University of Glasgow

Centre for Cell Engineering

Development of a Microfluidic Device to Test Nanoparticle Toxicity

Abhay U. Andar
Centre for Cell Engineering
University of Glasgow

Thesis Submitted to the Faculty of Biomedical and Life Science of the University of Glasgow for the degree of Doctor of Philosophy
September 2010

Author's declaration

I hereby declare that the research reported within this thesis is my own work, unless otherwise stated, and that at the time of submission it is not being considered elsewhere for any other academic qualification.

Abhay Uday Andar
Centre for Cell Engineering
University of Glasgow

September 2010

Acknowledgements

I would like to thank my supervisors Dr. Mathis Riehle and Dr. Nikolaj Gadegaard for their valuable help through out this thesis. Without whom there would be no hypothesis, no data and no thesis. I thank you both for your time, patience, dedication and guidance throughout my doctoral studies. The support provided was constant and you have been hugely influential in defining the scientist that I am today, and the future course of my career. I thank you sincerely.

I would also like to thank Drs Martha Liley, Thomas Overoltz, Philippe Neidermann, Melanie Favre and Nicholas Blondeux for their help with providing silicon nitride membranes and setting up the electrical systems for the TEER measurements. A special thanks goes out to my brilliant M.Res students and friends Mr. Sher Ahmed, Mr. Sultan Al-Shariff and Mr. Kazeem Olayiwola. Also would like to thank PhD student, Ms. Kristin Kirchhoff for her valuable time and dedication during our challenging joint project. Their input during the course of this PhD has been precious and extremely supportive.

I extend my gratitude to Prof. Adam Curtis, Dr. Matthew Dalby, Dr. Catherine Berry-Dalby and Prof. John Barnes for valuable advice and support during my time at the CCE. I would also like to thank all my fellow student, friend and colleagues, especially Mr. Andy Hart and Mrs. Anne Macintosh, who in their own way have been instrumental in the successful completion of my studies at CCE. Thank you for making my time at the CCE and the PhD process both enjoyable and rewarding. I acknowledge Mrs. Mary Robertson and Mr. Bill Monaghan for their help with clean room training and numerous mask plates for fabrication within the JWNC. This work was funded by the NANOSAFE2 – EC project; Grant Number: Contract no. NMP2-CT-2005-515843

Finally heartfelt thanks to my best friend and beloved wife Indira Rao-Andar, for bringing love, laughter and support to my life when I needed it most. Without your tireless encouragement, tolerance and devotion this thesis would never have reached completion. I would also like to thank my parents, Dr Uday and Deepa Andar and my beloved sister, Divya Andar-Batra, for their constant support and encouragement throughout the course of my education. I could not have possibly got this far without them. I am forever indebted to you all. Jai Parijnan.

Abstract

Recent years have seen a growth in the manufacturing of nanoparticles for their uses in various fields of science and technology. However, this explosion in the production and use of nanoparticles has in turn resulted in growing concerns regarding their impact on public health and the environment (Hoet, 2004). One major route of entry into the human body is through the air-blood barrier in the lungs. The air-blood barrier at the alveolar region in most mammals is normally about 500-600 nm in thickness (Bartels, 1979) and is mainly responsible for the selective transport of gases and certain vital solutes across the membrane (Theodore, 1975). This selective transport across these barriers is regulated by tight junction protein complexes that bind two adjacent cells in the tissue. This particular selective transport mechanism is highly attractive for the drugs industry due to which the lung epithelial barriers could provide a novel mode for delivery to patients (such a system already exist for patients suffering from asthama, where they use an inhaler to deliver their dosage). However, to develop such drug delivery systems it is necessary to study the effects either through *in vivo* and/or *in vitro* research methods. For the purpose of this thesis an *in vitro* system using the Calu-3 cell line (cultured on two types of membrane systems) was used in the attempt at mimicing certain barrier properties (mainly transport of solutes across the membrane and integrity/tightness of the cell monolayers) present in the *in vivo* state. Calu-3 cells were maintained on two different sets of porous membrane types, one was the commercially available Transwell® membranes (Costar/Fisher) and the other was the self-fabricated (at CSEM, Switzerland) silicon nitride membranes. The silicon nitride membranes were particularly unique, in the sense that their thickness was only 500nm (compared to the polymer Transwell® membranes) and also presented the possibility of miniaturising the Calu-3 *in vitro* system. Miniaturisation helps reduce the use of test solutions and allow the development of high throughput screening devices for biological applications (Beebe, 2002). When the possibility of miniaturisation occurs along side a biological application it is often the case that microflows would be necessary for maintaining cell culture within small areas inside the devices. Therefore, microfluidics was vital in providing the opportunity for miniaturised cell based systems. In this study PDMS (Polydimethyl siloxane) based microfluidic devices were used for developing the cell culture and concentration gradient devices. The final purpose of this poject was to create a scaleable modular integrated device allowing the analysis of the induced effects on Calu-3 cells against nanoparticle/solute translocation and assessing cell monolayer integrity using a real time TEER measurement system. This miniaturised *in vitro* multilayered microfluidic setup consisted of three main components, a top layer micro channel

(fabricated in PDMS), the middle silicon wafer bearing the silicon nitride membrane (also bearing the electrodes for measuring TEER of the cultured cell monolayer) and the bottom layer micro channel. This modular device would help assess Calu-3 cell monolayers resposes to toxic solutions and hopefully assist towards developing a novel analysis system device to study the effects of such toxic solutions in real time.

Table of contents

List of tables

List of equations

List of figures

Definitions / abbreviations

A549	Alveolar epithelial cell line
AFM	Atomic force microscope (microscopy)
AuNP	Gold nanoparticle
BSA	Bovine serum albumen
Calu-3	Cancer lung - 3
CC16, CC10	Clara cell secretory protein 16, Clara cell secretory protein 10
CFTR	Cystic fibrosis transmembrane conductance regulator
CSEM Centre	Suisse d'Electronique et de microtechnique
DAPI	4'-6-Diamidino-2-phenylindole
DMEM	Dulbeccos modified Eagles medium
EBL	Electron beam lithography
ECM	Extra-cellular matrix
E.coli	*Escherichia coli*
EDTA	Ethylenediaminetetraacetic acid
EMEM	Eagles Minimum Essential Medium
FBS	Fetal bovine serum
FISH	Fluorescent in situ hybridisation
FITC	Fluorescein isothiocyanate
16HBE14o	Human bronchial epithelial cells
hAEpC	Human alveolar epithelial cells
HBSS	HEPES buffered saline solution
HEPES	4-(2-hydroxyethyl)-1-piperazineethanesulfonic acid
ICP-MS	Inductively coupled plasma - Mass spectrometry
ICP-AES	Inductively coupled plasma - Atomic emission spectroscopy
IgG	Immunoglobulin G
IgM	Immunoglobulin M
JAM	Junction adhesion molecule
MDCK	Madin-Darby Canine Kidney
MTT	3-(4,5-Dimethylthiazol-2-yl)-2,5-Diphenyltetrazolium Bromide
PBS	Phosphate buffered saline
PDMS	Poly dimethylsiloxane
PMMA	Poly (methyl methacrylate)
PTFE	Poly-tetra-fluoroethylene
QD	Quantum dot
RF	Radio Frequency
RFU	Relative Fluorescence Unit
SE	Secondary electron
SEM	Scanning electron microscope (microscopy)
Si_3N_4	Silicon nitride
SP-A/B	Surfactant protein – A/B
STD	Standard deviation
TEER	Trans epithelial electrical resistance
TEM	Transmission electron microscopy
TCP	Tissue culture plastic
TiO_2	Titanium dioxide
UFPs	Ultrafine particles
UV	Ultraviolet
XTT	2,3-bis (2-methoxy-4-nitro-5-sulfophenyl)-5-[(phenylamino) carbonyl]-2H-tetrazolium hydroxide

Chapter 1 : General Introduction

1 Introduction

Living cells in the human body are typically 10s of micron in diameter and cell parts are much smaller ranging in the sub-micron level. Proteins which are smaller still, typically in the range of 5-50 nm (Figure 1) can be compared with the dimensions of some of the smallest artificially produced nanoparticles (Salata 2004). Nanoparticles are used and developed as materials in biotechnology and pharmaceuticals because of their “small size” (in the nanometer range). They have been shown to penetrate tissues quite well and allow the addition of a range of functionalities onto the same nanoparticle in order to be suitable for a particular application (Silva 2007, Salata 2004, Sperling 2008, Sukhorukov 2005, De la Fuente 2006). However, the question that arises is what effects do these nanoparticles have on human health and the environment; do they even pose a toxicological hazard? For example titanium dioxide (TiO_2) nanoparticles are often used in sunscreen lotions to absorb ultraviolet (UV) light. It has been reported, that some of these nanoparticles used in cosmetics have the ability to penetrate through the skin thus entering the body and interact with the bodies immune system (Hoet 2004). Effects of such nanoparticles could be long term or short term with respect to the exposure of vital organs in the human.

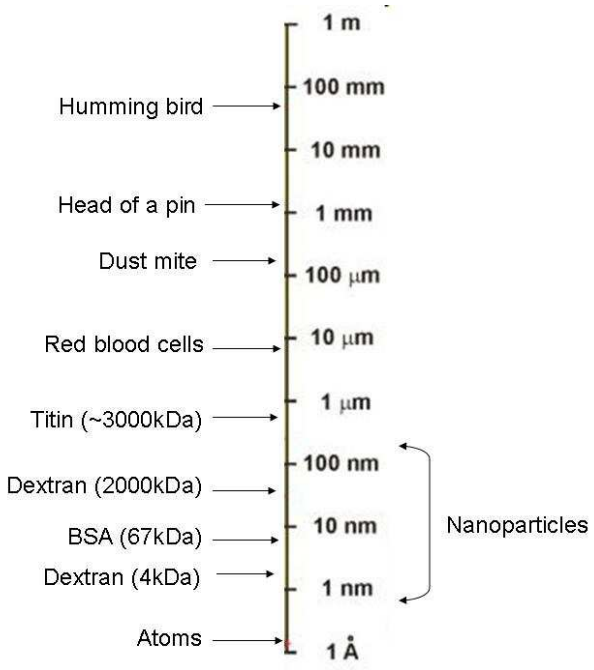

Figure 1: Size distribution scale
Scale of size distribution of various materials, proteins, cells, and animals (left) compared to nanoparticles

We are constantly exposed to various nanoparticles present in the environment due to air pollution. Particles released due to combustion of certain fossil fuels are one of the main concerns of environmental nanoparticle hazards with respect to inhalation (Stone 2000, Nawrot 2007, Nemmar 2003). The average human inhales approximately 15kg of air daily and when compared to the intake of 1.5kg of food and 2.0kg of water it becomes evident that the inhaled air can be a major source of harmful materials, chemicals, etc.. Due to the lung's unique morphology of airway conduction and large internal surface area ($70m^2$), these harmful chemicals are found to travel further across the air spaces and right up to the alveolar regions. The alveolar air-blood barrier region is responsible for gas exchange between the lungs and the capillary circulatory system. This air-blood barrier also works as a sieve against larger foreign materials (micrometer scale materials, aggregates, large dust particles, etc), where the much smaller materials (e.g 99_{Tc} technetium radioactively labelled carbon particles <100nm, certain therapeutic drugs – e.g asthama inhaler drugs like bambuterol and formetorol) tend to cross the barrier into the capillary circulatory system (Gardner 1993). Since the air-blood barrier is under constantly exposed to the enivornment or in the case of a disease (like asthma) under constant exposure to certain drugs, the repirstory system has several defence mechanisms. The various cell types within the lungs perform the task of excluding foreign toxic substances through other means like mucocilliary clearance mechanism and alveolar macrophage response that work along side the barrier function of the air-blood barrier (Asgharian 2001, Oberdörster 1997, Bernardin 1995, Gardner 1993, Stone 2007). Due to the presence of such defence mechanisms it becomes difficult to assess the actual effective dose delivered to the various target organs, from the concentration of pollutants in the air. There are however certain methods like *in vivo* or *in vitro* toxicity for vital organs (in animals) and cells respectively, which are the most commonly used techniques for evaluating the effects of exposures to harmful materials or nanoparticles (Seagrave 2005)[1]. While assessing *in vivo* exposure systems different parameters such as ventilation, frequency of respiration bronchial dimensions, bronchio-arterial blood flow, rate of elimination including the natural clearance, metabolic conversion and rate of retention have to be considered to postulate the effective dose (Gardner 1993). In addition to these factors there are certain physical and chemical

[1] Some researchers also use the *ex vivo* (certain tissue sample which is maintained outside the body under culture for approximately 8 -14 days, depending on the type of tissue, exposure experiment and length of experiment) conditions to asses toxicity (Sakagami 2006, Kashima 1996), but this will not be discussed with this thesis.

properties of the test materials that must be considered in determining the effective dose [2]. Diffusion coefficient, particle size, surface properties, surface area and solubility are some of the factors that may be considered (Oberdorster 2007, Stone 2006). For obvious ethical reasons nanoparticle testing in humans is substituted by *in vivo* animal models and *in vitro* analysis of human cells. *In vitro* studies can be a very useful approach to identify underlying mechanisms by which nanoparticles damage cells (Devlin 2005). New approaches in particle testing and cyto-analysis assays have made it possible to understand many of the underlying cellular pathways and biochemical processes involved in the cellular response to toxic- and other nanoparticles (Shim 2003). *In vitro* testing systems are relatively inexpensive and exposure results obtained from *in vitro* models of human cells can be compared to some extent with *in vivo* methods (Seagrave 2005). Cells in culture have on the other hand certain limitations considering growth potential, culture conditions, phenotypic expressions of proteins and retention of cell type specific function. The main disadvantages of having an *in vitro* system are that such lack the systemic physiological input (immune system, blood flow, temperature, etc..) available within an *in vivo* system. Meaning that under the influence of certain mechanical or chemical stresses there is no macrophage response or changed blood flow at the exposure sites, which is one of the important factors during healing or exposure repair (Seagrave 2005, Gardner 1993). However, inspite of these limitations *in vitro* systems can provide important information on interactions of potentially toxic materials with specific cell types. The *ex vivo* system, (tissue samples maintained in culture for approximately 14 – 21 days) can be used for experiments outside the body depending on the type of tissue and exposure routes studied (Seagrave 2005). The various established *in vitro* testing systems can give valuable and complimentary results to *in vivo* systems. However, the main disadvantage of *in vitro* systems is also to some extent their advantage, such that they lack the systemic input. In order to increase the *in vivo* likeness of *in vitro* models some complexities such as a 3D environment, flow, co-culture with other cells can be added. One of the techniques that aim at incorporating some such parameters into *in vitro* experiments can be achieved through microfluidic techniques. In microfluidic devices the environment can be well-controlled and parallelised high throughput systems could help maintain scalable cell cultures within a controlled environment with the scope to achieving better *in vivo* likeness.

[2] I will from here on concentrate on the specific problems associated with nanoparticle exposure.

1.1 Nanoparticle toxicity

1.1.1 Nanoparticles

As we steer towards a new age in technology, the field of nanoparticle-technology has found its way towards gaining tremendous importance for future applications in biomedical and pharmaceutical research. This field deals with the creation and/or manipulation of materials in the nanometer (0.1 – 100 nm) scale. Due to novel, exploitable properties that materials exhibit when structured, or made to be in the nano size range, nanoparticle-technology has had a great deal of impact on advancements in the scientific and technology community (Silva 2007, Salata 2007, Salata 2004, Stone 2007, Mazzola 2003, Whitesides 2005, Service 2004). Materials characteristics such as color, strength, and conductivity (heat and electrical) are drastically altered with slight modifications in particle size in the nano scale as compared to larger sizes or the bulk material. As a consequence, the field of nanoparticle-technology has generated substantial interest in many areas that aim to harness these changed properties of nanoparticles, so that they can be incorporated into products to enhance or improve existing properties, or can be used as novel stand-alone products (Salata 2004, Salata 2007, Soloviev 2007).

Examples of “nano-size” dependent properties and applications are seen in quantum dots, gold nanoparticles, magnetic nanoparticles etc.. Quantum dots (QDs) are nanoscale crystals of semiconductor material that fluoresce with a size dependant colour when excited by an appropriate wavelength of light. There has been a considerable amount interest in the use of QDs as inorganic fluorophores, owing to the fact that they offered significant advantages over conventionally used fluorescent markers. QDs have fairly broad excitation spectra–from ultraviolet to red light that can be tuned depending on their size and composition. They have narrow emission spectra, making it possible to resolve the emissions of different nanoparticles simultaneously and with minimal overlap. A valuable function being that they have a slow degradation making their fluorescence remarkably stable over long periods of time. By altering the surface chemistry of QDs, to make them more hydrophilic, they have shown to be used as tagging agents that can be specifically attached to cells, proteins and nucleic acids. In a study by De la Fuente et al 2005, they presented quantum dots (water soluble quantum dot conjugates using a cadmium sulphide core coupled with tiopronin, where the tiopronin made the surface hydrophilic and also reactive to proteins due to the presence of a free -COOH group) with surface immobilised cell-penetrating peptides (tagged with HIV-1-trans-activating-protein (Tat-protein)

molecules) that not only could penetrate the cell but also target components within, in this case the cell nucleus (de la Fuente, 2005). Their observations with the CdS@tiopronin-Tat showed penetration into the nucleus of fibroblast cells. Through this example, it is evident that nanoparticle surface properties can be modified, using surface coatings or tags, to create a link between themselves and their environment. In a review Salata (2004) explains that nanoparticle coatings or tags could be produced from protein and carbohydrate conjugates, antibiotics, fluorescent tags, biocompatible monolayers of small molecules, etc. These coatings depend on the specific applications to visualise and influence cell response, and could be used for various drug therapies. (Salata 2004, Kane 2007, de la Fuente 2005, de la Fuente 2004, Barrientos 2003). In an interesting review, Marie-Christine Daniel and Didier Astruc (2004), presented a number of applications of gold nanoparticles (AuNPs) for biomedical investigations and drug design. The use of AuNPs increased exponentially in applications related to biomedical sciences, electronics, catalysis and optical applications, with most of the particles being synthesised using a 'bottom up' approach (involves chemical synthesis and self assembly to generate the desired product - Silva 2004). The authors have listed various methods used to modify the surface chemistry of AuNPs in order to make these compatible with the needs of specific applications in various fields. This review also explains the functionalisation of AuNPs by alkanethiolate and various functional thiolate ligands forming very stable and monodispersed materials. These simple synthetic methods were shown to be particularly favourable for easy manipulation of AuNP surface properties. Of the many applications highlighted in this review, the most promising is the possibility of tagging AuNPs with DNA assemblies. For future biomolecular applications, such as labeling, detection, and transfer of drugs, including genetic materials the property of bio-tagging AuNPs or certain nanoparticles could be extremely useful (Elghanian 1997, Mirkin 1996). DNA was a good candidate for this task because of its specificity in base pairing, and it could be used at the nanoscale level for biosensing, (DNA strand thickness ~2.2nm and length of one nucleotide sequence ~0.3nm). The examples presented here showed an extraordinary variety of structures, properties and applications available for gold nanoparticles that will motivate fundamental sciences and interdisciplinary research in the future.

The above listed examples were just a few examples of the tremendous amount of work that has been carried out in the field of nanoparticle production and application.

1.1.2 Current situation with nanoparticle toxicity

Nanoparticles are currently being used within various consumer products like aerosols, cosmetics, paints, etc.. Some cosmetics like sun block, tooth-paste, paint etc. contain titanium dioxide (TiO_2) nanoparticles. In the case of sun block/screen creams, titanium dioxide works as a physical sun blocking agent that primarily reflects/absorbs ultraviolet light (It bocks UVB and short UVA (320-340 nm) (Benson 2005). Titanium dioxide is not irritating and more compatible with sensitive skin than chemical sunscreens (For example, Oxonica have recently developed a product known as OPTISOL™, which consists of microfine titanium dioxide with small amounts (0.67%) of manganese included in the crystal lattics structure of the particles. This allows absorbed UV energy to be dissipated, virtually eliminating the generation of free radicals. Manganese at the surface of the particle scavenge free radicals that are normally generated by other sunscreen components containing benzophenons, and salicylates) (Oxonica.OPTISOL™, data sheet 2009) The main issue with using titanium dioxide-based sunscreens is that they leave a white residue. By introducing TiO_2 nanoparticles into sunscreen products this issue has been partly resolved. TiO_2 nanoparticles have different optical properties and tend to leave much less whitish residue than regular powdered titanium dioxide. The TiO_2 nanoparticles retain the capacity to protect from UVB and short UVA wavelengths.

However, there are some concerns with the penetration and invasion of such particles into the blood stream through the skin. Effects of such nanoparticles are likely to arise in many different scenarios; they could be long term or short term, mainly with respect to the extent of exposure of vital organs in the human. For example TiO_2 particles have previously been reported to penetrate through the skin (Hoet 2004) thus interacting with the immune system. In a study by Ferin et al (1990, 1994), the authors demonstrated that when rats were exposed to an equal airborne mass concentration of ultrafine (range <100 nm) TiO_2 particles, there was excessive bronchoalveolar inflammation. In another comparative study by Warheit et al (2005), they tested TiO_2 particles with different surface coatings ranging from 0-6% alumina (Al_2O_3) and 0-11% amorphous silica (SiO_2). Their results demonstrated that only the TiO_2 particles with the largest proportion of surface coated produced mildly adverse pulmonary effects when compared to the TiO_2 control particles. This meant that the TiO_2 could be used as a control particle when setting standards for nanoparticle toxicity studies (for different nanoparticles). Such valuable experiments to produce standards for cell based systems, had also been conducted by Lu et al (2009), where the toxic effect of several different oxide based metal nanoparticles was determined.

Here TiO_2 was used as the baseline particle and revealed that NiO particles acted extremely toxic when tested for oxidative stress induced under *in vitro* conditions. There were several other experiments performed that tested the toxicity of nanoparticle colloids and fibres such as fine diesel- , or carbon black particles, etc. (Geys 2008, Xu 2004, Nemmar 2003, Ferin 1990, Warheit 2005, Warheit 2004, Stone 2007).

Hoet et al (2004) used an aerosol (Technigas) to test nanoparticle translocation across the lung epithelium into the blood stream (Hoet et al. 2004). They found traces of this radioactive aerosol (99m technetium-labelled carbon particles <100nm in diameter), in many of the vital organs. Radioactivity was detected in the blood of 5 different healthy human volunteers within a minute of inhaling the aerosol. (Duhayon 2008, Nemmar 2002) Technegas was a commonly utilised aerosol in diagnosing lung infections and for measuring the distribution of ventilation of the lungs. (James JM 1995, Isawa T 1991), but their potential hazards to human and environmental health were yet only vaguely understood. However, this study is not without its critics, in a paper by Brown et al (2002) and more recently in a paper by Mils et al. (2005) no translocation of nanoparticles was observed which would suggest that there are uncertainties in stability or imaging limitations in the detecting the radioactive technetium in an *in vivo* study. It is thus necessary to understand the toxicological effects of these particles and there is a need for developing a system that would accurately test such nanoparticles for their toxicity.

Rapid proliferation of nanoparticle production presents a dilemma to regulators (nanoparticle toxicologists) with regards to hazard identification. The aim is to be able screen nanoparticles for their toxicity and to implement their proper/safe usage in specific industries where nanoparticle-technology may be applied.,This is essential for risk and hazard management in areas where there was an extensive exposure to nanoparticles, for example in nanoparticle production industries, potential user of nanoparticles within labs, etc.. The risk evaluations required the generation of a data base related to the assessment of health hazards on exposure to such engineered nanoparticles. In order to understand the risks of nanoparticles, it is first vital to know the mechanisms that cause toxicity within various cells in the body or that can declare the particle as being toxic. Nanoparticle toxicity was shown to be largely dependant on the surface reactivity and on their variable particle size or by accumulation of surface area in contact with the nanoparticles (Stone 2006, Warheit 2004, Oberdorster 2007). For example in individuals who smoke, excess accumulation of smoke particles on the alveolar epithelium may cause a reduced surface area for the uptake of oxygen; in pneumonia, patients suffer due to an excess of water in

the lungs which may reduce the air accessible surface area of the alveolar epithelial cells, causing loss of cilliary activity and resulting in drying up of the mucus on the surface of the epithelium. Nanoparticles have also been shown to possess the potential to cause such changes within the human system and at the same time have a direct toxic effect on alveolar cells. (Stone 2006, Warheit 2004, Oberdorster 2007).

Although most of the validations for toxicity studies have been conducted using *in vivo* experiments, it was highly desirable for future research to follow the '3Rs' principle: Replace, Refine and Reduce animal testing in research. (for example UK based funding body 'The NC3Rs' look towards promoting new techniques at improving and implementing the use of *in vitro* techniques – NC3Rs – National Centre for the Replacement, Refinement and Reduction of Animals in Research). However, current *in vitro* methods for evaluating nanoparticle toxicity have some limitations in identifying or finding results for nanoparticle induced toxicity when compared to the same conditions for *in vivo* toxicity effects. For example considering the lungs, this is a complex organ consisting of different cell types and it is difficult to simulate the same reactions against nanoparticle as observed *in vivo* with the systemic environment in an *in vitro* system. In an interesting review by Sayes et al. (2009) the capacity of *in vitro* screening studies to predict *in vivo* lung toxicity of nanoparticles in animal models was investigated. There is a considerable amount of data where nanoparticle-technology has been utilised for the purpose of drug delivery via the lung (Forbes 2005, Foster 2000). However, there is a growing concern about the toxicity caused within the lungs by these delivery systems (Villa-Vega 2008). The following sections will discuss as to why pharmaceutical and drug companies are targeting the lung for nanoparticle-drug delivery technology and the significance of the defence mechanisms of the lungs with regards to such nanoparticles.

1.2 Lung as a target system

1.2.1 Pulmonary passage and barrier properties

For the purpose of this project the main area of interest were lung epithelial barriers. Components of the respiratory system are exposed to the environment and block the unwanted harmful materials and small particles, present in the air, from entering the body. Due to this very reason the lung is well equipped with several different defence mechanisms, for example the air-blood barrier regulating selective transport of gases, solutes and proteins, macrophage response to the affected sites and mucocilliary

movement. The lung epithelial cells, being one of the main defences, act as barriers between the external environment and the internal vascular system and form the air blood barrier.

The primary structure of the lungs and, the alveolar epithelium provide an extensive and thin surface for gas exchange. Besides this the pulmonary epithelium serves a number of other functions that help preserve the ability of the lungs to exchange gas. It provides a barrier (lung-blood barrier/air-blood barrier), which protects the host from the outside environment by controlling the transport of solutes, water and any inhaled foreign material. The lung epithelium also produces complex surfactant secretions, as well as several proteins necessary for defence against damage or pathogen attacks. The significance of the air-blood barrier was not only that those gases could diffuse across but also that it was known to be permeable to proteins and solutes. The alveolar to vascular permeation had been demonstrated in a number of publications and altogether they provided strong evidence for the respective transport mechanisms (Hermans 1999, Theodore 1975). Hermans and Bernard (Hermans 1999) stated in a review, that the air-blood barrier behaved like a molecular sieve, allowing the passage of solutes and macromolecules in both directions depending on their molecular weights and shapes, especially in the case of surfactant proteins. Surfactant proteins are secreted mainly within the lung cell area hence their presence in the vascular compartment of the system could be possible due to leakage through the barrier. Some surfactant proteins, like for example Clara cell secretory proteins (CC16, CC10), surfactant proteins (SP-A, SP-B) are studied in more detail with regards to protein transport (Broeckaert 2000, Hermans 1999, Robin 2002). To reach the blood stream proteins and solutes must cross the airway and/or the alveolar barrier. The epithelial barriers of the airways and the alveolar regions have several differences that can affect the passage of macromolecules to – or from the air space to - or from the blood stream. The permeability of this passage was likely to be determined by the relative pore size between adjacent epithelial cells. The alveolar barrier is estimated to have an average pore radius of about 1 to 5nm and the airway bronchial barrier has an effective pore radius of a about 7 to 12nm (Taylor 1970, Taylor 1965, Oberdorster 1986).

The ability of the air-blood barrier to act as a selective transporter between air and blood provides a promising route for drug delivery and biomedical applications (Forbes 2000, Forbes 2005, Kim 2007, Silva 2007, Salata 2004, Fiegel, 2003). Nanoparticles, due to their extremely small size, exist in the same structural domain as most proteins (Figure 1), which makes them useful for drug administration applications, considering also the

effective pore size of the inter-cellular junctions. However, the interactions of nanoparticles with the lung epithelium are poorly understood (Hoet, 2004, Oberdorster 1995, Stone 2007). The development of *in vitro* and *in vivo* systems has helped to asses the translocation of drugs and nanoparticles through lung cells.

1.3 In-vitro models

The human respiratory system is a complex organ consisting of numerous cell types that have specific roles within the different regions of the airways. In the lungs pathogenic effects of inhaled solid materials depend on achieving a certain lung burden [3]. When considering the lung burden, the chemical and physical properties of the particles themselves are important and influence deposition and clearance rates (Seagrave 2005, Marquis 2009, Oberdorster 2005). It was shown by some authors (Hoet 2004, Oberdorster 1995, Stone 2007, Strum 2009) that nanoparticles <100nm normally deposited in the alveolar regions, mostly at branching point, where a larger bronchiole splits into two bronchioles. In a theoretical view of particle deposition Strum et al. (2007) presented a model that explained how fiber nanoparticle deposit in the human bronchial and alveolar regions. They discussed the deposition of rigid and chemically stable fiber particles compared to the alveolar and bronchial clearance mechanisms using the aerodynamic diameter [4] of fiber particles. The bronchial clearance was driven by the mucociliary activity, which is an effective transport system that pushes mucus trapped nanoparticles moving them upwards through the airway canal. The alveolar particle clearance mechanism predominantly depends on macrophage phagocytosis. This process results in the activation of macrophages which induce the release of certain chemokines, cytokines, reactive oxygen species and reactive nitrogen species that can result in persistent inflammation and fibrotic changes (Ferin 1994, Cohen 1975, Muhlfeld 2008). However, some experimental evidence published by Absood et al. (2008), and Petty (2007), suggested that inhaled nanoparticles escape the alveolar and bronchial defence systems and can migrate into the regions of the air-blood barrier. Nanoparticle toxicity related to lung exposure has been investigated by authors like Donaldson 2002, Nemmar 2002, Oberdorster 2001, Stone 2007, Warheit 2005 etc., who also discussed the effects of particle

[3] Nanoparticle accumulation inside the lungs determines its lung burden dependent on the ratio of the rates of particle deposition and clearance

[4] Aerodynamic diameter is commonly applied to particulate pollutants and inhaled drugs to since their geometry is difficult to measure therefore the it is given an assumed geometry of a sphere

penetration and related pulmonary damage. All the above mentioned papers presented evidence that nanoparticles were mediators of adverse health effects probably due to their very small sizes, their surface reactivity, and their ability to produce surface free radicals to cause oxidant damage.

In a nanomaterial toxicology review, Oberdorster et al. (2007) highlighted the significance of *in vitro* testing methods for nanoparticle toxicity testing. They stated that there are several parameters to consider with regards to the application of *in vitro* testing methods. Also that there are several issues concerning such methods to detect the nanoparticles, due to possible dose mismatches within *in vivo* conditions, and the need for a positive and a negative control particle (bench mark particles of known toxicity) as well as differential protein adsorption onto the nanoparticles (also mentioned by Lundqvist 2008, Lynch 2007). To aid with methods of determining toxicity and setting up certain control values several analytical methods have to be considered for cytotoxicity due to the possible uptake and translocation of nanomaterials. Marquis et al. (2009) recently reviewed various analytical methods available to assess nanomaterial toxicity with *in vitro* techniques. They showed that due to the complexities involved with assessing nanoparticles (explained before as size and surface area properties, etc.) that many of the techniques used to derive the information about toxicity had often to be used collectively (meaning that only one or two analysis techniques are not enough to estimate the toxicity of one type of particle and that a combination of techniques would be better suited to determine toxicity. Within this review, nanoparticles were identified using: transmission electron microscopy (TEM), inductively coupled plasma atomic emission spectroscopy (ICP-AES), fluorescence spectroscopy, flow cytometry and video enhanced differential interference contrast (VEDIC) to relate to the amount of uptake and transported through cells. The techniques to test nanoparticle toxicity however included a variety of metabolic assays [e.g. MTT, XTT [5] and Alamar blue assays], necrotic or apoptotic assays [lactate dehydrogenase testing for leaking cells by showing up released lactate, Trypan Blue a dye excluded by living cells, neutral red (as for trypan blue), annexin-V a marker for apoptotic cells, and live/dead (using ethidium homodimers together with SYTO-stain) assays]. These cytotoxicity test assays were useful for most types of cells and could help to generate a valuable database to classify nanomaterials according to their toxicity. These techniques are used as part of a group of three or more techniques (the minimum number is 3 types of different techniques) which gives a comparative analysis for the toxicity of nanoparticles (according to the

[5] Full forms given in abbreviations section

authors Marquis et al 2009). In this case, one technique is dedicated to testing the size and distribution of nanoparticles (e.g ICP or TEM) and the other two are used to test the effects on cell stress and changes in metabolic acticvity in cells (e.g. MTT, apoptotic cell assays, etc.)

There are currently several cell lines being used as *in vitro* model systems for the lungs, these are: Calu-3 and 16HBE14o which are human bronchial epithelial cell lines and then the human alveolar cell lines hAEpC and A549, as well as others. These cell lines have been vital tools to understand drug delivery and metabolism, and are now being utilised to postulate the behaviour of inhaled nanomaterials. The Calu-3 cell line is the most commonly used cell model for drug delivery studies and toxicity analysis (Calu-3 are derived from airway adenocarcinoma human bronchial epithelial cells type II and commercially available from ATCC-LGC – Promochem). They exhibit both a serous (secretory) and sometimes a ciliated phenotype and were shown to form very good epithelial barriers which can be utilised for different applications, e. g. to investigate drug transport, and toxicity testing of harmful aerosols and particles, etc (Florea 2003, Fogh 1977, Forbes 2000, Forbes 2005). Test materials and applications of Calu-3 cells are listed in Table 1.

Respiratory cell type	Application	Test materials	Authors
Calu – 3	Nanomaterial Screening	Polystyrene particles (amine/carboxy-modified)	(Geys, 2006)
		Poly(lactic-co-glycolic)acid particles	(Fiegel, 2003)
		Single/multi-walled carbon nanotubes (CNT)	(Rotoli, 2008)
		Chitosan particles (Microspheres formulated at NP:mannitol ratios)	(Grenha, 2007)
	Drug screening	Cyclodextrins (α-, β-, γ-, HP-α/β, RM-β-CD)	(Matilainen, 2007)
		FITC-dextrans,Caffein, Lucifer yellow, antipyrine, chromoglycate, insulin, leucine, uridine, salbutamol	(Mathia, 2002)
		Albuterol sulfate, sucrose, fluorescein tranferrin	(Foster, 2000)

Table 1: Calu-3 cells used as a screening tool for drugs and nanoparticles.
This table lists the two main areas for the applications for Calu-3, nanomaterial screening and drug screening, showing the different nanoparticles and drugs utilised. The relevant literature is listed in the table

1.4 *In-vivo* models

In vivo models have been specifically designed to establish a relation between the potential toxicity of nanoparticles under the true physiological conditions of the test organs (i.e lungs in this case). *In vivo* inhalation experiments used to test the potential toxicity of some nanoparticles have shown that they can travel much deeper into the body (into vital organs) passing through the air-blood barrier in the lungs (Nemmar 2002). There are a number of exposure techniques, most of which are reviewed in much detail by Garner et al. (1993). In this review the authors analysed several experimental techniques where animals were made to inhale particle contaminated air. They categorised these techniques as being either static - or dynamic- systems, depending on the way in which the air was supplied to the animals. Following their categorisation under "static conditions" the test material was initially introduced inside a chamber and allowed to mix with the air in the system. The animal was later introduced into this chamber and the apparatus was kept sealed. In such a system there is no ventilation of air hence over time oxygen is depleted, and carbon dioxide

increased, which may exasperate the materials toxicity. Due to this inherent problem such static systems were abandoned for recent studies. Under “dynamic conditions” there is constant flow of air mixed with the material to be tested, and hence oxygen/carbon dioxide levels did not affect the animals. Other parameters such as temperature- and humidity- could also be controlled within the experimental setups, allowing one to match environmental conditions. Experimental inhalation exposure techniques are categorised depending on the type of exposure to the host. Gardner et al (1993) described three different types: A) whole body exposures, where the host animal can be tested within a controlled environment and all the organs provide a valuable and large base for results. However, this method proved to be quite expensive considering the costs of the chambers, materials, and animal maintenance. The animals also had to be exposed continuously or sporadically to airborne nanomaterials and exposure is not restricted to the respiratory system (It was difficult to determine the extent of toxicity caused through the organ of interest and other routes of entry such as transdermal, oral uptake due to grooming, etc, have to be considered). B) Head or nose exposure, where the delivery system is focused towards the introduction of test particles through the lungs, via inhalation and the exposure of any other body parts is reduced. This system used up less amount of the test material as compared to the whole body exposure systems. This system was however stressful to the animals since they were exposed to the test material within tiny ventilation zones and may have not had access to either food or water for long periods of time due to inaccessibility once the animals were loaded. C) The ‘lung only’ exposure included deep lung exposures (to specific lung sites) by intubation. Each technique has its advantages and disadvantages. These techniques were implemented depending on the test materials and on the host species. Inhalation toxicology systems and methodology are more widely discussed in reviews by: Barrow 1982, Wong 2007, Phalen 1976, Phalen 1984, Gardner 1993, Cannon 1983, and Cheng 1995; (Some schematics of exposure systems are shown in Figure 2). The techniques and methods described above produced a steady exposure atmosphere, however, in most cases the amount of material that was absorbed by or deposited into the animals could still differ between subjects. This was possible because of differences in the respiratory physiology and anatomy, e.g. breathing the frequencies may differ between subjects leading to significant differences in the total amount of test material inhaled (Gardner 1993).

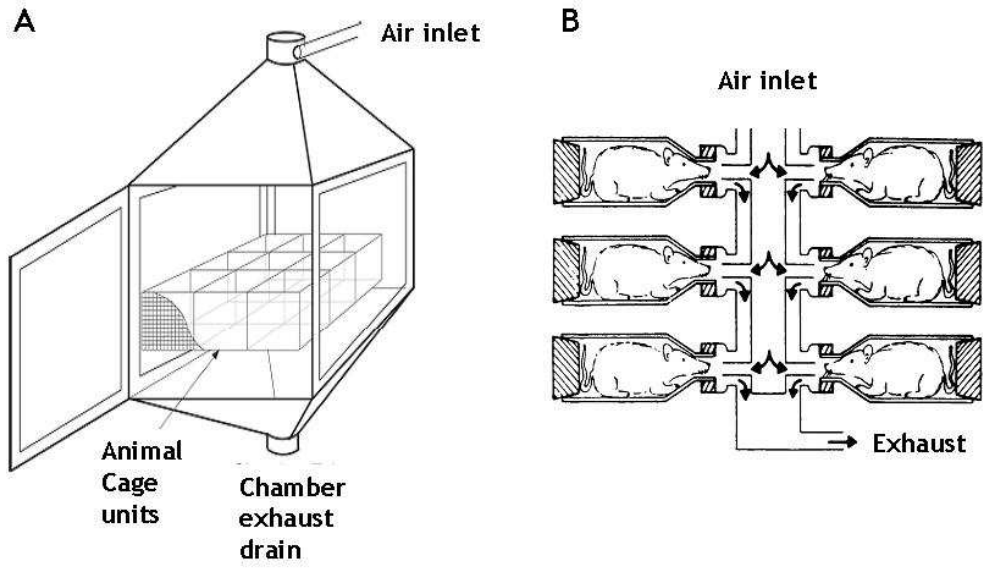

Figure 2: In-vivo inhalation exposure systems
A) The chamber represents a schematic of a whole body exposure system (Wong 2007), the air enters from above and leaves the chamber at the exhaust below. B) This is a schematic of a nose only exposure system adapted for rats, the steady flow of air through the central pipe has to be faster than the exhalation speed (Cheng 1995, Cannon 1983)

To reduce these systemic differences local dose methods were used especially when dealing with expensive test materials. Techniques such as intratracheal instillation, intratracheal inhalation, oropharyngeal aspiration, tracheostomy and endotracheal inhalation allow direct dosage to specified respiratory tract areas, but have the drawback of being a far more invasive procedure (Wong 2007).

In vivo toxicity assessment included the use and sacrifice of several animals. This allowed for the examination of animals after long term exposures, as well as studies of localisation, systemic biodistribution, excretion and retention of the administered materials (Barrow 1982, Wong 2007, Phalen 1976, Phalen 1984, Gardner 1993, Cannon 1983, Cheng 1995). There are a number of methods established to detect nanoparticles that get localised within live specimens, recently sacrificed specimen or fixed tissue samples (e.g. full body analysis using fluorescent/radioactive tags, homogenized tissue sampling using ICP-MS or ICP-AES [6], protein and serum assays from tissue samples- explained in the previous section). However, most in vivo methods are labour intensive and costly (Gardner 1993). The maintenance of animals is very expensive and also involves many ethical issues concerning live animal exposure and the number of animals used/killed for a particular experiment.

[6] ICP-MS (inductively coupled plasma – mass spectrometry) and ICP – AES (inductively coupled plasma – atomic emission spectrum) are highly sensitive methods to detect small volumes (few nanolitres) of metal present in given test solutions.

Hence there is a desire to move towards *in vitro* technologies that can be closely related to *in vivo* conditions.

1.5 Epithelial barriers and the significance of Transepithelial electrical measurements (TEER) systems

1.5.1 Epithelial barrier and tight junctions

The epithelium is a series of tissues that form the topological outside of the body, including its cavities, apart from the gut. It can be composed of either several cell layers (stratified epithelium) or just a mono-layer (simple epithelium). For example, the skin epithelial cells called ceratinocytes form a boundary and protective barrier shielding the organs within the body from the environment. In the case of the lungs, the air-blood barrier serves as a transport zone, which protects the circulatory system from harmful substances. The epithelial cells posses directionally organised intra/inter-cellular protein complexes that facilitate the transport across surfaces, and show patterns of absorption and secretion appropriate to the environment confronted. For their barrier function to work epithelial cells are polarised where the so called apical part of the cell face the topological outside and the basolateral to the topological inside of the body. In order to separate these two faces of the epithelium, and allow for a tight seal when needed the cells have specialised cell-cell contacts where junctional proteins reside. These protein complexes are mainly classified into tight junctions, gap junctions and adherens junctions.

The epithelial tight junctions form a functional and morphological boundary between the apical and basal surface of cells and regulate the diffusion of water, ions and larger solutes along the paracellular pathway (Schneeberger 2004, Weiss 1983, Schneeberger 1992). The process allows a selective and passive form of transport of solutes across the barriers. Figure 3, A) shows the junctions between the cells. For example in the lungs, the alveolar region is responsible for gas exchange and certain protein solutes These junctions between adjacent cells consist of the tight junction proteins connecting cells, the adheren junctions and desmosomes which interconnect to the actin filaments and intermediate filaments within cells that have the ability to regulate signal transduction pathways and cell surface receptors (Balda 2008). These tight junctions are involved in regulating cell proliferation, differentiation and contributed to vesicle transport. The tight junction architecture is composed of transmembrane protein networks between adjacent cells and this protein complex is made up of occludins, claudins, tricellulins and JAM (junction adhesion

molecule) proteins (Balda, 2008). Recent work into the cellular functions of these proteins have revealed how tight junctions are formed and which of their components contribute to their characteristic morphological appearance, as well as how they are regulated and how they signal to regulate changes in epithelial cells. They are linked to cytoplasmic plaques that are formed by a network of adaptor proteins (e.g ZO-1, ZO-2, ZO-3, etc), signalling components and actin-binding cytoskeletal linkers (e.g F-actin). (Balda 2000, Balda 2008, Schneeberger 2004, Gonzalez-Mariscal 2003, Brandner 2009, Aijaz 2006, Matter 1999, Matter 2003, Lapierre 2000, Chiba 2007). In a cross sectional profile (Figure 3, B) of transmembrane protein complexes, they seem to form 'kissing points' (via binding sites (charged amino acids) within the transmembrane protein structures to form a tight junction that were produced as a result of binding sites between adjacent transmembrane proteins).

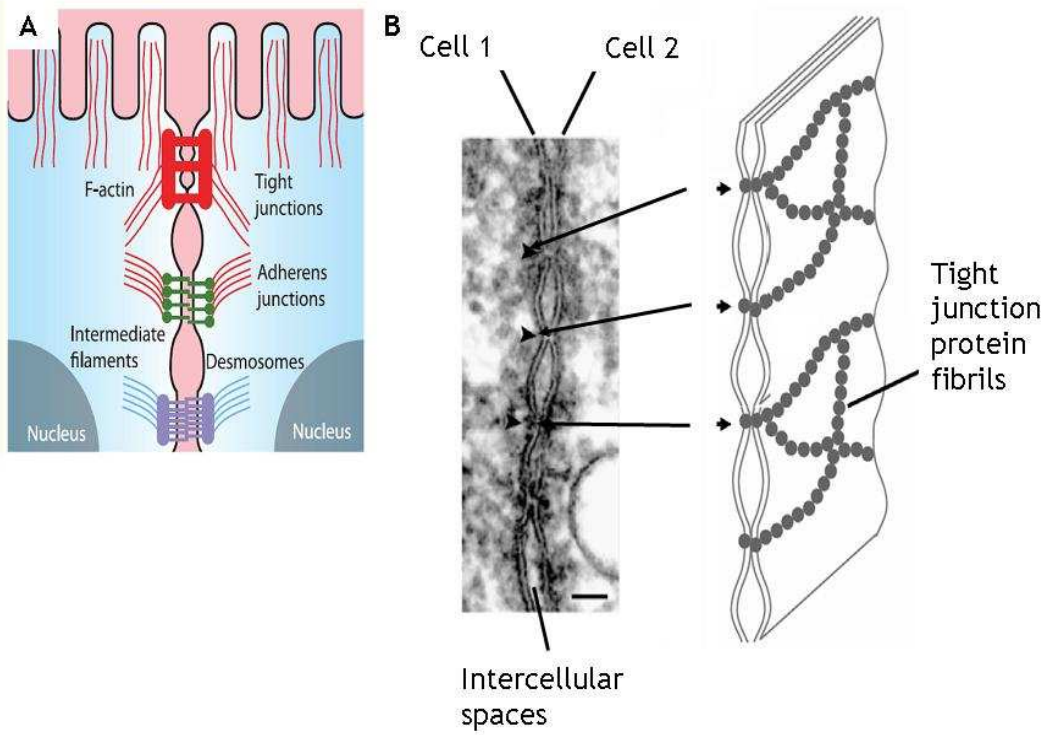

Figure 3: Tight junctions
A) This picture shows the various connecting junctions between adjacent cells and their intercellular connections with actin and intermediate filaments from (Balda, 2008) B) The picture is a TEM and a sketch showing tight junction protein kissing points and fibrils inside the cell membrane. Scale bar is 50nm (Brandner 2009).

Tight junctions are virtually impermeable to large moleculecular weight tracers and are arranged in a seal. Such junctions can be either classified as 'tight' or 'leaky' barriers according to their physiological significance (Balda 2008). Meaning that epithelial barriers in different organs or in different areas of such organs have different epithelial junction properties, for example junctions in the urinary bladder are extremely tight, but leaky in the

renal proximal tubule which is valuable for re-absorption of solutes and maintains the water and solute contents in the blood. There are methods to measure the permeability and integrity of the epithelial tight junctions, for example using fluorescence or radioactive transport measurements and electrical resistance (Hediger 2002, Geys 2006, Geys 2007, Nemmar 2006, Nemmar 2002). Moreover, defects in tight junction components can result in a loss of barrier properties and may contribute to inherited diseases, cancer, and several junction proteins related problem. In some cases they can be targeted by viruses, bacteria and other pathogens (For example *Pseudomonas aeruginosa* patients with cystic fibrosis) (Saavedra 2002, Kazmierczak 2004). This suggests that tight junction associated processes have an important role in the pathogenesis of a range of diseases and it is important to maintain the barrier and fence functions. Cell culture technology enables us to study cell growth, differentiation, metabolism and functionality, response to external stimuli and transport phenomenon in *in vitro* systems. The progress of *in vitro* techniques has helped reduce the use of animal testing in recent times (Pollard 2002). The main attention is on epithelial cell types and their barrier properties.

1.5.2 Measuring Trans epithelial electrical resistance (TEER) of epithelial cells

Adjacent cells are linked by tight junctions, which play an important role in conserving epithelial tissue functions. The ‘tightness’ or integrity of such epithelial monolayers can be determined according to the electrical resistance created by the epithelial layer known as the Transepithelial electrical resistance (TEER). The TEER system measures the total resistance created by the cell membrane area cultured between a set of electrode (pair of current injection electrodes and pair of voltage measurement electrodes). Therefore the resultant TEER is calculated from the measured resistance value for cell monolayer cultured on membrane per unit area. (TEER = Measured resistance * Effective area, therefore Ωcm^2) (Stiles 2005, Wegener 1996, Clausen 1979, Clausen 1981).

TEER is a valuable tool to study cell barrier properties and there are some commercially available macro-scale systems to conduct these experiments. The EVOM™, system was one of the first commercial instruments developed for measuring TEER (commercialised by WPI (World precision instruments) Inc.) and is normally used in combination with Transwell® cell culture polymer membranes (produced by companies like Corning Costar®, Falcon®, etc). The EVOM™ comes equipped with a pair of silver/silver chloride electrodes known as the STX2 (The STX2 are a fixed pair of double electrodes, 4 mm

wide and 1 mm thick where each stick of the electrode pair contains a silver/silver-chloride pellet for measuring voltage and a silver electrode for passing current. The small size of each electrode is designed to fit into Transwell® cell culture inserts. STX2 electrodes are used with almost all tissue culture inserts currently available on the market; however this system seemed to work best with the culture wells of sizes that were ≥6 mm diameter (WPI, World precision instruments). TEER measurements are also sometimes non-reproducible and show problems with possible sample contamination and varied TEER values over sets of samples due to the manual insertion of the electrodes (Geys 2006). WPI also make Endohm™ chambers used in combination with the EVOM meter that can provide reproducible resistance measurements of endothelial cells in Transwell culture inserts. The transwell inserts need to be transferred from their current culture wells and into the Endohm chambers when measuring the reisistance of the cell layer. The base of the chamber and the cap contain a pair of concentric electrodes (a voltage-sensing silver/silver chloride pellet in the center plus an annular current electrode). This Endohm setup allows a more uniform current density to flow across the membrane than compared with the STX2 electrodes and the background resistance of a blank insert is low compared to that in measured using the handheld STX2 electrodes (reduced from ~150 Ω for WPI's hand-held STX2 electrodes to less than ~5-10 Ω when using the Endohm chambers). However the minimum diameter for this culture well system again was 6mm. The setup is such that the transwell inserts can be transferred into the holders and then measured within this chamber (closed system), rather than using handheld electrodes. However, the Endohm device holders need to be regularly sterilised and can be susceptible to handling errors and contamination. The REMS AutoSampler™, which is another resistance measurement system developed by WPI, is an automated computer controlled setup which offers reproducibility, accuracy, flexibility and ease-of-operation. Such an automated measurement system provides the advantages of speed, precision, decreased opportunity for contamination and real-time availability of measurements on the computer. The REMS AutoSampler consists of a robotic sampler arms that moves the electrode over each well of the microplate (24-96 well plates) resting on the base plate tray. The measurements are read through a Microsoft Windows operating system-based data acquisition card and the REMS software to operate the system using a Microsoft Windows based computer. Therefore this setup may reduce loss of cell cultures due to contamination and all the measurement data can be obtained in real time on the computer. However, the cost of such a machine is quite high and the problem of minimum surface used is again restricted to a 96 well plate Transwell inserts setup. There is thus the motivation among researchers to

develop a cost effective method and a high throughput miniaturised system for TEER measurements.

In an interesting review by Hediger et al (2002), the authors suggested that a miniaturised system could prove to be an advantageous method for the purpose of epithelial resistance measurements. Miniaturised systems could decrease the analysis time due to their small channel dimensions. This could reduce reaction times inside the fluidic chambers and also would reduce the quantities of analytes. Their multilayered device system presented here was used to measure TEER values for epithelial cells grown on polycarbonate membranes. This sort of device could be useful to analyse many other parameters within one system which could reduce the cost of running the experiments. When designing such methods for parameters like movement of the conducting ions between or across the cell/membrane barriers, the quality of electrodes and the type of circuit system need to be considered. The setup used by Hediger et al. (2002) was a resistance measurement using 2-point and 4-point measurements to determine the real part (resistance) of cells monolayers on nanoporous membranes sandwiched between two silicon or glass chips bearing platinum or Ag/AgCl electrodes. When using a 2 point measurement setup Ohm's law is used in order to determine a resistance: Resistance (R) = Voltage (V)/Current (I). Here the measured voltage that develops across the resistance (when a current flows through an unknown resistance) is obtained by dividing the voltage by the sourced current. However, a problem that occurs when using a 2-wire setup is that the voltage is measured not only across the resistance in question, but this also includes the resistance of the leads and contacts. This becomes a problem when trying to measure small resistances or if the contact resistance is high, then it may be difficult to obtain accurate results with this kind of system. In the case of the 4-point configuration the paths of the current generating electrodes and voltage sensing electrodes are separate; this then reduces the chance of detecting any resistance caused by the wire contact or lead resistance (Hediger 2002). Therefore, the 4-point measurement setup was considered to be the preferred system, because this kind of measurement system uses 4 separate electrodes, a pair for current-injection and another pair for voltage measurement. This system is similar in working to the conventional EVOM™ TEER system and as shown by Herdiger et al. (2002) produced comparable results. Therefore, this sort of system could be used to obtain the best way possible to anticipate the behaviour of epithelial tight junction barrier properties with the use of an electrical resistance measurement system integrated with microfluidic device system.

1.6 Why microfluidics and automation?

1.6.1 What microfluidics can offer to toxicity testing

Microfluidics is a science that can be applied to manipulate and understand the properties of liquids at a miniaturized level and recent years have seen an exponential increase of its applications (Kamholz 2004, Whitesides 2006, Beebe 2002). This field has gained international recognition and has immense potential as well as widespread applications in various fields of science (Whitesides 2006, Beebe 2002). A study by Andrew Kamholz (2004) emphasises on the expansion of microfluidics, both in technical publications and as a part of issued patents in recent years. Microfluidic systems provide a powerful way of exploring and exploiting fluid behaviour at a scale where the dominating factors are viscosity, diffusion and capillarity rather than turbulent flow and mixing (Beebe 2002). The ability to work with small volumes, the resulting short reaction times and the possibilities of parallel experiments makes this technology extremely useful.

Microfluidics has opened avenues for lab on a chip technology which allows us to integrate an entire laboratory process on a single microfluidic chip (Haeberle S 2007, Knight 2002, Haswell 2006, Reyes 2002). Miniaturization of such lab systems have found their use in areas of research such as toxicology, biotechnology, cell biology, drug discovery, sensor technology etc. It was therefore hoped that such devices would prove to be cost effective, time saving, portable and easily disposable. In biotechnology, there are a large number of applications that included the analysis of DNA protein interactions, chromosome screening, systems biology etc. which require miniaturized systems, in which case microfluidic systems are ideal candidates (Chang 2006, Sieben 2007, DeMello 2003, Zhang 2005, Breslauer 2006, Chien LJ 2009, Beer 2008, Sun Y 2006, Sieben 2007). Beer et al (2008) developed the possibility of performing RNA extractions, reverse transcription and PCR amplification analysis on one chip. They presented a method where by they combine real time and reverse transcription PCR assays with digital microfluidics to isolate single copies of viral RNA for gene profiling. The chromosomal staining presented by Sieben et al (2007) shows one of the first on-chip implementations of FISH (Fluorescent in situ hybridisation) on chip which is vital in detecting several chromosomal abnormalities, associated with multiple myeloma, with a ten-fold higher throughput and 1/10-th the reagent consumption as compared to the traditional slide-based method. Sun et al (2006) reviewed different polymer devices used for a variety of different applications in microfluidics of which the most commonly used polymers for cell sorting devices and

DNA were Poly methyl methacrylate (PMMA) and poly dimethyl siloxane (PDMS). Similarly in cell biology there have been numerous publications presentation the use of miniaturized systems for single cell and culture based assays (Beebe 2005, Khademhosseini 2006, Yeon 2007, Tanaka 2009, Tanaka 2007, Lee PJ 2009, Hung P 2005, Lu 2004, Chiu 2000). Hung et al. (2005) presented a multilayered microfluidic device which performed the task of creating a multiple concentration gradient that formed along fluid channels and were relayed through the cell culture reactors within the device. The multiple cell culture wells allowed growth and proliferation of cells under a continuous perfusion system running perpendicular to the gradient channels. This approach could be valuable for optimizing mammalian cell bioreactor performance. The microfluidic gradient model could also be used to characterize the effect of culture medium components, pH, cell density, and perfusion rate on protein expression. The microfluidic gradients similar to these have been used in understanding chemotactic behaviour of cells (Abasolo 2004, Walker 2005, Aijaz 2005, Jeon 2002).

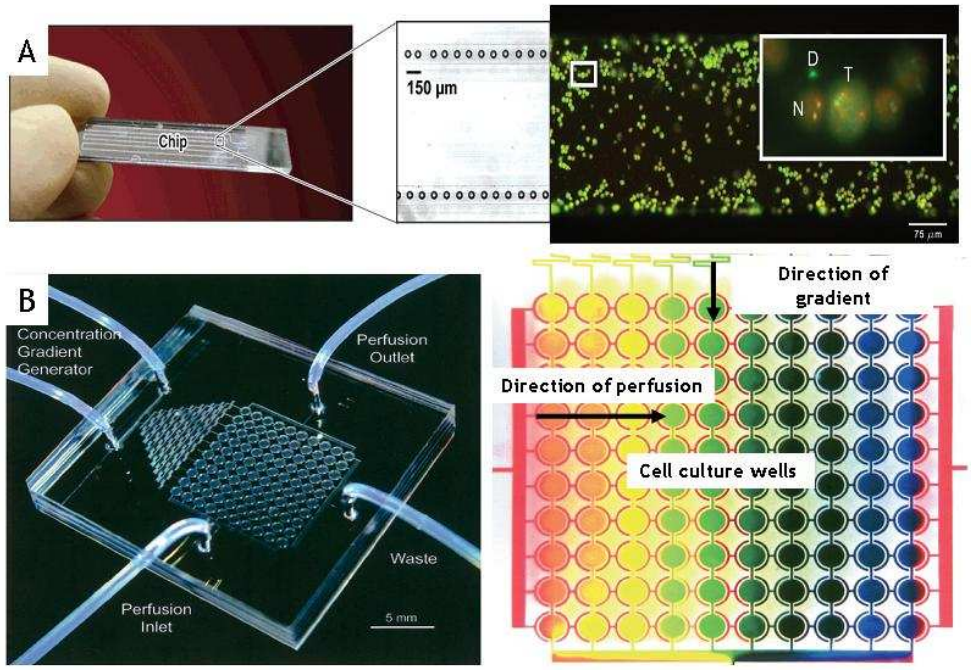

Figure 4: Some examples of microfluidic devices.
A) This device is an example of using a microfluidic device for in –situ hybridisation experiments. (Sieben, 2007), the microchip shown in the image was able to analyse cells and test Chromosomal activity using FISH dyes B) Multiple culture wells with a useful concentration gradient and cell culture medium perfusion device is represented in this picture (Hung P, 2005).The concentration gradient was able to dilute test solutions within the different parts of the device. The unique part about the perfusion channels was that they were flowing perpendicular to the gradient device and was not much disruption in the gradient.

Microfluidics had been used for toxicity studies and to produce dilutions of certain drugs, testing chemotactic activities of cells, cytotoxic testing assays (Walker 2005, Mao 2003,

Lin 2005, Torous 2006, Bang 2004, Jiang 2003). Many of these systems use microfluidic gradient mixers and in work presented by Tirella et al (2008), they showed that such gradient mixers being used to prepare dilutions of conventional local anesthetics (bupivacaine and lidocaine) used against myoblast cells. All these experiments have shown a potential use for testing nanoparticle toxicity by using such kind of a gradient mixer device to dilute the stock particle solutions and analyse them in an array of parallel experiments. However, In order to understand and work with microfluidics it is necessary to understand the physical phenomenon behind the behaviour of fluids and materials dissolved/suspended within if the fluid is confined in micrometric containers. The effects that become dominant at such scales in fluidics are laminar flow, diffusion, fluid resistance, surface area to volume ratio and surface tension. Some of these phenomena will be discussed in more detail in the following.

1.6.2 Basic concepts in microfluidics

1.6.2.1 Laminar flow and the Reynolds number

Laminar flow is an important characteristic of microfluidics in which a fluid flows in parallel layers, with no disruption between the layers. Under laminar flow the viscous forces dominate over the inertial effects of the fluid inside the channels. Laminar flow conditions are determined by the Reynolds number *(Re)* (Equation 1). The Reynolds number gives a relation between the inertial and viscous forces. This tells us whether the flow in microchannels is laminar or turbulent. When the Reynolds number is less than 1 ($Re \ll 1$) (where the viscous forces are dominant), the flow is predicted to be laminar (Beebe 2002, Tabling 2005). When fluids flow through microfluidic channels under laminar conditions, then mixing is expected to occur only by the phenomenon of diffusion. This diffusive mixing is dependant on the characteristics (viscousity and diffusion coefficient) of the two (or more) fluid streams flowing along the length of the channels, to equiliberate their concentrations (Beebe 2002, Tabling 2005).

$$Re = \frac{\rho u l}{\eta}$$

Equation 1: Reynolds number
The Reynolds number 'Re' is the ratio of the inertial forces, where the density 'ρ' , velocity of fluid (flow velocity) 'u' and the length scale or channel diameter as 'l' (this can also be known as the hydraulic diameter 'D_h') are presented (Purcell 1977) (where the cross sectional geometry of the channels is considered) and the viscous forces (viscosity of fluid 'η'). (Brody 1996, Tabling 2005)

The Reynolds number is derived from the Navier-Stokes equation governs fluid flow laws for both compressible and incompressible fluids. Equation 2 is the basic equation that represents the Navier-Stokes equation for incompressible fluids. This equation is a representation of Newton's law for fluids, where forces per unit volume is on the right-hand side, which is dependant on the pressure gradient '$-\nabla P$' and the viscosity '$\eta \nabla^2 u$'. The left-hand side gives the mass per unit volume 'ρ (density)' times the acceleration of the fluid, where 'u' is the fluid velocity over time 't' (Brody 1996).

$$\rho\left[\frac{\partial u}{\partial t} + (u \bullet \nabla)u\right] = -\nabla P + \eta \nabla^2 u$$

Equation 2: Navier – Stokes Equation
In this equation 'u' is the fluid velocity (flow velocity), 'ρ' is density (of fluid), 't' is time, 'P' is the pressure and 'η' is the fluid viscocity.(Brody 1996)

Considering the micrometer dimensions in microfluidic systems, laminar flow conditions are achieved due to the low Reynolds numbers. The Reynolds number for such devices is normally achieved once the test fluid flowing through the microchannels crosses what is known as the entrance length (L_e). The entrance length 'L_e', is the length needed for the fluid to develop the velocity profile after entering the fluid channels or passing through components, e.g. valves, inlet/outlet entry points, bends, etc. The entrance length for laminar flow conditions can be calculated as $L_e = 0.06*Re*D_h$ (hydraulic diameter of channel) (Brody 1996, Tabling 2005). Once the fluid has crossed this entrance length it will develop laminar flow conditions where the fluid profile inside the channel has a 'No slip' boundary conditions and hence the velocity at the walls of the fluid channels is zero. The flow velocity builds up slowly from zero at wall to a uniform velocity towards the center of the fluid channel. Therefore, Newtonian fluids [7] inside such fluid channels flow in the direction parallel to the flow along the length of the channels. Also, if there are no-slip conditions, then a shear stress is exerted at the wall of the channels. Cells can adhere to a substrate up to a certain degree of shear (Korin 2007, Lu 2004, Leclerc 2006). Above the shear threshold, which depends on the type of cells, substrate and time, cells may detach from the substrate.

[7] (Newtonian fluids are those for which the shearing stress is linearly related to the rate of shearing strain)

The shear stress at the walls is represented by:

$$\tau_{wall} = 6\eta \frac{Q}{h^2 w}$$

Equation 3: Shear stress equation
Where 'τ_{wall}' is the shear stress at the walls, 'Q' represents the channels flow rate, 'η' is the viscosity, 'h' is the height of the channel and 'w' is the width of the channel. (Korin 2007, Lu 2004) Q is calculated by the following equation

$$Q = \pi \frac{\phi_{syr}^2}{4} V_{syr}$$

Equation 4: Channel flow rate
Where the 'Φ_{syr}' is the syringe diameter and 'V_{syr}' was the velocity of fluid within the in channels (translational velocity of the pump).

1.6.2.2 Diffusion

Diffusion is the process in which particles in a given volume move from higher chemical potential to a lower chemical potential, by Brownian motion, to maintain a equal or constant concentration of particles throughout the volume. The phenomenon of diffusion is important for a microfluidic device when dealing with the mixing of solutes and solutions under low Reynolds number conditions. In a turbulent flow the liquids mix quickly and efficiently; whereas under laminar flow conditions liquids not mixed but equiliberation of concentrations occur only via diffusion. It is understood that under micrometric conditions the flow regime is laminar and the solutes or particles mix mainly through diffusion. These properties are exploited inside microchannels where gradients of concentrations can develop by altering channel length and allowing time dependent equilibration of fluid concentrations running in parallel within a device. The first microfluidic devices depended on parallel lamination using two fluid input channels and a main broad channel. The time taken to completely euiliberate the concentration profile of the two test fluids depended on the length of the channel and on the diffusion coefficient of the test fluids..These microfluidic devices were ideal to understand the basic transport phenomenon at the microscale and can be used to calculate diffusion coefficients of test fluid molecules. [The concept was initially illustrated within the 'T' (Figure 5) and 'Y' – channel mixer devices (Nguyen 2005, Kamholz 1999, Ismagilov 2000)]. Diffusion can be modelled using the diffusion equation (Equation 5), as shown inside a 'T' channel mixer device (Figure 5). The diffusion equation is dependent on the diffusion coefficient of the test material solubilised/non-solubilised in a fluid. This diffusion coefficient is derived from the Stokes-

Einstein equation (Equation 6) for spherical molecules through a liquid through fluidic channel with low Reynolds number.

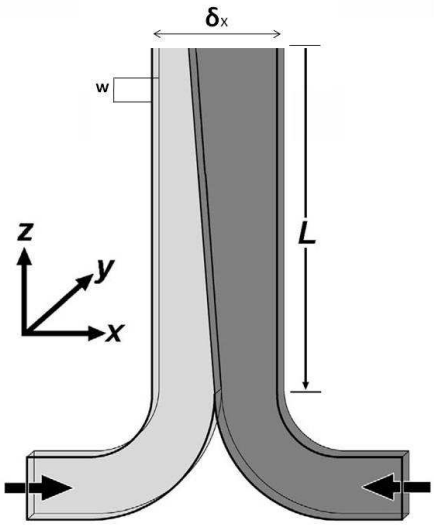

Figure 5: Diffusion analysis across a 'T' shaped channel.
This image was obtained from the work presented by Kamholz et al (1999) and modified to fit equation 5, which shows the diffusion profile of a test liquid (in grey) that is diffused across the length of the channel 'L' where the width is 'w' and spreads across the diffusing 'δ' dimension along the x axis

$$\delta_{(x)} = 2\sqrt{Dt}$$

Equation 5: Diffusion in one dimension
This equation where 'δ' represents the thickness of the diffusive front in the 'x direction' after time 't' for a diffusing particle along the length channel (ref to image) and 'D' is the diffusion coefficient. (Tabling 2005)

$$D = \frac{kT}{6\pi\eta\, a}$$

Equation 6: Diffusion coefficient
This equation explains the Diffusion coefficient 'D' of a circular (sphere) shaped particle, where 'k' is the Boltzmann constant, 'T' the absolute temperature and 'a' it the radius of the particle. (Brody 1997, Tabling 2005, Brody 1996)

1.6.2.3 Fabrication of devices in PDMS [Poly (dimethylsiloxane)]

Since the introduction of miniaturised systems silicon, quartz and glass have been the favoured materials for microfluidic device fabrication. However, attention was diverted towards polymers which posed a more cost effective and simplified method of fabrication as compared to glass and silicon (Becker 2002).

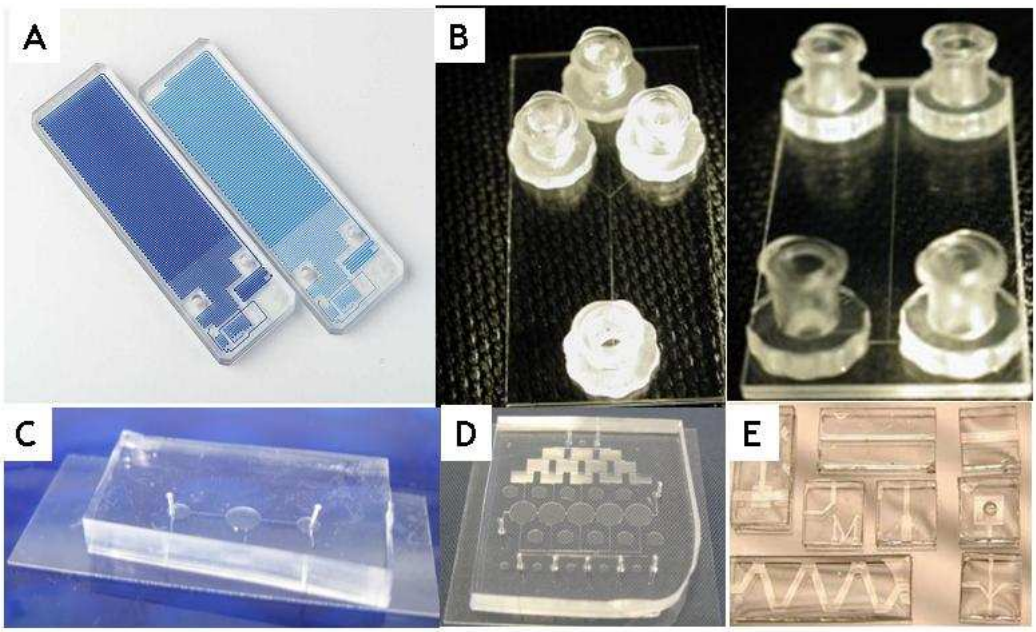

Figure 6: Microfluidic chips
A) These chips are glass devices produced by the Dolomite Centre Ltd. B) Pictures are of Y- and H- channels in glass produced by Translume Ltd. C) and D) are chips produced using PDMS elastomer at the Center for Cell Engineering, University of Glasgow. E) Chips produced by (Rhee 2008), University of Michigan.

Microfluidic device fabrication techniques have been mostly derived from the microelectronics and microprocessor industry. There a large number fabrication techniques adopted for microfluidics for example, replica micromolding, embossing techniques, micromachining, casting, injection moulding etc (Madou 2002, Becker 2008). The most commonly used and relatively accessible method for polymer fabrication is photolithography and polymer casting techniques. This involves the fabrication of a negative master substrate and uses an elastomer (PDMS) to generate a negative replicate of the master – the positive channel structure. PDMS is a soft polymer that has been most commonly used as a sealant for waterproofing, as a mould release agent and is several biomedical products (contact lens materials). It has recently found applications within the microengineering and microelectronics industry (Becker 2008). PDMS has been widely used for cell based microchannels systems since it is gas permeable, optically transparent to about 280nm, cures at low temperatures, is nontoxic to cells, can be reversibly deformed, and also allows to seal devices reversibly and irreversibly to itself or other materials, and finally that it is elastomeric in nature. (Kallio 2006, McDonald 2000, Wu 2006).

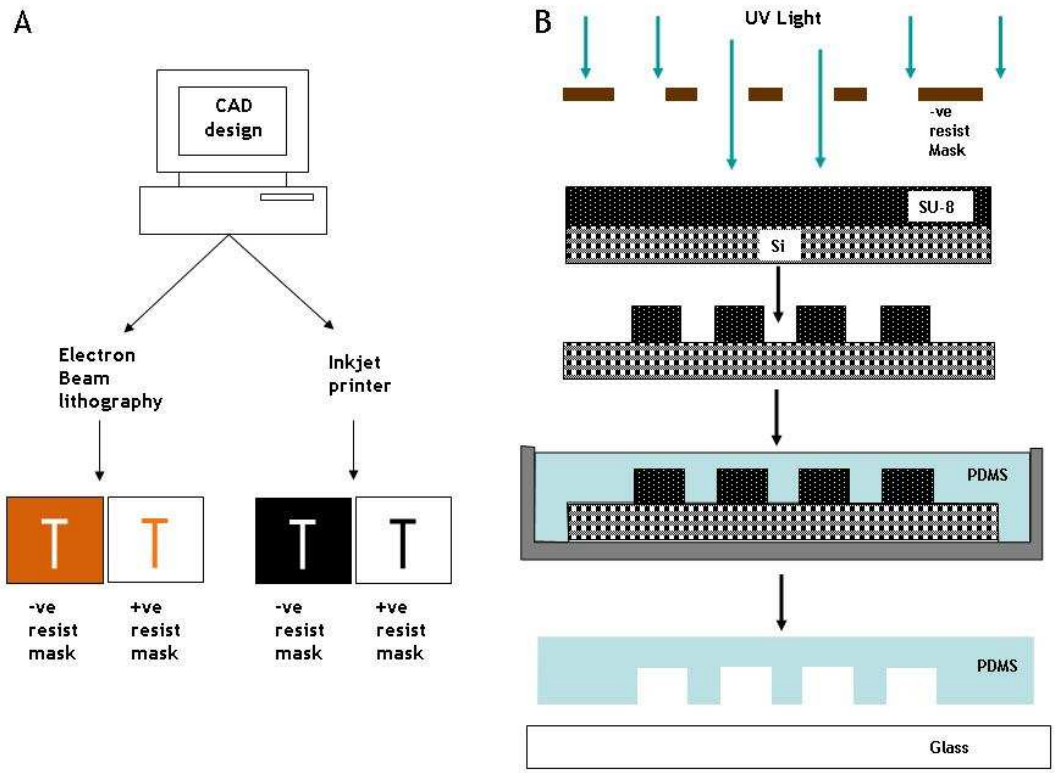

Figure 7: fabrication methods for rapid prototyping of PDMS microfluidic devices.
A) This illustration explains the process of mask development using CAD designs which are transferred onto masks plates with the help electron beam lithography. The masks can be designed according to the type of resist commonly used in photolithography. For a negative resist like SU-8 you would use a mask in which the designed area is transparent. This is because SU-8 when exposed to U.V light polymerises to form the desired 3D structure. B) The illustration is an explanation to rapid prototyping of microfluidic devices using PDMS.

Some issues to consider when fabricating devices are that the method should be quick, readily available, relatively easy and reproducible, and last but not least the process should be cost effective. Fabrication of microfluidic devices using PDMS ticks most of these boxes. The process of photolithography is the major expense in the process which requires the preparation of a silicon master mold against which the PDMS devices are cast. The casting process is quick and within hours we can rapidly prototype devices. Prototyping begins by creating the design in a CAD (computer aided design) program. These designs are transferred either on mask plates via electron beam transfer (in our case) or some prefer to transfer them to transparencies via a high definition inkjet printer. These masks are used to transfer the design patterns on substrates spun with a positive (AZ456) or negative photoresist (SU-8) to a desired thickness and hardness. These substrates prepared by photolithography techniques in the clean room are used as molds to cast PDMS devices.

Chapter 2 : PDMS based microfluidic devices for cell culture and concentration gradients

2 Introduction

Microfluidics is the science of manipulating fluids inside microchannels. The flow regimes inside devices are governed by factors like laminar flow, diffusion and shear stress (Beebe, 2002). Microfluidic systems have become increasingly important in the past two decades due to their application in various fields of science, mainly biomedical research (Weibel 2003 & 2006, Haeberle S 2007). With new and improved fabrication technologies their small dimensions are easy to achieve (Reyes 2002, Sia 2003, Collard 2008). Early microfluidic systems were fabricated on silicon or glass by micromachining and bonding technologies (Becker 2002, Becker 2008). However, this area has really taken off after the development of SU-8 EPON epoxy photoresist (MicroChem.) and introduction of polymer based devices. This EPON epoxy resin is sensitive to wavelengths of UV light (365 – 436nm). SU-8 contains acid-labile groups (Bisphenol A Novolak epoxy oligomer) and a photoacid generator (triaylsulphonium hexafluroantimonate). Upon irradiation the photoacid generator form an acid that protonates the acid labile epoxy groups and forms a series of cross linked bonds on being heated (during bake steps). This photoresist is able to achieve high degrees of cross linking as a result of photothermal activation which produses high mechnical and thermal stability for structures after development. (Nguyen 2006, Del Campo 2007) (Collard 2008, Puleo 2007, Hill 2007). SU-8 photoresist is well established with micrometer and millimetre sized structure development, and it also is used for preparing microfluidic devices in combination with PDMS elastomer. The PDMS elastomer allows the fast formation of high fidelity topographically inverse copies (with accuracy in nanometers) by replica casting (McDonald 2000, Zaouk 2006). PDMS is also often used to prepare microfluidic devices for cell culture based devices due to its compatibility with cell culture procedures, chemicals (e.g. salt solutions, ethanol, etc..), as well as its gas permeability and biocompatibility (Lee 2003). This Chapter focuses on the optimisation of fabrication protocol for such devices using SU-8 photoresists (type – SU-8 2050, 3050, 3025) and finally on the development of PDMS based microfluidic devices for the specific experiments.

The schematic design of the multilayered microfluidic device shown in Figure 8, where a silicon nitride porous membrane is sandwiched between the top and bottom microfluidic channels, the microchannels were fabricated using PDMS and the design was meant for a single cell culture well design shown in Figure 8 a) and b). The PDMS microchannels were designed such that a pair of single cell culture device could be used together, where one formed the top microchannel and the other formed the bottom microchannel forming the

multilayered device (described in more details in Chapter 3). One of the main challenges for this PhD project, was to multiplex the designs for each of these layers (top microfluidic device design, Figure 8 a) and the bottom microfluidic design, Figure 8 c) into a five cell culture well systems, which is described in more detail in Chapter 4 (Section 4.1.1.1). The multiplexed version of the top microchannel device was also intended to include a concentration gradient generator that would dilute test solutions (e.g. fluorescent dyes, antibiotics, nanoparticles, etc.) among these five cell culture wells. To design such concentration gradient it is vital to first understand the functioning and principles of diffusive mixing phenomenon within these devices. Basic designs for diffusive mixing devices consist of two parallel fluid flow channels and shaped in either like a 'T' or a 'Y', each had two fluid inlets, and a mixing channel ending in one outlet, the chemical gradient develops perpendicular to the flow of fluid (Nguyen 2005, Kamholz 1999, Ismagilov 2000). Such fluid mixing devices are ideal to understand basic transport phenomenon at the microscale and often used to calculate diffusion coefficients of particles and solutes but are in general limited to less than 300µm width. An extension of the same principle are so called 'Christmas Tree' devices, developed by Jeon (2000) and Dertinger et al. (2001), where a series of dilutions are established according to the same principle as within the T junction device and then combined to form a wide channel with a chemical gradient perpendicular to the flow. The concentration gradient mixer design implemented in this Chapter, was a modified version of the devices presented by Joen et al and Dertinger et al. The main intention behind such a device was to use it in conjunction with a project that dealt with the layer-by-layer (LBL) deposition of polyelectrolytes (PEs). LBL is a very versatile and inexpensive method by which nanometric PE layers are adsorbed onto a charged, hydrophilic surface by alternating the deposition of positive and negatively charged PEs. The deposition of the individual layers can be controlled by parameters like pH values, ionic strengths, temperature, etc.. The gradient generator was intended to develop a pH gradient across the broad observation channels (explained in Figure 11) and by such influence the deposition of chitosan and heparin. The reason was that it had been shown in previous experiments that the adsorbed alternating layers of chitosan and heparin had differential cell-adhesive properties, depending on pH regime used during deposition (Kirchhof 2008, 2009). Therefore, the gradient generator device was intended to create LBL gradients of PEs deposited at different pH across the channel, which then would assist in the study haptotaxis[8] of adhesive osteoblast cells. The fabrication, handling and cell

[8] Haptotaxis is the directional motility of adhesive cells in reaction to an immobilised chemical gradient. (e.g. axonal outgrowth during development).

culture protocols were taken into account and modified accordingly when designing the multiplexed version of the single cell culture device explained above.

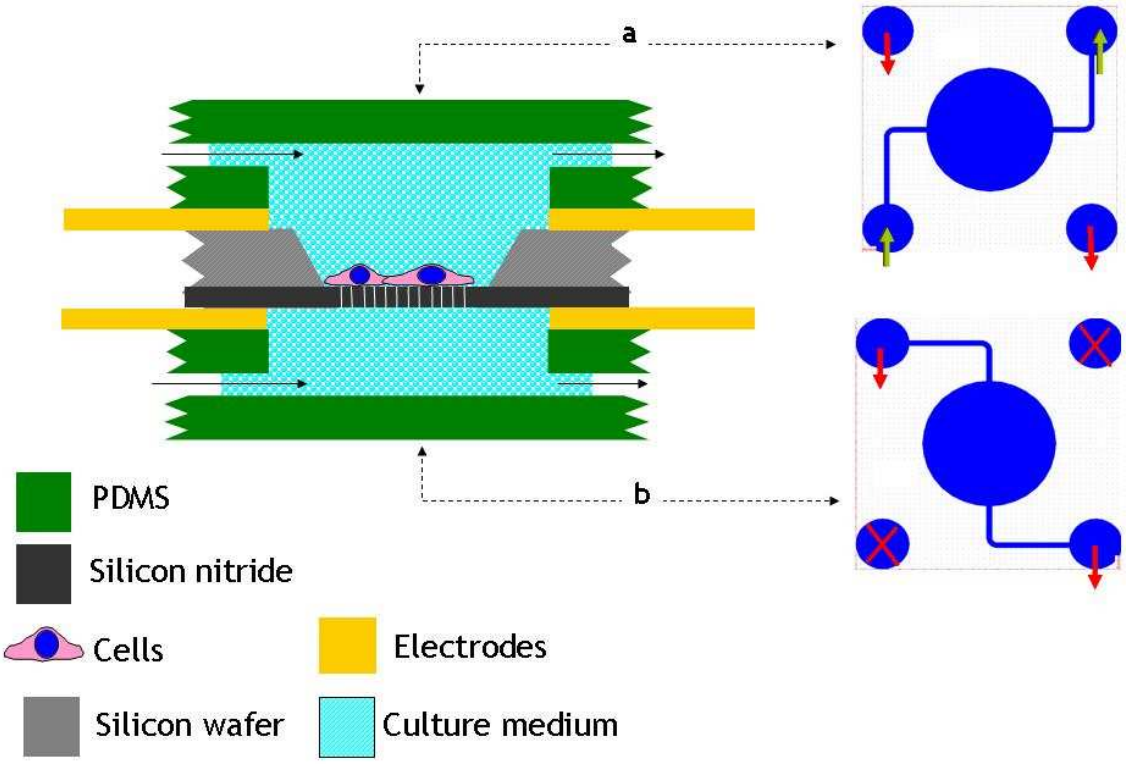

Figure 8: Schematic representation of the device idea.
The schematic representation A) The multilayered device design. The components of the device were made up of different materials. The microfluidic channels fabricated from PDMS (green), the silicon nitride membrane (black) suspended on silicon wafer (grey), the wafer was coated with platinum electrodes (yellow). Cells were cultured on silicon nitride membranes and medium (blue) was perfused through the device channels [The black arrows represent the direction of flow inside the device]. a) shows the design for the top microfluidic channel and b) showed the design for the bottom channel. [The upward pointing (green) arrows represent the flow of fluid from the top channels and the downward pointing (red) arrows signify the connections made to allow flow through the bottom channel and the fluid connectors were inserted through the top side. The red crosses in the bottom channel connectors show the un-used connectors].

2.1 Materials and methods

2.1.1 Making silicon masters

CAD programs such as L-Edit, CleWin and WAM were utilised to generate the 2-D images of the specific designs. These were later transferred onto a chromium coated 5 x 5 inch quartz plates using electron beam lithography. The quartz plates were often referred to as ‘mask plates’, and allowed users to transfer the patterned design onto silicon wafers coated with resist. When using certain resists like SU-8, which can be extremely sticky and difficult to clean or remove once they had hardened or polymerised, therefore in most cases copies of the original mask plate (bearing a chromium lining) patterns were prepared. The design was transferred onto a cheaper ferric-coated mask plate, which was used instead of the chromium mask to avoid damaging the original. The silicon wafer coated with SU-8 photoresist was then patterned using this ferric mask (Figure 9). The pattern was transferred by aligning the mask plate to the wafer, bringing the two almost into contact and exposing it to ultraviolet light using the MA6 mask aligner (SÜSS Microtech) (with an exposure energy of ca. 7.1mW/cm^2 for every second). The exposed SU-8 wafer was then processed (steps explained in detail in section 2.1.1.3 from this Chapter) and several PDMS devices bearing the relief pattern were cast using this silicon master (Process of casting against silicon masters is explained in detail in section 2.1.2 from this Chapter).

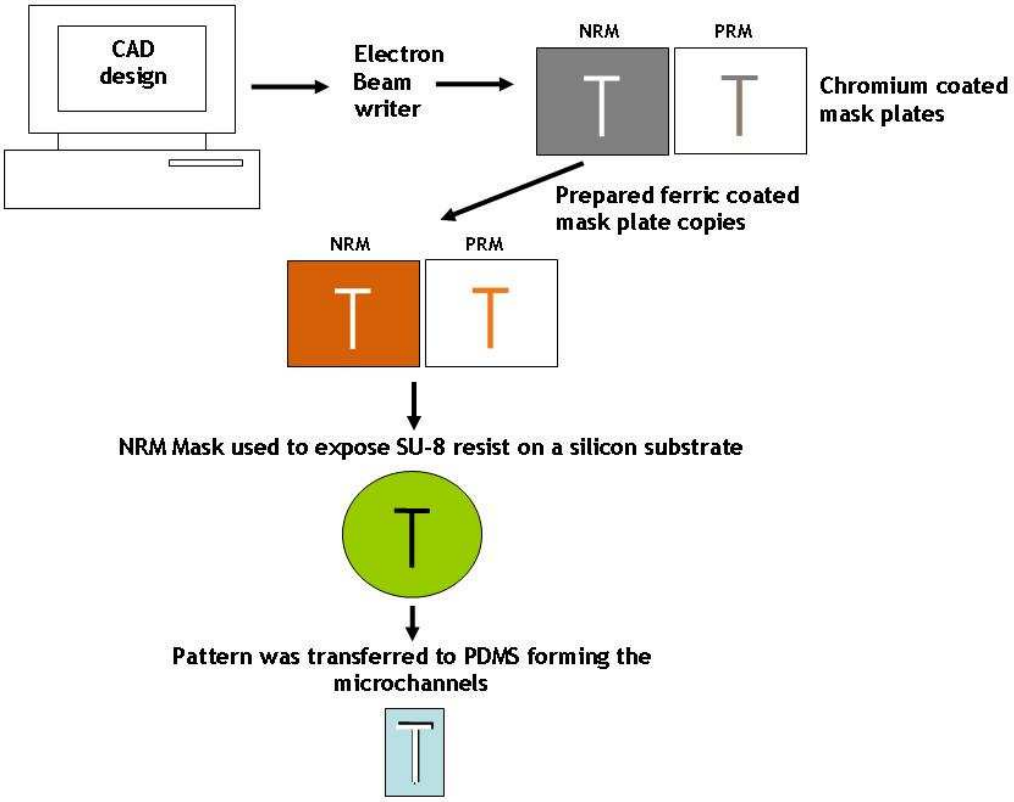

Figure 9: Steps for designing devices
Devices were designed in 2D using CAD software. These designs were fed into an electron beam writer and the patterns were transferred onto a chromium coated mask plate. Ferric-coated mask copies were prepared and used instead of the original chromium mask (since we were using SU-8 photoresist). The ferric mask were used when exposing the resist to form the silicon master. The silicon master consisting of the resist pattern was developed and processed. Finally a negative copy of the resist pattern was prepared in PDMS which formed the microchannels. [NRM – negative resist mask (created resist patterns of SU-8 and microchannels in PDMS), PRM – positive resist mask (used with SU-8 only if microchannels were to be developed on silicon substrate and surrounded on two side with SU-8)]

2.1.1.1 Device designs

The devices implemented in this Chapter include a single cell culture device (Figure 8, a) and a gradient mixer (Figure 10). The single cell culture device consisted of a cell culture well having a chamber diameter of 5 mm and a inlet/outlet with 4mm channel lengths with a width of 200 µm. It could be used either as a standalone cell bioreactor or it be integrated with the multilayered device. The design was such that the device could form both: the top and the bottom channel/cell culture well for the multilayered setup with the silicon nitride membrane chip sandwiched in the middle. On the device were a pair of connectors adjacent to each inlet/outlet channel, which indicated the equivalent position of the through channel connecting top and bottom microfluidics, when it was to be integrated into a multilayered device. This device could, when bonded to glass coverslips, also be used as a standalone device to investigate cell behaviour and optimise culture conditions in preparation for the more complex experiments.

The concentration gradient mixer design consisted of 7 rows of 'serpentine' channels. Each serpentine channel was approximately 7 mm long and 50 µm wide. Each subsequent row of serpentine channels was connected by a 100 µm wide perpendicular channel. The gradient 'observation' zone (this broad channel was 0.9 mm wide and the width was related to the number of channels in the last row – this design had 9 serpentine channels in row 7) was where the resultant diffusive mixing through the device would form the gradient profile. This allowed the dilutions from each of the nine serpentine channels (the final row) to flow parallel to each other under laminar conditions inside the broad channel forming a diffusion gradient profile across the width of this channel. The fate of mixing two test solutions through this device is shown in Figure 11, where a dye at two hypothetical concentrations C0 [0%] (e.g buffer) and C100 [100%] (e.g a dye dissolved in the same buffer) were pushed in through the inlets of the device. The concentration, from C0 (one control) and C1 - C8 (8 different concentrations left to right), were formed in the last row of the serpentine channels (row 7). The dilutions developed from C0 – C8 in the last row of serpentine channels were, assuming complete mixing at the end of each channel, expected to be: 0, 0.8, 6.2 22.7, 50.0, 77.3, 93.8, 99.2 and 100%. These non-linear concentrations met inside the broad channel (gradient observation channel) and the dilutions were allowed to mix again through diffusion, along the length of this channel developing a profile that is shown in Figure 11.

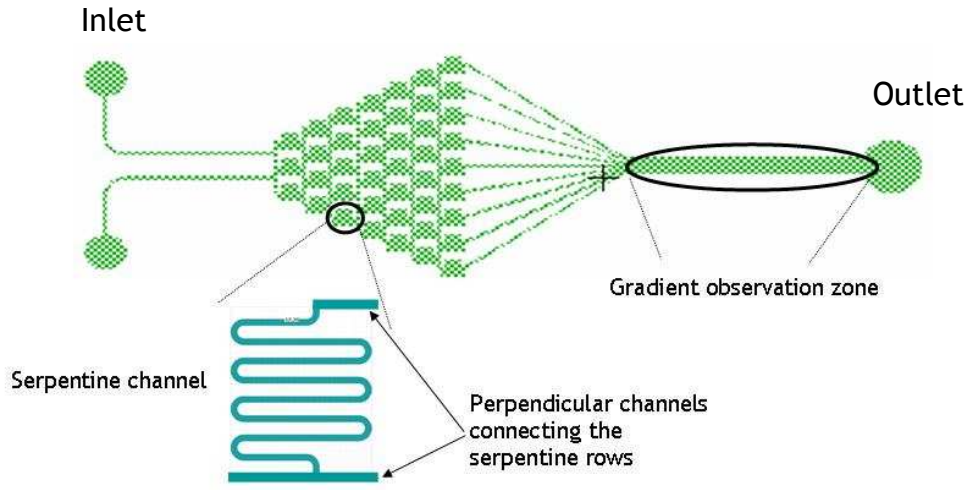

Figure 10: The concentration gradient mixer
This was the gradient mixer design showing the 7 rows of serpentine channels that finally commence into the broad gradient observation channel (observation zone). Each serpentine channel (enlarged in the inset, which is rotated by 90° with regards to the design image) is connected at its beginning and end by a perpendicular channel, which connects all the serpentine channels to each other. Each serpentine channel is 7 mm long and 50 µm wide. The final row contains 9 serpentine channels creating: 1 loaded and 1 unloaded control as well as 6 different dilutions of the solutions entered into the inlets.

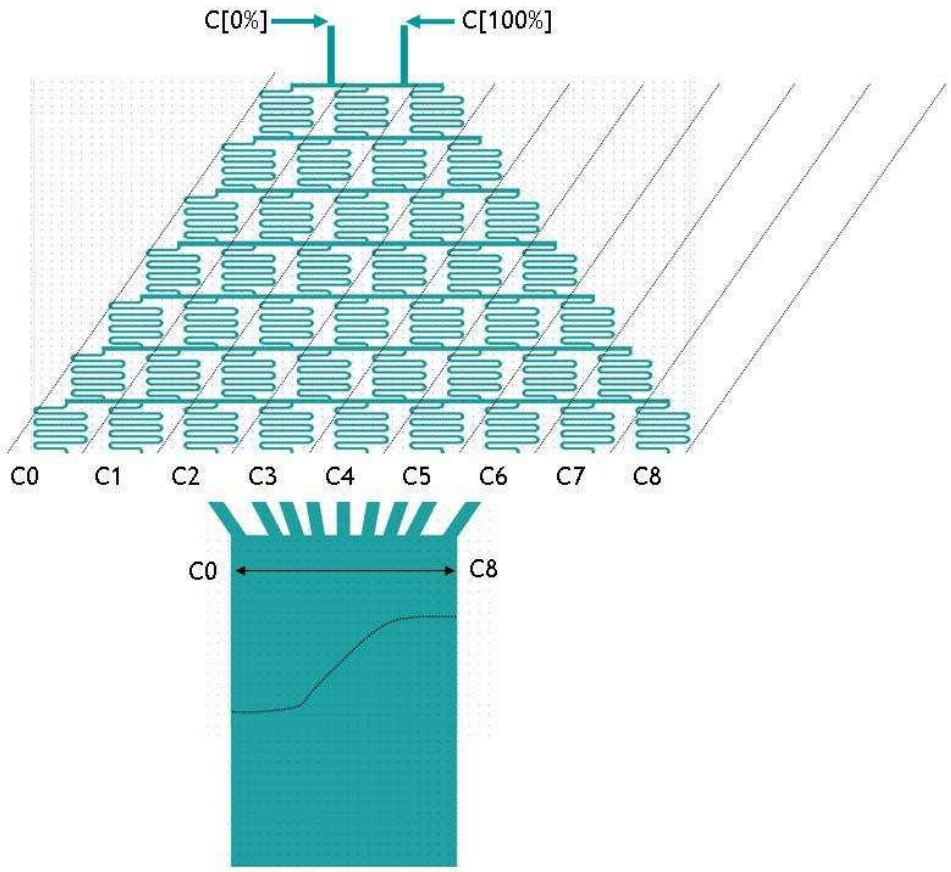

Figure 11: Gradient of concentration formed in the serpentine mixer device
The serpentine channels form a 'christmas tree 'like structure shown here. The entrance concentration C[0] and C[100] for a certain test solution was diluted such that the percentage of dilutions formed range from 0 – 100% [C0 – C8 in the last row of serpentine channels show expected non-linear dilution values of 0, 0.8, 6.2, 22.7, 50, 77.3, 93.8, 99.2 and 100%]. The non-linear gradients formed at the entrance length of the broad channels are mixed again due to diffusion along the length of the channel resulting in a concentration gradient that is close to being linear.

2.1.1.2 Cleaning the wafers

Silicon wafers were cleaned in opticlear [9], acetone and propan-2-ol each for 5 mins under sonication.[10] The wafers were then dried at 180°C for 30 min in the oven to remove any traces of moisture on the surface which could affect photoresist adhesion.

[9] Opticlear – cleaning solution (lens cleaner) used in the clean room to clean silicon wafers.

[10] If the silicon wafer surface seemed very dirty after scribing and cutting them into smaller pieces they were washed using a Piranha solution (hydrogen peroxide and sulphuric acid in a ratio of 1 : 3 respectively)

2.1.1.3 Coating and processing

The silicon masters were fabricated using photolithography with different types of SU-8 photoresist; SU-8 - 2050, 3025 and 3050. This SU-8 was a negative photoresist, which meant that the area exposed to light would remain on the surface of the substrate and the rest would get washed away during the development process. The SU-8 photoresist used was able to produce heights of up to 200 µm. The height and width of the fluidic channels were important for cell culture purposes. To avoid clogging cells inside the channels and also to reduce the stress within the system, for cell culture purposes the channel width was expected to be around 100-200 µm and the height to be 50-100 µm. (Korin 2007, Korin 2009)

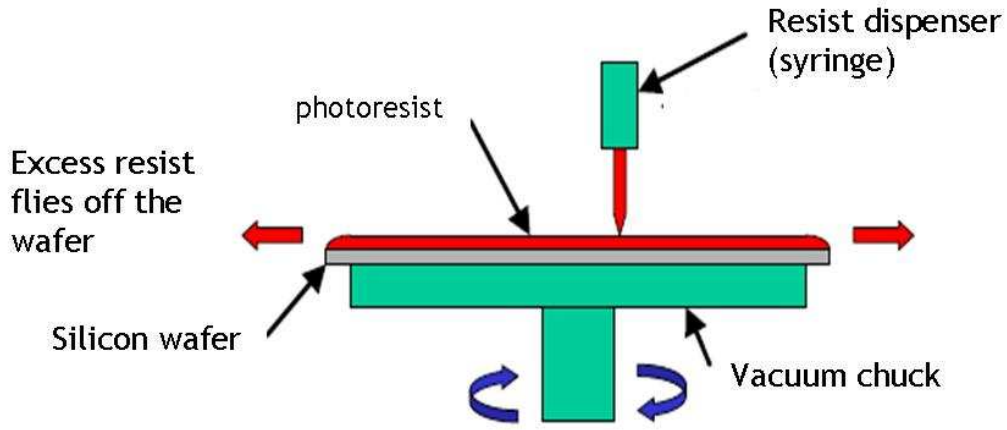

Figure 12: Spin coating on silicon wafer.
Photoresist was first deposited as a homogenous layer on top of the wafer. The wafer was spun at 3000 rpm for 30 s which produced a height of 50 µm for the photoresist SU-8 3050 (MicroChem data sheet for SU-8 3000 series). For the initial 5-10 s all the excess resist was jolted off and the remainder developed the required thickness (Darling, Accessed 21st August 2009; Madou, 2002; the picture is a modified version from Darling, Accessed 21st August 2009).

The silicon wafer, kept in the 180°C oven to dry after the washing steps, was removed and allowed to cool inside the flow cabinet for a few minutes. The resist was poured onto the wafer surface and initially spun at 500rpm for 10-15 seconds. This allowed the resist to settle evenly onto the substrate surface. This wafer was then spun at a slightly faster speed to attain a well covered and flattened layer of resist of a desired height. The spinning was followed by a pre exposure bake step at 65°C and then at 95°C. The baking times varied depending on the type of resist used and the thickness of the spun layer (Figure 12).

Photoresist	SU-8 2050	SU-8 3050	SU-8 3025
Thickness at rpm	75µm at 2000rpm	50µm at 3000rpm	50µm at 1500rpm
Pre exposure bake	95˚C for 20-30min	95˚C for 20-30min	95˚C for 20-30min
Exposure	25-30sec	35sec	25-30sec
Post exposure bake	10-15min	10-15min	3-5min
Development	7-10mins	10-15min	5-8min
Hard bake	180˚C for 30min	180˚C for 30min	180˚C for 30min
Silane coating (evaporation method)	30-60min	Not required	Not required

Table 2: The different types of SU-8 photoresist and spinning protocols used to prepare microfluidic masters.
This information was made available form the data sheet provided with SU-8 photoresist (MicroChem). The table showed the different SU-8 types; 2050, 3050 and the 3025. Each resist type had slightly different protocols for heights between 50-75 µm. The interesting part was that the 3000 series SU-8 was very stable after exposure and baking steps hence did not require a silane coating (explained in section 2.1.2.1 from this Chapter)

2.1.2 Microfluidic device fabrication using PDMS

SU-8 being a negative photoresist (meaning that whatever part is exposed gets polymerised, hardens and remains on the substrate surface), the area exposed to UV light remained on the silicon wafer and the rest was washed away by the developer solvent (EC solvent – ester based solvent [11]). This was then dried and placed in a petri dish or a silicon wafer holder for replica casting using PDMS. (Processing steps are explained Figure 13)

PDMS (Sylgard 184) (purchased from Dow Corning), is an elastomer and consists of two components, the siloxane pre-polymer base and the curing agent. The base and curing agent were mixed at the suggested ratio of 10:1, base to curing agent by mass (Corning, 1998, Data sheet for Sylgard 184; Dow Corning). The two parts were mixed thoroughly to ensure uniform distribution of the cross-linker. In order to remove all the gas in the uncured PDMS mixture (introduced due to the constant agitation), it was degassed under vacuum. The degassed PDMS was poured onto the silicon master and left to cure at 80ºC inside an oven for approximately 1-2 hrs (If left overnight then the temperature may be

[11] To check for residual resist a rinse with propan-2-ol was used. The propan-2-ol solution reacts with any residual un-developed resist and turns it white in colour allowing the user to see if development is complete.

adjusted to 60°C). The PDMS was either poured into a petri-dish containing the silicon master or injected into a casting chamber, Figure 13 B and C, which was specially developed for replica casting. This casting chamber was designed also to produce PDMS devices that would be similar in thickness as to better fit into the designed microfluidic device holders. The casting chamber had a gap between the substrate bed and the cover of approximately 2.5 mm. The PDMS devices that were cast using this chamber had a thickness of about 2 mm and most importantly had a very smooth top layer. The smoothness of the top layer and the precise thickness was important when these devices were used inside their device holders, which also gave them a better conformation to the structures of the holders. The PDMS casts were pealed of from the master substrate and were bonded to glass slides/coverslips. (Bonding explained in section 2.1.2.2)

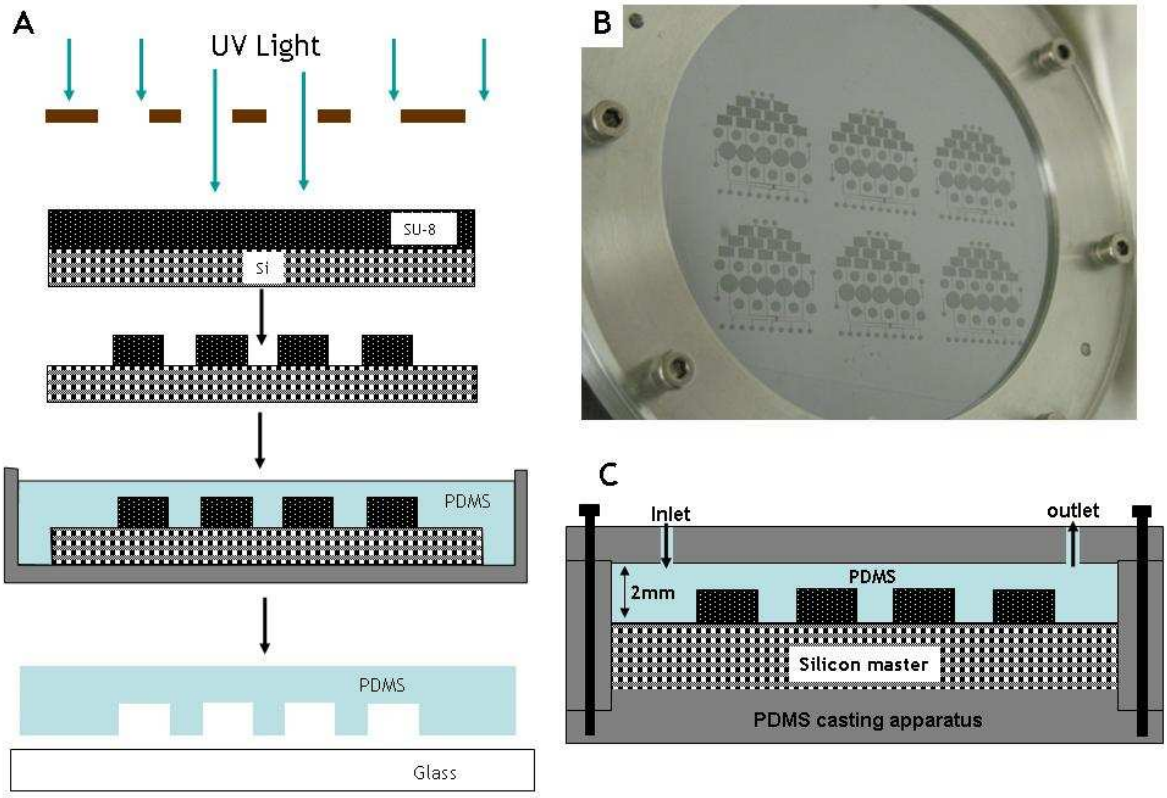

Figure 13: Silicon wafer (master) fabrication using photolithography and PDMS casting method.
A) This illustration highlights the steps for fabricating a silicon master using SU-8 negative photoresist by photolithography techniques inside the clean room. The SU-8 photoresist was exposed to UV light against a photomask designed with a specific design and a replica cast was prepared from PDMS. B) PDMS was cast against the silicon master inside a casting chamber specifically developed to maintain a constant thickness of PDMS and to improve bonding capability inside device holders. Controlling the thickness and producing a much smoother top surface allowed better conformation inside a device holder designed for some of our multilayered devices. C) The transverse section of the casting chamber showed the silicon wafer held inside the holder, while the PDMS was poured through the inlet. The outlet allowed the easy flow of PDMS through the system. A controlled height of 2 mm was produced almost every time and which helps to maintain the thickness of the devices.

2.1.2.1 Silane coating

During the process of detaching PDMS from the silicon masters, in some cases, the SU-8 photoresist would stick to the PDMS and get peeled off the surface of the silicon substrate. This was common with the SU-8 2000 series (SU-8 2050). This adhesion of the SU-8 to PDMS was prevented by a silane (perfluorinated alkane silane – [*tridecafluoro-1,1,2,2 – (tetrahydrooctyl)trichlorosilane*] coating (~1 nm coating). This stopped the SU-8 from peeling off the surface and allowed the master wafer to be used several times for casting patterns in PDMS. The coating of a silane was used and allowed to self-assemble on the surface through adsorption. A single drop of the silane solution was placed next to the silicon substrate wafer, kept in a Petri dish. This was placed on a hot plate at 150ºC and covered using another petri dish. The silane was allowed to adsorb on the surface, leaving a 1 nm thick layer of Teflon coating, as illustrated in Figure 14. This layer was sufficient to prevent the adhesion of SU-8 to PDMS.

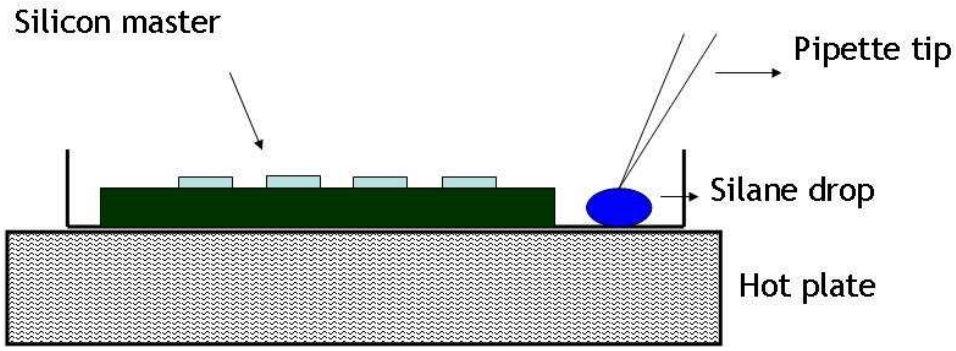

Figure 14: An illustration of silane coating using evaporation.
Once the silicon master was developed it was allowed to dry for 30 mins in the oven at 180°C to remove any moisture from the sample. The wafer was then placed into a petri dish and left on a hot plate at 150°C. A drop of silane was placed on the side and allowed to evaporate onto the surface for an hour until the entire sample was coated.

2.1.2.2 Bonding microfluidic devices

To prepare microfluidic devices it was important to make sure that both the PDMS mold and substrate surfaces were absolutely clean. The substrate (glass coverslips/slides/silicon device) was cleaned by immersing it into Piranha solution (see above). This was followed by a series of washes with distilled water, acetone and then propan-2-ol, each for 5 min under sonication. These substrates were dried off using a flow of particle free air or nitrogen. The PDMS microchips were rinsed in propan-2-ol and blow dried using a flow of nitrogen gas. All substrates and the PDMS microchips were exposed to an air plasma for 30-60 sec (bonding side facing up) using a plasma cleaner (Table 3) (HarrickPlasma

website – http://www.harrickplasma.com/products_cleaners.php, referenced on 19/03/2010). Then each set was bonded to produce the final microchannel device. These were transferred to an oven for 20-30 min at 60 ºC (this seemed to seal the devices better). PDMS surface is hydrophobic in its natural state, hence the surface needed to be modified when using it for the purpose of cell culture and microfluidic applications. By using the air/oxygen plasma treatment via the Harrick plasma machine bonding between the PDMS device and glass/silicon chip was enabled. During oxygen plasma treatment, the CH_3-groups on the PDMS-surface are oxidized and OH-groups formed, similarly on the glass/silcon chip when oxidised, therefore creating strong seal between the two surfaces by covalent bonding. (Bhattacharya 2005, Kallio 2006, Lee 2003, McDonald 2000, Sia 2003).

Low power (RF)	716V DC	10mA DC	7.16W
Medium power (RF)	720V DC	15mA DC	10.15W
High power (RF)	740V DC	40mA DC	29.6W

Table 3: Harrick plasma settings.
This table was obtained from the Harrick plasma website (http://www.harrickplasma.com/products_cleaners.php). (RF – Radio frequency setting on the plasma cleaner)

2.1.2.3 Device holders

In some cases the bonding strength was not sufficient; therefore external pressure was applied to press the device and substrate together. To assist the bonding, device holders were designed and machined in the mechanical workshop according to the specifications of the designs. Glass slides (25 x 25mm) were used to evenly apply pressure and had fluidic connector access holes drilled through them. The burs needed to drill the holes were purchased from Diama Int. (500 series diamond dental burs; 545, 544, 525 and 522- depending on the sizes of connectors used)

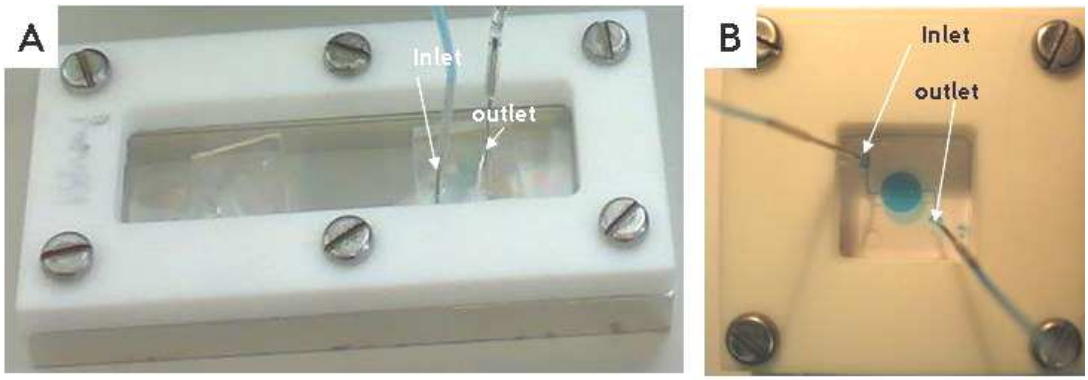

Figure 15: First clamp design: Aluminium and PTFE.
A) This device holder was useful for the single culture well system since it was used to fit a maximum of 2 devices together. Syringe needles attached to polymer tubing were used as inlet and outlet connectors to flow desired liquids. The device holder was designed at the C.C.E and machined in the mechanical workshop, University of Glasgow, James Watt bld. B) shows the top view of the another device holder setup for single cell culture well devices. Also showing inlets and outlet inserts.

2.1.2.4 Inlets/outlets connectors and tubing

To drive liquid through the devices syringe pumps (KD scientific series 2000, syringe pumps) were used and the syringes were coupled with needle connectors attached to a flexible polymer tubing (Tygon tubing) and specially prepared inlet/outlet connectors.

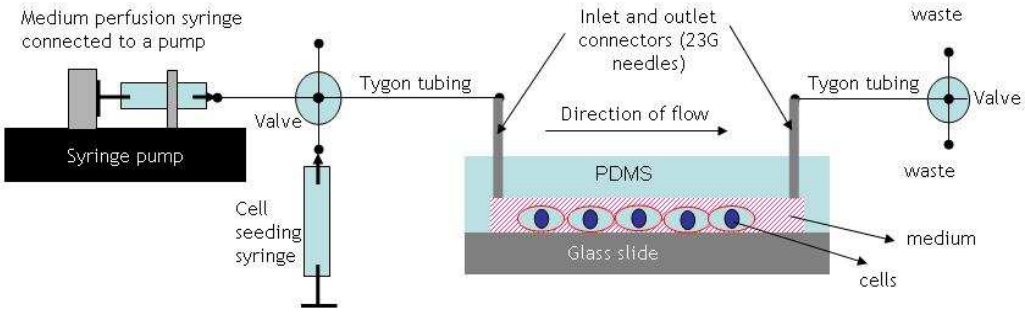

Figure 16: Perfusion system setup for microfluidic devices.
This illustration shows the setup for the perfusing medium and fluids through a microfluidic device. The syringe is supported by a syringe pump that drives the liquid through the tubing at a certain controlled rate. The fluid is passed in through the tubing and finally into the microfluidic device. The device is connected via syringe needles to the tubing. The fluid flows from the inlets to the outlets where it gets either collected or thrown away depending on its contents.

For all the inlets and outlet connectors a Microlance gauge size 23G 1 ¼ (0.6 x 30 mm) (BD Scientific, Microlance) was used. These 23G needles were filed at their ends to make them blunt and inserted into the tubing connectors [The tubing was bought from COLE PARMER - tygon tubing (sku# 06418-02) inner diameter (ID) = 0.02 inches (0.5 mm) and outer diameter (OD) = 0.06 inches (1.5 mm)]. Their other Luer lock end was cut off and

smoothened using a file to make a blunt rounded inlet connector to be inserted into the device. The 21G 1 ½ (0.8 x 40 mm) (BD Scientific, Microlance) needle tips were cut and smoothened. Once they were blunt and rounded enough these needles were used to puncture holes into the PDMS at the inlet and outlet marks on the device. The PDMS microchip was punctured very slowly and care was taken not to cause any cracks within the channels. Once all the holes were punctured, the chip was rinsed in isopropanol and left to dry. To get rid of any dust and dirt a small clean strip of sticky tape was used to clean the bonding PDMS surface before put in contact with the substrate of interest (glass or silicon).

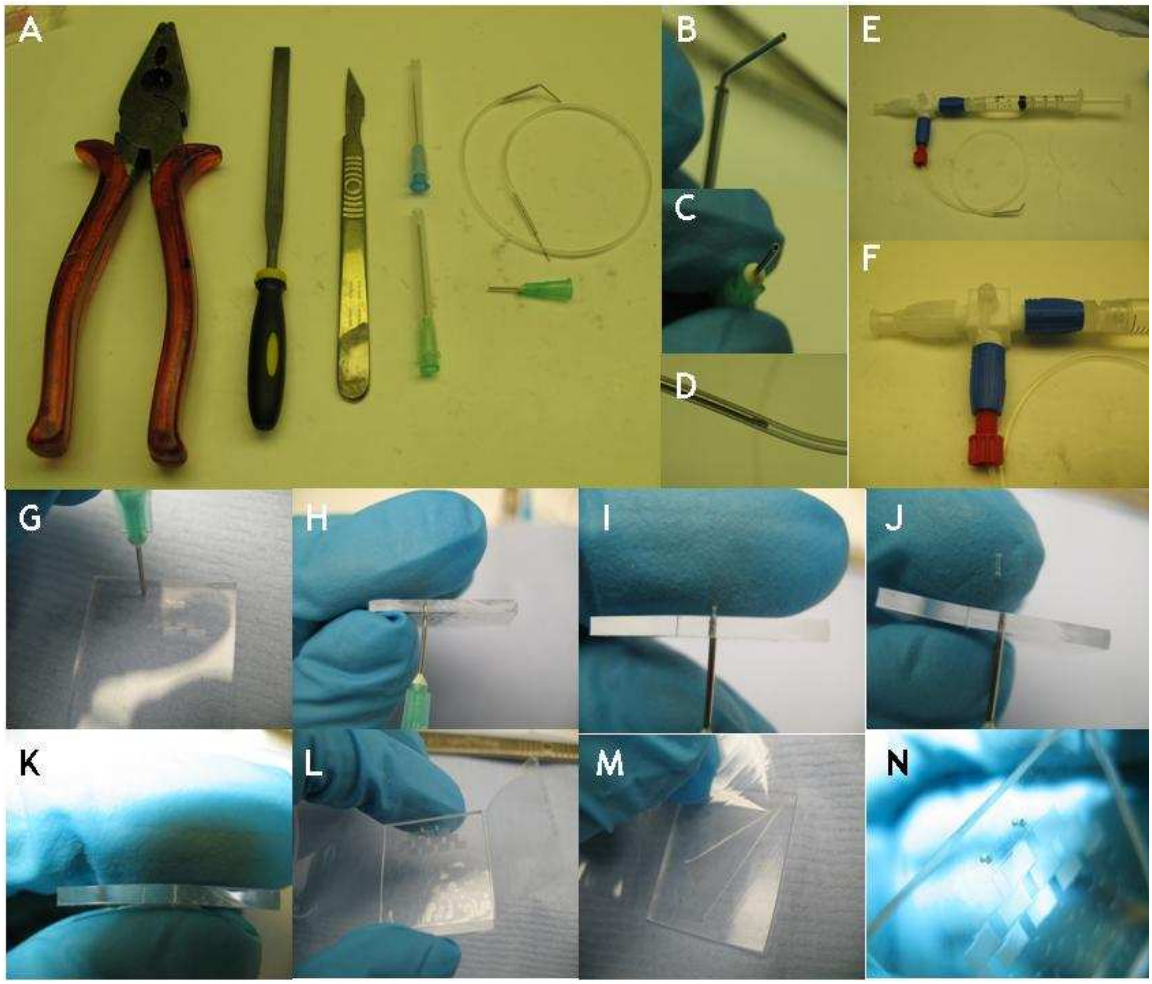

Figure 17: Device tools
A) This image showed the tools used for preparing the different components of the device B) The inlet connector was prepared using the 23G needle, where one side was connected to the tygon tubing and the other end was filed to be inserted into the device. C) The 21G microlance was filed to be used to punch holes into the PDMS inlet/outlet connector channels. D) The inlet connector was connected to Tygon tubing. E) F) The tubing and syringe was connected to a PTFE valve. G) to N) were the steps that indicated the protocol for puncturing holes and cleaning the PDMS surface using sticky tape.

2.1.3 Cell culture

2.1.3.1 Calu – 3 cells

Calu-3 cells (an adenocarcinoma derived, human bronchial epithelial cell line, type II lung epithelia) were obtained from ATCC-LGC Promochem and maintained in Eagles minimum essential medium (EMEM) also purchased from ATCC. EMEM medium was supplemented with 10% foetal bovine serum (FBS), 2% antibiotic mixture with added glutamine (Glutamine-114 µM, penicillin/streptomycin-1905 µM and fungizone-11.9 µM). The cells were maintained as a monolayer in tissue culture plastic (TCP) 25 cm^2 flasks at 37 °C and 5% CO_2 in a incubator. The medium was renewed every 2-3 days. When almost confluent (after about 4-5 days in culture), the flasks were washed with HEPES saline and incubated for approximately 10-15 mins with a 0.1% solution of trypsine/versine (trypsine – EDTA) solution in a 37 C, 5% CO_2 incubator. Once the cells detached from the surface of the flask they were collected and re-suspended in FBS (This was repeated twice). The cells were centrifuged at 1400 rpm for 4 min, re-suspended in 1 ml of EMEM, counted in a modified Fuch's haematocytometer and their concentration suitably adjusted. For culture maintenance 0.7 x 10^6 Calu-3 were seeded into a 25 cm^2 TCP flask. Alternatively or in parallel the required amount of cell count adjusted suspension was used for experiments.

2.1.3.2 Fibroblast cells

The hTert fibroblast (Infinity^{TM} Telomerase Immortalised primary human fibroblasts (hTERT-BJ1,) were obtained from Clonetech Laboratories, Inc.,USA. These cells were maintained in 75 cm^2 TCP flasks. The DMEM mixture medium used was 71% Dulbeccos Modified Eagles Medium (DMEM) (Sigma, UK), 17.5% Medium 199 (Sigma, UK), 9% FCS (Life Technologies, UK), 1.6% 200 mM l-glutamine (Life Technologies, UK) and 0.9% 100 mM sodium pyruvate (Life Technologies, UK). The cells were maintained in the incubator at 37 ºC with a 5% CO_2 atmosphere. The medium was renewed every 2-3 days. When almost confluent (after about 4-5 days in culture), the flasks were washed with HEPES saline and incubated for approximately 10-15 mins with a 0.1% solution of trypsine/versine (trypsine – EDTA) solution in a 37 °C, 5% CO_2 incubator. Once the cells detached from the surface of the flask they were collected and re-suspended in DMEM mixture medium (This was repeated twice). The cells were centrifuged at 1400 rpm for 4 min, re-suspended in 1 ml of DMEM mix, counted in a modified Fuch's haematocytometer and their concentration was suitably adjusted. For culture maintenance 1 x 10^6 hTert

fibroblasts were seeded into a 75 cm^2 TCP flask. Alternatively or in parallel the required amount of cell count adjusted suspension was used for experiments.

2.1.4 Preparing the device for Cell Culture

To make the environment inside the device favourable for cell growth and proliferation a methodical washing protocol was adopted, as detailed below. The device connectors and tubing were prewashed with 96% ethanol and left to dry in the flow cabinet. They were then connected to the fluidic device at one end and to the syringes at the other (via high pressure valves). Precautions were taken to prepare completely bubble free syringes and connectors. Once all the necessary components were prepared there were a number of sterilisation steps that had to be done prior to the inclusion of culture medium and cells. To minimise the amount of bubbles forming in the medium during perfusion its gas content had to be reduced. To allow for better cell adhesion the device were coated with ECM (e.g. collagen and fibronectin) proteins. The various methods detailed below explained each of these steps.

2.1.4.1 Wash steps for sterilising the device

A series of wash steps were tried and tested to improve the environment inside the device for cell proliferation. Immediately after bonding the devices, their microchannels allowed liquids to easily wet the channel walls and the substrate. Hence the wash steps were implemented soon after the bonding since the liquids would flow smoothly through the microfluidic channels. The channels were washed with ethanol to maintain the hydrophilic nature of the channels and also to begin the sterilization procedure. In most cases if the device had just been prepared, then the use of ethanol for sterilization was more than sufficient, but in some cases pre-filtered 0.1 N HCl (hydrochloric acid) was also used after ethanol to help kill off bacterial and reduce protein residue. The solutions were then rinsed out with a long 30-60 min rinse with distilled water. This was necessary to remove any traces of ethanol from the PDMS (solvents are sometimes absorbed by PDMS if used for a long time inside channels) (Lee 2003, Mukhopadhyay 2007). This was followed by another 30-60min rinse with a saline buffer (either phosphate buffer saline; PBS: NaCl -136.89 mM; KCl - 26.8 mM; KH_2PO_4 - 73.7mM; Na_2HPO_4 -14.7 mM and the pH is adjusted to 7.5 using 1 M NaOH) or 4-(2-hydroxyethyl)-1-piperazineethanesulfonic acid (HEPES) saline – containing NaCl – 140 mM, KCl – 5 mM, HEPES – 10 mM, d-Glucose – 5 mM and 0.001% of a 0.5% phenol red solution). The channels were then perfused with cell culture medium composed of EMEM with antibiotics and 10-15% FBS for approximately

15-20 mins. The entire setup was then allowed to settle under static, no flow, conditions inside the incubator until cells were ready to be seeded.

2.1.4.2 Medium preparation

The medium was left for 1-2 hr in the CO_2 incubator to equilibrate before being used in the device to reduce the potential gas content and that way help avoid bubble formation alternatively the medium was pre-warmed to 40°C in a water bath for 1 hr, then left to cool to 37 ºC.

2.1.4.3 ECM protein coating

In order to increase the biocompatibility of the devices and encourage cell adhesion the devices were best coated with an extracellular matrix protein. The washing steps mentioned earlier section (2.1.4.3) was followed by the addition of a collagen mix consisting of EMEM (excluding FBS) containing 3 mg/ml solution of collagen type I [(Cellagen solution, Biomedical/ICN Biomedicals (cat.no. 152393) type I collagen, pH 3.0) dissolved in HEPES solution (section 2.1.4.1)]. This was prefused through the device and allowed to adsorb to the inside of the device at 37 ºC for 1-2 hr. The solution was finally washed off using EMEM (including FBS). The cells were subsequently seeded into the device.

Type	Reagents	Volume [ml]	Ratio
Collagen solution MP Biomedical/ICN Biomedicals (cat.no. 152393) Type 1 collagen, pH 3.0, Cellagen solution AC – 3	HEPES saline (section 2.1.4.1), pH 7.5/plain EMEM	2	20
	Cellagen Solution AC or PC (0.5 or 0.3% wt/vol- supplied as 3mg/ml solution 0.01 M acetic acid)	0.1	1
Collagen type I solution Sigma Aldrich	Plain EMEM	2	20
	Collagen (Supplied as 3 mg/ml solution - 0.3% wt/vol in 0.01 M HCl (pH ~2.0).	0.1	1
	Maintain the pH to 7.4 using 0.1M NaOH and 0.1M HCL (use phenol red indicator)	Colour change-orange to light pink	

Table 4: Different types of collagen type I used for surface coating and a list of their respective preparation/dilution.

2.1.4.4 Cell seeding into the device

Once the microfluidic cell culture chambers had been sterilised and coated with collagen, cells were seeded into the device via there inlet/outlet channels. The seeding was done using either one of the three methods explained below.

The Figure 18,A) illustrated the method implemented to introduce cells into the cell culture chambers via the outlet channels. This helped to control the flow of cells into the inlet channels and prevented clogging of the inlet channels or the connector tubing (if cells adhered to the either of these). The flow of cells when seeded was controlled by a syringe driver or by hand. However, care was taken to prevent any inclusion of gas bubbles or contaminants during this process. The inlet channel seeding method on the other hand, seemed to work better and had fewer inclusions of gas bubbles. The inlet seeding method was illustrated in Figure 18 B). Seeding cells through the inlet gave better control and reduced both the number of gas bubbles and more importantly contamination. This method however could not completely avoid the clogging of the channels by cells. However the inlet/outlet seeding method illustrated in Figure 18 C) reduced gas formation and to some extent the clogging of cell slightly better. Here both the inlet and outlet channels were connected to valves, which allowed selective seeding and fluid insertion.

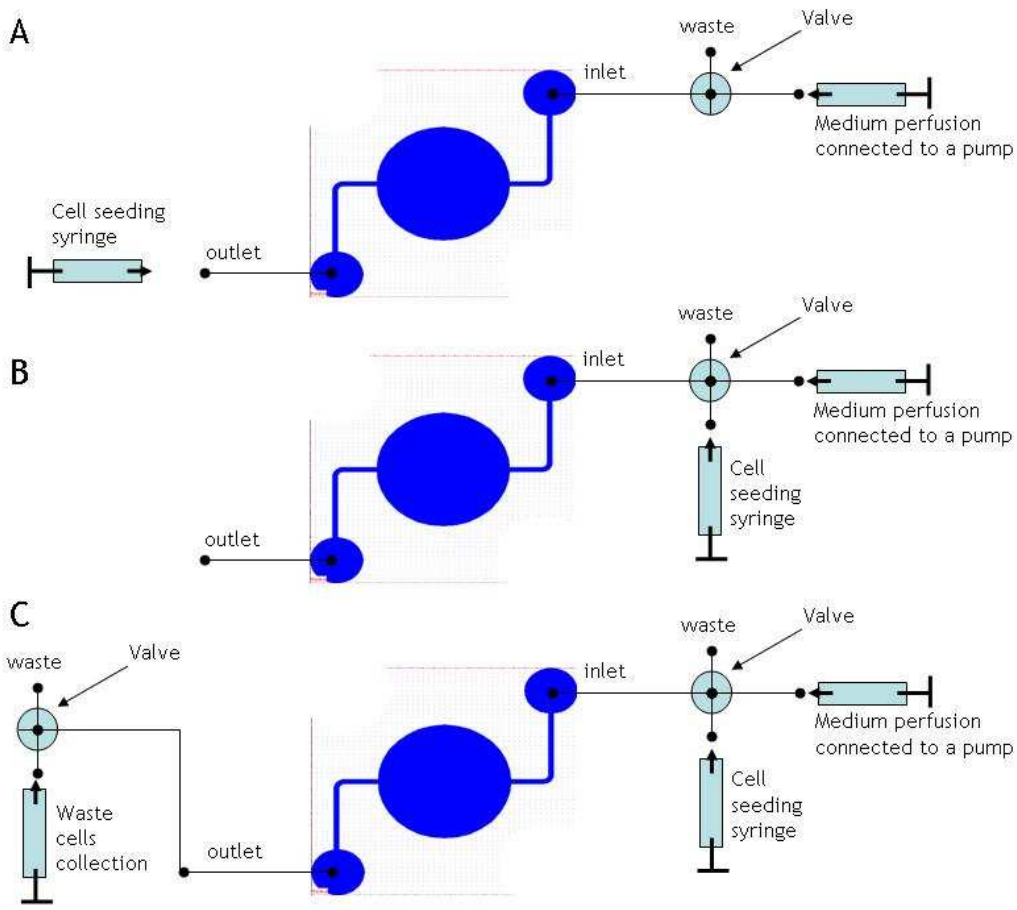

Figure 18: Cell seeding inside a culture single cell culture wells
These images show the various methods used for cell seeding into microfluidic devices in this project. A) This explains the outlet seeding method, where the direction of medium perfusion is from the inlet opening to the outlet opening. The cells however are seeded through the outlet opening. B) This explains the Inlet seeding method, where the direction of medium perfusion is same as in 'A', but the difference being that the cell seeding is performed through the inlet channel C) The inlet/outlet seeding method explains that the flow of medium is the same as in 'A', however there is a two step seeding method involved. The cells are initially seeded from the inlet side and any lost cells are collected inside the outlet side syringe. If cell are lost during medium perfusion or death due to air bubbles, then cells can be are seeded through the outlet side using the cells available or can prepare a fresh sample of stock cells.

2.1.5 Cell staining using Coomassie blue dye

Cells were grown on 13 mm diameter glass coverslips placed inside a 24 well plates for 24 hrs, under static (no-flow conditions). These cells were washed several times with PBS to remove any extracellular matrix proteins and traces of FBS. The fixative solution, made up of 4% formaldehyde (vol/vol) in PBS with 2% (wt/wt) added sucrose, was added and left to incubate at 37°C for 15mins. The fixative was then removed and cells are washed again with PBS several times to remove all fixative. Coomassie (0.2% Coomassie blue dye (wt/vol) (This stain was commonly used for gel electrophoresis to stain proteins - here it was used to stain the fixed cells), 7.5% acetic acid (vol/vol) and 50% ethanol (vol/vol) all dissolved in distilled water) was used added at room temperature. This is rinsed off with

PBS and the cells mounted onto glass slides with PBS. In the case of microfluidic devices the above solutions were pumped through the system via pressure driven flows. This procedure did cause some cells to detach from the substrate. In order to reduce such, and avoid multiple syringe changes the fixative was directly added to the device channels through the inlet channel connectors, to make sure that the cells get stuck onto the substrate surfaces. This made it possible to stain most of the cells in the culture chamber. Once the cells were stained all sample could be viewed under the light microscope.

2.2 Results

2.2.1 Fabrication techniques

2.2.1.1 Fabrication using SU-8

The microfluidic devices were all fabricated using photolithography techniques described earlier in this chapter. Three different types of SU-8 (2050, 3050 and 3025) negative photoresist were used to fabricate the silicon masters. Each resist type was used under different conditions depending on the required thickness. In general the pre-treatment of the substrate, spin coating, baking and other processing steps were adopted from the data sheets provided for the relevant SU-8 resists (MicroChem). However, during processing the protocol had to be adapted according to the specific application. Table 5 lists the processes used to achieve the desired height (a list of the SU-8 types and protocol given in the data sheet was previously explained in Table 2). The heights obtained were measured using a Dektak (Table 5). Each of the photoresists showed slight variations between the expected heights (given in the data sheet) and the measured heights. The SU-8 3050 was easier to predict as the same heights could consistently be achieved when using a two step spinning method as laid out in detail in discussion section (Pg. no 76).To perform the step method, first a base layer of photoresist was spun on the substrate and after pre exposure bake, a second layer was spun on top to gain the desired height; this was used mostly with the SU-8 3000 series due to its better adhesive properties. The relationship between spin speed and resist thickness was assumed to be consistent over time and used as a means to determine the height of the channels. The dimensions obtained were used to calculate the flow rate, shear stress experienced by the cells and the diffusion coefficients of particles within the microchannels.

Fab. No.	Resist	Steps to coat Si with SU-8 photoresist				ht (data sheet) [µm]	Exp. Time [s]	Height ± SD [µm]
		Spin coating 1 [rpm]	Pre-bake [°C]	Spin coating 2 [rpm]	Post-exposure bake [°C]			
1	Su-8 2050	2000	95	----	----	75	30	73±3 (n=4)
2	SU-8 2050	2000	95	2000	95	150	40	135±7 (n=3)
3	SU-8 3025	2000	95	2000	95	90-95	35	83±1 (n=3)
4	SU-8 3050	3000	95	----	----	50	35	48±4 (n=5)
5	SU8-3050	2000	95	----	----	75	35	74±1 (n=3)
6	SU-8-3050	2000	95	3000	95	125	40	112 ± 5 (n=3)

Table 5: SU-8 fabrication scheme showing the nominal and measured resist heights.

2.2.1.2 Single culture well device fabrication

The single culture well was designed using the L-Edit/CleWin software. Figure 19 A) shows the silicon master for the single well device. The diameter of the main cell culture well was designed to be 5 mm in diameter and the lengths of the inlet and outlet channels were designed to be 4 mm. The fabrication scheme 6 in Table 5 was used and the height was measured height after processing using the Dektak machine to be 112µm, shown in Figure 19 C). The total volume of the channel was calculated to be 2.379µl. .

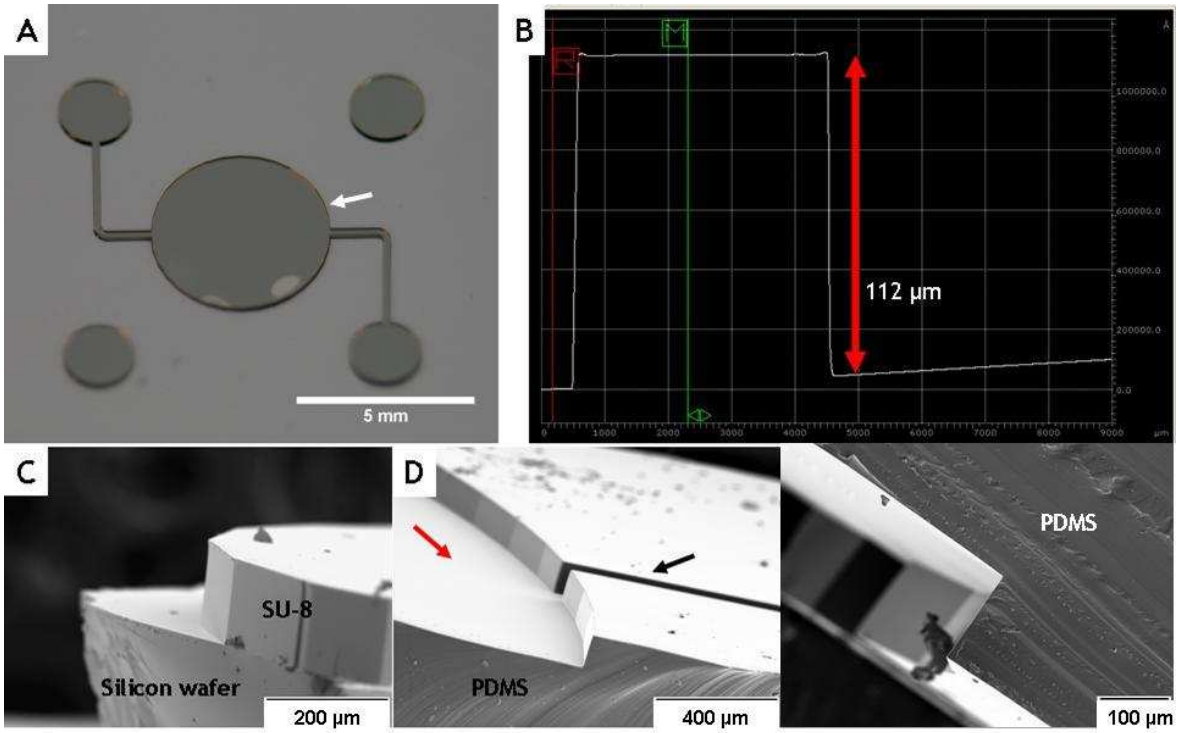

Figure 19: Single culture chamber microfluidic device.
A) Photograph of a silicon master with the SU-8 photoresist pattern on top (the arrow indicates an area of the resist B) Dektak height profile of the developed SU-8 3050 photoresist, here the height of the feature was 112µm. C) SEM profile of the chamber on the silicon master. D) SEM image of the PDMS device showing the channels (marked by the black arrow) and chamber (marked by the red arrow). E) SEM image of a crossection of the inlet/outlet microchannel in PDMS (ht was ~100 µm and width was 200 µm).

2.2.2 Cell culture

2.2.2.1 Seeding densities

In order to optimise the seeding densities Calu-3 cells were seeded on 13 mm diameter glass coverslips. The cells were seeded at five different densities: 0.015, 0.03, 0.07, 0.3 and 0.7 x 10^6cells/cm^2, equivalent to an expected surface coverage of 0.2, 2.9, 7, 29 and 70% on seeding, and cultured for 3hrs, 14hrs and 24hrs, after which time they were stained with a solution of Coomasie blue, observed under the light microscope, and their respective area coverage measured. The results show that the cell density of 0.7 x 10^6 cells/cm^2 lead to complete cell coverage of the reference area (field of view) by day 1. In order to ensure early coverage of the culture area within the microfluidic device this seeding density was adopted.

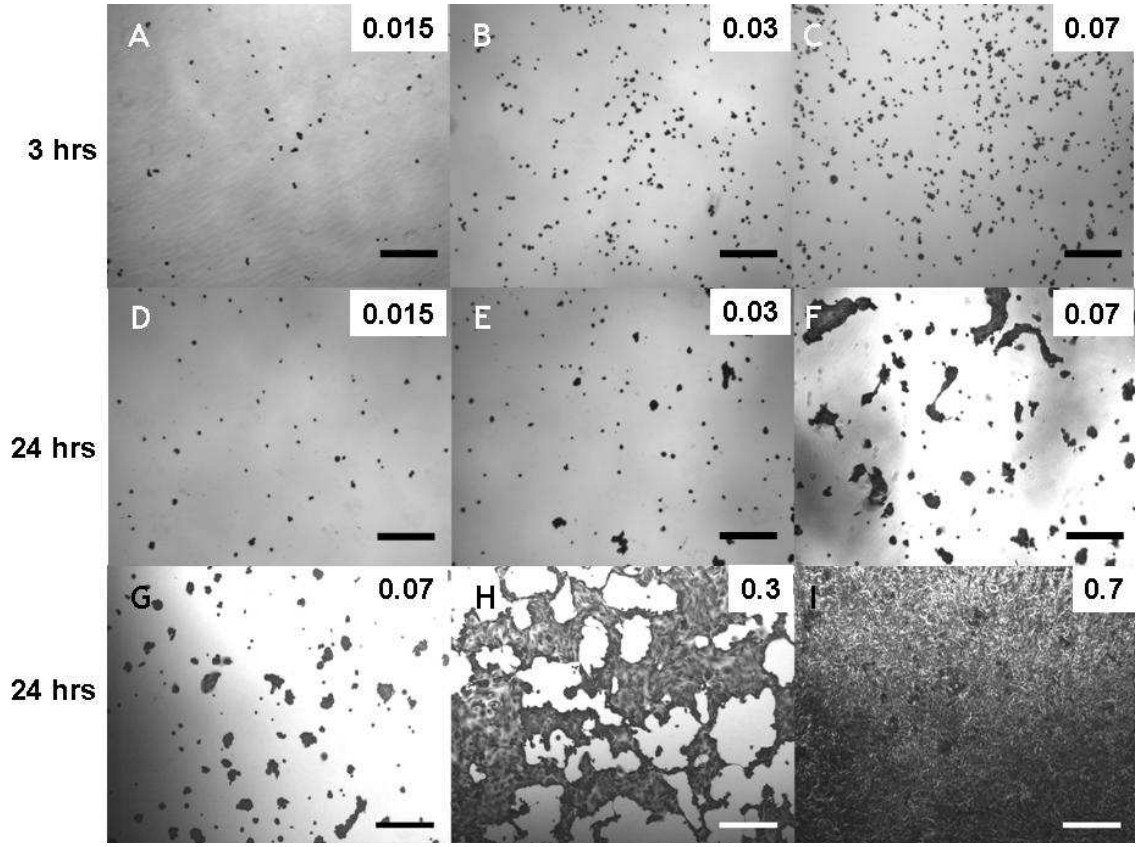

Figure 20: Coomassie blue staining
Calu -3 cells seeded at the different densities indicated in the top right of the respective images (x 10^6 cells/cm^2) onto 13mm diameter coverslips, fixed and Coomassie blue stained at 3h (A-C), and 1 day (D-I). Scale bars 250µm.

2.2.2.2 Cell culture inside the single cell culture well device.

The cell culture protocols used were outlined/described in the Materials and Methods section under (2.1.3 and 2.1.4); in short; cells were seeded through the inlet using the method described for the single culture well devices. Initially hTert fibroblast cells were used to establish a base line methodology for culture conditions as these cells grew faster and needed less time to reach confluence, and also to optimise the pressure driven flow regimes when using the syringe pumps. The cells in Figure 21 A, B, and C are hTert fibroblast cells which were allowed to proliferate inside the single well culture chambers at a flow rate of 1µl/min for 3-4 days. The shear stress calculated using the equations, presented by Lu et al (2004) and Korin et al (2007), were 0.6 and 1.2 mPa in the middle of the cell culture chambers while using a constant flow rate of 0.5 and 1 µl/min respectively (for a 10 ml syringe). The shape of the cell culture well is round and hence the shear is less towards the middle of the chamber than compared to the inlet and outlet entrance points (which were calculated to be 15 and 30 mPa at flow rates of 0.5 and 1 µl/min respectively). Once cells were seeded inside the device, they were allowed to settle for about 3-4hrs to allow for initial cell attachment. The cells thereafter were maintained at intermittent flow

(Korin 2007) (6-8 hrs the pump was on, then for 1 hr the pump was off, then the flow was started again for 6-8 hrs) with a rate of 1 µl/min for 3-4 days in culture. The results presented in Figure 21, showed proliferation of hTert fibroblast cells (forming confluent monolayers) and for Calu-3 cells (healthy but still had not reached confluence). After day 3 the hTert cells completely covered the entire culture area inside the device. However the Calu-3 cells seeded at 0.7 x 10^6 cells/cm^2 only covered about 20-25% of the total area inside the device on day 3, suggesting that longer culture periods and maybe also lower shear stress conditions were needed to allow faster growth of confluent monolayers.

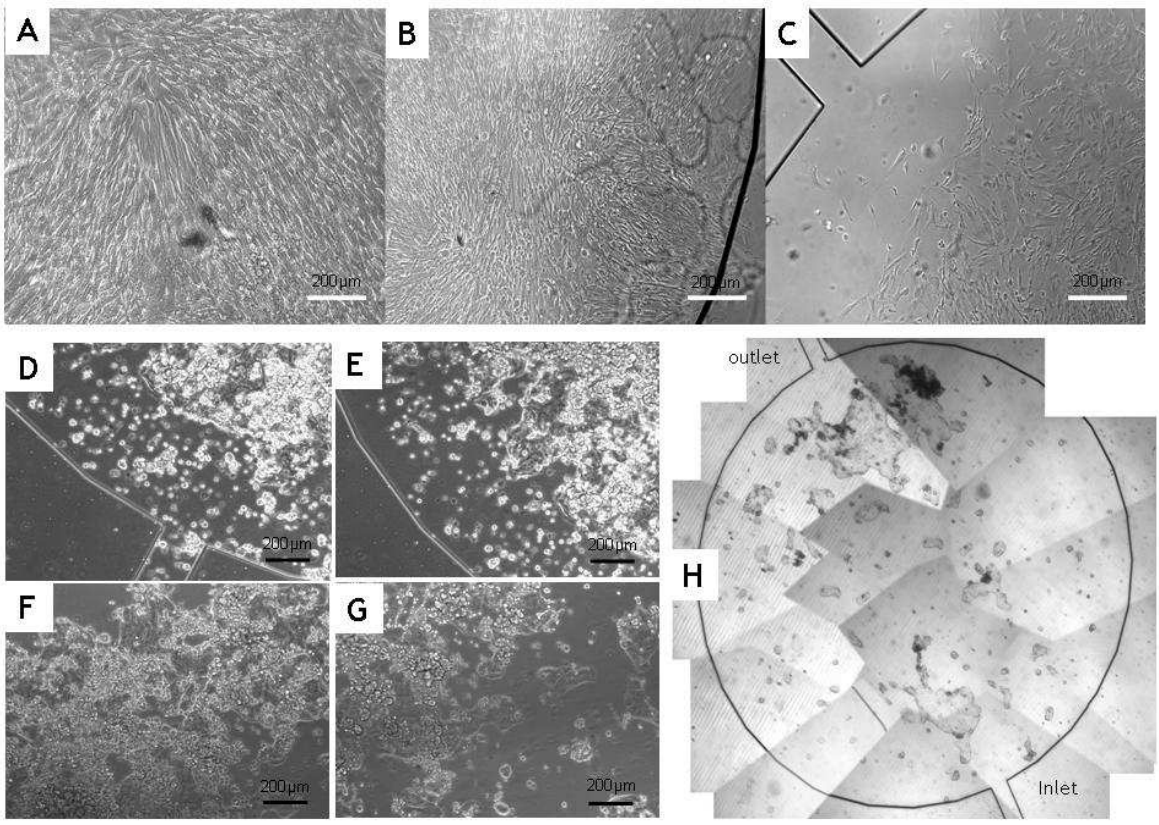

Figure 21: Cell culture in single culture well channels
A) B) and C) hTert cells cultured inside the single culture well device. Pictures taken on Day 3 of maintained at an intermittent flow rate of 1µl/min. The syringe pump was programmed for intermittent flow (6 - 8 hr flow, 1h no flow, then again 6 – 8 hr flow) Scale bars = 200µm. D) E) F) and G) Images of Calu-3 cells cultured under the same conditions as the hTert in A. H) Composite micrograph of Coomassie stained Calu-3 seeded at 0.7 x 10^6 cells/cm2, after 3 days in flow culture. The image covers the entire culture well showing the distribution of Calu-3 inside the well.

2.2.3 Concentration gradient mixer (joint experiments with Kristin Kirchoff - PhD Student)

The intent was to use the gradient generator for layer by the layer deposition of gradients of two weak polyelectrolytes. If weak polyelectrolytes are deposited in a layered fashion on surfaces at differening ionic strength or pH their resulting surface properties (topography, charge, viscoelasticity) change accordingly (Kirchoff 2008, 2009). The purpose for Ms Kirchoff was to investigate the cells interpretation of such gradients. The gradient device worked as described in section 2.1.1.1; in short; the two entry channels are constantly split and mixed in successive rows of channels with interconnecting serpentine channels that extended the time the fluid spent in the channel and thus allowed for diffusion to occur. Our device had 7 rows of serpentine mixers ending in 9 outlet channels that joined up to form a 0.9 mm wide channel. In order to reveal the underlying differential in pH two dyes were used: fluorescein-thioisocyanate (FITC) at a concentration of 1mM, and 2'-7'-bis(carboxyethyl)-5(6)-carboxyfluorescein (BCECF) as a pH indicator. The following experiments were conducted to achieve an understanding of gradient device. The pictures in Figure 22 and Figure 23, show the formation of a FITC gradient across the broad channel under the influence of different pressure flows. The aim was to achieve repeatably the same, broad and consistent gradient of dye across the channel. The profile of the gradient seen in Figure 23 B) and D) were the best obtained with the device. Table 6 shows the results obtained from using the different dye with different flow rates. In order to get a good gradient profile the syringe pumps needed to run at low flow rates (>1 µl/min), which may often cause pulsatile flow. To avoid these effects the pump was adjusted to run at a higher volume while using a low volume syringe (250µl volume Hamilton syringe). This meant that the actual flow rate would be much lower than that displayed on the pump.

Fluorescent Dye	**Flow rate displayed on the pump (µl/min)**						**Results (flow rate that creates the best fit linear concentration gradient)**
	Actual flow rate using 250µl syringe at pump set to a 10ml syringe (µl/min)						
FITC in Tris-HCl	1	5	10	50			1µl/min or 0.025µl/min (from **Figure 22** and **Figure 23**)
	0.025	0.126	0.252	1.261			
BCECF in water	1	5	10	50	100	500	50µl/min or 1.261µl/min (from **Figure 24**)
	0.025	0.126	0.252	1.261	2.523	12.6	
BCECF in PEI	1	5	10	50			10µl/min or 0.252µl/min
	0.025	0.126	0.252	1.261			

Table 6: Summary of the gradient experiments from Figure 21, 22 and 23

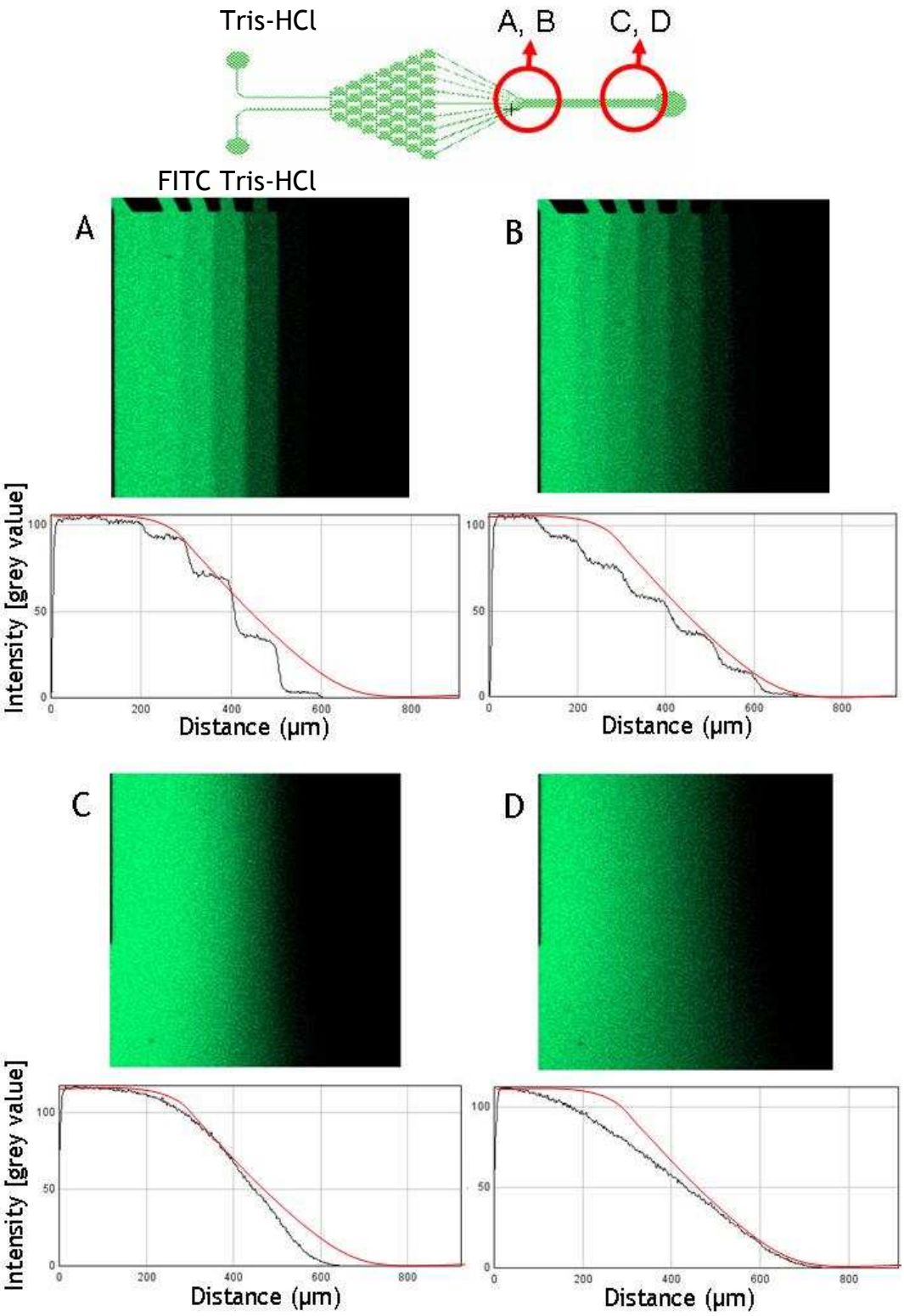

Figure 22: FITC intensity profiles at the beginning and end of the wide channel – perfusing with FITC in Tris-HCl on the left against plain Tris-HCl on the right - Part I
A) Intensity profile across the gradient for a flow of 50 µl/min and B) Profile for a flow of 10 µl/min at the beginning of the broad channel. C) Profile for a flow of 50 µl/min and D) Profile for a flow of 10 µl/min at the end of the broad channel. The graphs show the intensity values of FITC fluorescence in arbitrary units along a line in the midle of the images in black, the expected gradient is plotted in red. The smoothing of the gradient between beginning and end is a result of the diffusive mixing that occurs along the broad channel of the device. All flows were performed applying 10ml syringe settings on the pump while using a 250µl volume glass Hamilton syringe.

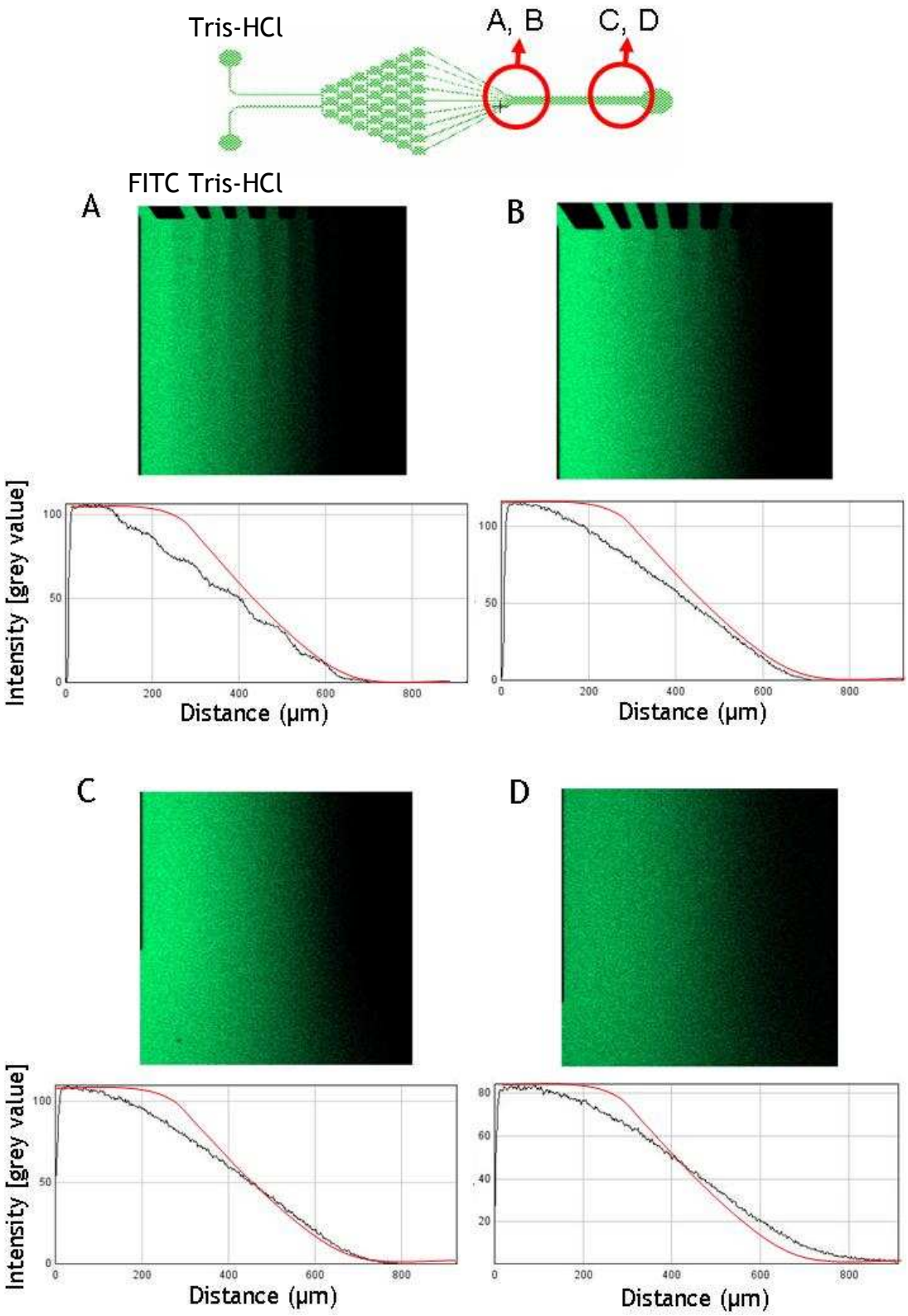

Figure 23: FITC intensity profiles at the beginning and end of the wide channel – perfusing with FITC in Tris-HCl on the left against plain Tris-HCl on the right - Part II
A) Intensity profile across the gradient for the flow of 5 µl/min and B) Profile for 1 µl/min at the beginning of the broad channel C) Profile for the 5 µl/min and D) profile for the 1 µl/min at the end of the broad channels. The graphs show the intensity values of FITC fluorescence in arbitrary units along a line in the midle of the images in black, the expected gradient is plotted in red. The smoothing of the gradient between beginning and end is a result of the diffusive mixing that occurs along the broad channel of the device. All flows were performed applying 10ml syringe settings on the pump while using a 250µl volume glass Hamilton syringe.

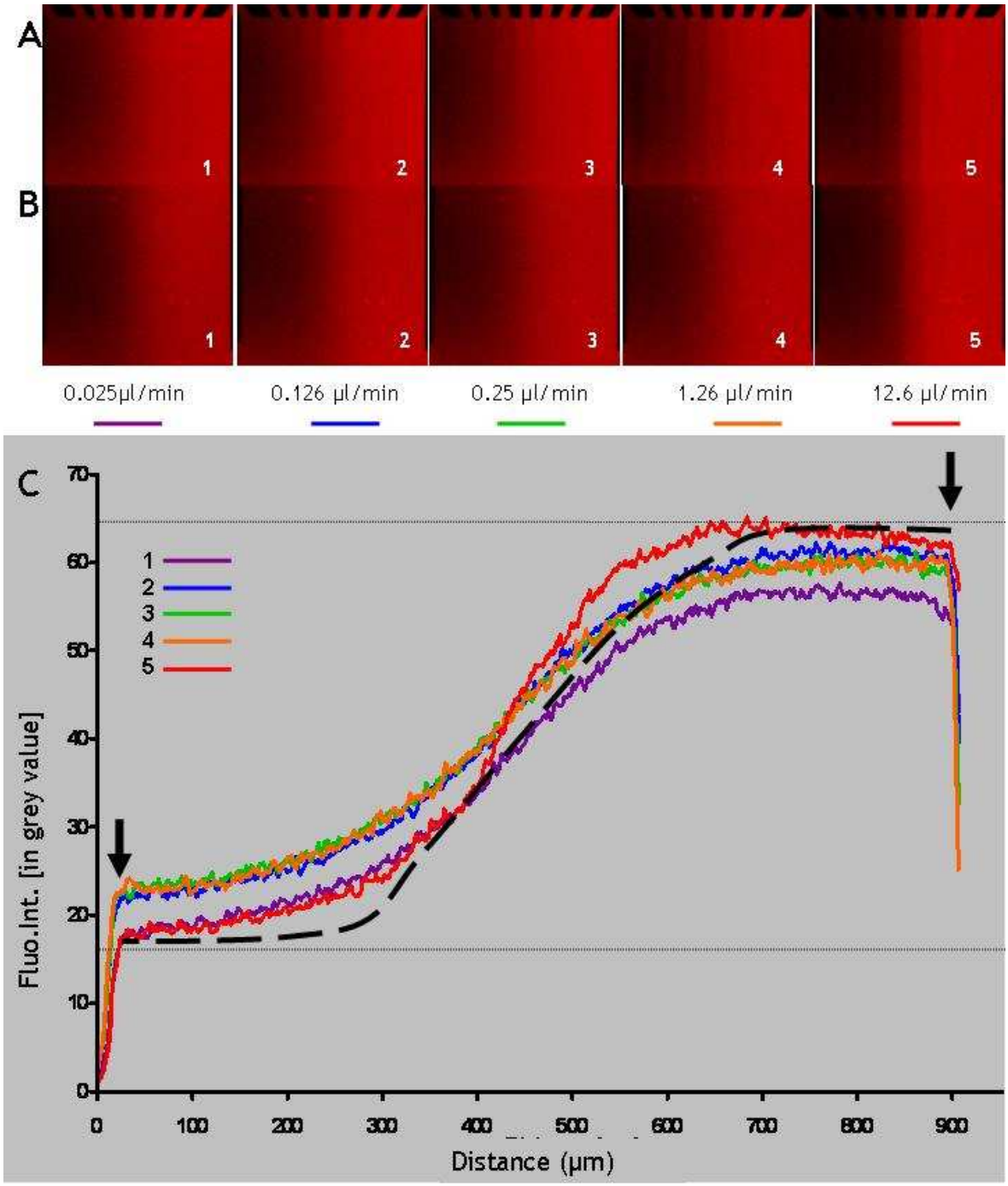

Figure 24: BCECF fluorescent dye intensity profiles at the beginning and end of the wide channel - perfusing with BCECF in water on the right against plain water on the left.
A) Intensity profile of the gradients developed at the beginning of the broad channel and the numbered images signify the different flow rates used for the experiments (1 = 0.025µl/min, 2 = 0.126µl/min, 3 = 0.25µlmin, 4 = 1.26µl/min, 5 = 12.6µl/min) B) Intensity profile of the gradients developed along the end of the broad channel. The numbers signify different flow rates (1 = 0.025µl/min, 2 = 0.126µl/min, 3 = 0.25µlmin, 4 = 1.26µl/min, 5 = 12.6µl/min). C) The graph is a representation of the fluorescence intensity across the broad channels from pictures shown in the set (B1 = lilac, B2 = blue, B3 = green, B4 = orange and B5 = red). The black dotted line represents the desired fluorescent intensity profile of the gradient (for 0, 0.8, 6.2, 22.7, 50, 77.3, 93.8, 99.2 and 100%). The arrows mark the broad channel width. All flows were performed applying 10ml syringe settings on the pump while using a 250µl volume glass Hamilton syringe.

2.3 Discussion

This chapter focused on the development of microfluidic devices using SU-8 photolithography and PDMS replica moulding. The techniques used in developing microfluidics involved micromachining, soft lithography, embossing, injection moulding and laser ablation and have been described throughout the literature (Beebe 2002, Nguyen 2006). Each technique had its associated set of advantages and disadvantages according to the envisaged application of the devices. In case of the designs for the multilayered device, the technique of choice was to use a patterned photoresist as master substrate to cast replicate microfluidic devices. Here SU-8 Epon epoxy was used and this resist was spin coated to thicknesses in excess of 75 μm, patterned by mask based photolithography, and allowed full control over all design parameter. However the methods suggested within the data sheets provided by MicroChem Inc. for this resist type had to be optimised for the purpose of this project. The changes to the protocol were mainly due to different working conditions within the labs. For example depending on the substrate cleaning solutions (different methods of cleaning used in different labs), the adhesion of SU-8 could vary. (Another reason being that different labs have varying working conditions for SU-8). This photoresist has many advantages but also comes with some disadvantages due to its long and uncertain exposure times and high viscosity. The mask aligner exposure time and energies may vary from lab to lab due the differences in the Mask aligner machines. This could be due to the differences in the light filters (between 365–436 nm depending on the type of UV lamp) used inside such mask aligner tools produced by different companies (Mask aligner machines are produced by different manufacturers, e.g SUSS MicroTec, Midas System Co., Ltd, etc..) (Nguyen, 2006). Sometimes, due to under-exposure, the developed photoresist walls tended to form inverted ‘V’ shaped structures. This can influence the secondary pattern transfer process when using PDMS casting as a means of replication for microfluidic devices. The exposure times had to be tested and optimised in this case to avoid any irregularities in the patterning process. In Figure 25, A) the effects of under exposure are seen, where the side walls are slightly ‘inverted V’ shaped and B) shows straight walls once the exposure times were optimised according to the height of the walls. The viscosity of SU-8 for the resist used (i.e. SU-8 2050, 3050 and 3025) also made it tricky to handle in the lab, in relation to spin speeds and adhesion. During spinning, the resist sometimes develop a wavy irregular resist surface along the wafer for a low spin speed (<1500 rpm). In order to achieve tall structures (~100 μm) this needed to be improved into a more reliable protocol. As this was quite unreliable when using a single layer focus was then diverted towards a double coating, which meant that the photoresist

(e.g SU-8 3050) was initially spin coated, soft baked and then second layer of resist (e.g SU-8 3050 again) was applied at either the same, higher or lower speed depending on the required height for the structures (see Table 5). This double layer approach reduced the incidence of wavy surfaces and helped obtain smooth layers of photoresist. The methods used for fabricating the structures in SU-8 were adopted and slightly modified versions from various publications discussing multilayered SU-8 fabrication (del Campo 2007, Sato 2006).

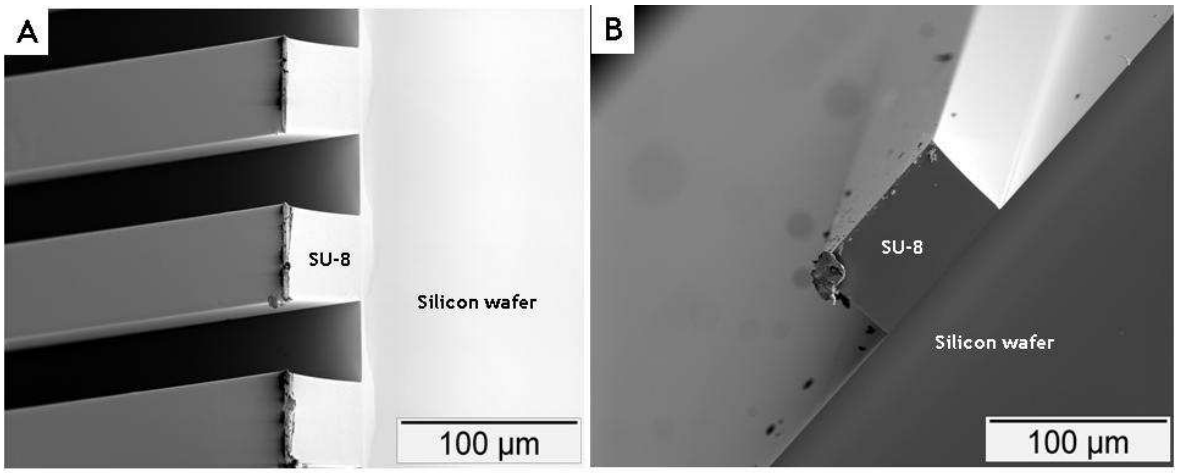

Figure 25: SU-8 photoresist exposure SEM images.
A) This SEM image shows the inverted 'V' shaped wall irregularities due to improper exposure of SU-8 (serpentine channels, ht ~58 µm width intended to be 50 µm) B) This SEM image shows the straight walls developed due to optimized conditions of exposure times (inlet channel for seeding, ht ~ 58 µm and width 100 µm).

The silicon masters had SU-8 features on top, which were used as molds to cast PDMS replicates to form the microfluidic devices. PDMS has a good reputation for rapid prototyping of microfluidic device, as sealing is easily achieved using an air, or oxygen plasma etch. Also PDMS is gas permeable, biocompatible, and transparent even in the UV range (Leclerc 2004, Kallio 2006, Lee 2003, McDonald 2000, Sia 2003). This makes it an attractive choice for cell culture devices. The devices were bonded to glass coverslips and used for their specific purposes. The single cell culture well was designed to observe cell behaviour inside devices and establish a basis for long-term cell culture analysis.

When dealing with long-term cultures several parameters had to be considered in order to improve cell proliferation within the PDMS microchannels. For example, the sterile working conditions inside microchannels, sufficient supply of nutrients and gases to cells and most of all flow conditions with a minimum of fluid shear. Inside microfluidic channels, adherent cells often face the risks of being exposed to mechanical forces exerted

by fluid motion or gas bubbles, therefore having to deal with shear stresses (Walker 2004). The fluid motion is however necessary for the replenishment of nutrients and waste removal. [Shear stress is experienced by cells when a tangential force is applied across its surface and a variety of different cell types experience varying amounts of shear under physiological conditions (Lu 2004, White 2007, Korin 2007, 2009, Frangos 1988)]. As explained by Leclerc et al. (2006) mouse osteoblastic cells were successfully cultured for long periods (>7 days) at shear stress rates of 5 mPa in a microfluidic environment but the same cells failed to proliferate at a shear of 35mPa. However, osteoblastic cells endure shear stresses of about 600 – 3000 mPa under physiological conditions (Leclerc 2006). In the single cell culture system, (explained in this Chapter) fluid shear was applied to fibroblasts, as well as lung- and kidney-epithelial cells. These cells in their respective physiological conditions are also exposed to shear stress but this can be very different from that experienced by osteoblastic cells and hence their endurance to shear stress may be different (Leclerc 2004, Leclerc 2006, Korin 2007). The single cell culture device used for maintaining hTert fibroblast and Calu-3 cells, had a calculated shear stress value of 1.2 mPa experienced inside the cell culture well region (at the broadest part of the chamber, for a flow rate of 1 µl/min having a velocity of 0.4×10^{-3} mm/sec). The shear stress calculated at the inlet/outlet channel points was about 30mPa. This device, therefore had shear stress conditions favourable for cell culture over long periods of time, suggested through literature (Korin 2007, Leclerc 2004). The shear stress levels that were permissive for long-term culture of human fibroblast cells within microfluidic channels, was in the range of 5-20 mPa (Korin 2007). For the Calu-3 cells however there were no existing data in the literature about their resistance to fluid shear. Therefore Calu-3 cell proliferation was tested inside the single channel devices using the same flow regime as that successfully used for culturing the fibroblast cells.

The other device discussed in this chapter is the Christmas tree/serpentine concentration gradient generator that was used to produce chemical gradients of fluorescent dyes and pH of solutions. This device was a slight alteration of the work presented by Dertinger et al. (2001) and Joen et al. (2000). The main purpose for this device was two-fold: In the context of the work presented in Section 2.2.3, the serial dilution of nanoparticles in a defined reliable, and predictable way was the intended application for this gradient generator, which served as a demonstrator, at the same time this device was intended to be used for LbL deposition of PEs to study cell haptotaxis. Similar microfluidic devices had been shown to be useful in the study of cell chemotaxis and seemed to offer an avenue for LbL techniques (Agrawal 2008, Lin 2005, Jeon 2002, Gunawan 2006). Similarly to LBL

there were other applications in mind for this device. One of them which was creating gradients in concentration for cytotoxicity testing, for example like the device shown by Tirella et al (2008). They used the gradient device for the purpose of testing commonly used anesthetic solutions against myoblast cells. Such studies proved that concentration gradient mixers had a potential use in nanoparticle toxicity testing too. The gradient device shown in this chapter was to be used in conjunction with cell culture and designed for the sole purpose of understanding and realising their potential for different applications within cell biology. Therefore, the next step was to integrate such a system with cell cultures similar in working to devices presented by Hung et al, (2005). Their device showed the successful use of such gradient devices connected to an area of cell culture wells within the same system.

2.4 Conclusion

The main focus for this chapter was to establish the basis for the fabrication, cell culture and working of certain microfluidic device channels. The work here had shown that the control of cultures over long periods of time was possible within the single cell culture devices. Also, the fabrication of these microfluidic devices using SU-8 and PDMS had proven to be a valuable method for the rapid prototyping of microfluidic devices. It was evident that the flow rates to be used with such a device were approximately between 0.5-1µl/min which resulted in very low rate of shear within the system. Therefore, it was also possible to use this device for long-term cultures. This was vital in the case of the Calu-3 cells at least, since these cells needed much longer culture times as compared to the fibroblasts. When developing complex gradient mixer devices the results showed that a good profile for mixing was achieved at very low flow rates (~0.025µl/min). Such a device could prove to be a valuable tool for cell and tissue engineering.

These results were carried forward when developing the final set of multilayered devices, which would be explained in the next two chapters. Therefore, the next stage (Chapter 3 and 4) focuses on up-scaling the single cell culture device and used in combination with microfabricated silicon nitride membranes. These nitride membranes in the following Chapter were tested for their cell compatibility and compatibility inside a multilayered microfluidic design. The gradient mixers on the other hand, were incorporated within such multilayered devices in Chapter 4 and designed to serve the purpose of combining cell cultures with different dilutions of test solutions.

Chapter 3 : Optimisation of cell culture conditions on silicon nitride membranes

3 Introduction

Under normal physiological conditions the tracheal, bronchial and alveolar lung epithelia come constantly in contact with the air during the process of breathing. The bronchial and alveolar epithelia are responsible for blocking unwanted harmful materials, example small particles and air borne pathogens present in the air, from entering the blood stream and vital organs of the body (Gardner 1993, Cohen 1975). These epithelia show the capacity to selectively transport gases and solutes between the two compartments (lung alveolar and blood capillaries). The transport mechanism is made selective by tight junctions between adjacent epithelial cells, which form this barrier. Tight junctions are virtually impermeable to large molecular weight tracers and thus solutes and nutrients have to be transported either paracellular or transcellular (Chiba 2007, Gonzalez-Mariscal 2003). Epithelial tight junctions can either be classified as 'tight' barriers or 'leaky' barriers according to their physiological function (Schneeberger 1992). This means that different organs can have different junctional properties, for example the tight-junctions of the urinary bladder epithelium are extremely tight, but tight-junctions in the epithelium of the renal proximal tubule are leaky. Whereas the former example requires an absolute seal the later sits at an important site for osmoregulation requiring more transport (Schneeberger 1992). The specific functional requirements of the lung-blood barrier, that it should allow selective transport of gases and solutes provided a promising new route for drug delivery and biomedical application (Forbes 2005, Taylor 1965, Piiper 1971). The development of safe and effective drugs administered via the lungs, however, requires a good understanding of the selective transport mechanisms in the respiratory air-blood barrier. The development of *in-vitro* and *in-vivo* systems has helped to assess the rate of translocation or the way in which selective transport occurs across the air-blood barrier. For example, the integrity of epithelial tissue barriers can be analysed through *in vivo* methods using radioactive/toxic solutes, by exposing either whole animals or specific sites (such as can be achieved by intratracheal, oropharyngeal, endotracheal exposure) (Geys 2008, De Boeck 2003, Warheit 1997, Warheit 1988, Bryce 2008, Oberdorster 2002, Wong 2007). Measuring the integrity of the epithelial tight junctions is also possible via electrical measurement systems, such as the plythesmograph, which is a non-invasive method for whole body experiments or for specific body parts that monitors changes in the electrical impedance of the test tissue epithelium, due to changes in the volume of air or blood inside specific organs. (Vanoirbeek 2004, Yamamoto 1992, Babu 1990).

For tissue culture models of the epithelial barrier *in vitro,* the tightness of the cell monolayer has been assessed using either the diffusion of marker solutes (radioactive, or fluorescent molecules with known size and charges) or systems that measure TEER (see Section 1.5.2 from Chapter 1) an inherent property of cell monolayers with well developed tight junctions (Hediger 2002, Geys 2006, Geys 2007, Nemmar 2006, Nemmar 2002, Manford 2005, Matilainen 2007). There are several cell lines available that are being used as models of the lung epithelial barrier *in vitro*: e.g. Calu-3 (human bronchial epithelial type II airway adenocarcinoma cells) and 16HBE14o (human bronchial epithelial cell lines) (Manford 2005, Forbes 2003, Florea 2003, Mathia 2002), hAEpC and A549 (the human alveolar cell lines) (Forbes 2005, Geys 2007). These cell lines have been used in drug delivery and nanoparticle toxicity experiments. The most commonly used cell model of these are the Calu-3 cells (Foster 2000), they form both excellent tight junction properties and good epithelial barriers (Florea 2003, Fogh 1977, Forbes 2000, Forbes 2005). They were therefore quite an attractive cell line to form the base for developing novel *in vitro* analysis systems.

In most cases the epithelial cells *in vitro* are cultured inside culture well apparatuses consisting of porous polymer Transwell® membrane filters (produced by companies like Corning Costar®, Falcon®, etc). The membrane inserts divide the culture well dish into two compartments, apical and basal. Using the measurement system provided [12], epithelial cell cultures can be classified according to TEER values across the culture substrate-membranes which determines their tightness and integrity. The TEER for such an apparatus, is measured using a pair of electrodes generating an alternating current (AC) (mainly to prevent accumulation of proteins on the electrode surfaces or electrolysis of solutions) which is applied across the epithelial cell layer and another pair of electrodes detect the corresponding voltage drop in the system on account of the resistance created by the monolayer of cells. The apparatus for measuring these TEER values is based on the 4-point probe method and uses silver and silver-chloride electrodes (the significance of the 4-point sensing system and the difference between using a 2-point and 4-point system is explained in Section 1.5.2, Chapter 1)(The apparatus for measuring the TEER is described in Chapter 3 [12]). The setup used for this project was similar in working to the electrical

[12] EVOM™ commercialised by World Precision Instruments Inc., was one of the first instruments developed for measuring TEER. This was normally used in combination with transwell cell culture polymer membranes and the STX2 electrodes (pair of double electrodes, 4 mm wide and 1 mm thick, each consisting of an electrode pair of a silver/silver-chloride pellet for measuring voltage and a silver electrode for passing current).

setups shown in the PhD thesis of Hediger (2002). This sort of system measured the total resistance of the cell-covered culture-membrane.

Hediger (2002), in his PhD thesis highlighted the advantages of miniaturised and automated systems for the purpose of cell monolayer TEER analysis and suggested that such systems could prove to be a valuable tool for testing various epithelial barrier functions. Hediger (2002) presented a device consisting of polycarbonate micro/nano-porous membrane sandwiched between two silicon or glass chips and the measurement system consited of platinum or Ag/AgCl electrodes (Using the 4-point probe setup). The device presented by Herdiger (2002) maintained and measured epithelial barriers for MDCK cells. This device setup gave a valuable insight on the development of miniaturised systems.

This Chapter describes the cell culture protocols developed for Calu-3 cells cultured on silicon nitride membranes and the use of FITC dextrans to test the leakiness of cell monolayers in combination with TEER measurements. Polymer membranes used through literature (explained above) are quite thick (>5 µm), hence, focus for this project was shifted towards fabricating thin, ~500 nm, silicon nitride membrane chips that would better relate to lung barrier systems under true physiological conditions (lung epithelial barriers range from approximately 500 – 600 nm thick). Thin films of silicon nitride are often used in the semiconductor industry as passivation layers for integrated circuits. This material however, has recently gained importance for its application within biology [blood-brain barrier (Ma 2005) and liver-blood barrier (Zhang 2008)]. The use of such membranes to study barrier functions for lung epithelial cell (Calu-3) is not evident through literature and culture conditions with measured TEER values for these cells on silicon nitride membranes were also absent. These results for the micro-scale system were compared to the commercially existent macro-scale Transwell membrane system. Such a micro-scale setup with the combination of the lung epithelial cells (Calu-3), the silicon nitride membranes and the TEER measurement system could prove to be a very useful tool in biology, both for fundamental research and clinical diagnostics.

3.1 Materials and methods

3.1.1 Silicon nitride membrane fabrication (CSEM, Neuchatel, Switzerland)

The fabrication steps for the silicon nitride membranes are explained in Figure 26. The silicon wafer was cleaned using a Piranha solution (3:1 v/v of concentrated H_2SO_4 to H_2O_2) at 120 °C for 30 min. The cleaned wafers were coated with a 500nm layer of Si_3N_4 using a low-pressure chemical vapor deposition (LPCVD) technique. The wafer was then spin-coated with an AZ7220 photoresist (EVG 101 Advanced Spray Coating System, St. Florian am Inn, Austria), exposed under UV light for 5 seconds by a manual precision alignment system (mask aligner) and exposed using a standard photolithography mask definining the opening of the well and the pores. The resist was developed in AZ300MK developer (made up of Tetramethylammonium hydroxide 2% vol/vol in water) (ChemTrec, Arizona). The developed features were etched by ICP Dielectric Etching System (Adixen AMS 100, Annecy, France). The residual AZ7220 photoresist was removed by immersing the wafers in n-methylpyrolidone (NMP) solution and sonicating them at 70 C for 30 min. After rinsing with deionized (DI) water and drying with nitrogen, the same process was repeated on the other side of the wafer and had a new mask to define the pattern in silicon nitride on the backside of the wafer to finaly produce the silicon etching zones for back etching. Finally, the porous Si_3N_4 membranes were developed after the back-etching of the silicon wafer using with potassium hydroxide (KOH) at 90°C for 7–8 hr, where the KOH etches the silicon around the Si_3N_4 (forming the trench/seeding well).

The membranes were designed in a way that would best fit the purpose of the different experiement (like, for static conditions and microfluidic device conditions explained along the course of this Chapter). The initial set of membranes were developed for cell compatibility experiments Figure 27, A) and a). The membrane chips were fabricated to bear an array of membranes, either 5x5 array (membrane area 1.5 mm^2) or 9x9 array (membrane area 1 mm^2). The membrane arrays allowed several cell culture experiments in parallel. Since the Si_3N_4 membranes were meant to be used inside a microfluidic device, the membrane arrangement needed to be slightly altered to best fit their respective device design. The membrane chip designs were modified to be compatible with the single cell culture multilayered device layout. Figure 27 B) and b) have one membrane (1 mm^2) in the centre of the chip. Figure 27 C) and c) showed the design for the five adjacent membrane layout, which allowed for five different experiments to be performed in parallel. The advantage of having such a layout was that there was enough spacing between the adjacent

membranes to be to use them separately as compared to the arrayed layout (which was more complicated to separate from sample to sample) due to closely packed membranes.

The main area of focus for these membrane chips was to develop an automated system to test the TEER of epithelial monolayers. In order to achieve these resistance measurements, electrodes were fabricated around the membrane areas within the chips (shown in Figure 28). These electrodes were prepared using metal deposition, where a 100 nm layer was deposited onto the surface of the silicon chips. The metal surrounding the electrodes was wet etched (Aqua regia HCl:HNO_3::3:1 (vol/vol), etch rate 25-50 µm/min) leaving the electrodes on top of the silicon chip. The membrane chip design and fabrication were all performed by our collaborators at CSEM in Neuchatel, Switzerland. The people involved in this project at the CSEM were Drs Martha Liley, Thomas Overoltz, Philippe Neidermann, Melanie Favre and Nicholas Blondeux.

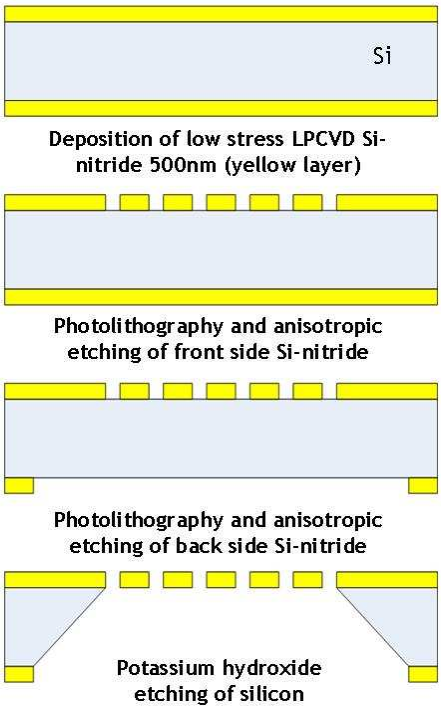

Figure 26: Schematic representation of the fabrication method for silicon nitride membranes.
Silicon nitride membrane fabrication steps presented in this image; Silicon (Si) (blue), Silicon nitride (yellow) had 500nm thickness. The process from the first step of deposition of silicon nitride on the silicon wafer until the final back etch of silicon to finally reveal the nitride membrane structures were shown from top to bottom.

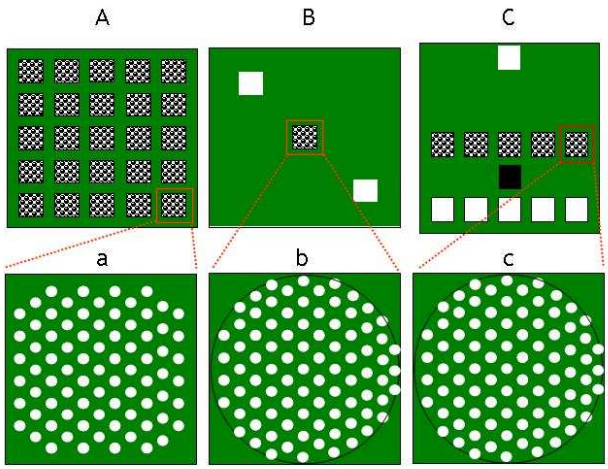

Figure 27: different membrane layouts
A) This was the initial silicon nitride membrane array chip design used for cell culture optimisation protocols and consisted of either a 5x5 membrane layout (membrane area 1.5 mm^2) or a 9x9 membrane layout (membrane area 1 mm^2 and the chip was ~15 x 15 mm). The magnified design of the membrane was shown in a). B) This was the design layout of the membranes to fit the single culture well device, (membrane area 1 mm^2 and chip was ~15 x 15 mm). The magnified image shown in b) where the pores were oriented such that they formed a circular perimeter leaving the corners with no pores. C) This five adjacent membrane layout was fabricated to allow for five different experiments to be performed in parallel on one chip. The magnified image was shown in c) (membrane was 1 mm^2 and chips were ~20 x 20 mm). (The black and white checkered squares in A), B) and C) represent the membrane area. The white squares represented holes in the silicon chip and were meant to connect the bottom microfluidic channels. The black square is the observation zone for the microchannels). All membranes pore sizes of 1 µm diameter (pore fill rate was 5% and the pore period 4.2 µm) [Please also see SEM images in Figure 35]

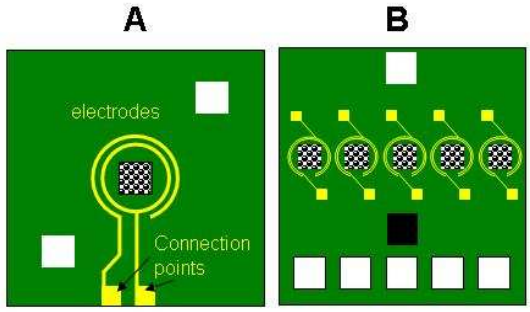

Figure 28: Electrodes for measuring TEER.
A) This represented the single membrane chip (membrane area was the black & white checkered squares) and a pair of platinum electrodes (yellow) on the top and bottom side of the chip (total area was ~15 x 15 mm). [The white squares represented holes in the silicon chip which were meant for connecting the bottom layer microfluidic channels when used in the multilayered device setup]. This single chip was used for the initial experiments to test the principle of the system and circuitry. B) This represented the five membrane chip (membranes were the black & white chessboard) which was designed to perform a set of five experiments in parallel (total area 20 x 20 mm). [The white squares represented holes in the silicon chip and were meant to connect the bottom microfluidic channels. The black square is the observation zone for the microchannels.

3.1.2 Cell culture

The Calu-3 cells used for cell culture experiments were maintained in culture conditions (explained in detail in 2.1.3 from Chapter 2) and prepared for seeding onto Transwell membranes or silicon nitride membranes.

3.1.2.1 Cell seeding onto polymer Transwell® membrane inserts

The Transwell membrane inserts [kept inside a sterile 24 or 12 Tissue culture plastics (TCP) well plate] were initially they were immersed in EMEM medium (when using Calu-3 cells) for 5 min. The medium was removed and a solution of collagen was slowly pipetted on the apical side of the membranes. The inserts were allowed to incubate at 37°C for 1 hr prior to cell seeding (preparation of the collagen solution was described in Chapter 2: Section 2.1.4.3 ECM protein coating). After incubation the insert membranes were rinsed with HEPES buffer solution and then left immersed in EMEM medium until cells were ready to be seeded (approximately 15-20 mins). Cells were seeded onto clear transwell polyester inserts of 0.33 cm^2 area (Costar, Cole Parmer and Fisher scientific), with pores of either 0.4 µm or 3 µm diameter. The Calu-3 were cultured in EMEM medium and supplemented with 15 % foetal bovine serum and 2 % antibiotic mixture [13]. The cell monolayer was examined optically and monolayer integrity was monitored using the TEER setup (EVOM® with the STX2 electrodes setup [12]).

3.1.2.2 Cell seeding onto porous silicon nitride membranes

Cell seeding onto silicon nitride was performed via two methods, as illustrated in Figure 29. Either a plastic holder to support the membranes (Figure 28, A) or using PDMS wells to support the silicon chip and placed on the apical side of the chip to confine cells to the membrane area (Figure 28, B). The plastic holder was mainly used as a support for the silicon nitride membrane chips to prevent the bottom side from touching the surface of the cell culture wells (since the membranes themselves were extremely delicate). The use of the PDMS support wells created an apical compartment and a basal compartment for the silicon nitride membranes, which proved to be useful when performing FITC-dextran diffusion experiments. Each different membrane design had a specific set of PDMS wells developed for this very purpose. The PDMS wells were prepared by pouring the PDMS

[13] Antibiotic mixture as shown in Chapter 2, Section 2.1.3. Cell Seeding, Calu-3 cells.

mixture [14] into a Petri dish to approximately 1/4 th the depth and left to solidify at 80ºC inside an oven for approximately 60 min. Then, using a scalpel, the PDMS sheet was cut to fit the membrane containing devices (ca. ~ 20 x 20 mm for the five well membrane chip and ~15 x 15 mm for the single membrane chip and the 9 x 9 or 5 x 5 array membranes chip) (Figure 30). To create wells for cell culture holes of 4 mm diameter were punched into the PDMS using a hole punch. These PDMS sheets were sterilised in 70% ethanol and left to dry. At this point, silicon nitride membrane chips were washed with acetone, propan-2-ol and ethanol in a series of wash steps (Only if membrane chips were re-used after one set of cell culture experiments, they were immersed in Pirahna acid solution (included 3 parts H_2SO_4 , 1 part H_2O_2) for 30 min). They were left to dry inside a sterile environment flow cabinet until they sandwiched between two PDMS sheets (placed on either side of a silicon nitride membrane chips). These devices were dried for 30 minutes in an oven at 60ºC for 15-20 min and then exposed to an air plasma cleaner (on high power - 740 V, 40 mA and 29.6 W, Harrick plasma machine, for 30 sec;) to make the membrane surfaces and the PDMS slightly hydrophilic and wettable (Ye 2006, Mukhopadhyay 2007, Arafat 2004, 2007). [The preparation of microfluidic devices also included this step to ensure a good bond between the chip and the PDMS microchannels]. Prior to cell seeding, membrane surrounded by the PDMS wells were rinsed once again with 70% ethanol, and then rinsed with HEPES buffer twice. The nitride membranes were coated with a ECM protein solution of either, collagen (preparation of the collagen solution was described in Chapter 2: Section 2.1.4.3 ECM protein coating) or fibronectin (sigma)(1:20 vol:vol, in HEPES buffer), and a polypeptide solution, poly-l-lysine (1:20 solution vol/vol in HEPES buffer)(sigma) for 1 hour prior to cell seeding. They were then rinsed in a HEPES buffer solution and left in EMEM medium (~40 µl of medium fill up the wells of this device) (15% FBS) until cells were ready to be seeded (approximately 15-20 mins). The culture medium was changed every 12- 24 hrs [15].

It was a lot less complicated to setup the silicon nitride membrane chips using the plastic holders compared to using the PDMS wells. The silicon nitride membranes were cleaned as described above and exposed to air plasma. They were then placed on top of sterilised plastic supports (designed specially for these chips) and sterilised using 70% ethanol. The membrane-chips were rinsed with a solution of HEPES buffer, coated with the respective

[14] PDMS mixture was prepared as explained in detail in Chapter 2, Section 2.1.2. Microfluidic devices using PDMS.

[15] These experiments were performed under static conditions (there was no continuous fluid flow) unless mentioned otherwise

ECM or polypeptide as described above, and the entire setup left in EMEM medium (15% FBS) until cells were ready to be seeded (approximately 15-20 mins). Cell culture medium was substituted every day when using both these setups.

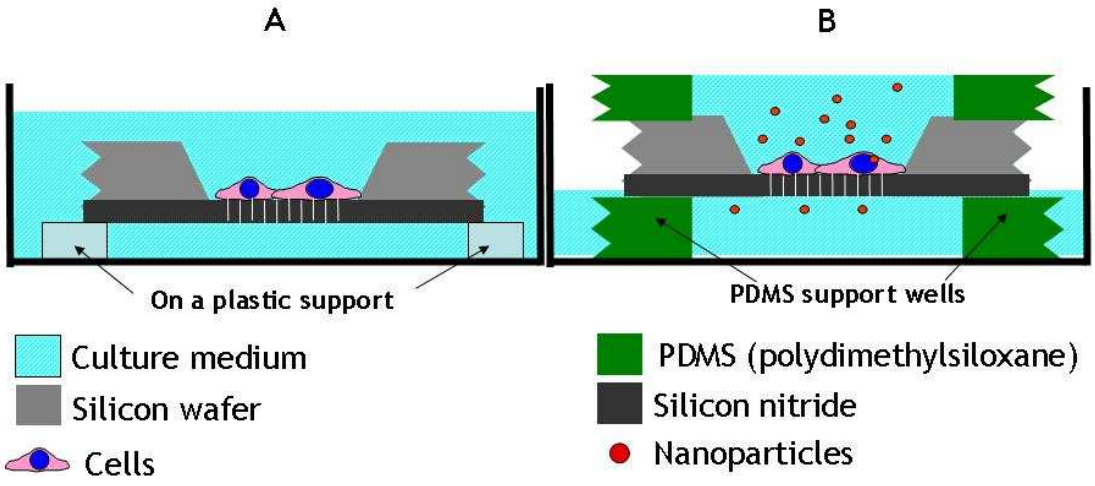

Figure 29: Seeding techniques adopted for our silicon nitride membranes
A) Using plastic holders to support the membranes and B) Using PDMS wells to support the membranes.

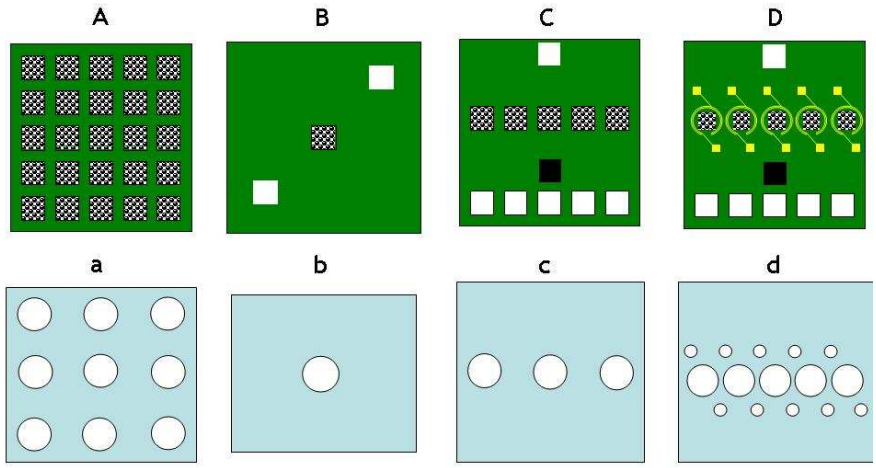

Figure 30: PDMS (Polydimethylsiloxane) constructs for silicon nitride membranes
A), B), C) and D) represent the various layouts used for silicon nitride membrane chips (green) during the course of this thesis project. a), b), c) and d) are the PDMS sheets (blue) with wells (white circles) punched in to fit the layout of their respective membranes. (the black and white checkered squares in A), B) C) and D) are the silicon nitride membranes).

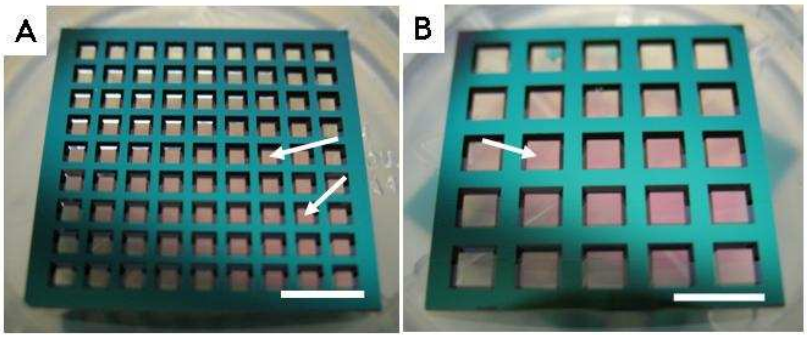

Figure 31: The different membrane sizes used for cell culture experiments.
A) The 1 mm^2 (9x9 array) membrane structures in each trench. B) the 1.5mm^2 (5x5 array) membrane structures. (Scale bars 3 mm)

3.1.2.3 Single cell culture well multilayered microfluidic device bearing the silicon nitride membranes

This multilayered device was prepared by bonding a pair of single cell culture PDMS microchannels (described in Chapter 2: section 2.1.2.2) to either side of a single membrane chip (design described in section Figure 27: different membrane layouts). The resultant multilayered device was sterilised by a series of washes with ethanol, water, HEPES saline solution and finally with culture medium (described in Chapter 2: 2.1.4), introduced through the inlet channels of the top and bottom layers at a set flow rate (10 µl/min). (Devices were prepared with and without collagen step, to test the difference of having surface coating). Cells were seeded (preparation explained in Chapter 2: 2.1.4.4) into the top layer membrane area of the multilayered device. The connection through the top layer microfluidic inlet channels (TI) (Figure 32) by gently inserting them through (similar to cell seeding methods described in Chapter 2: 2.1.4.4), with the help a syringe and allowing them to settle for approximately 4-6hrs inside the incubator (at 37°C), before beginning the perfusion of culture medium. The fluid in the top and bottom channels were allowed to flow at 1 µl/min. (The connectors and device parts were described in Chapter 2: 2.1.2). The cells were maintained for a period of 4-5days inside this device device on the nitride membranes or until they were confluent.

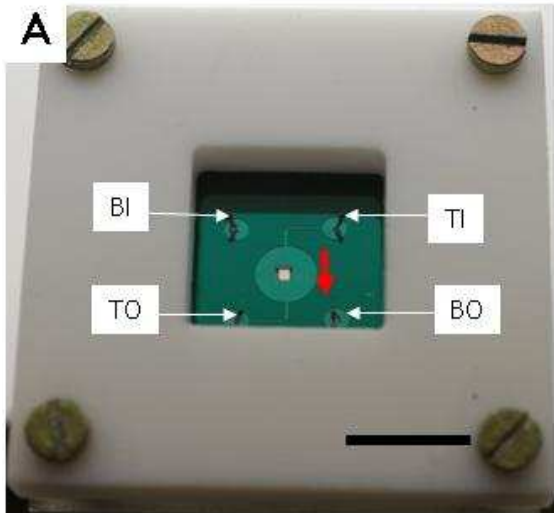

Figure 32: Single cell culture well multilayered microfluidic device.
This image shows the single cell culture well microchannels used with the silicon nitride membranes. The silicon chip is sandwiched between two PDMS microchannels and held together inside the device clamp. The device consists of a top microchannel and a bottom microchannel and the fluid is introduced through the inlets and outlets (Top inlet – TI, top outlet – TO, bottom inlet – BI, bottom outlet – BO). The red arrow marked the direction of fluid flow.

3.1.2.4 Cell confluency measurements on the silicon nitride membranes

The cell coverage area on the silicon nitride membranes during was measured using Adobe Photoshop's magnetic lasso tool. As shown in Figure 33, the cell area was calculated by selecting the cell-covered areas and comparing it to the total surface area of the membranes.

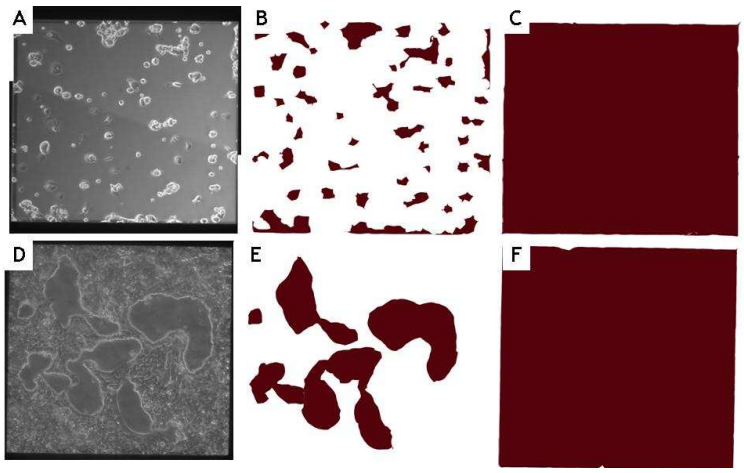

Figure 33: Calculating the cell coverage area
A) This image was of a collagen coated sample observed at day 1 after seeding. B) To measure the area of the membrane covered by the cells, the magnetic lasso tool was used to draw around a cell cluster. In this image the areas marked were the cell covered areas. (15% cell coverage) C) This was a picture with the membrane area filled. D) After 5 days in culture the cells in (A) grew and multiplied to form the clusters seen E) In this image the area not covered by the cells was marked to simplify the calculation of area covered by the cells. (78%) F) Image of the membrane area used to calculate the area covered by the cells.

3.1.3 Immunocytochemistry

Cells were fixed using a fixative solution (PBS containing 4% formaldehyde (v/v) and 200 mM sucrose) for 15 minutes. The fixative was removed and a permeabilisation buffer (PBS containing 300 mM sucrose, 50 mM NaCl, 3 mM $MgCl_2 \cdot 6H_2O$, 20 mM HEPES, 0.5% Triton X 100, pH 7.2), which was added to the samples and kept at 4°C for 5 minutes. The permeabilisation buffer was removed and blocking buffer (1% bovine serum albumin (BSA) (wt/vol) in PBS) added for 5 minutes at 37ºC. The PBS/BSA was then removed and the primary antibody (2% ZO-1 N- term rabbit or Occludin N- term rabbit (vol/vol), 2% Oregon green-phalloidin (vol/vol) – (Invitrogen), 1% methanol (vol/vol) in PBS) added and left for an hour in the dark at 37ºC. The antibody was then removed and the sample washed 3 times for 5 minutes with 0.5% Tween 20 (vol/vol) in PBS. Finally, the cell nuclei were stained using DAPI contained in the mounting medium (Vectashield, Vector Labs).

3.1.4 Electron microscopy sample processing

The cells were fixed with 1.5% glutaraldehyde (Sigma, UK) buffered in 0.1 mM sodium cacodylate (Agar, UK) (4 ºC, 1 hr). The cells were then post-fixed in 1% osmium tetroxide for 1 hr (Agar, UK) and 1% tannic acid (Agar, UK) was used as a mordant. Samples were dehydrated through a series of alcohol concentrations (20%, 30%, 40%, 50%, 60% and 70%), stained in 0.5% uranyl acetate, and followed by further dehydration (90%, 96% and 100% alcohol). The final dehydration was in hexamethyl-disilasane (Sigma, UK), followed by air-drying. Once dry, the samples were sputter coated with gold-paladium before examination in the scanning electron microscope (SEM) (Digital SEM 6400).

3.1.5 Translocation studies

3.1.5.1 Translocation method using FITC-dextrans with polymer Transwell® membrane supports

Once the cells reached a high TEER value, the culture medium was removed from both the apical and basal compartments and membranes were washed with PBS [16]. Then a volume (250 µl) of FITC-dextran MEM[17] was added to the apical compartment. The same MEM

[16] PBS was prepared in the same way as explained in Chapter 2 (Wash steps for sterilising devices)

[17] 1 mM solution of either 2000 kDa, 500 kDa, 70 kDa or 4 kDa FITC-dextran (Sigma) dissolved in colour-less MEM (with non-essential amino acids and antibiotics and excluding phenol red) (Invitrogen)

culture medium, but without the dextrans was added to the basal compartment (ratio of the volume in apical compartment v/s the volume in basal compartment was either 1 **:** 1 or 1 **:** 2). The membranes were left for about 60 mins in a CO_2 incubator (5% CO_2, 37ºC) to test for any diffusing FITC-dextrans molecules. After incubation, the apical and the basal solutions were each collected inside a 1.5 ml Eppendorf tube. The collected samples were measured for their fluorescence intensities using a fluorescent plate reader (Fluorescent spectrophotometer, Envision)[18]. The fluorescent measurement readings taken for each sample in the plate reader were represented by a standard reading unit known as the 'relative fluorescence unit (RFU)'. [The RFU reading for each apical compartment solution (A)(consisting of the test dye solution) was subtracted by the RFU reading for plain MEM solution (M)(no dye). Therefore the final apical RFU (A_f) = A – M. The RFU reading for the basal compartment solution (B)(translocated dye sample) was subtracted by the RFU reading for the plain MEM (M)(no dye). Therefore the final basal RFU (B_f) = B – M. The percentage of translocation across the membrane (T) = A_f/B_f * 100].

3.1.5.2 Translocation method using FITC-dextran particles with silicon nitride membranes.

The collection of the apical and basal fluid, from silicon nitride membrane static culture devices, for translocation experiments were slightly different compared to the Transwell inserts (since the volume of liquid collected from the silicon nitride devices was 40µl as compared to the 250 µl for the transwell supports). Once the cells reached a high degree of confluence (100%) on the membranes (this was observed under the microscope), the culture medium was removed from both the apical and basal compartments and washed with PBS. Then the device was turned over and a volume (40µl) of plain MEM was added into the basal compartment. The basal compartment was then capped using a thin sheet of PDMS (this managed to seal and hold the liquid inside due to surface tension, when the device was inverted again). Then a volume (40 µl) of FITC-dextran MEM[17] was added to the apical compartment. The device was then left for 60mins in a CO_2 incubator (5% CO_2, 37ºC). The solutions were collected, from the apical and basal wells, in an Eppendorf tube and their fluorescence intensity measured using the same intensities and filter mentioned for the Transwell supports.

[18] The Fluorescent plate reader was set to measure using a 480/485 nm wavelength excitation filter and 535 nm wavelength emission filter for FITC-dextran particles.

3.1.6 Measuring the integrity of cell monolayers

3.1.6.1 TEER measurement method for measuring cell monolayer TEER on polymer Transwell® inserts

TEER was measured using an EVOM system (volt-ohmmeter[19] supplied with STX 2 electrodes. (World precision instruments, WPI). Measurements were made 10-20 mins after refreshing the culture medium (any debri/dead cells would removed from the cultures). The resistance of a cell-free transwell insert was subtracted from the resistance measured across each cell monolayer to yield the TEER of the cell monolayer. This value was then multiplied by the surface area of the membrane to give the TEER value. In this case polyester inserts of 0.33cm^2 (6.5 mm), with pores of either 0.4µm or 3µm diameter were used.

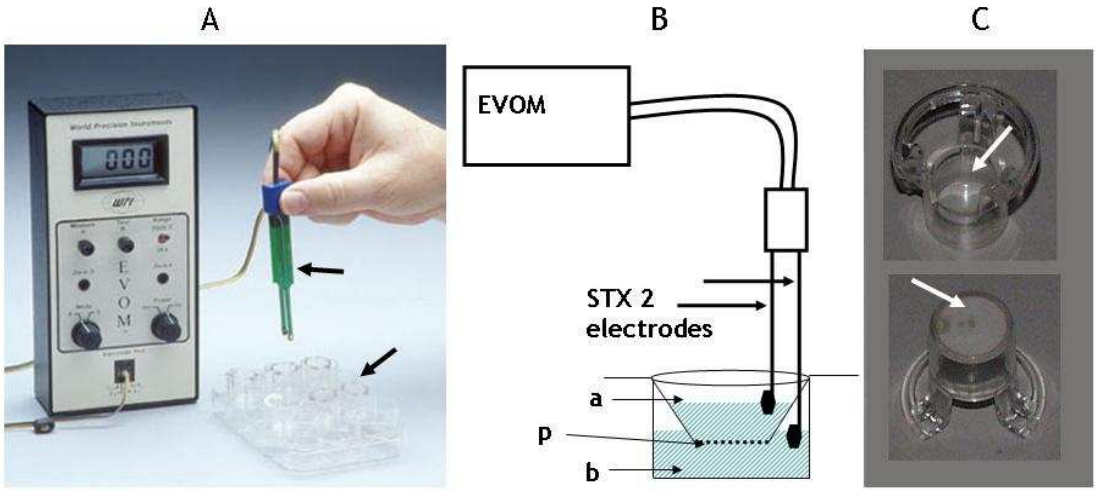

Figure 34: EVOM setup with the transwell supports.
A) EVOM system developed by WPI for TEER measurements. (image from WPI website given in the bibliography) B) STX 2 electrodes were immersed into the culture transwell supports to take resistance measurements. (image obtained from the WPI website was modified to fit this explanation). Cells were grown inside the apical compartments (a) on top of the polymer membranes (p). The basal compartment (b) collected the diffusive test solutes. C) These images show the polymer transwell supports that bear the polymer membrane (marked by the whit arrows)(images from WPI website).

3.1.6.2 TEER measurement method developed for measuring cell monolayer TEER on silicon nitride membrane chips

TEER on the the silicon nitride membrane device was measured using two types of setups, designed specifically for the particular device in use. There are two setups explained in this section, the single membrane device setup and the five membrane device setup. The

[19] A volt-ohmmeter is an electronic measuring instrument that combines several measurement functions in one unit, like measuring voltage, current and resistance.

schematic diagram in Figure 35 and the circuit diagram in Figure 36 give an idea of the setup scheme for the single membrane system. (All the designs for the device holder and electrode described in appendices) (Also in Figure 50 and Figure 51). For the single membrane setup the EVOM was used in combination with the specially designed micro-electrodes to read out the TEER measurements. The principle of this technique was to use separate electrodes for the current-injection and the potential measurement, similar to the STX2 electrode system (4-point measurement system in AC). Two wires current injecting wires (I1 and I2) were connected to an AC current source (in this case the EVOM (V1) was used for current injection. I1 was connected to the apical compartment electrodes and I2 was connected to the basal compartment electrodes. The electrodes M1 and M2 were used to make the potential measurements using EVOM (V2) multimeter. In that case, the impedance measured relates directly to the impedance of the solute liquid (and of the cell layer**).** In Figure 35on the right side a current (I) is injected through the system through I1 and I2. This main current is compared to a reference resistance 'Rref' and is measured in V1 by the multimeter. Therefore the current here can be calculated (according to Ohms law) as being I=V1/Rref. On the left side of this figure you find that the current (I), flowing through the system, is measured by M1 and M2 at the multimeter where the recorded change in potential is given as V2. This change in potential is measured in reference to the resistance of the cell monolayer on the membrane, given as Zm. Therefore, the current measured on left side is represented as I= V2/Zm. Taking both sides into consideration the impedance/resistance of the cell monolayer can be represented as Zm=Ref*V2/V1. The circuit diagram shown in Figure 36 shows the connections to the various parts of the device.

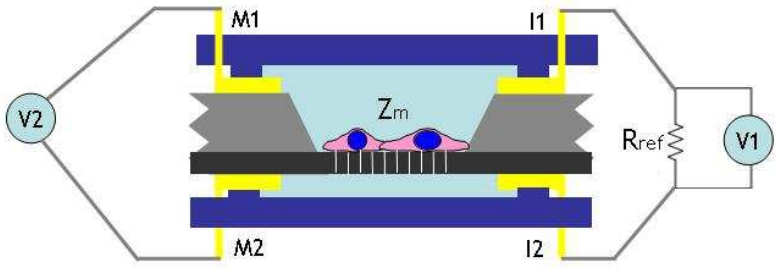

Figure 35: Schematic representation of the measurement system setup for porous silicon nitride membranes
A) Schematic of the electrode connections used for the multilayered silicon nitride device, where I1 and I2 represent the current electrodes and M1 and M2 represent the voltage. I1 and I2 are connected to an AC current source with internal impedance of 'Rref' which is ~1 – 20kΩ. The Z_m is the resultant impedance measured for the cell monolayer.

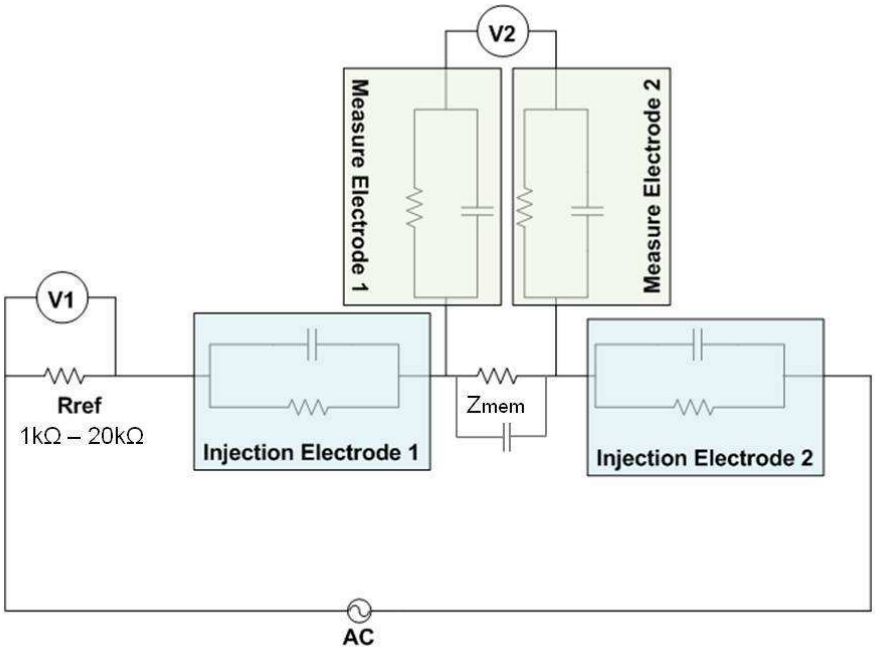

Figure 36: Circuit diagram for the single membrane device
Here 'Z_m' is the resistance measured for the cell monolayer cultured on the silicon nitride membrane. The 'Rref' is the reference internal resistance of the EVOM volt-ohmmeter, which works as the current supplier (AC) (V1) and measures the change in potential when travelling across the cell membrane (V2). There are two current injection electrodes (1 and 2) and two potential measuring electrodes (1 and 2).

The five membrane measurement system was more complex as compared to the single membrane device (device parts, connectors, etc. are shown in the appendices section). The electrodes used for this setup and the design for the membrane chip was very different (Figure 28) as compared to the single membrane chip setup. However, the principle behind the circuit connections were similar to the circuit diagram shown in Figure 35 and Figure 35, for each of the parallel placed membranes on the chip. The electrodes were connected via gold coated electrode connectors. The readings were relayed between each parallel membrane after every 10s interval. The relays were monitored via the Labview software programme through a laptop input. This was meant to measure TEER for five adjacent membrane wells. The five membrane setup consists of two sets of five electrodes each for the current injection I1 and I2 are the main sets of five and each membrane well has its own set of current connector $I1_{w(x)}$ and $I2_{w(x)}$, where x = w1, w2, w3, w4 or w5 depending on the membrane well (w). The voltage measurement (M1 and M2) also has one set for the top compartment and one for the bottom compartment, where each membrane well has its own set of of voltage measurement connectors $M1_{w(x)}$ and $M2_{w(x)}$. Each membrane TEER was measured at every 10 sec interval and each measurement is an average of 100 measurements taken. The resultant TEER is produced through an excel spreadsheet.

3.2 Results

3.2.1 Membranes types: silicon nitride and Transwell® polyester membranes

Silicon nitride membrane chips were fabricated at the CSEM using photolithography and etching techniques. The membrane pores were 1 µm in diameter and the spacing between each pore was 4.2 µm (centre to centre and had a fill factor of 5% in nitride with thickness of 500 nm). The SEM images (Figure 37) showed the pores and the thickness of the membrane. These membranes had a well structured array of pores on the membranes unlike the random orientation of pores found on the Transwell polymer membranes. The transwell inserts had porous polyester membranes and were available in different pore sizes (varying pore diameters). The two polymer nucleopore membranes used in this project had either 0.4 or 3.0 µm diameter pores. The thickness of the membranes as measured from the SEM images in Figure 38 was approximately 5 µm. The pores in the membranes were randomly distributed, and hence some of these pores overlapped with each other resulting in some much larger irregular pores. The pore densities were 4 x 10^6 pores/cm^2 (0.4µm) and 2 x 10^6 pores/cm^2 for the 3.0µm ones respectively (Data sheets for Transwell® membrane supports – Corning).

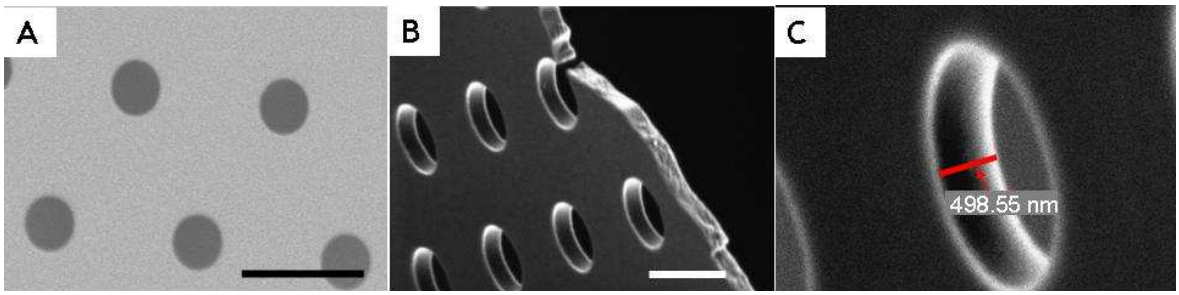

Figure 37: SEM images of the silicon nitride membrane
A) This image shows a top view of the nitride membrane. From the image we can see that the membrane pores diameter is 1 µm and the distance from centre to centre between the each pore is about 4.2 µm. (scale 5 µm) B) This image was taken to determine the thickness of the membranes. (scale 2 µm) C) The thickness of the membranes is 500 nm.

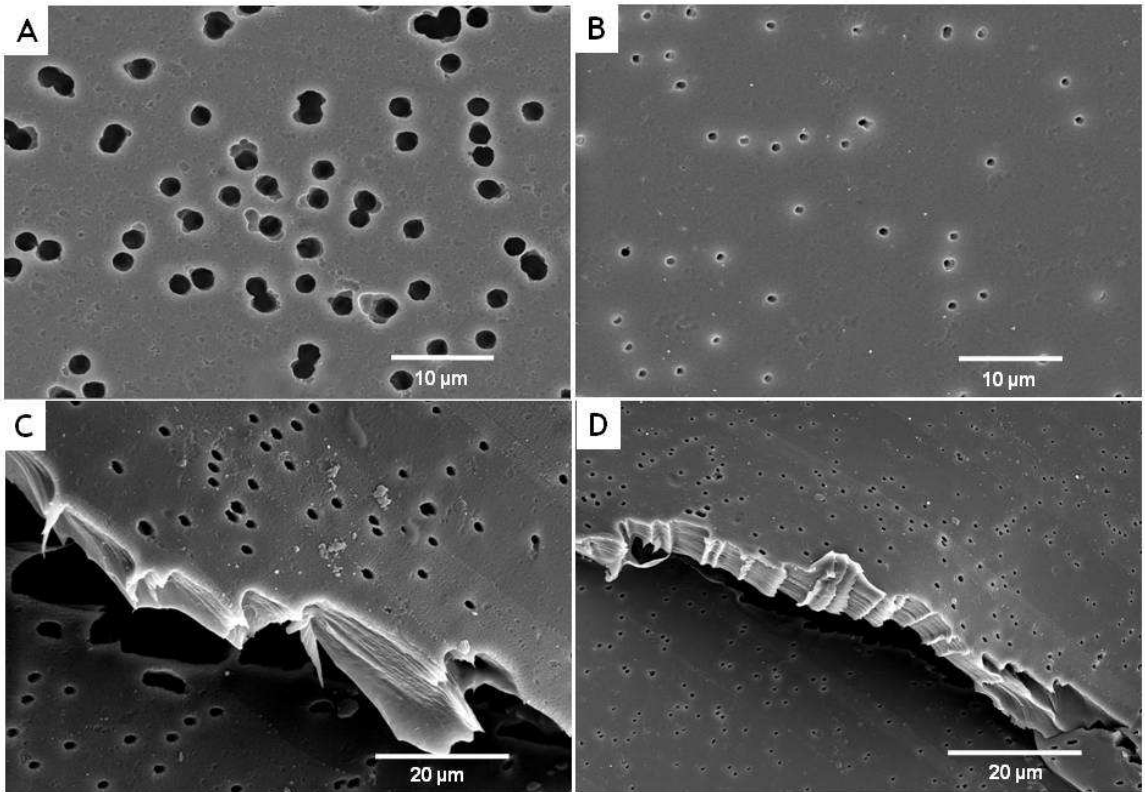

Figure 38: SEM images of the Transwell polymer (polyester) membranes.
A) This SEM image shows a top view of the 3.0µm diameter membranes. (scale 10 µm) B) This showes an SEM image of the 0.4 µm diameter membranes. (scale 10 µm) C) The thickness of the 3.0µm was approximately 5µm, (scale 20 µm) D) thickness of the 0.4µm membranes is about 5 µm (scale 20 µm).

3.2.2 Initial experiments of cell culture inside microfluidic device

Experiments were carried out using the single culture well microfluidic device system, described in the previous chapter, in combination with the silicon chip bearing a single membrane. These tests revealed however that cells failed to attach to and grow on the porous silicon nitride membranes. Figure 39 A, showed the initial setup of the device when put together with the porous membranes and the balling up of cells was observed here at day 1, being maintained inside the device (the observed area was the porous membrane area and held together with PDMS microchannels inside the device holder). It was thought that the surface of the membranes was unfavourable for cell proliferation and therefore the surface properties of these membranes needed to be altered. In order to determine the surface properties contact angle measurements were performed in the same way PhD of Elena Martines (2005). The pictures in Figure 40 shows a contact angle measurement on a porous silicon nitride membrane. The values for contact angle obtained for the membranes same as used for the cell experiments were 88± 3 ° (n = 5, average±SD), on the flat silicon nitride the contact angle was 65±8 ° (n = 5, average±SD). This difference in contact angle between the flat, and the porous membrane could be considered to be due to the missing

surface fraction. The approach developed by Cassie and Baxter (Cassie 1944), suggests that a drop that sits on a composite surface made of air and solid "experiences" a mixed substrate where the relation between the apparent contact angle θ_{ACB} and the ideal angle on a smooth surface of identical chemistry θ_Y (Young's angle) can be described by the following formula:

Eq: $cos\theta_{ACB} = r_f f cos \theta_Y + f - 1$

Where 'r_f' is the roughness [20] factor of the wetted area and 'f' is the area fraction of the projected wet area. The product of the '$r_f f$' is refered to as the solid fraction 'Φs'.

When the contact angle obtained for the flat silicon nitride and the non-pore surface fraction (0.9), as well as the solid fraction (1/0.9) were inserted into this equation the expected angle on the porous silicon nitride membranes was 71 º. The measured contact angle of 88 º corresponds to a missing surface fraction of 40% rather than the 10% that were missing. This discrepancy could be due to the fact that in contrast to many other measurements here the water droplet sits over relatively large pores in a very thin membrane, thus having direct contact to non-water-vapour-saturated air on the other side of the membrane. In measurements of contact angles on rough surfaces the substrate pores/missing surface fraction is in most cases limited in depth, thus allowing the substrate pores to equilibrate and thus be filled with air saturated with water vapour, this can happen very fast as in most cases the surface pores are very small indeed.

[20] The roughness factor of a surface is the ratio: $r_f = A_r/A_g$ where A_r is the real (true, actual) surface (interface) area and A_g is the geometric surface (interface) area.

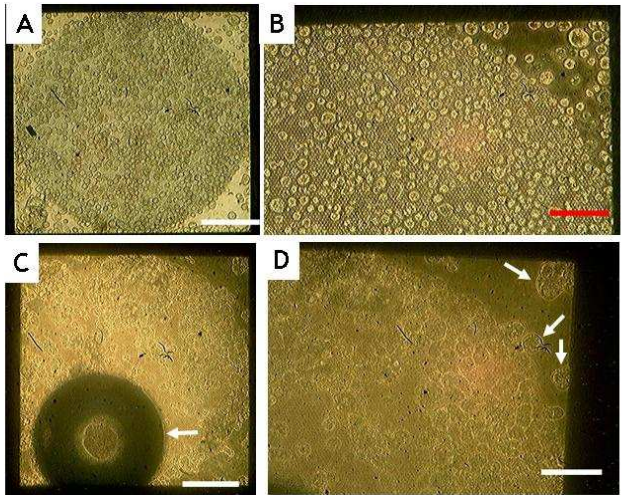

Figure 39: Initial experiments with the silicon nitride membranes in microfluidic devices
A) This image was taken 3 hr after cell seeding and showed the porous membrane area (scale bar – 250 µm). B) The magnified image of the membrane area in A). (scale bar – 50 µm). C) This image shows the cells on the membrane inside the device after 1 day in culture (scale bar – 250 µm). The arrow marks an air bubble trapped inside the system. D) The magnified image of the cells shows very little spreading, most remained rounded. Arrows indicate some rounded cells. (scale bar – 50 µm)

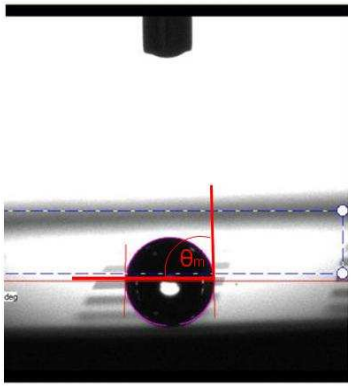

Figure 40: Contact angle test to check surface properties.
This image was taken to present the contact angle measured on the membrane surface. The angle measured was approximately 88° (θm = measured angle) (the number of membranes tested for contact angle = 5 and the SD of measured angles for 5 samples was ± 3°).

Improvements in device: Starting with the microfluidic device, several problems arose due to the following difficulties: The microfluidic connectors would exert tremendous strain on the microchannel inlet/outlet connection points in the PDMS, that the sheet would either be pulled out or crack at these connection points. Thus developing leaks in such areas of the device. Leakages would also appear at the point due to improper sealing between the PDMS device surface and the silicon chip surface, especially the areas near the inlet and outlet connectors. In order to improve the device sturdiness and to improve the bonding between PDMS channels and the silicon chip, a new device holder was designed to clamp the device together (Figure 40). The design parameters provided ease of

use, inter-connector stability, tight contact between PDMS mcrofluidics and silicon chip and transparency. Cell culture within these devices was improved with this new plastic clamp design and it worked well to hold the entire setup together including the microfluidic inlets and outlets (Figure 41).

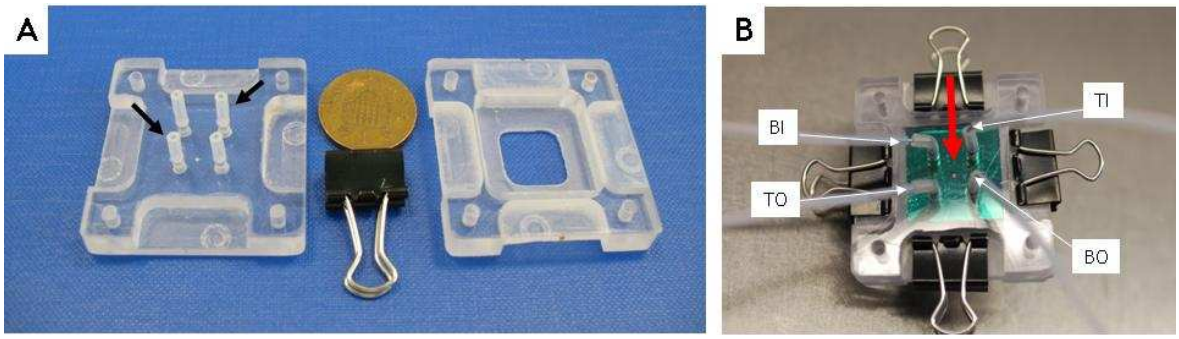

Figure 41: New device clamp for the single multilayered system
A) This shows the top and bottom parts of the new device developed for the single membrane device. The entire system was clamped down together using bulldog clamps. The arrows mark the silicon tubing connections used to provide the connectors some sturdiness. B) This is an image of the device when put together, here TI= top inlet, BI=bottom inlet, TO= top outlet and BO= bottom outlet and the red arrow mark the silicon nitride membrane inside the device.

Figure 42 shows cell culture results achieved when using the new clamp system. For these experiments the membranes were also coated with collagen. The devices seemed to be more stable and the collagen coating provided better cell growth. From Figure 41 cell growth inside the plasma etched sample device (without collagen coating) was not very successful, since the cells appear to be balled up. This is because after etching the surface the properties are lost over time and therefore an immediate coating of some ECM protein would be necessary to provide cells a better adhesive surface. (~6 out of 10 devices would work) (Section 2.1.2.2 from Chapter 2 to refer to the Bonding techniques).

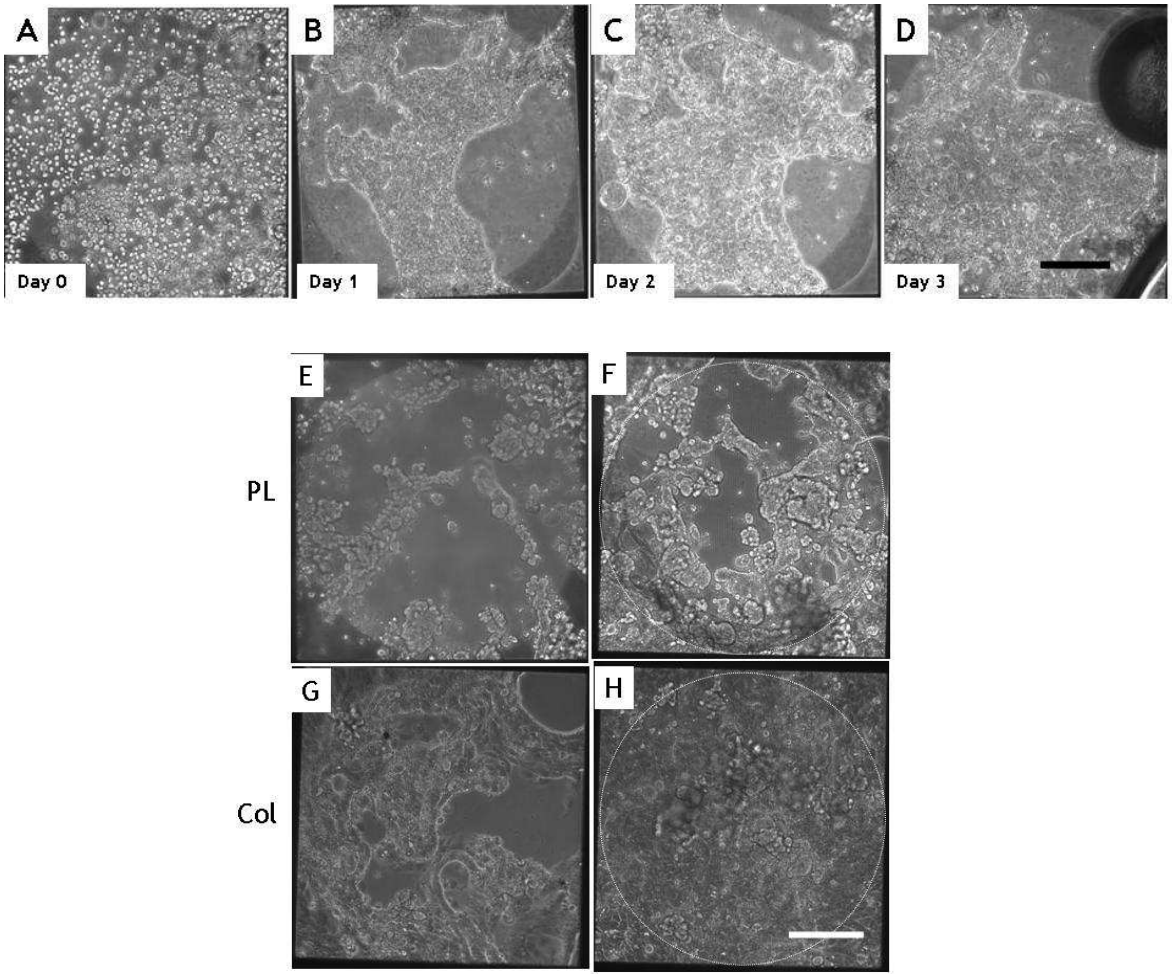

Figure 42: Cell culture results with the improved device holder design.
The cell culture images shown in A) B) C) and D) show the cells being maintained at 1 µl/min under continous flow. They were observed at different stages from Day 0, Day 1, Day 2 and Day 3. (scale bar 250 µm) These samples were coated with collagen after being bonded to the PDMS microchannels. However the presence of air bubbles made this extremely hard to culture comfortably and required constant agitation. Hence a loss of cells is seen in image B). However once the bubbles were removed they reached about 80% confluence by day 3. The images in E (day 1) and F (day 4) were sample exposed to only plasma etch and then bonded with the PDMS microchannels. The samples in G and H were exposed to plasma etch and then bonded as well, but the steps also included a collagen coating step. The dotted circles mark the membrane areas

3.2.3 Cell culture optimisation on silicon nitride membranes

The surface properties of the membranes were altered to make them more amenable to long term cell culture. The silicon nitride membrane porous surfaces were shown to be more hydrophobic, therefore to make the membrane surfaces more hydrophilic, they were exposed to air plasma using a Harrick Plasma machine at high energy for 30secs (shown in Table 3: Harrick plasma settings.). These were later treated with different solutions of collagen, fibronectin, and poly-l-lysine. The first stage, Figure 43 and Figure 44, the membranes were supported by a plastic (poly carbonate - PC) support and the entire apparatus was immersed in medium. (However, contact angle measurements would not be necessary once the membranes were coated with ECM proteins or the poly-l-lysine, since it was assumed that the surface coatings were cell friendly). Prior to immersion into cell

culture medium, these membrane samples were exposed to air plasma or coated with collagen, fibronectin, poly-l-lysine and compared to the non-treated membrane pores. The results showed that both the coatings could achieve about 80% of confluence for cell cultures within 5 days in culture. The second stage presented in Figure 44, the membranes were placed in between two PDMS wells and then coated with their specific coatings, either air plasma exposure, collagen, fibronectin, and collagen/fibronectin mix (50/50:vol/vol). The non-treated membranes were abandoned due to the slightly hydrophobic nature of PDMS since it was difficult to fill the wells with culture medium when unexposed to plasma etch (explained in section 2.1.2.2 Chapter 2) and (Bhattacharya 2005, Mukhopadhyay 2007). Also, from the above mentioned experiments it was evident that when these silicon nitride membrane surfaces were not exposed to plasma etch, they seemed unfavourable for cells. The images (Figure 43) and graphs (Figure 45) showed that the membranes exposed to air plasma and collagen/fibronectin mix showed the most promising results and reached about 80% confluency within 5 days in culture. Optimisation experiments were initialised in order to provide a rational basis to improve culture conditions on silicon the nitride membranes that were to be used with our microfluidic devices.

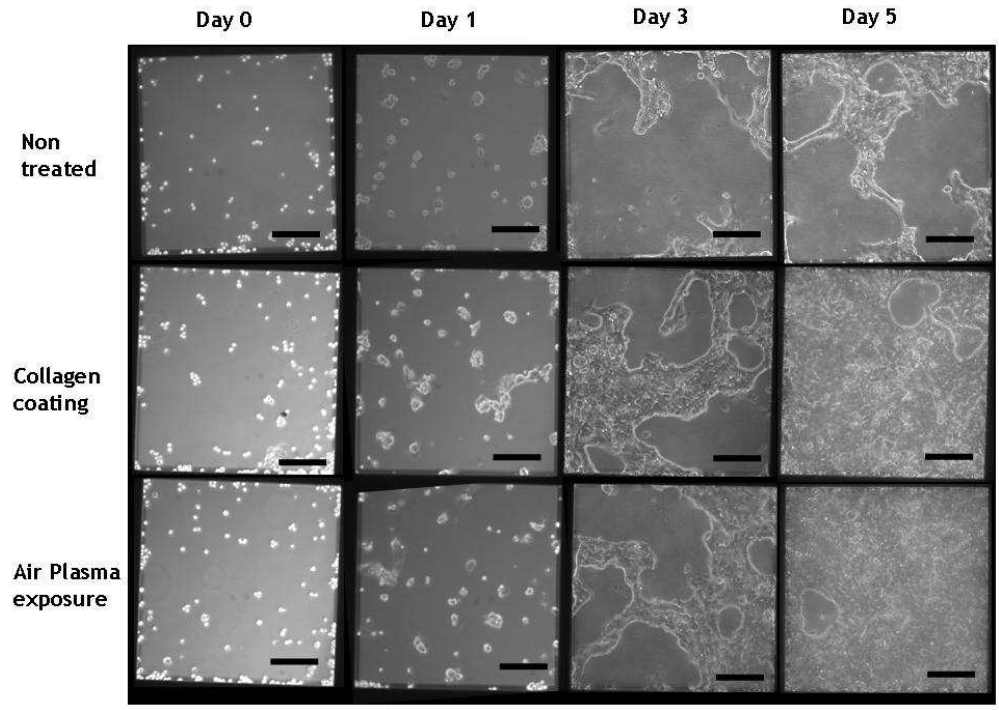

Figure 43: Cell culture on silicon nitride membranes
Phase contrast time series (left to right) of the same 1 mm^2 membrane following cell growth and proliferation from Day 0 (seeding) until Day 5. The samples were uncoated (top) coated with collagen after air plasma treatment (middle) or just air plasma treated (bottom).

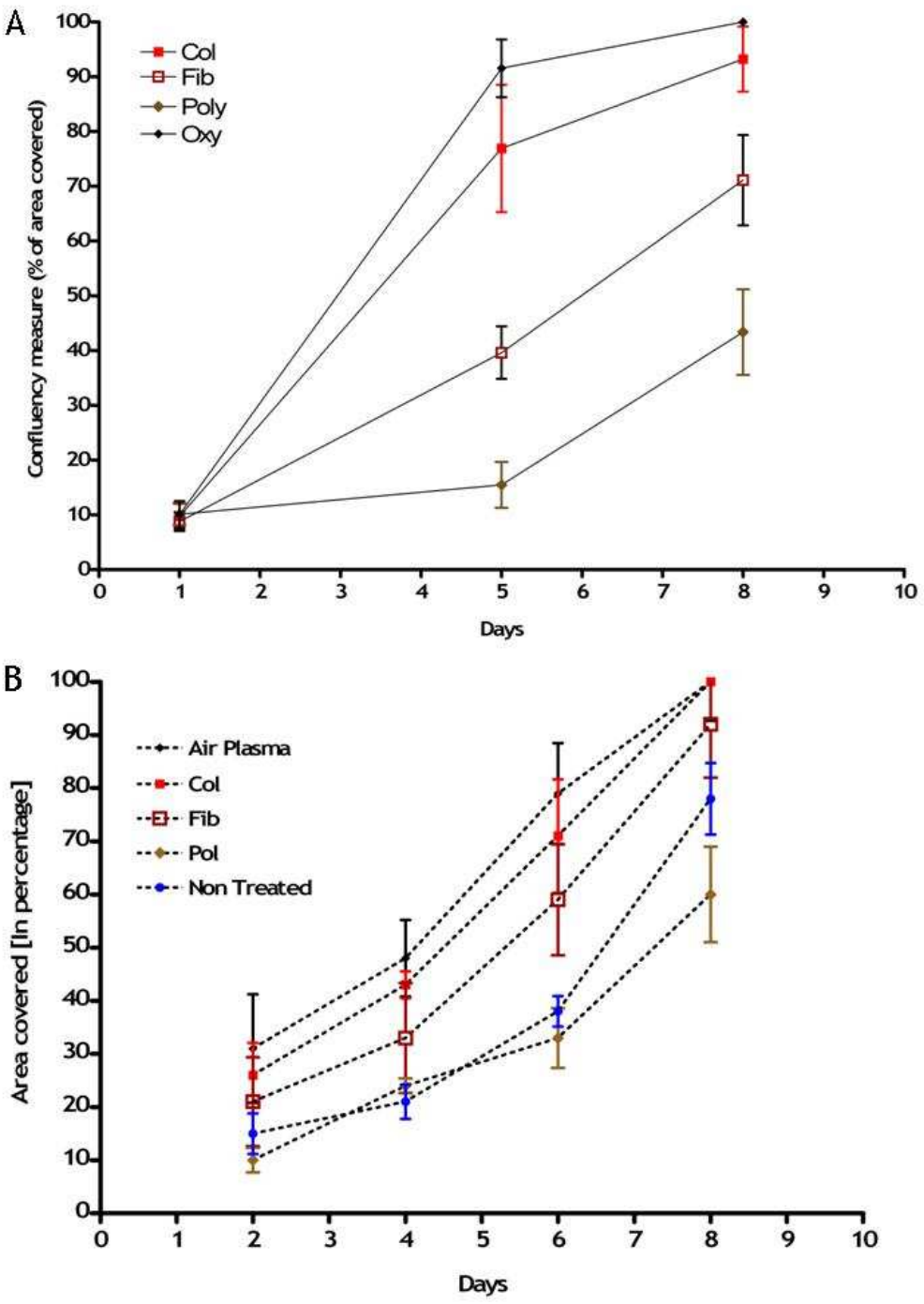

Figure 44: Confluency measurements using plastic supports.
A) These experiments were performed to test the 1.5 mm^2 area membranes at a seeding density of 700 cells per membranes well. B) This graph showed the 1 mm^2 show similar progression of the growth and proliferation as compared to the bigger membranes. (All the confluency measurements were performed using the magnetic lasso tool just to show the increment of cell coverage on the surfaces and the data presented here was the mean percentage for n=3 samples, showing the ±SD).

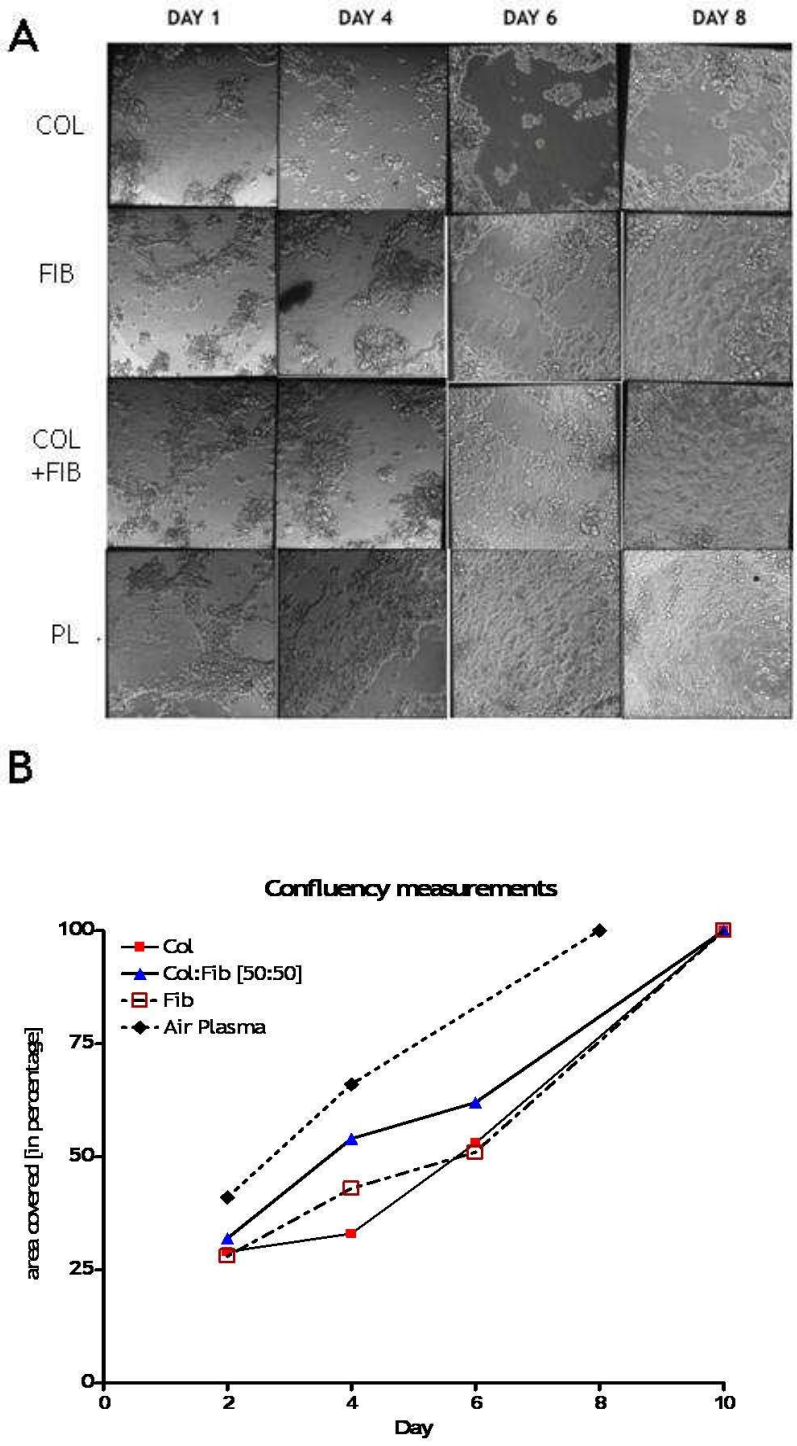

Figure 45: Confluency measurements using PDMS wells above
The images in A) presented the set of experiments performed using PDMS wells that sandwiched the silicon nitride membranes inside culture plates. The samples presented showed the cell growth and proliferation profile over Day 0 until Day 8. (COL- collagen coated, FIB- fibronectin coating, COL+FIB- collagen and fibronectin coating, and PL-air plasma exposure) B) The graph represented the percentage of confluent area for the cells. The graph showed that the air plasma and the col:fib (50:50) samples reached 100% confluence by day 8. (mean percentage calculated for n=3 samples)

3.2.4 Cell culture and TEER measurements on polymer Transwell® membrane inserts

The cell culture optimisation experiments on the silicon nitride membrane static devices were carried out along side cell culture experiments performed on polymer membrane transwell system. This helped derive a certain relation between the different membrane systems, the commercially available polymer membranes and the fabricated silicon nitride membranes. This gave an idea of the TEER values and cell growth expected for the cell monolayers tested after regular intervals of days in culture. The cell monolayers cultured on the polymer membranes were tested for the TEER using the STX2 electrodes provided with the EVOM resistance measuring system. The peak in TEER value was reached by day 9 on the 0.4µm membranes and on the 3.0µm membranes at day 14 (see Figure 46). Once the samples reached the desired TEER values (between 300-500 Ωcm^2 (Foster 2000, Geys 2007)), Geys et al (2007) also suggested that minimum value for TEER needed for a tight monolayer was 129 Ωcm^2). TEER values for the 0.4µm pores of 586 ± 12 Ωcm^2 were on samples coated with collagen (in the graph denoted as - C) and 577 ± 10 Ωcm^2 for non-coated samples (NC) (at day 9) and the 3.0µm pores showed TEER values to about 606 ± 8 Ωcm^2 for the non-coated samples (at day 14). The value of almost 600 Ωcm^2 were represented a tight monolayer that was suitable to perform translocation measurements. The TEER measurement was discontinued once these samples were used for translocation experiments. (However, TEER has been shown to be quite stable for long term culture, where cells reach maturity and TEER values stay stable for few days and then values gradually reduce (Florea 2003, Foster 2000, Geys 2007). The images in Figure 47, show the ZO1 protein staining for the different membrane pores. These gave an idea of the tightness of the monolayers. (Since ZO1 was one of the main tight junction proteins)

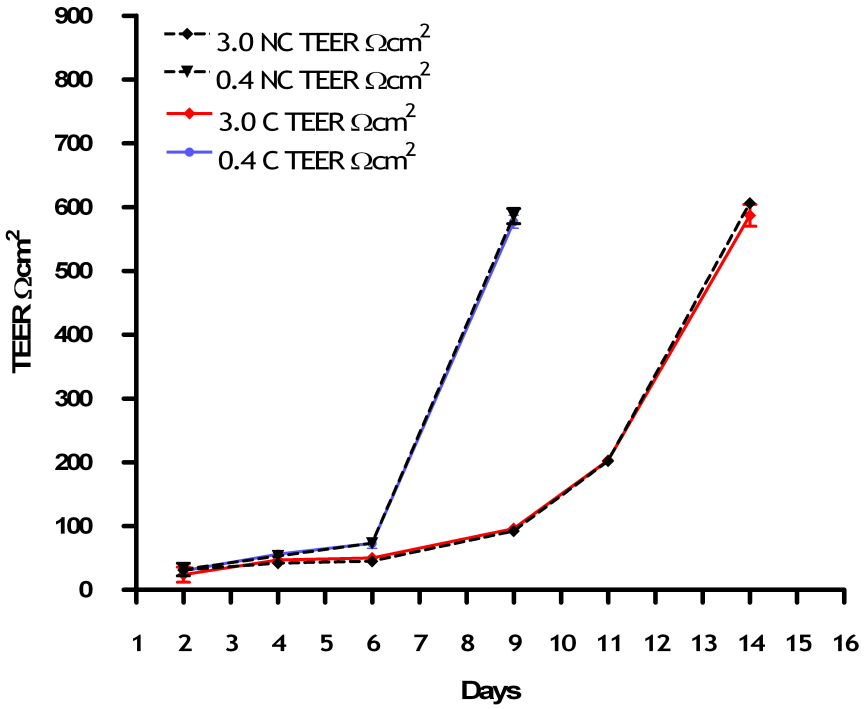

Figure 46: Development of TEER over culture time on transwell inserts
These were tested in dependency of pore size (3.0µm and 0.4µm) and surface coating. Collagen coating had less influence than pore size on the time at which the maximum TEER was reached.. Once this is reached the samples are used for translocation experiments with FITC dextrans. The graphs are average for n=4, ±SD) [NC – no collagen coating, C – collagen coated]

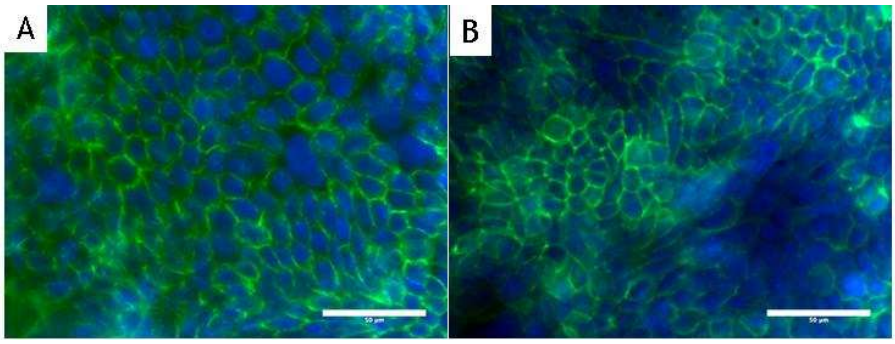

Figure 47: ZO1 protein staining for tight junctions
A) Calu-3 cells grown on 3.0 µm pore size membranes. B) Calu-3 cells grown on 0.4 µm pore sizes. The images shows the ZO1 proteins stained in oregan green stain and the nucleus stained blue using DAPI stain. The scale bars were 50 µm. These illustrate the tightness of the monolayers before translocation experiments were performed.

3.2.5 Translocation measurements comparing polymer Transwell® membranes with silicon nitride membranes

The translocation measurements on the transwell membranes were performed once the cell monolayers reached a good enough TEER (such that the monolayer was tight). The

measurements were carried out using a fluorescent plate reading spectrophotometer. The fluorescence intensity measured in relative fluorescence units (RFU) was normalised in order to compare the stock solutions, control- (medium without dye) and test-samples. Figure 48 showed the normalised translocation as percentage of FITC-dextrans translocated through the membranes to compare the cells grown over transwell with 3.0µm and 0.4µm pores. The FITC-dextrans used to test the translocation had different molecular weights (4kDa, 70kDa, 500kDa and 2000kDa) estimated the size of the still existing spaces/gaps between cells. The comparisons show that when used in presence of cells the 4kDa being the smallest sized particles showed a higher percentage of translocation than the 2000kDa particles. This was also evident on both types of pore sizes. (size of dextrans were presented in Stokes radius -Table 7)

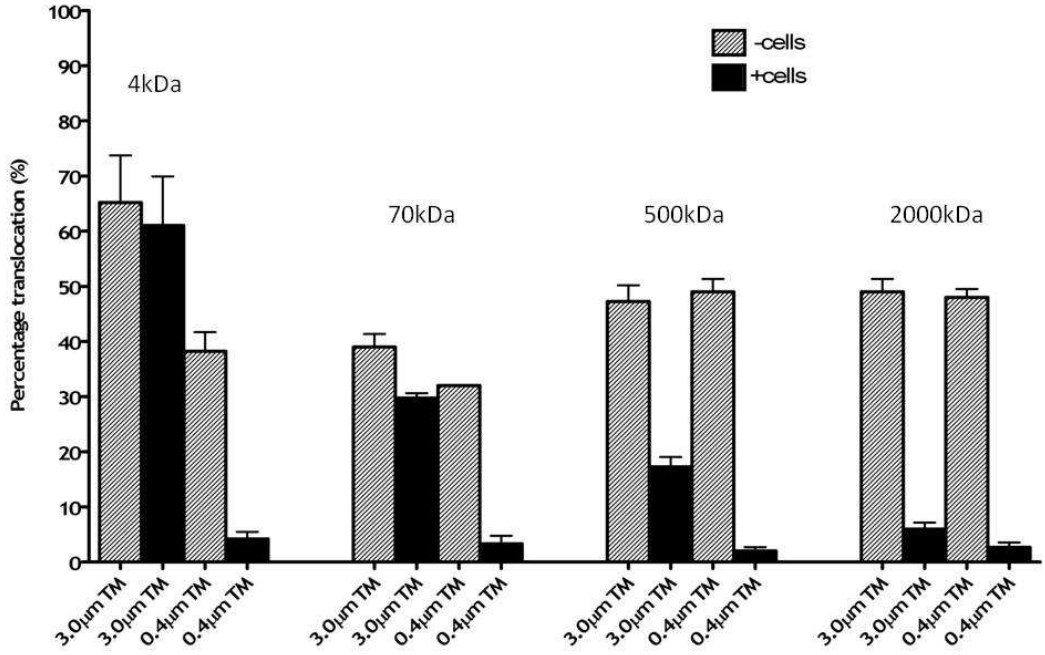

Figure 48: Comparison graph of FITC- dextran translocation through the transwell membranes.
This graph shows the comparison between the 0.4µm and 3.0µm pore size polyester membranes. The graph shows a comparison between the different sizes of FITC- dextrans, the 4kDa, 70kDa, 500kDa and 2000kDa. The percentage of translocation is calculated using arbitrary values for fluorescence intensity and plotted against the type of membranes use (each membrane is also compared to a -cells and +cells of respective samples for n=3 samples, ±SD) (TM=trans membrane supports)(kDa = Kilo Daltons).

Comparing translocation across cell monolayers on 1 µm pores silicon nitride membranes and 3.0µm transwell membranes revealed major differences especially for the smaller dextran particles (see Figure 49). The translocation of the 4kDa dextran particles showed the most significant differences where the outcome was in favour of the silicon nitride

membranes which resulted in less translocation in the presence of cells as compared to the Transwell membranes.

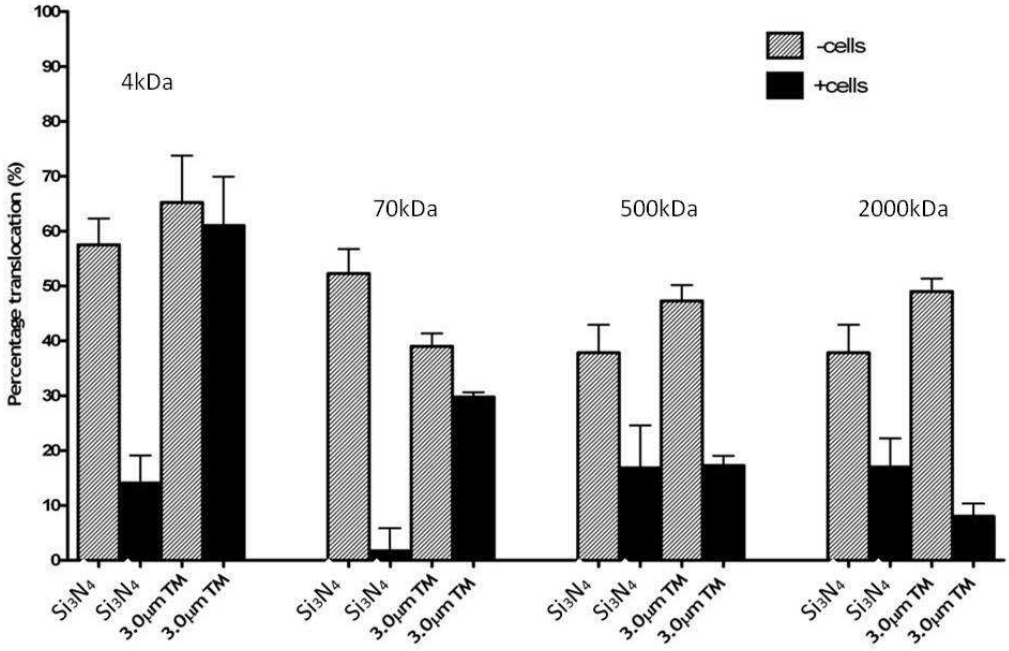

Figure 49: Comparison of FITC- dextran translocation across silicon nitride and polymer Transwell® membranes
FITC-dextran particle translocation across the 3.0µm pore size polyester membranes and 1 µm pores silicon nitride membrane with and without cells over 60 min. The graph shows a comparison between the different sizes of FITC- dextrans, the 4kDa, 70kDa, 500kDa and 2000kDa. The percentage of translocation was plotted against the type of membranes use (each membrane is also compared to a -cells and +cells of respective samples for n=3, ±SD) (TM=transwell membrane and Si_3N_4 = silicon nitride membrane)(kDa = Kilo Daltons)

FITC- Dextrans (molecular wt in kDa –kilo Daltons)	**Sizes (stokes radius in nm)**
4	1.4
70	6
500	14.5
2000	27

Table 7: comparison between the different dextran molecules
The molecular weights for the Dextrans were presented with respect to their stokes radius (de Belder – Amersham Bioscience handbook no. 18-1166-12, Lin 1997). This would help give a relation between the tranlocation effects seen due to the sizes of dextran molecules.

3.2.6 TEER measurements in single and five silicon nitride membrane system

These experiments were performed to establish measurement protocols for continuous TEER assessment on the single and five membrane systems using the micropatterned platinum electrodes on the silicon nitride membrane chip. The following experiments were done under static (no-flow) conditions, Figure 50 summarised experiment for the single membrane cell culture system: once the cell monolayers reached a desired degree of confluence (~100% confluency – viewed under phase contrast microscope) their TEER was measured using an adapter that clamped the nitride membrane chips and established electrical contacts to the electrodes at the same time. In order to establish an immediately measurable effect on the TEER cadherin based cell-cell adhesion was disrupted using a buffer (Versine buffer [21]) which contained 0.5mM EDTA. The homotypic cadherin based cell-cell adhesion is calcium dependent, after calcium removal cells will not be able to maintain their cell-cell adhesion and separate, leaving open gaps that allow electric continuity between the apical and basolateral aspect of the cells. The single membrane setup was the initial design for TEER measurements on silicon nitride. The TEER values measured on the single membrane system were in the range of 15 Ωcm^2. After addition of the versine solution a rapid decrease in TEER was observed, as expected. However, the TEER measured before adding the versine solution was still quite low compared to the TEER values observed through literature (on polymer Transwell membranes between ~129 – 600 Ωcm^2)(Geys 2006, 2007). This could be due to the lack of a completely confluent monolayer or due to problems in the testing system itself. The cell culture protocol was simultaneously being improved at the time when the single membrane setup was being tested. Once the cell culture was improved, as shown previously from Section 3.2.3 where the cells were confluent after 5-8 days in culture, the single membrane setup was abandoned and work was focussed on developing the five memebrane measurement setup.

The five membrane system explained previously was adapted to allow the measurement of five membranes in parallel Figure 27). When using the five well culture systems the initial TEER values were measured to be about 20 $k\Omega cm^2$ and on addition of the versine solution TEER gradually decreased [22]. The TEER measured here was far greater than that

[21] Sodium chloride – 140 mM, Potassium chloride - 5mM, Hepes - 10mM, EDTA - 0.5mM, Phenol red 0.5% - 0.001% (vol/vol), d- Glucose – 5mM

[22] The peaks on the graphs are missing due to over saturation of the reading – the reading of TEER maybe higher than $20k\Omega cm^2$, however this in unknown since the maximum reading for the EVOM was 20 $k\Omega cm^2$ (WPI-World precision instruments).

measured on the single membrane setup. The electrode setup designed for the five membrane chip comprised of five separate current injection electrodes & five separate voltage measurement electrod, each for the apical and basal sides. The graph showed the TEER measurements taken using this systemand each well is measured separately in after every 10 second interval and for every measurement shown in the graph from Figure 51 is the average TEER for 100 measurements per every 10 seconds. The TEER measured for well 1, 2 and 3 achieved 20 $k\Omega cm^2$. (However, wells 4 and 5 did not show a high measure of TEER). Once the culture wells were added with versine buffer (The 'black arrow' on the graph in Figure 51, was when versine buffer was added into the apical well and the TEER then gradually dropped).

The high values in TEER in well 1, 2, and 3 were thought to be due to healthier and more confluent cell layers. Also the measurement setup and connectors, were different compared to the single membrane system. For the five membrane device, gold coated spring micro-connectors were used to connect the circuits to the membrane chip electrodes (shown in appendices Figure 84). The five membrane static-device system has proven to be useful in detecting the cell membrane TEER for five independent experiments in parallel. The five measurement system also has shows the use of the versine buffer solution as being a benchmark solution by which the tightness of a certain monolayer can be tested. Therefore, such a system could be used to identify effects of either toxic or non-toxic soulutions when compared to the TEER results obtained from the versine buffer influence. Another important advantage of this measurement device is the ability to measure TEER changes accurately in real time. The real time effects seen within each of the samples gradually reduce suggesting a loss in cell membrane tightness. The five membrane TEER measurement system was a much more reliable system compared to the single membrane device explained above. However, experiments with the five membrane system were conducted under static conditions and therefore, the next step was to integrate the microfluidic devices to this setup, as demonstrated in Chapter 4, (Section 4.1).

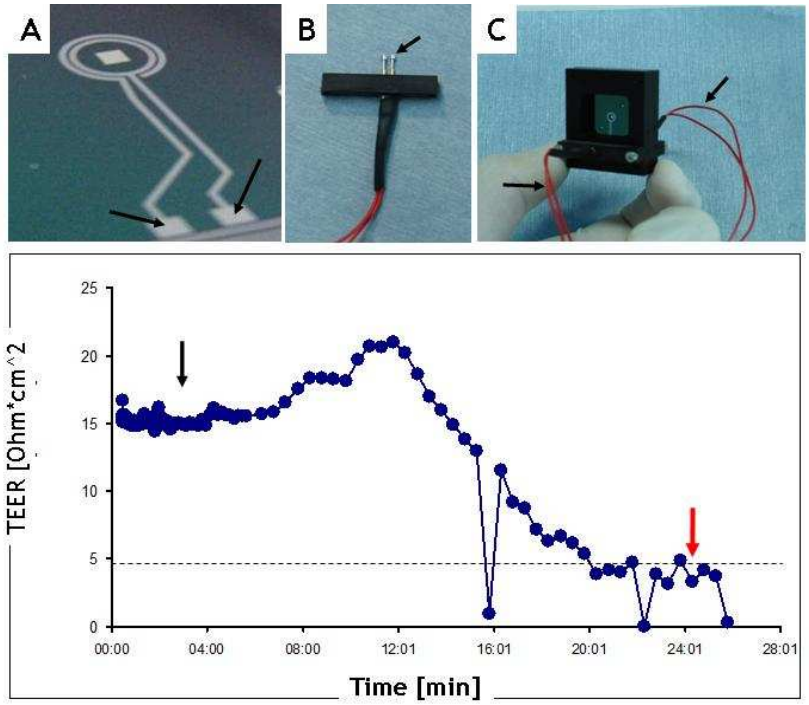

Figure 50: TEER measurements for single membranes
A) The image showed the single membrane chip and the arrows mark the contact points on the chip that connected the circuit when using the electrode setup shown in B). B) The electrode setup designed for the single membrane chip and the arrows mark the electrode contacts. (one current injector and other for voltage measure. C) This showed the entire apparatus when put together. Arrows marked the apical connectors and basal connectors. The graph showed the TEER measurements taken using this system. The TEER was measured at 15 Ωcm^2. The black arrow marked the point when Versine buffer was added into the apical well and the TEER then gradually dropped to the 4 Ωcm^2 (the red arrow marked the point when the measurements coincided with the TEER values for membranes without cells.

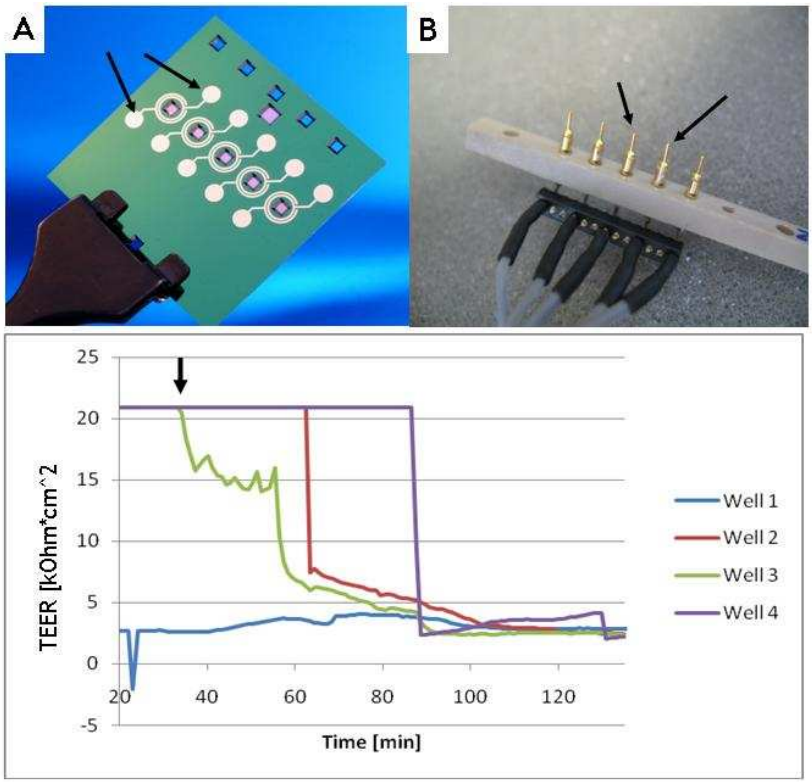

Figure 51: TEER measurements for silicon nitride membranes
A) The image showed the multiple membrane chip and the arrows mark the contact points on the chip that connected the circuit when using the electrode setup shown in B). B) The electrode setup designed for this chip (five for current injection electrodes & five for voltage measure each for the apical and basal sides) and the arrows mark the electrode contacts. The graph showed the TEER measurements taken using this system. The TEER was measured at 20 kΩcm^2. The black arrow marked the point when Versine buffer was added into the apical well and the TEER then gradually dropped. (Well1 – without cells (blue), Well2, 3 and 4 – with cells, Well 5 did not show a measure but it too had cells).

3.3 Discussion

The initial experiments performed with Calu-3 cells on silicon nitride membranes inside the single chamber microfluidic devices (when nitride membranes were not coated with proteins) often resulted in rounding up of cells, and finally cell death. This was thought to be the result of insufficient nutrient supply, gas bubbles or unfavourable hydrophobic membrane surface. However, when the device was properly sealed and used with the new clamp design the results were improved, showing a much higher percentage of reproducibility (~60%). The improvement in cell culture was also dependant on the collagen coating step which was included in the washing steps. The problems with certain devices producing gas bubbles persisted inspite of these improvement and bubbles needed to be pushed out to ensure that the flow of fluid was continuous and avoid drying up the cultures. Problems with gas bubbles have been reported previously through literature and can often be dealt with by slight agitation or other methods mentioned in the review by Young et al (2010).

Realising that the Calu-3 cells were never before used with silicon nitride membranes, it was necessary to first optimise cell culture conditions on these substrates for this cell type. Silicon nitride membranes were fabricated inside the clean room using photolithography and deep reactive ion etching techniques. Deep reactive ion etching techniques often use harsh chemicals that often include fluorine and chlorine compounds. These chemicals can be extremely hazardous to cell cultures and hence the surface properties of Si_3N_4 membranes needed to be cleaned and protein coated, to render the surfaces more cell compatible (Harris 2003, Ma 2005, Zhang 2008). Figure 40, illustrates the hydrophobic nature of these membranes where the contact angle was almost 90° on microporous areas. In order to change the surface properties the membranes (wettability) were initially cleaned using an acid solution (Piranha) and kept in a solution of propan-2-ol until required. Before performing cell culture experiments the membranes were dried under the flow hood and their surfaces were exposed to air plasma. The exposure to air plasma oxidises the surface resulting in a more hydrophilic surface. To improve the adhesion of cells to the membrane surfaces, extracellular matrix (ECM) proteins (mainly collagen and fibronectin) and a polypeptide poly-l-lysine were used to coat the membrane surface. Through the cell culture optimisation results it was evident that the collagen coating and the 50:50 mixture of collagen:fibronectin worked well in improving cell adhesion and proliferation on the Si_3N_4 membranes. The membranes exposed to air plasma alone also had a similar effect (Figure 43, Figure 45). The membranes showed evidence of good cell growth and proliferation

when used with the plastic holders, but since our main aim was to use them within microfluidic devices, it was necessary to use them in conjunction with PDMS wells. An apparatus using PDMS wells on either side of the membranes was engineered to derive a better understanding of cell proliferation inside such confines. However, the PDMS presented certain problems when attempting to fill the culture wells with liquid during the washing steps. Such problems, with the hydrophobic nature of PDMS, have been made evident through literature (Mukhopadhyay 2007) and therefore, the wettability needed improving. The solution was to expose the entire static device to air plasma (Ye 2006) which was later followed by the sterilisation and washing steps.

In the static experiments from Figure 43 and Figure 45, the medium was substituted with 15% of FBS, regardless of the surface coating to test whether it was because of serum starvation that cells would 'ball up' (Cells typically exhibit this morphology when they are starved of serum). This helped towards the formation of tight monolayers of cells for both the experiements (with plastic holders and with PDMS). The increase in the FBS content of culture medium was also adopted when using the Transwell® membrane supports. This helped to achieve high TEER values (~600-700 Ωcm^2) when using the transwell insert membranes. The effects of FBS content on TEER values have been explained by Geys et al (2006), where they previously had tested cell culture samples cultured using 2% and 10% content of FBS within their culture medium. Their mean TEER values observed were ~400 $\Omega.cm^2$ for the 3.0µm and ~1000 $\Omega.cm^2$ for the 0.4µm diameter pores respectively (Geys 2006, Geys 2007). The TEER values observed in Section 3.2.4, for the 3.0µm pores were much larger (600 Ωcm^2) and well above the value reported for a measurable tight monolayer. The values observed on the 0.4µm diameter pore size were however lower than stipulated in literature, but enough to suggest that the monolayers were tight [(Agu 2001) suggested that the TEER should be around 129 Ωcm^2 that correlates to be a tight monolayer]. Foster et al (2000), suggested that a TEER value of 300 Ωcm^2 was sufficient to represent tightness since their experiments using Luciferase yellow transport flux levels showed very little changes for the higher TEER values. Therefore, in the experiments presented in Section 3.2.4, once the measurements for TEER in the 0.4 µm and 3.0 µm samples fulfilled the criterion for a tight monolayer, they were immediately used for translocation experiments with fluorescent dextran particles. These dextran particles have often been used to test the transport of molecules across epithelial barriers. The range of size of the dextrans used varied between ~54 nm for the 2000 kDa dextran to ~8.9 nm for the 4 kDa molecular weight dextran with the 500 kDa and 70 kDa molecular weight dextrans possessing 29 nm and 12 nm respectively (radius of particles given in Table 13:

Diffusion coefficients of the dextran particles). The translocation studies performed using Transwell® inserts of two different pore sizes (0.4 µm and 3.0 µm diameter) showed significant differences. The re-distribution of the dextran particles, after 1 hr of incubation, between the apical and the basal compartments of the Transwell insert was initially examined without the presence of cells. This redistribution is simply based on diffusion of the particles across the membranes and depends only on the size of the molecules. The results showed a variation in the percent of translocation according to the size of the dextran particles. Ideally the percent particles translocated from the apical to the basal should decrease as the size increases, however the percent of translocated 500 kDa and 2000 kDa particles was slightly higher than that observed for 70 kDa ones. This was not the case in presence of cells. In the presence of the cell monolayer the percent translocated decreased according to the size of the dextran particles. The translocation of the FITC-dextran (4, 70, 500 and 2000 kDa) across the 3.0 µm Transwell® membranes was compared to the translocation across the silicon nitride membranes (1 µm pore diameter). The particles translocated less across 3, and 0.4µm polymer Transwell® pores with increase in size, this was expected as the coefficient of diffusion is inversely proportional to the particle size (Equation 6: Diffusion coefficient). The measurement of translocation of the different sized dextranes across the Si_3N_4 membranes showed again the phenomenon where the translocation followed the size profile of the particle (meaning that the smaller FITC-dextran particles translocated more than that compared to the bigger sized particles). The translocation values for the 70 kDa particles were slightly lower than both the 500 and 2000 kDa molecules. Particle size did not influence the probability of translocation across the cell coated nitride membranes, which was unexpected. An explanation for these unexpected results could be handling errors, or a previously unreported cellular interaction with these different dextran particles. A possible explanation that would result in similar transocation probability would be an active paracellular transport, which means that smaller particles would be just as slow as larger ones. The translocation observed for the three larger dextrans through cell-free inserts was roughly the same. This could also presumably be explained by the fact that even the biggest dextran is over 50 times smaller than the diameter of a single pore and that a plateau may have been found in particle size through this size of membrane. But this result is just as likely to be due to human error or a machine malfunction. Beck et al (1970) suggested that even when molecular size was a fraction of pore size there was a marked decrease in the rate of diffusion. However, these results allowed to correlate the cells behaviour on conventional Transwell membrane with that on the Si_3N_4 membranes. These discrepancies could be analysed by using TEM or

confocal imaging to section the cells and thus be able to follow whether there was any cellular uptake, active translocation.

3.4 Conclusion

This chapter mainly focused on the optimisation of culture conditions for Calu-3 cells on these silicon nitride membranes and showed that certain ECM protein coatings could possibly improve the surface properties of these membranes making them a more suitable system for biological experimentation. These membranes when combined with the TEER apparatus could prove to be useful for toxicity studies when using epithelial cells and would provide real time analysis in an automated system. Silicon nitride membranes are a novel system developed to transfer the conventional Transwell membrane setup into an on-chip automated measurement system. Also, the thickness of these membranes is unique and approximately in the range of mammalian epithelial air-blood barriers, which are between 500-600 nm thick from within a range of animals (Bartels, 1979). The advantage of having these thin silicon nitride membranes is that the diffusion of the particles through the miniaturised system across the membranes is un-hindered and the thickness f the membrane can virtually be neglected when performing diffusion experiments across the cell membranes. These properties made these membranes quite attractive in their uses. Translocations through the silicon nitride membranes were of prime importance to the overall project and it was imperative to derive a comparison between results obtained from the silicon nitride membrane and the Transwell inserts. The culture conditions that were modified to suit the nitride membranes were important for the microfluidic device experiments within Chapter 4.

Chapter 4: Development of a multilayered microfluidic analysis system for epithelial cells

4 Introduction

In the previous two chapters; Chapter 2, focused on the development of concentration gradients and cell culture microfluidic devices. In Chapter 3, the cell culture protocols for Calu-3 cells cultured on silicon nitride membranes and inside single cell culture well multilayered silicon nitride membrane devices, was the main focus point. Both these Chapters assisted the final goals for the project, which was to develop a microfluidic multilayered device to help test the toxicity of nanoparticles. Chapter 4 has been split into three sections; Section 4.1 explains the steps taken towards improving and developing a new multilayered microfluidic device having five cell culture wells. This device was aimed at being a refined version of the multilayered single layer device, explained in Chapter 3, Section 3.1.2.3. The top layer fluidic channel of the new multilayered device also included a concentration gradient to create five dilutions (four solute and one control dilution) for their respective cell culture wells. The top layer concentration gradient model was a modified version of the 7 row - gradient mixer device discussed in Section 2.1.1.1 in Chapter 2, the new device had 3 rows and into corresponding five cell culture wells rather than into one wide channel. The top/gradient part of the new multilayered device was unique in the sense that it could be used as a stand-alone device. This meant that the device could be tested separately which also helped to understand the working of the gradient. The different dilutions that developed when using certain test liquids (red dye, fluorescently labelled dextrans of different molecular weights suspended in culture medium, etc.) with this gradient device could easily be observed under the microscope. The observed intensity profiles acquired from the tests could be modified to get the best fit dilutions by simply altering the flow rates of the inlet channels (The expected dilutions were 0, 12.5, 50, 87.5 and 100% within the fluidic cell culture wells also explained in the following section, 4.1). The top/gradient layer of the new multilayered device had other potential uses when being used as a stand-alone device. One such project is demonstrated within this Chapter 4, in section 4.2, where this device was used for testing epithelial cell culture interactions with *Pseudomonas aeruginosa (P.aeruginosa)* (4.2). This project was designed for the purpose of a Masters thesis (for student Sultan Al Sharif - MRes in Biomedical Sciences - 2009), demonstrating initial experiments and highlighting the possible uses of such a gradient device.

As mentioned above, most of the work listed in Chapter 4 involved the development of the top/gradient device, cell culture optimisation and TEER measurements for the final new multilayered five well device. In parallel to this project there was another Masters project

designed (for student Kazeem Oliyawola *(MSc in Electronic Engineering- 2009)* using SU-8 to develop techniques needed to make an SU-8 based multilayered multiple analysis device (4.3). The idea behind this was to have a completely sealed device and to make the fabrication process quick as compared to the number of steps taken to prepare one of the silicon nitride based devices.

4.1 Optimisation of the top/gradient layer and the development of the multilayered microfluidic device

The following sections will cover the device design, fabrication techniques involved, fluid flow and cell culture experiments for the top/gradient device, both as a stand-alone device and as a part of the new multilayered silicon nitride membrane based microfluidic device.

4.1.1 Materials and Methods

4.1.1.1 Design and fabrication of the microfluidic gradient device

The 2D design, shown in Figure 52, is the microfluidic gradient model designed using the CleWin computer software (engineering CAD tool). The image shows the different components of the gradient device; firstly, the two inlets (green) that lead into the concentration gradient channels and the middle inlet (mauve) that lead into the bottom channels (when using this with the multilayered microfluidic setup). (The design for the bottom microfluidic channels is shown in Figure 53). Secondly, the concentration gradient consisted of three rows of serpentine channels approximately 6 cm each in length that split into five cell culture wells creating four different concentrations of a test solution and a control. The serpentine channels aided diffusive mixing of test solutions along their lengths that would create expected dilutions of 0, 12.5, 50, 87.5, 100%, across the device. The concentrations formed would be viewed at the observation channels at the end of this device. The significance of these observation channels was to help view the resulting concentrations in a single field of view under the microscope. Thirdly, the five cell culture wells (blue) were given a separate cell seeding inlet and outlet channel to avoid blocking the gradient channels during cell seeding. Fourthly, the round discs were meant for the electrical contacts points. These round disks were puncture points in PDMS to allow the connection between electrical contacts and the electrodes on the silicon nitride chip when this device was used in a multilayered microfluidic measurement setup. Finally, the outlet connectors (green) were designed to collect the five different concentrations of test solutions for analysis and the outlet connectors (mauve) that were connected to the bottom

channel device (when using this with the multilayered microfluidic measurement device setup).

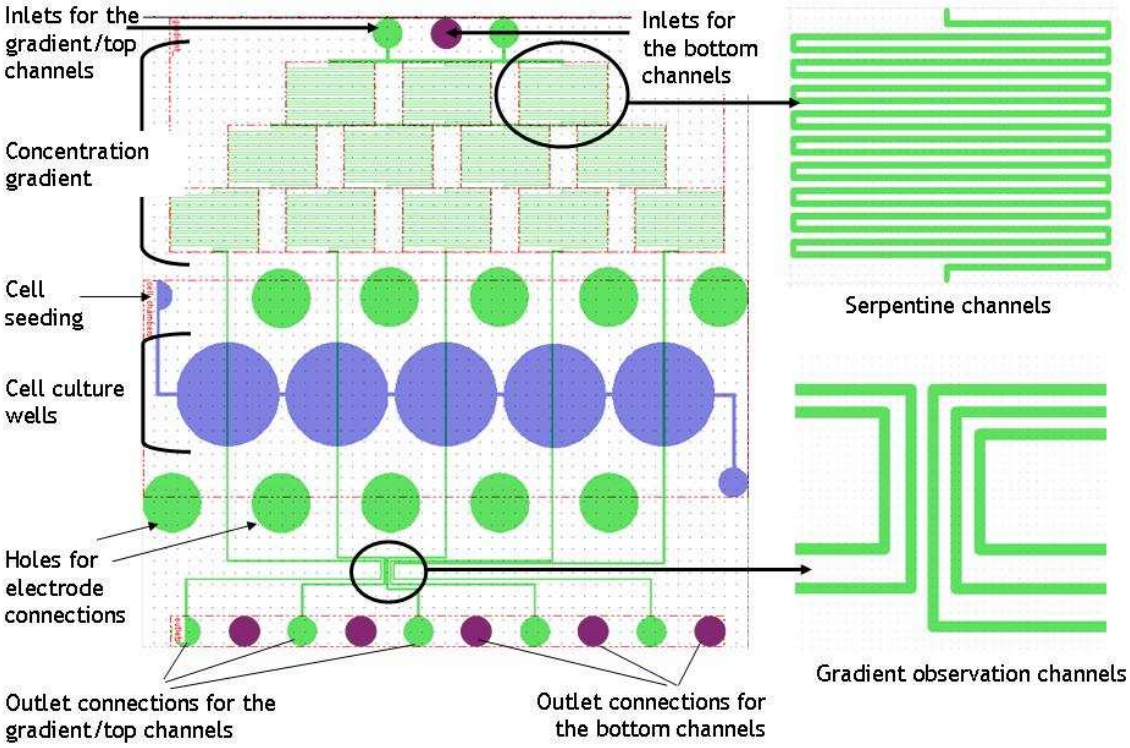

Figure 52: Design for the gradient/top microfluidic channels
This is a printout of the design file of the concentration gradient device created using the CleWin designing software. The image showed the different components of the design. The gradient/top device inlet channels (green), concentration gradient generator showing three rows of serpentine channels (serpentine channel length = 6 cm), gradient splits into five cell culture channels (blue) resulting in a different concentration of test solution in each respective well, the outlet channels (green) for the gradient/top device, the outlet channels (mauve) meant for collecting samples from the bottom channels, the gradient observation channels, holes as markers for the electrical contact points. Dimensions – cell culture well diameter = 3.5mm, serpentine channel width= 50µm, observation channel width= 50µm, cell culture seeding channel width= 100µm, electrode holes = 2mm diameter, outlet/inlet connectors = 1mm diameter.

The design in Figure 53 shows the bottom microfluidic channels and was designed using the CleWin software. This device was used only in combination with the gradient/top microfluidic and the silicon nitride membranes when integrating the final multilayered measurement setup. The bottom microfluidic device was used specifically for the multilayered device experiments only and never on its own. The device consisted of serpentine channels, however these were not meant for mixing test samples but trying to balance out the flow of liquid between the top and bottom channels (to try to make both the fluid in the top channel and the fluid in the bottom channel flow together). The five separate serpentine channels would lead into five different cell culture wells (test sample collection wells - blue) and finally towards the outlet channels. The outlet channels were

connected to the outlet channels (mauve – in Figure 52 and 53) in the multilayered microfluidic device setup.

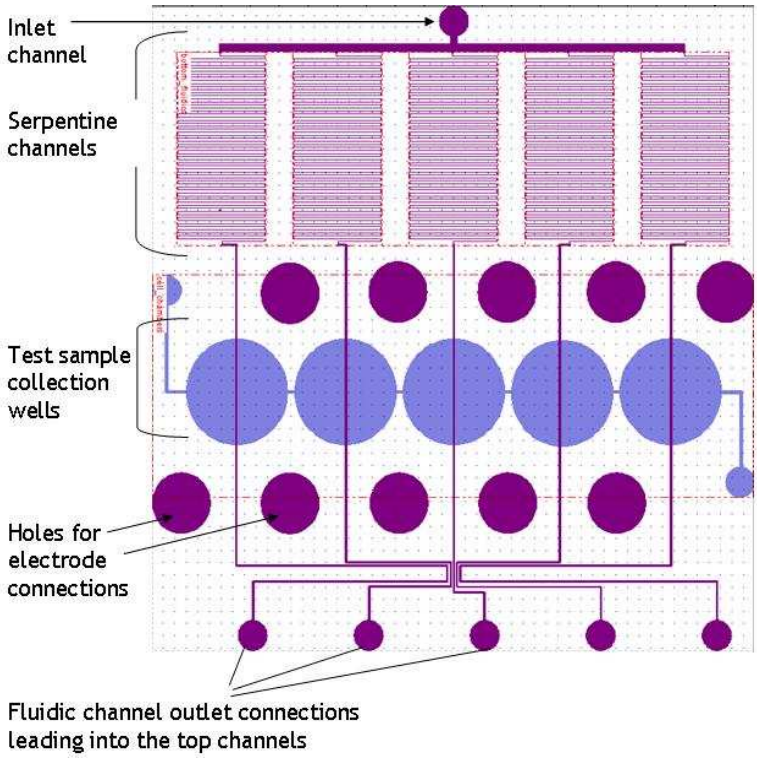

Figure 53: Design for the bottom microfluidic channels
The design for the bottom microfluidic channels designed using the CleWin software, showed the inlet channels, Serpentine channels to balance out the flow of liquid in the gradient device, the cell culture/test sample collection wells (blue), fluidic outlet channels and the holes for the electrical contacts which puncturing markers on the PDMS. Dimensions – cell culture well diameter = 3.5mm, serpentine channel width= 50µm, observation channel width= 50µm, cell culture seeding channel width= 100µm, electrode holes = 2mm diameter, outlet/inlet connectors = 1mm diameter.

The design was transfered to a mask plate using an electron beam writer and 6 copies were transferred onto a 5 x 5 inch mask plate. The mask plates bearing the designs were used to expose the photoresist (SU-8 3050) spun of a silicon wafer. The SU-8 3050 was poured (directly from the bottle – this avoided any contamination when using glassware or spillage when using a syringe, as an intermediate) onto a silicon wafer spun initially at 500 rpm for 10s and finally at 3000 rpm for 30s to achieve a thickness of approximately 50 µm. The wafer was then baked on a hot plate at 95 °C for 30 min. The spun resist was exposed for 35s to UV light (power density rating of ~ 7.1 mW/cm^2 using the MA6 – mask aligner system (Section 2.1.1 in Chapter 2). Fabrication and processing step were followed as per the protocol for SU-8 3050 from section 2.1.1.3 Chapter 2. To prepare the devices the silicon master was placed inside the PDMS casting chamber (Explained in materials method section 2.1.2 from Chapter 2). A pre-prepared mixture of PDMS (10 parts Sylgard

184 and 1 part curing agent – explained in 2.1.2 from Chapter 2) was injected into the casting chamber. The casting chamber was placed inside the oven for 1-2 hrs at 80 °C. Once cured, the casting chamber was dismantled and the PDMS microchannel devices were peeled off from the silicon master.

4.1.1.2 Integration of layers for the multilayered toxicity testing device

The different components of the multilayered device were integrated together (Figure 54) as follows: A) The silicon nitride membrane chip was sandwiched between the top and bottom microfluidic channels thus forming the core of the device. The PDMS microchannels were bonded to the membrane chip using an air plasma exposure step (explained in section 2.1.2.2 from Chapter 2). B) This device was placed inside a device holder (plastic holder) to reduce the potential for any leakages and to give the apparatus sturdiness when connected to the electrical contacts. C) PDMS microchannels were supported with a glass slide on either side to provide support to the core device, since PDMS is a soft polymer and is easily compressed these glass slides provided some sturdiness to the device. D) On clamping the device together, it was then ready to be used for experiments and connected with fluidic connectors. This device was meant to test the integrity of the cell monolayers using the TEER method via the electrical contacts (section 3.1.6.2 Chapter 3) and attempt to detect any changes in TEER values under the influence of toxic solutions.

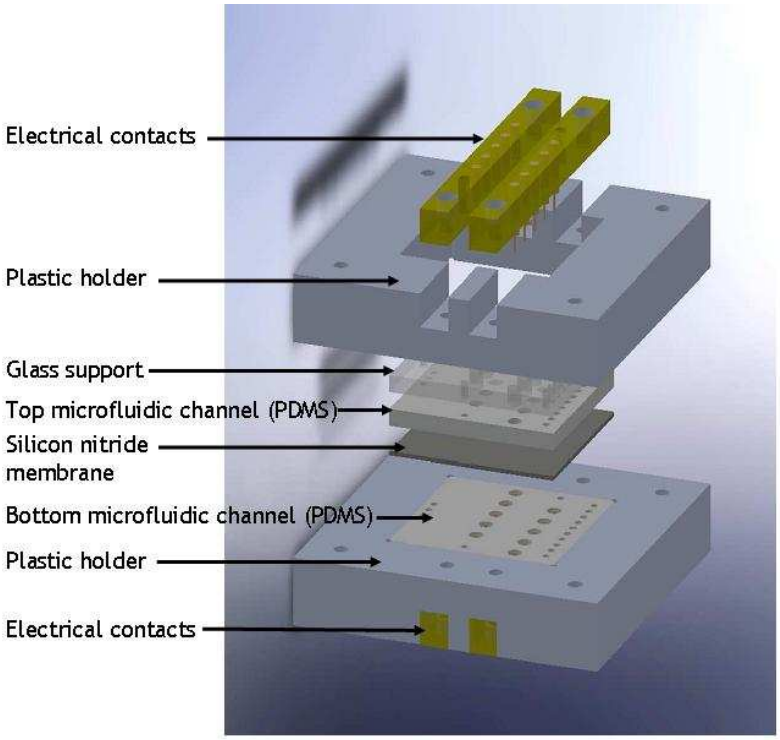

Figure 54: Clamping together all the parts of the final testing device
The image showed the different parts included in the device; electrical contacts (yellow), plastic holders on the top and bottom side to clamp the device together, glass slides on either side of PDMS microchannels, Top and bottom PDMS microfluidic channels bonded to the silicon nitride membrane chip. (Diagram courtesy of Nicholas Blondeaux, CSEM, Switzerland)

4.1.1.3 Cell culture in the top/gradient device

The cell culture technique involved an initial device rinsing step using different solutions to wash and sterilise the devices. All solutions used in the rinsing steps were inserted through the inlet channels (signified by the downward pointing arrows at the top of the image; Figure 55). The steps involved an initial rinse with a solution of 70% ethanol for approximately 10 min and this was washed out with distilled water for another 10 min. This step was followed by a 1 hr rinsing step with HEPES saline solution and a 10 min rinse with plain cell culture medium (without FBS) (EMEM when using Calu-3 cells, and DMEM for MDCK cells) which was important to assure a safe and alcohol free environment for the cells. This was followed by a rinse with cell culture medium containing FBS. To improve the attachment of cells inside the cell culture wells, a solution of culture medium with collagen (section 2.1.4.3 from Chapter 2) was included as part of the wash steps. The entire device was kept in the hot room/incubator, at 37°C for 1 hr, to allow the medium to warm up. During the wash steps the cell seeding inlet and all outlets were left open to allow for easy fluid flow through the device. Once cells were ready to be inserted through the cell seeding inlet channel, the outlets were plugged using tubing

valves or by inserting tube endings, connected to syringe needles, into solid thick blocks of PDMS. At the same time, the gradient inlets were also closed, preventing cells from entering the serpentine channels. (Cell culture techniques using epithelial cells were explained in section 2.1.3 from Chapter 2 and cell seeding into microfluidic devices is explained in section 2.1.4.4 from Chapter 2 and 3.1.2.3 from Chapter 3).

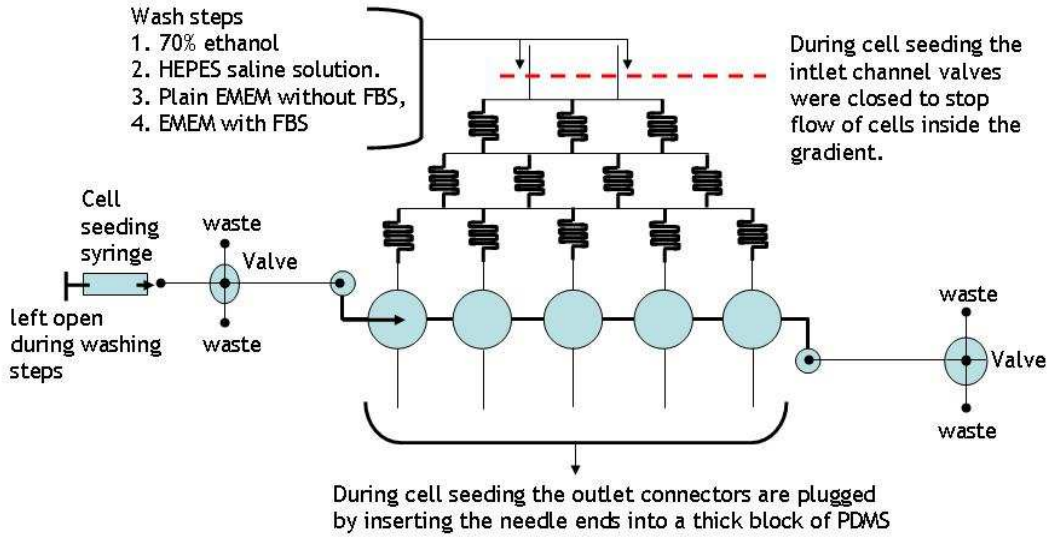

Figure 55: Seeding cells into microfluidic cell culture wells of the gradient device
The schematic showed the various steps involved in the sterilisation and preparation of devices for cell culture. The steps involved introduction of alcohol, HEPES saline solution, plain EMEM, and EMEM with FBS into the device channels. Once the rinsing steps were complete the device is ready to be seeded through the cell seeding channels.

4.1.1.4 Cell culture inside the new multilayered toxicity testing device

The multilayered toxicity device apparatus consists of 15 fluid connectors; 9 top microchannel connectors and 6 bottom channel connectors. The image in Figure 56 A), shows the different connectors prepared from Tygon tubing and syringe needles (section 2.1.2.4 from Chapter 2). The image in B) present the entry points for the tubing connectors into the device microchannels; top inlets points (white dots on blue), bottom channels inlet point (solid blue), electrical contact points (yellow circles), top outlet points (solid black) and the bottom channel outlet points (white dots in black). The cell washing steps and the cell seeding methods were similar to the previous section 4.1.1.3 from this Chapter.

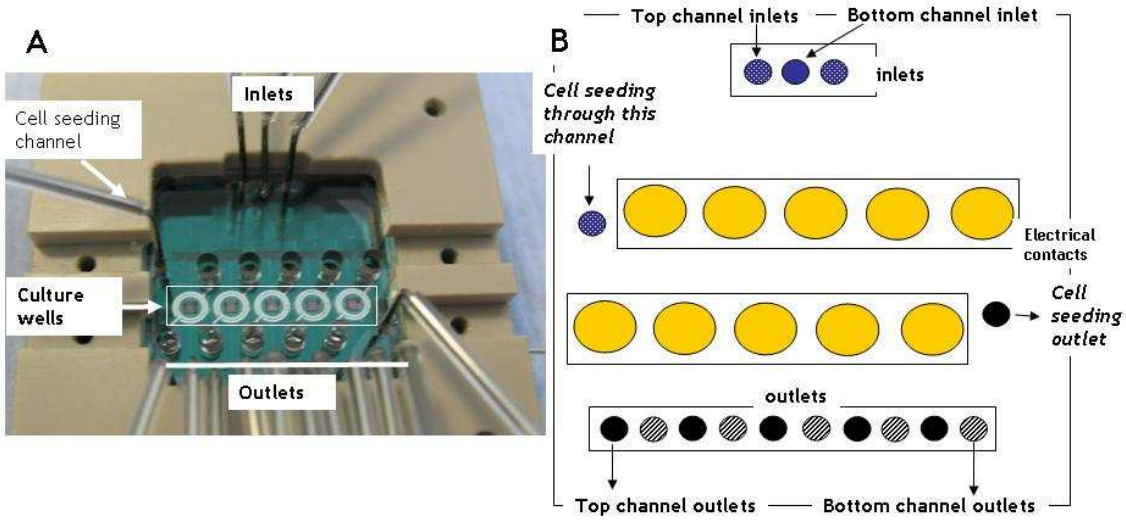

Figure 56: Fluidic connections for the device
The image A) showed the microfluidic device held together using a device holder. The fluid was introduced into the device via inlet channels. The device had a separate cell seeding channel which delivered cells straight into the cell culture wells. B) This schematic showed the different inputs and output areas for the fluid. The bottom channel has separate inlet and outlet connectors than the top microfluidic channel. The yellow areas mark the electrical contact points which are not connected to any of the microfluidic channels.

4.1.2 Results

4.1.2.1 Fabrication

To develop the mutilayered toxicity device it was necessary to first understand the workings of the gradient/top fluidic part of the device in more detail. The top layer of the device consists of a microfluidic network that included a set of serpentine channels that led into five separate cell culture wells. The serpentine channels were responsible for developing the dilution gradient with the help of diffusive mixing. The flow of a test solution alongside a clear buffer resulted in four different concentrations including a control at the clear end of these serpentine channels. The channels consisted of 3 horizontal rows of serpentine channels that would meet at the row ends and allow for the two concentrations to mix again (gradient mixing rows and channels were also explained in the Chapter 2) The resultant four concentrations and the control were delivered to the five different cell culture wells. The device microchannels were cast in PDMS against the silicon master wafer bearing the SU-8 3050 structures (SU-8 structures seen in Figure 57, A). The processing steps were explained in section 2.1.1.3 from Chapter 2. The SEM picture shows clearly some of the serpentine channels, and the inlet channels for the top gradient device. The height was 58±3 µm as measured in the Dektak. (see Figure 57 B).

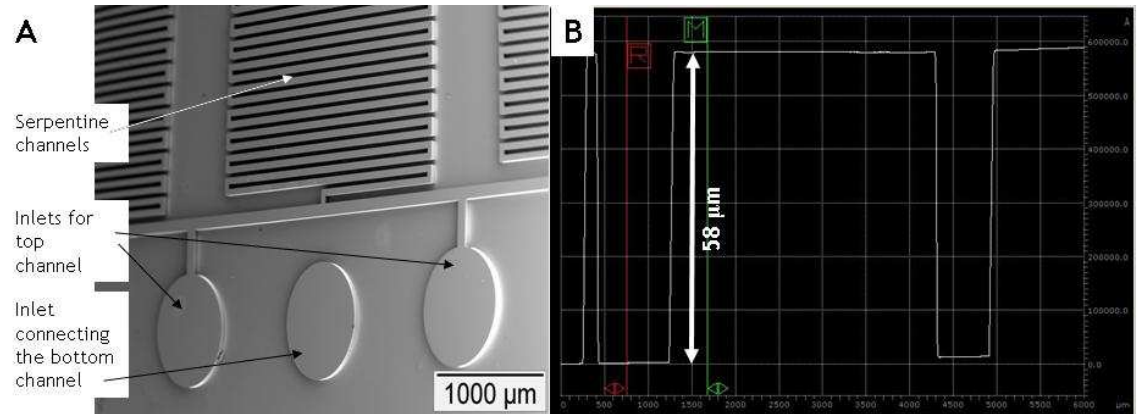

Figure 57: Fabrication results for the multiple cell culture well device.
A) SEM image of the SU- 8 master. The image showed the two device inlets leading into the serpentine channels, the middle is the connector to the bottom microfluidic device channels. B) The height of this device after fabrication was measured to be 58 µm, using a Dektak (Dektak 6M Veeco, Metrology group)

4.1.2.2 Dye intensity gradient profiles inside the top/gradient device

It was possible to use the top layer as a standalone device as shown below, in Figure 58, where it was used for diluting red coloured food dye (into four dilutions and one control). The gradient device was designed to combine the serpentine channels with separate cell culture chambers. The serpentine channels increase the channel lengths resulting in much longer times for diffusive mixing, at the flow rates used (1 µl/min to 5 µl/min). To demonstrate the successful generation of a concentration gradient a red food dye manufacturer) was used in one and clear water in the other inlet, the resulting concentration gradient is presented in Figure 58, B. The dissolved red dye and water were inserted through the two inlet channels resulting in four separate concentrations of red dye developed, ranging from a 0% control and a 12.5% to 100% within the five culture wells. The results obtained when running the experiments, when red dye was used against water dilutions were found to be in the range of 0.2% (w1), 24.8% (w2), 60.7% (w3), 87.3% (w4) and 100% (w5). This varied slightly from the expected results that were 0, 12.5, 50, 87.5 and 100% in the respective wells.

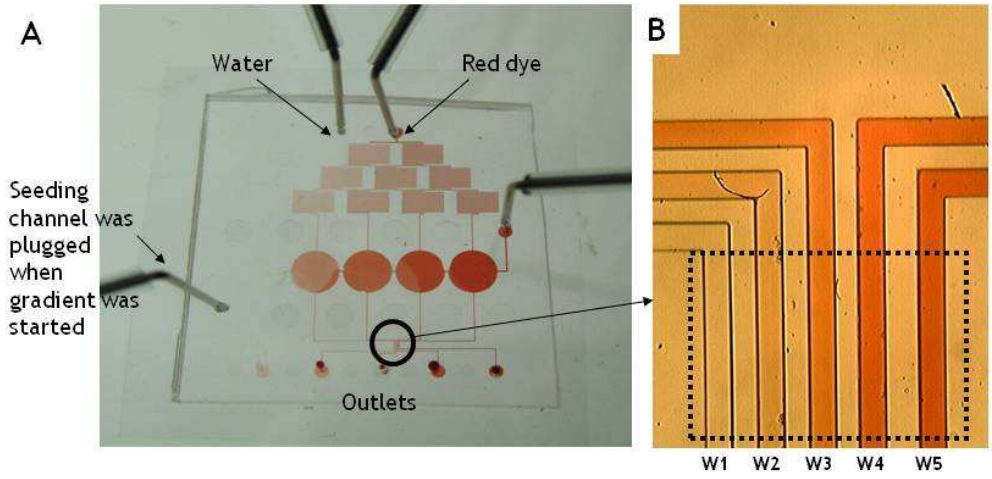

Percentage of red dye	Well 1 (W1)	Well 2 (W2)	Well 3 (W3)	Well 4 (W4)	Well 5 (W5)
Expected percentage	0 %	12.5 %	50 %	87.5 %	100 %
Measured percentage	0.2 %	24.8 %	60.7 %	87.3 %	100 %

Figure 58: Calculations for the percentage separation of test red dye.
A) The gradient device was used to dilute a solution of red food dye to illustrate the working of this device. The red dye solution in water was added through the right inlet and water through the left inlet. The perpendicular seeding channel was plugged (using a valve or the needle ends were stopped up using blocks of PDMS) when the gradient was running. B) This image shows the observation channels (each with width 50µm) and the marked area signifies the reference area for measured percentage of intensity of red dye (marked with a dotted rectangle). In the table, the expected percent for dilutions were 0, 12.5, 50, 87.5 and 100%, and the calculated mean percent for dilutions were as 0.2, 24.8, 60.7, 87.2 and 100 % in their respective wells. (Well 1, 2, 3, 4, and 5 corresponds to W1, 2, 3, 4 and 5)(1µl/min).

Fluorescently labelled dextrans (FITC-dextrans) were used to study the gradient generation through this device. These FITC labelled dextrans, discussed in Chapter 3, have different molecular weights. The ones used in this thesis included the 4, 70, 500 and 2000 kDa FITC dextrans. Due to their difference in mol.wt, they have different effective hydrodynamic diameters and hence diffuse at differing rates (Xu 2001). To study the development of dilutions within our devices, a 1mM solution of FITC-dextran of mol.wt 2000 kDa (Sigma, Poole, UK) was dissolved in transparent (exclusive of phenol red) MEM (containing 5% non-essential amino acids and 2% antibiotics, 10% FBS). The FITC-dextran MEM mixture (introduced through the right inlet of the gradient device) was run against plain MEM (introduced through the left inlet of the gradient) and results were observed under the fluorescent microscope at the level of the observation channels at the end of the device (Figure 52). (The device was placed on microscope stage heated to 37°C). The concentrations observed with this device were: 2% in channel 1, 24% in channel 2, 74% in channel 3, 99.2% in channel 4, 100% in channel 5; when used at a flow rate of 1.26 µl/min. However, through this graph it was evident that the mixing within these channels was not

complete since the intensity peaks for the each channel were tapered and not homogeneous, mainly in channel 3 (middle channel). This meant that the mixing has not completed, or that the flow rate is too high. On lowering the flow rate to 0.63 µl/min the percentage of dilution seen were 23.5% in channel 1, 41% in channel 2, 78.2% in channel 3, 100% in channel 4 and 97.2% in channel 5. These still seemed to have slightly tapered peaks, but there was more homogeneity in channels 2, 4 and 5. However, similar problems of non-homogeneous peaks were observed in channels 1 and 3 (from left to right in Figure 62). This meant that there could be a possibility of homogenising the peaks either at lower flow rates or either by addressing the problems that the channels leading from the cell culture chambers towards the outlet observation channels were of different lengths resulting in varied fluid resistance (explained in the next section).

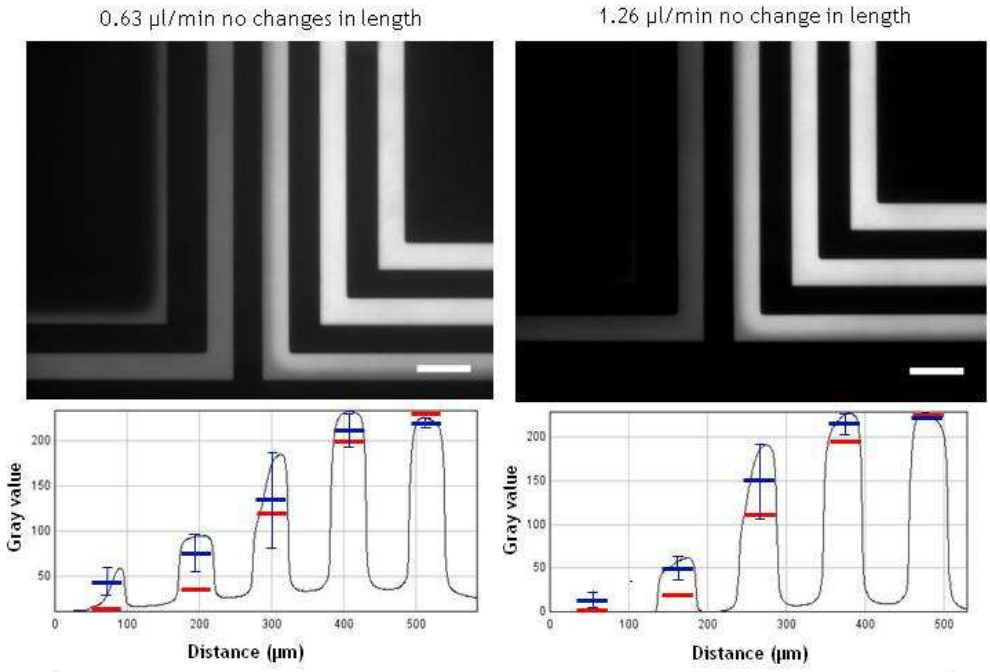

Obv. Channels	1	2	3	4	5
0.63 µl/min	23.5%	41%	78.2%	100%	97.2%
1.26 µl/min	2%	24%	74%	99.2%	100%
Expected percentage	0%	12.5%	50%	87.5%	100%

Figure 59: Intensity profile in the observation channels of the multiwell device - perfusing FITC dextran in MEM medium through the right inlet and plain MEM medium through the left. The images and graph show the profiles of the dilutions developed when using FITC-dextran 2000 kDa. The red lines mark the expected percentages for each channel (left to right; 0 - 100%). The blue lines mark the measured mean percentages for their respective channels (from left to right in the images for n=4 values, with ±SD). The black line represents the intensity profile for one experiment with each of the two flow rates used, 0.63µl/min and 1.26µl/min (using a 250µl SGE glass syringe set to the 10ml syringe setting on the pump). The percentage dilutions observed in each channel are presented in for the intensity profile represented by the black line is given in the table. 1, 2, 3, 4 and 5 are numbers for the respective channels seen in the images from left to right).

4.1.2.3 Alterations in the outlet channel lengths of the top/gradient device

The results from the previous section suggested that there were certain problems with the development of the dilutions when viewed within the five observation channels. The improper mixing observed inside the channels led to a deviation from the expected values for dilutions. The observation channels were meant to simplify the viewing of the five dilutions of a test solution under the microscope and to achieve this, the outlet channels needed to be parallel to each other at that stretch of the device. However in doing so, each outlet channel (leading from the cell culture wells towards the outlet connectors) had a different length (evident from the measured values in Table 8). This meant that the resistance faced by the fluid when entering these channels was different from each other as well, since the relation between the resistance and length was explained as being directly proportional to each other (Walker 2007, Beebe 2002) (resistance was given as $R = 12\mu L/wh^3$, where 'L' is the length, 'w' is the width, 'h' is the height of channels and 'μ' is the fluid viscocity, explained in Figure 60: Resistance v/s length of outlet channels hypothesis). This means, that when there is an increase in length of a channel then the resistance increases. This resistance is also dependent on the width and height of the channels where if these parameters change, then the resistance would be inversely affected. The measured lengths in the table show that 'L5' was the longest channel and 'L3' was the shortest. This meant that when fluid attempts to flow through these channels it would prefer to flow faster through 'R3' (the resistance would be lower) than it would through 'R5' (resistance would be higher). Once the serpentine channels complete the mixing process, the dilutions would flow into the respective cell culture chamber and subsequently through outlet channels. However, if the outlet channels have different resistances it would cause a differential of flow/pressure between the cell chambers and since they are connected the fluid would attempt to flow into the channels with least resistance, until equilibrium is reached. This could be one of the causes for the unexpected values for the mixing regimes seen in the observation channels, where there is mixing again due to the invading fluid from adjacent cell chambers. Therefore it was thought that, if the lengths of the outlet channels were adjusted to be of the same value, then the resistance too would be the same, which would in turn lead to an even mixing according to expectations. Meaning that L1, L2, L3, L4 and L5 would be equal in length which would mean that $R1 \approx R2 \approx R3 \approx R4 \approx R5$.

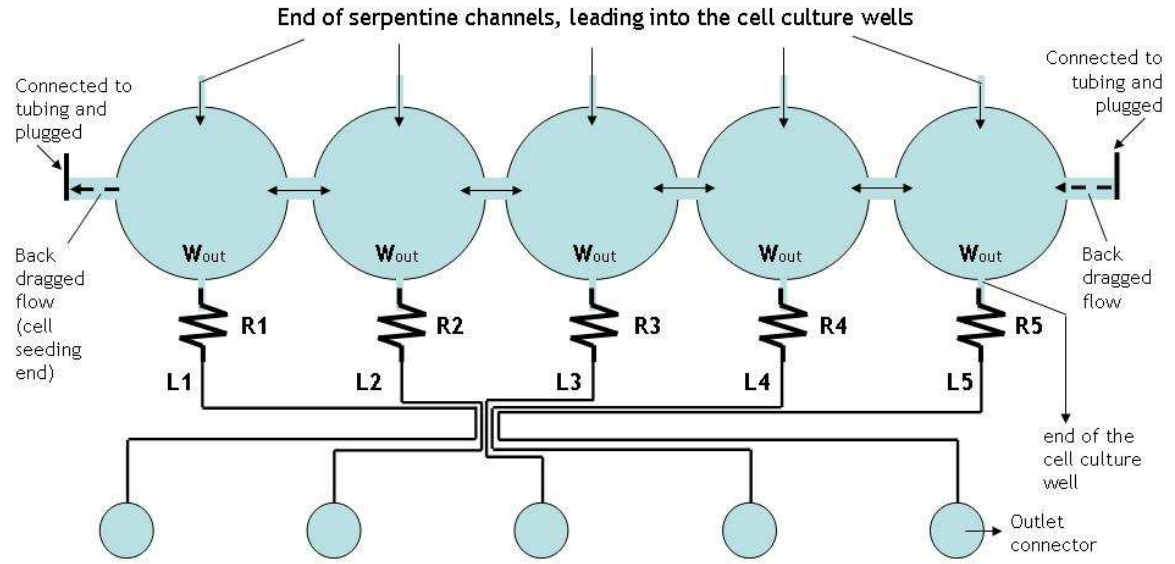

Figure 60: Resistance v/s length of outlet channels hypothesis
This is a hypothesis of the reasons for variable percentages (when compared to the expected values) inside the multiwell gradient device. Fluidic resistance 'R' is directly proportional to length of channels 'L', and is inversely proportional to the width of channels 'Wout' and cube of the height 'H'. Meaning that when 'L' increase there is a higher resistance and when 'Wout' and 'H' increase then the R in the channels is reduced. L5 is the longest channel, therefore this channel has the highest resistance, 'R5'. L3 is the shortest channel and therefore it has the least resistance. In this device, all the outlet channels are of the same width and device has an even height, then, L5>L1>L4>L2>L3 (from Table 8), therefore R5>R1>R4>R2>R3.

Outlet channels (L)	L1	L2	L3	L4	L5
Lengths (mm)	17.72	10.2	8.8	16.2	23.89
Resistance calculated (Pascal/m^3sec)(N/m^5sec)	1.6 x 10^{-5}	0.9 x 10^{-5}	0.8 x 10^{-5}	1.4 x 10^{-5}	2.2 x 10^{-5}

Table 8: Calculated lengths of the outlet channels and fluidic resistance.
The lengths were calculated from the end of each respective cell culture well until each outlet connector (shown in the schematic above)

To test the hypothesis, that the performance of the gradient device deviated from the expected dilution values due to the difference in channel lengths of the outlet channels, these were adjusted to be of the same length in a new design. Figure 61 showed the channels leading from the bottom of the cell culture wells (blue) to the observation channels (marked inside the dotted rectangle) and finally to the outlets had different lengths and explains the alterations made near the observation channels. To increase the lengths of channels serpentine structures were used, which meant that the size of the device would remain the same. This allowed the same device holders to be used when using different device designs.

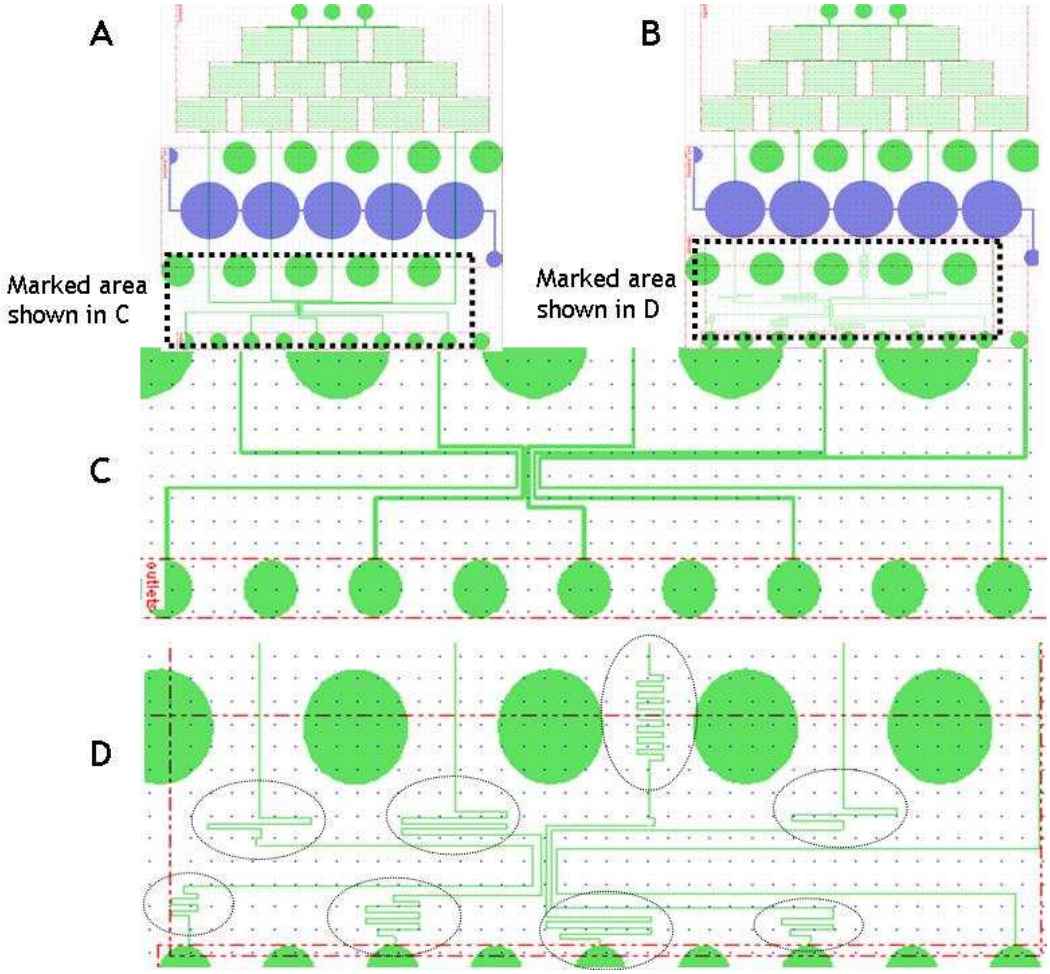

Figure 61: Changes in the lengths of the outlet channels.
A) This drawing represented the initial device, where the outlet observation channels were marked using a dotted rectangle – magnified in image (C). The length of these channels was not the same. B) This picture showed the new device bearing the corrected lengths of channels. The corrected region was marked by the dotted rectangle – magnified in image (D). The magnified image of the dotted area for the corrected design, showed serpentine like shapes were adopted to increase the length of the channels and to keep the size of the device the same (circled by the dotted circular lines). This helped in designing the same device holder for both these devices.

The FITC-dextran MEM mixture was on this occasion was introduced through the left inlet of the gradient device) and was run against plain MEM (introduced through the right inlet of the gradient) and results were observed under the fluorescent microscope at the observation channels at the end of the device. The different concentrations, shown in Figure 62, were results obtained for the 2000 kDa dextran in MEM when run against plain MEM. The fluorescence intensities observed using this device were tested for four different flow rates, 0.025 µl/min, 0.25 µl/min, 0.63 µl/min and 1.26 µl/min. The observations revealed that the homogeneity of the peaks for dye dilutions intensities was seen to homogenise as the flow rate was reduced. However, when the flow rate dropped below 0.63µl/min the dilutions were disrupted tremendously and the percentage of intensities varied a lot compared to the expected values (indicated by the red dotted line

and values were expected to be 100, 87.5, 50, 12.5 and 0%, from left to right). The best results were seen for the 0.63µl/min flow rate where the values were very close to the expected percentages and the peaks were slightly more homogeneous than the 1.26µl/min flow rate. The lesser flow rates showed good mixing but they had a very irregular dilution gradient.

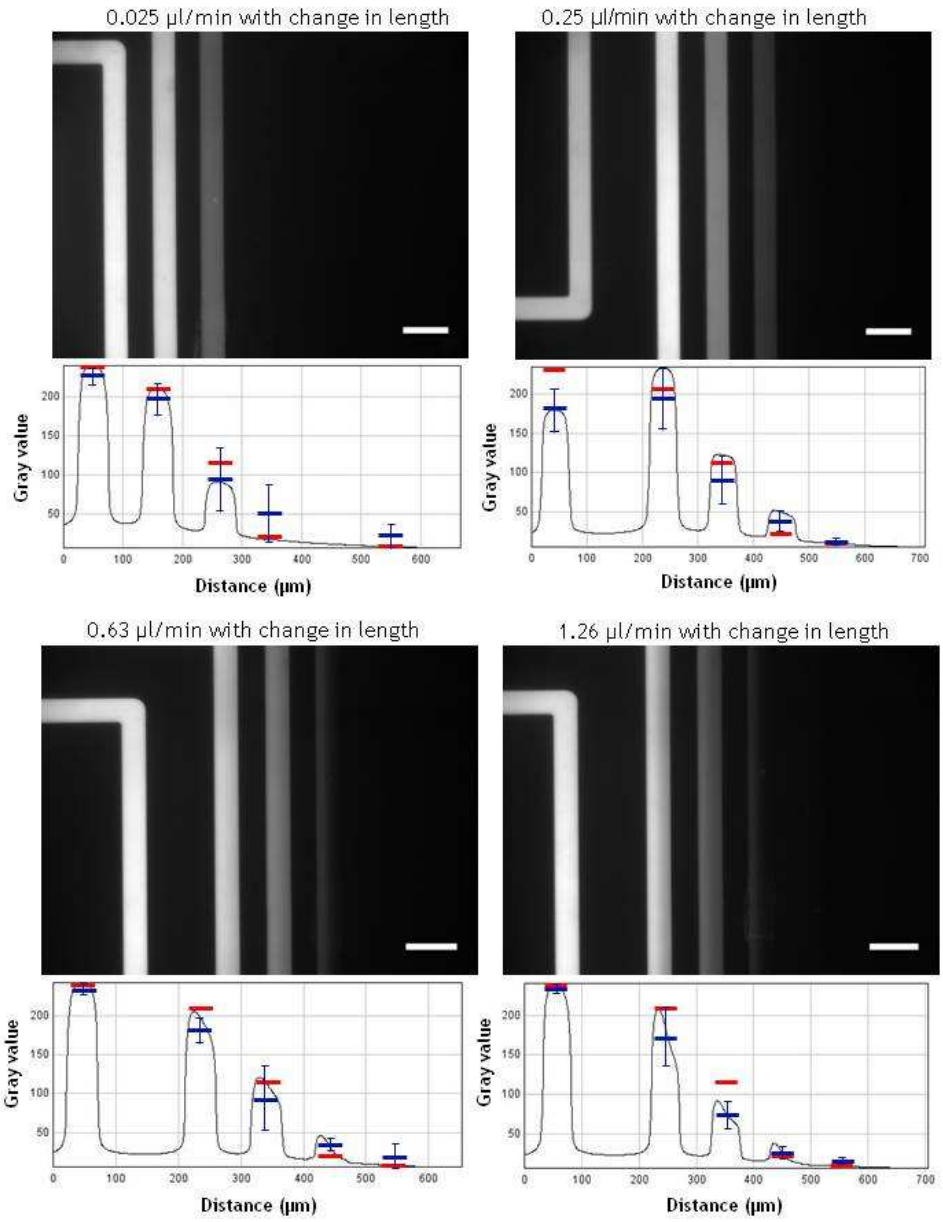

Obv. Channels - with changes in length	1	2	3	4	5
0.025 µl/min	100%	87%	36%	2.03%	NA
0.25 µl/min	75%	100%	51%	18.3%	NA
0.63 µl/min	100%	82%	44.4%	9.2%	0.2%
1.26 µl/min	100%	84.3%	34.2%	11%	0.7%
Expected percentage	100%	87.5%	50%	12.5%	0%

Figure 62: Intensity profile in the observation channels in the multiwell device with changes in the outlet channel length - perfusing FITC dextran in MEM medium from the left inlet and plain MEM medium from the right

The images and graphs show profiles of the fluorescence intensity for dilutions developed when using FITC-dextran 2000 kDa. The red lines mark the expected percentage intensity for each channel (from left to right; 0 - 100%). The values marked by the blue lines are the show the mean percentages for their respective channels, for n=4 samples showing ±SD (from left to right in the images). The black line marks the intensity profile for the images shown above each graph at their respective flow rate (where a 250µl SGE glass syringe was used with pump setting for a 10ml syringe). The table shows the different percentage of intensities obtained for each flow rate represented by the black line in each graph. (1, 2, 3, 4, and 5 are numbers for the respective observation channels in the images from left to right).

4.1.2.4 Epithelial cells cultured inside the gradient device

Initial experiments included improvements in seeding protocols and growth conditions in the attempt to adapt the cell lines Calu-3 and MDCK to prolong (>14days) cell growth within these multiwell microfluidic devices. The capacity of each cell culture well within these gradient devices and the ability seed the cells evenly inside each of the five cell culture wells was vital to allow comparison between the wells (cell seeding experiments shown in Figure 62, were carried out to arrive at this). Cells were seeded into the device via the cell seeding channels on the device and left to settle for an hour inside the cell culture wells. They were then fixed with 4% formaldehyde in PBS, and later stained with Coomasie blue. The stained cells were counted under the microscope.

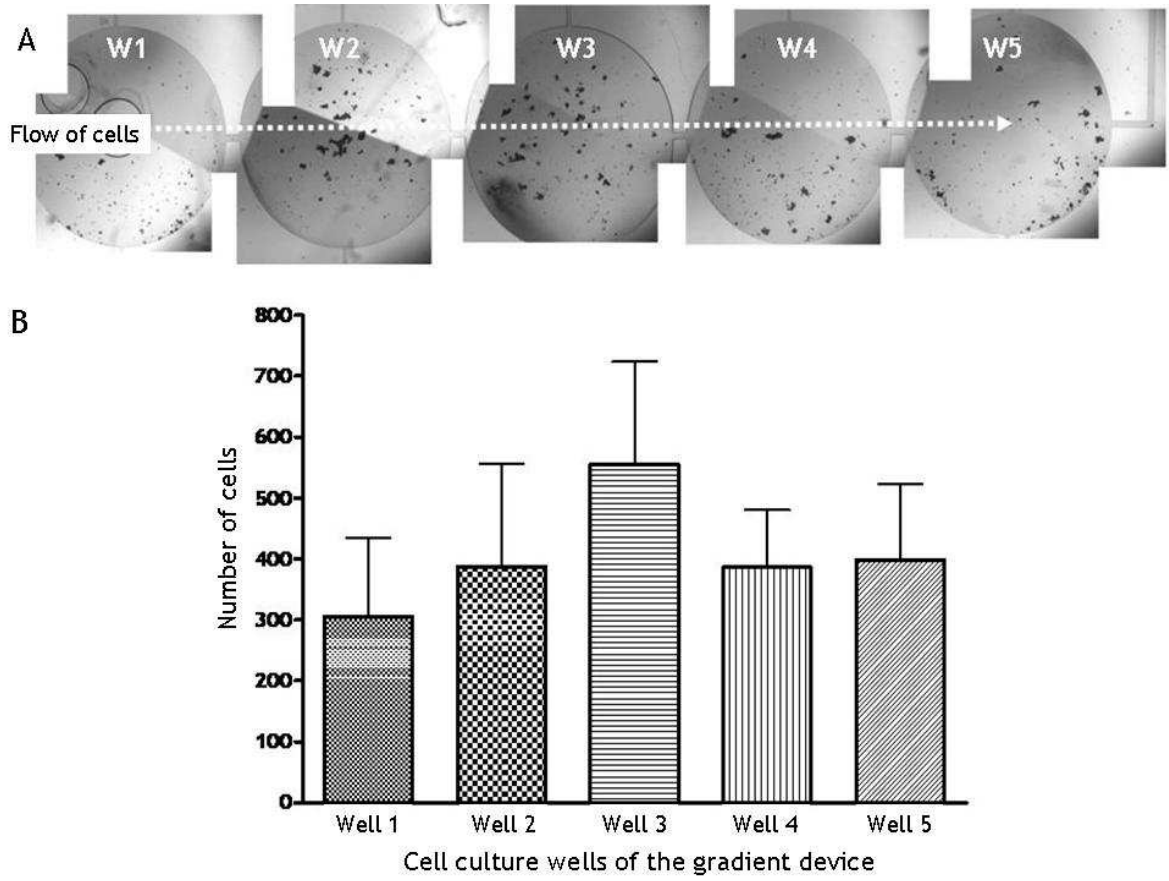

Figure 63: Cell counting
The image in A) was an example for the cell densities achieved at seeding using the multiple cell culture wells. The cells were introduced from the left to right and seeded at 2.9 x 10^6 cell/cm^3. using 2ml solution in total. After settling in the chambers for 1hr they were stained with Coomasie blue, see text for detailed results. The graph in B) shows the average cell density on the different wells (n=9, detailed values in Table 9).

W1	W2	W3	W4	W5
300 ±128	280 ± 168	522 ± 168	380 ± 94	432 ± 125

Table 9: Number of cells counted within each cell culture well of the device.
All wells showed a high value for the SD and hence there in principle the variation from well to well for the cell densities resulting in each well could be assumed to be similar. However, the middle well mostly showed larger number of cells within each the microfluidic device tested.

The middle culture well (W3 – indicated in the Table 9) consistently contained more cells. This could be due to differences in flow and pressure when the cells were introduced into the devices. An alternative explanation could be that, when seeding stops and the syringe with cells (used for seeding) is removed, cells are dragged backwards from the high flux areas (small channels connecting the last wells to the exit wells) but not from the low flux areas in the cell seeded wells. The limited amount of volume in the "high flux areas" limits the amount of back-dragged cells such that only the last three wells are "reseeded" (see Figure 60). When imaged over time (Figure 64) the seeded wells showed continuous "normal" cell growth. The Calu-3 cells were maintained inside the device for up to 14 days (Figure 64 E). The long culture times required to allow Calu-3 cells to mature (>14d) meant that the medium needed to be exchanged at regular intervals, on each occasion it was possible that air bubbles could be introduced leading to disruption of cell cultures. Care also had to be taken to equilibrate any medium in a 37 ºC incubator for before use with the devices which reduced the propensity for air bubbles, thus reducing the occurrence of air bubbles inside the devices. Due to the long time it took for the Calu-3 to become confluent MDCK cells were used for further experimentation, reducing culture time from more than 14 days to a confluent cell layer by day 4. This meant that the medium only needed to be changed once if at all necessary. Also MDCK cells have shown through literature to form good tight junctions and also posses the CFTR receptor protein. This meant they could be used as a substitute cell line for Calu-3 cells for such cell culture optimisation experiments.

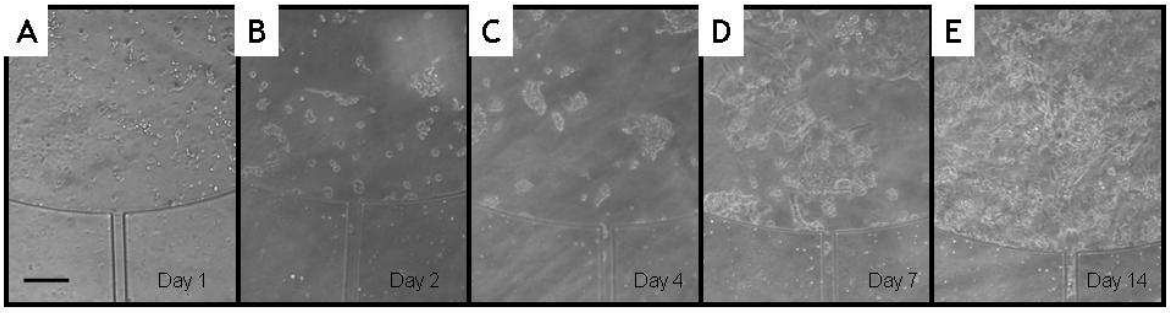

Figure 64: Seeding and growth of CALU-3 cells inside a cell culture well
The Calu-3 lung epithelial cells were seeded as described above and maintained inside the device for a period of 14days. The phase contrast micrographs show the exit part of the central cell culture well of the device. The cells proliferated and formed a confluent monolayer by day 14. Cells at culture days: A) 1, B) 2, C) 4, D) 7, E) 14. The scale bar (A) is 100μm.

4.1.2.5 The new multilayered toxicity device bearing the top/gradient device

The new multilayered toxicity device integrated with the top/gradient device, was ready to be used for cell culture optimisation experiments. Figure 65 shows the top/gradient device (A) and bottom microfluidic channels (B), where the both these devices microfluidic channels were adapted specially to fit the silicon nitride membrane chips in between them.

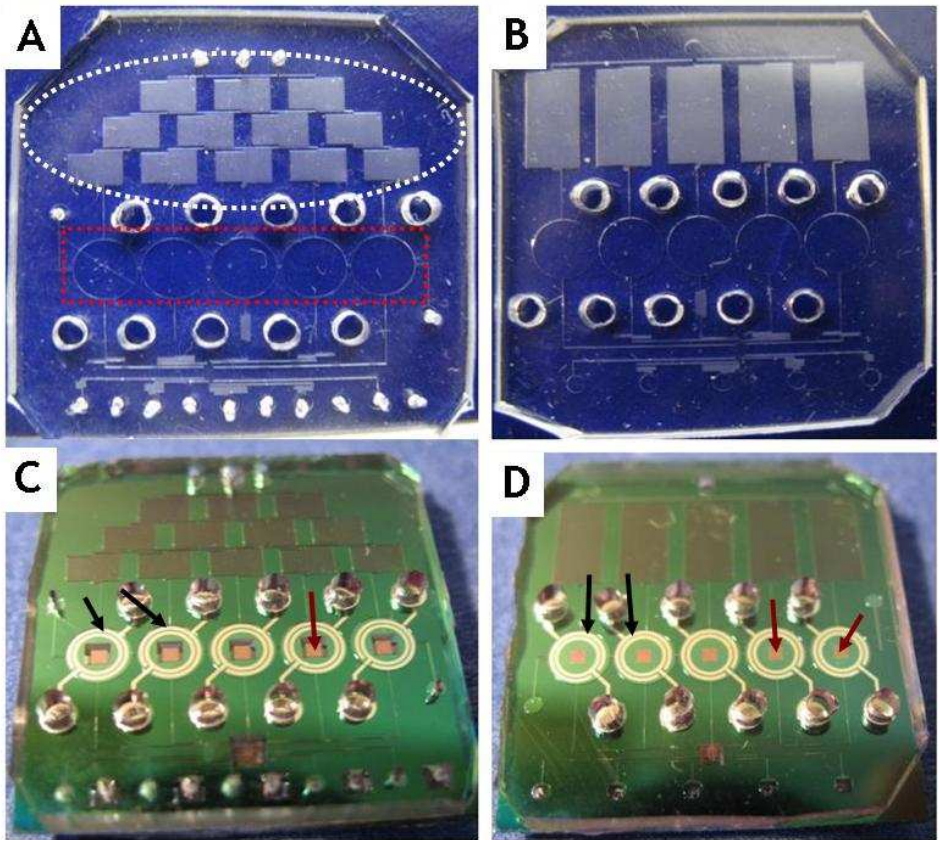

Figure 65: Final device parts
A) This image showed the top microfluidic channel which bears the concentration gradient (marked inside the whit circle) which leads into the cell culture well (marked inside red rectangle). The length of outlet channels had been altered to reduce the effect of pressure change within the system B) The bottom microfluidic channel. The length of the outlet channels have been altered in this case as well. C) This image showed the top view of the device when bonded to the silicon nitride membrane chip, showing the electrodes (black arrows). The electrodes surround the membranes (brown arrows) on the apical and basal compartments of the device. D) This is the bottom view of the device and where you can see also the membranes (brown arrows).

This device helped to measure the integrity of the cell monolayers using an integrated TEER measurement electrode setup designed specifically for this particular device (setup explained in Chapter 3, section 3.1.6.2. In order to achieve a sufficiently high (>129 Ohm/cm^2) TEER (Geys 2007) cell cultures would have to develop tight monolayers on the microporous silicon nitride membrane surfaces. The results seen in Figure 66, where experiments were carried out using Calu-3 (seeding density ~ 0.7 x 10^6 cells/cm^2) cells in order to test the quality and efficiency of cell culture and seeding into the device. The cells were seeded through the inlet channels in a direction perpendicular to the concentration gradient flow (explained in material method section of this chapter).

Problems with the development of gas bubbles arose very regularly, these would develop in the corners of the membranes, which proved to be a tough obstacle to tackle. However TEER in some wells of the devices without bubbles did show some TEER values of ~20

$k\Omega cm^2$. The average TEER was measured at every 10s interval and there were ten repeat measures for each interval (Figure 67). The electrical system setup and working is explained in Chapter 3, Sections 3.1.6.2. The culture system however, could not be maintained for a longer period than the amount of time analysed. Therefore, to get rid of the bubbles the sterilisation washing steps were very crucial and needed meticulous handling. During the washing steps there would always be an air bubble covering the membranes. Many methods to exclude them were attempted as listed here;

1) During the cleaning steps for the devices, ethanol was allowed to flow only through the top layer micro-channels. This would cause the fluid to seep through the silicon nitride membrane pores, preventing air bubbles being formed on the silicon nitride membrane trench (area, where the cells were to be seeded). Once the membranes were free of gas bubbles the flow in the bottom channels was started. This proved successful only until cells were seeded into the system after which sometimes air bubble would emerge.

2) Once culture medium was being perfused through the system, by day 2 or 3 bubbles developed at the corners of some, or all the silicon nitride membrane trenches. To attempt to eliminate them small amounts of CO_2 gas was pumped in through the seeding channel alternating with the inclusion of fresh cell culture medium. The CO_2 would help break down the bubbles and dissolve them into the medium along with itself.

3) The other method was to pump the liquid at a high flow rate (5, 10 or 50 µl/min) and agitate the device in order to break down the air bubbles into smaller parts, which would then slowly dissolve into the medium (within a few minutes). This method would however lead often to cracking of the delicate silicon nitride membrane and was therefore not deemed ideal.

4) Before the inclusion of cell culture medium into the devices, the medium was kept inside the CO_2 incubator to let it equilibrate (this could reduce the possible formation of bubbles later on during cell culture). All these attempts would sometimes be futile in eliminating the development, and or introduction of gas bubbles. Gas bubbles are detrimental to the functioning of any microfluidic chip as they can interrupt or divert the flow of medium and thus negatively affect cell growth. Most importantly gas bubbles can cause serious disruptions to the concentration gradient. In microfluidics gas bubbles are a very big issue and can often cause pressure differences and erroneous experimental results (Young 2010).

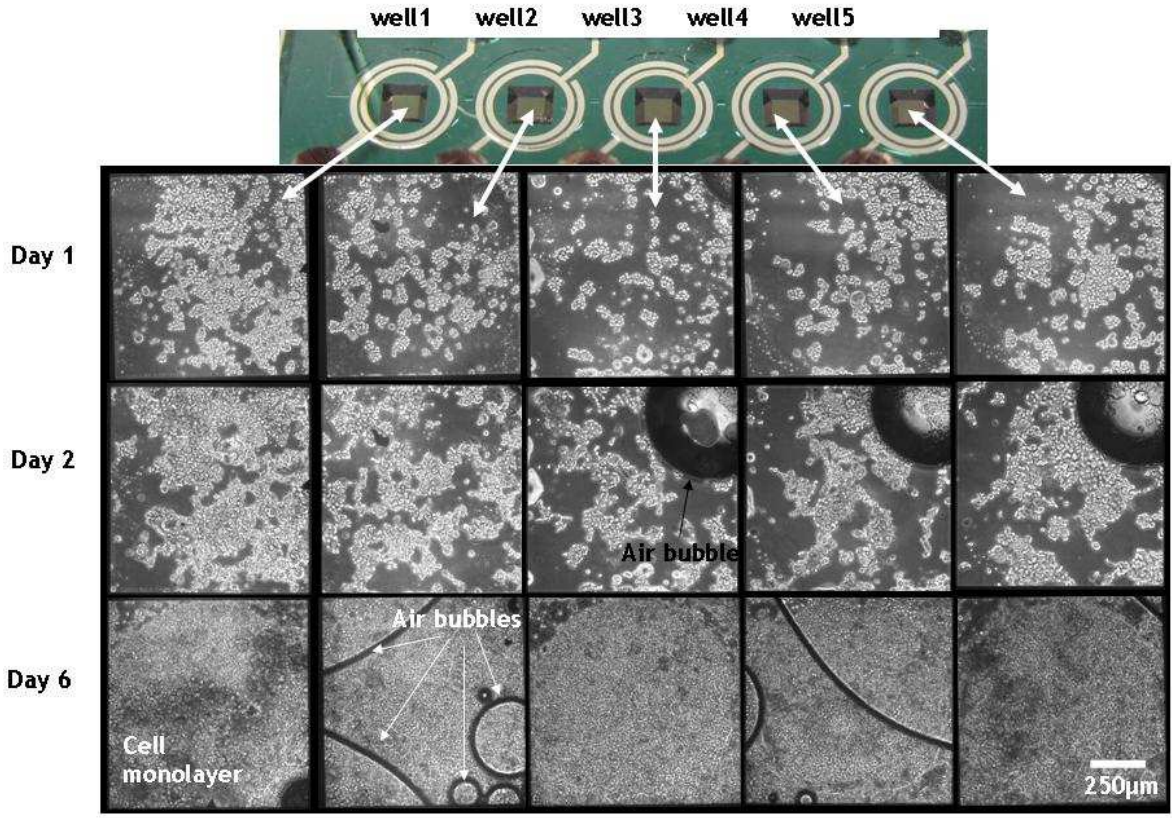

Figure 66: Cell culture in the final device.
This image shows cells being cultured on the porous membranes within the device. Cells were maintained for 6 days inside the device. The images show air bubbles in some of the membrane areas where the cell monolayers are being maintained. The scale bars in the bottom right hand side corner image is 250 µm.

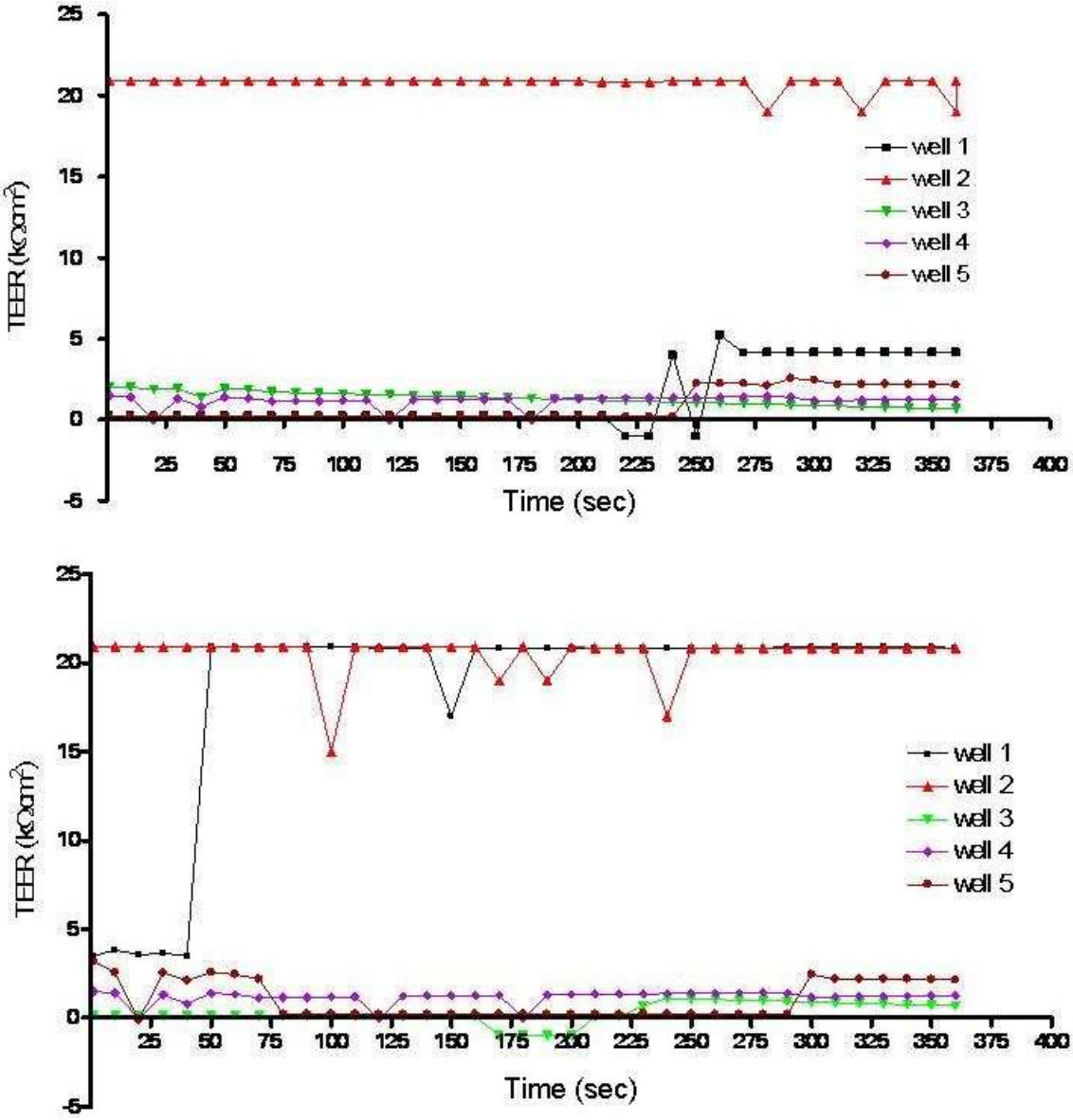

Figure 67: TEER on the multilayered device
These graphs show the TEER measurements for the respective wells in the device. The TEER was measured at every 10s interval and each interval took 10 readings. The final TEER measured was the average of the ten readings per each interval. The sudden drop of resistance or climb of resistance peaks were caused due to the loss of/contact between electrodes and electrode contacts in the system.

4.2 Discussion

The gradient device was adopted from a paper by Dertinger et al (2001) and Jeon et al, (2000) with the intentions of applying it to a different practical problem, i.e. the feeding of a series of cell culture wells with a series of different dilutions of toxins, here specifically nanoparticles. The design implications of some of the adopted changes in the design of the gradient generator which were necessary to incorporate the wells, and further to allow for on-chip assessment of the dilution gradient complicated the flow regime within. The idea of incorporating the gradient systems with cell culture was previously presented by Hung et al (2005). Their integrated system included a microfluidic device consisting of the gradient system leading in to a chain of cell culture wells. The uniqueness of their device was that they had fabricated perfusion channels on a different plain to the underlying cell culture well channels. The gradient formed would therefore not be disrupted and the perfusion channels would flow perpendicular to formation of gradient. Therefore, within their device once the cells reached a certain confluence they could use the gradient system to influence cells and administer various cytotoxic drugs. This however, was a much more complicated device than device where the gradient channels were with broad channel ends were used to study chemotaxis and hepatotaxis and others where the broad channels (cells seeded through the outlet channels) were connected by a separate seeding channels to introduce cells through (Song 2004, Walker 2005, Lin 2005, Jeon 2002). The top/gradient device explained in this chapter was on the lines of developing such a device where it would be possible to culture cells in the presence of a certain influence and also the perfusion channel would be the gradient channels since it would carry and dilute the test materials. As the entire device was more than 400 mm^2 the microfluidics design also included an “outlet observation point” which could be easily viewed under the microscope. This allowed microscopic, optical access to the different output channels in the five different channels within one field of view (dependant on the magnification). The results obtained from using the dye to study the behaviour of the device were shown to form dilutions that were slightly away from the expected values of the gradient dilutions (of 0, 12.5, 50, 87.5 and 100), which meant that there was a problem with the device shown in Figure 68 . The results obtained from such experiments, when red dye was used against water, the dilutions were found to be slightly less varied from the expected result. This was also evident when using FITC–dextran dye through the device. There could be several possible reasons for this divergence from the expected values, such as:

A) Difference in lengths of the outlet channels, this would cause a difference in resistance to flow, which in turn would lead to differential flow through the parallel channels of the system;

B) The interconnects between the wells, which were intended for cell seeding may interfere by allowing the mixing of the dye in adjacent cell culture wells and hence the resultant dilutions observed at the observation channels (see Figure 62 for observation channels) may be slightly varied from the expected values. An example for such cross-contamination via the cell culture well interconnects is shown in Figure 68, where the red dye flows from one well into an adjacent one through the interconnecting channels.

The observation channels were designed such that the outlets leading from the cell culture well to the outlet connectors would run parallel to each other for a certain distance to allow them to be viewed simultaneously. This meant that the individual exit channels were not of the same length due to the varied distances between cell culture wells. The measured resistance in each channel was different, due to which the fluid mixtures showed a tendency to exit through the channel(s) of least resistance. In order to overcome this problem the lengths of these exit channels were changed and the new devices tested. As Figure 61 shows this resolved the problem to some extent, where the different channel lengths were increased using serpentine channels. This meant that the device holder designed for the old device could be used again for the new device in which the lengths of its outlet channels were changed.

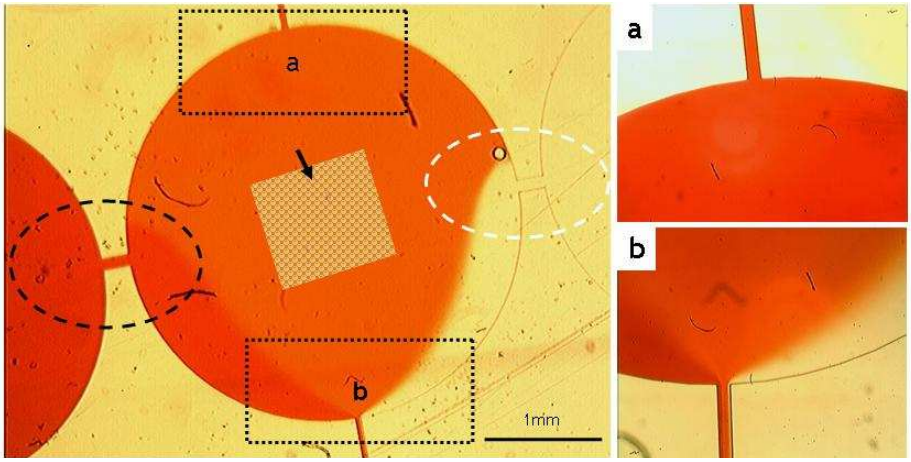

Figure 68: problems with the device.
A) The picture here shows the interference from the adjacent cell culture channels. On the left the darker red colour is seeping into the lighter compartment. On the right the water is seeping into the lighter red colour well. The block 'a' is the dye when it enters the middle chamber after passing through the gradient. The block 'b' is the outlet leading into the observation channels.[The darker red dye invades the adjacent wells marked by the black dotted circle and the buffer leaking into the adjacent well marked by the whit dotted circle. The arrow marks the membrane area when using this device in the multilayered setup TEER measurement setup]. The black arrow points towards the area marked by a red checkered box approximately 1 x 1 mm, like the size of the silicon nitride membrane. This signifies that the area where the checkered box is situated major area surrounding it is the part of the device where the dilution is unaffected by the flaws in the device.

Once these alterations were made, the modified device was tested and the fluorescence intensities across the exit channels (Figure 62) at a flow rate of 0.63 µl/min, were more in line with expected percentages (0, 12.5, 50, 87.5 and 100%). As expected the changes in the length of channels had an effect on the resistance of the monochrome system and quality of mixing. However, the images of some channels (mainly the middle in the graphs of Figure 62) showed a tapered orientation in the graph, suggesting that the mixing was incomplete. Therefore, it was thought that there could be cross contamination between two adjacent cell culture wells through the interconnected parts (seeding channel) which could be causing the incomplete mixing observe at the observation channels.

4.2.1.1 Problems associated with the new multilayered toxicity testing device

Gas bubbles were a major problem when using this device. The problems with gas bubbles start right with the assembly, sterilistaion, and continue during cell seeding, cell feeding and further perfusions (Figure 69). When starting the sterilisation steps for the devices bubbles would form in the region of silicon nitride membrane trench (where cells are to be seeded). This would occur on every occasion when using the device. To rid the device of these bubbles was achieved by either constant agitation, or increased fluid flow rates.

However care needed to be taken when increasing flow rates as the silicon nitride membranes were delicate and could crack if the differential pressure across the membrane was too high (effects of pressure on silicon nitride membranes are discussed in (Nguyen 2006) pages 420 – 422). The following treatments/protocols were developed to address these problems:

A) The microfluidic channels in PDMS were exposed to air plasma which makes the surface more hydrophilic (explained in Chapter 3) therefore allowing the fluids to flow easily, inspite of which these bubbles would appear.

B) Another way was the development of a rinsing protocol: during the washing and rinsing steps the 70% ethanol solution would be initially allowed to flow through the top/gradient channels and into the silicon nitride trenches. This would force the air bubbles from the membranes surface and push them through the pores of the membranes into the bottom microchannels. Both these methods would work only 30-40% of the times and were detrimental to the cell cultures because these bubbles had the potential to rupture cell membranes. Also since the multilayered devices were fabricated with PDMS microchannels the air bubbles have the potential to enlarge with time (This was due to the gas permeable nature of PDMS)(Mukhopadhyay 2007, Young 2010).

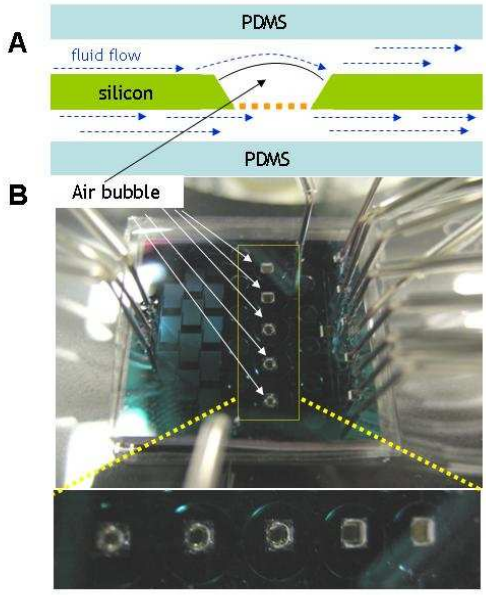

Figure 69: air bubbles problems
A) The image shows the gas bubble were trapped this could have been due to the fact that the silicon surface was slightly more wettable than the sides of the trench and silicon nitride membranes. exactly on top of the membrane surfaces of the devices and disrupting the flow of fluid also preventing any fluid flow through the membranes. B) This is an image of a working device in the sterilisation stage and the only areas that have the air bubbles are the silicon nitride trenches.

These gas bubble problems persisted, although many devices showed the presence of gas bubbles present in either 2 or 3 membrane trenches rather than all of them. The results seen in Figure 66, show the cell monolayers being maintained inside the device on the silicon nitride membranes. These pictures show the presence of air bubbles within some of the culture wells and some without any air bubbles. These problems not only affected the multiwell, but also the single well device, here the problem could be resolved easier, since it was only one silicon trench surrounding the silicon nitride membrane. Hence, in Chapter 3 the results for cell maintenance within the single cell culture wells were more successful (with 60% success rate). However, the aim for this PhD was to develop a device that would allow miniaturising and parallelising the measurement setup as well as allowing in-line measurements. Therefore, the integrated TEER measurement system needed to be used when testing the tightness of the monolayers. The presence of gas bubbles within the multilayered devices interfered with TEER readings and is often read as an error (the gas bubble meant that there would be a break in the circuit and therefore resulting in no reading). Due to such problems, the TEER readings were difficult to acquire (compared to the static condition TEER values) when cells were being maintained under flow conditions inside this device.

4.3 The top/gradient device used for testing the effects of *Pseudomonas aeruginosa* on epithelial cells

Pseudomonas aeruginosa (P.aeruginosa), an opportunistic bacterium species, is part of a vast group of aerobic gram-negative microorganisms found in soil, water and other moist environments. This pathogen causes morbidity and mortality, particularly in patients with impaired clearance within the respiratory system. Especially in patients with cystic fibrosis (CF) where normal clearance mechanisms within the respiratory system are impaired, these bacteria are known to colonise the lungs and cause diseases (can cause the onset of pneumonia). The ciliated epithelium that lines the airways possesses several mechanisms to prevent colonisation by inhaled bacteria, thus the lower respiratory tract usually remains free of bacteria. In CF patients the defective function of the CF transmembrane conductance regulator (CFTR) in airway epithelium and submucosal glands has been shown to be associated with invasion of the virulent bacterial species. (B. Goldberg 2000, Mendes 2004, Pier 2002, Kato 2002, Taccetti 1996, Gomez 2007, Moreau-Marquis 2008, Boucher 2002). The CFTR in the lungs result in excess re-absorption of sodium inside the airway epithelium causing an excess of water in the airway surface liquid. This excess of

water inside the airway system immobilises epithelial mucus and inhibit ciliary activity on epithelial surfaces resulting in mucus plaques forming on the surfaces. *P.aeruginosa* penetrates these plaques and is protected from phagocytosis or anti-microbial activities, hence allowed to colonise and cause chronic infections (Hull 2003). *P. aeroguinosa* rapidly switch from dormant behaviour to a more indolent mode of growth, turning off the expression of immunostimulatory products such as flagella-proteins, and initiate the formation of a protective biofilm; this adaptation played a critical role during chronic infection with *P. aeruginosa* (Gomez 2007, Saavedra 2002, Jacob 2002). The commonly used cell lines in cystic fibrosis studies in the literature were Calu-3 and Madin Darby canine kidney (MDCK) cells, since they express the CFTR receptor and display the protein on their plasma membrane. This therefore would create an affinity towards infection from *P.aeruginosa* leading to the formation of bacterial biofilms on cell surfaces (Jacob 2002, Vikströma 2009, Saavedra 2002, Mendes 2004, Saavedra 2002, Campodónico 2008, Terheggen-Lagro 2005).

The microfluidic top/gradient device is being used here as a stand-alone device to investigate the effects of *Pseudomonas aeruginosa* on Calu-3 and MDCK. This microfluidic device setup could offer a new avenue in the study of pathogen-cell interaction, as this device allows this interaction to be interfered with using a range of soluble factors in a contained and parallelised way. The device used is the same top/gradient device with the five cell culture well system introduced above, and illustrated below (in Figure 52). The concentration gradient system offers the opportunity to (A) generate different seeding densities of bacterial species and (B) different concentrations of antibiotic solution (expected concentrations of 0, 12.5, 50, 87.5 and 100% concentrations). By diluting the bacterial colonies amongst the five cell culture wells, their effects on mammalian cell cultures (maintained within the five wells of the device) could be investigated in a density dependant manner (as each well would be supplied with a different inoculum). Similarly once the bacterial colonies have established themselves inside the culture wells and at the stage of forming biofilms on epithelial cell, it would be advantageous to administer different doses of antibiotics and drugs to test their reactions.

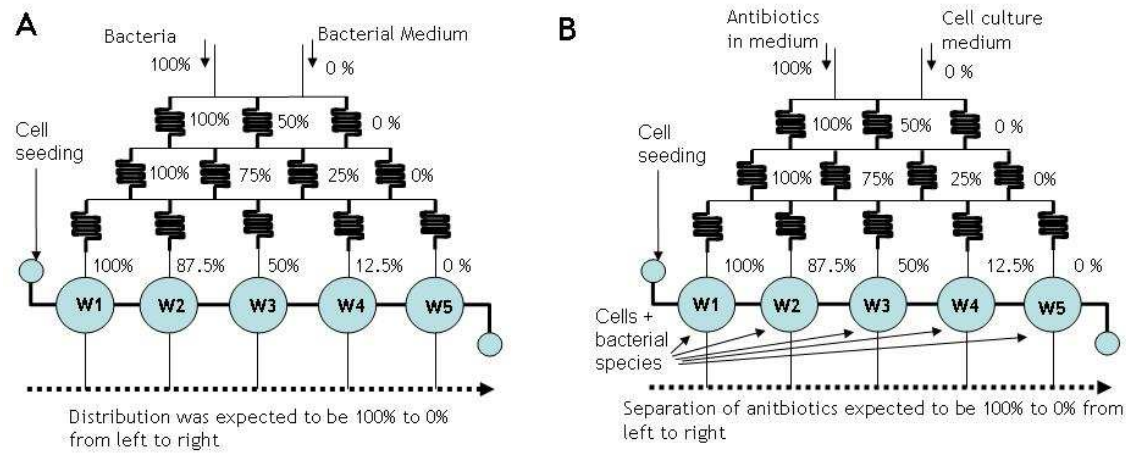

Figure 70: project ideas
A) This model showed how the device could be used to generate different seeding densities of bacteria. B) This showed how different concentrations of antibiotics could be administered using the device.

4.3.1 Materials and Methods

4.3.1.1 Handling the bacterial colonies

The bacterial colonies were maintained in a small 1.5 ml vial containing 1 ml Luria-Bertani (LB) nutrient medium (0.1 mM tryptone, 0.05 mM yeast extract, 171.2 mM NaCl, pH 7). When cells were not in use they were kept refrigerated at ca. 4 °C. When bacterial colonies were needed for experiments these vials were warmed up and centrifuged to obtain bacterial cell pellets. The old medium was substituted with fresh medium and the vial was incubated for 1 hr before use. To count the colonies forming units (CFUs) petri plates were used which were prepared by pouring LB agar (125 mM agar – pH 7) followed by autoclaving. The bacteria were smeared onto these sterile plates in order to determine the CFU, before they were used in experiments. Once the CFU were known, a measured quantity of (~4.8 x 10^5 CFUs within 100µl of bacterial broth) was added to the cell monolayers and incubated for 6 hrs before analysis or staining. When being used with the gradient (standalone) devices, 20 µl solution of bacterial stock solution mixed in 1 ml LB medium (when used with cell cultures then the stock was mixed in 1 ml of EMEM/DMEM medium) was introduced through one of the gradient inlets and plain medium was introduced through the other (at a flow rate of 0.63 µl/min, using the 250 µl glass syringe). When using the cells the bacteria were allowed to flow through while observing the effects with time-lapse setup on the phase contrast microscope (in the hot room kept at 37°C). When used without cells the colonies were collected off chip through the outlet channels and plated onto LB agar plates (To check the dilutions developed due to the gradient).

4.3.1.2 Live/dead staining

In order to determine the proportion of bacteria affected cells whilst minimising contact, the reduced biohazard viability/cytotoxicity kit 1 (Invitrogen, Paisly, UK) was used to test the epithelial cell monolayer resistance to *P.aeruginosa* in the presence of different concentrations of antibiotics [23]. This staining depends on the permeability of the two stains SYTO-10 (green fluorescent nucleic acid stain which is membrane permeant and labels all live cells, including the ones with intact plasma membranes) and "DEAD Red" cell impermeant and labels only cells with ruptured plasma membranes. To wash the cell monolayers, cell culture medium was replaced with clear (without phenol red) HEPES – buffered saline solution (HBSS - 135 mM NaCl, 5 mM KCl, 1 mM $MgSO_4$, 1.8 mM $CaCl_2$ and HEPES solution pH 7.4). The cells were then incubated in the dye mixture containing 2µl of SYTO-10 (Component A) and 2µl of DEAD-Red (Component B) into a common 1ml volume of HBSS (1:500 dilution of each vol/vol). The dye solution was removed and the cells were washed with HBSS, followed by fixation in 4% glutaraldehyde in HBSS for 1 hr (1ml of glutaraldehyde in 25ml of HBSS). The fixative was substituted by HBSS and then immediately examined under the fluorescent microscope.

4.3.2 Results

4.3.2.1 Live/Dead staining

To study how the epithelial cells can be affected by the presence of *P. Aeruginosa*, experiments using a so called "live/dead" staining for Calu-3 and MDCK cells, was used. The effects of different antibiotic concentrations on such *P. aeruginosa* infected cultures were also tested. (The images in Figure 71 shows the live/dead staining) In A) and B), Calu-3 and MDCK cells were infected with bacteria and incubated for 1hr at 37ºC. Then these cells were fixed and stained with the live/dead stain. Calu-3 and MDCK showed a large number of dead cells associated with the low concentrations of the antibiotic as expected. These experiments were also useful in working towards creating a control experiment to test the reactions of cells in presence of different antibiotic solutions[23] required for experiments in combination with *P. aeruginosa* inside the concentration

[23] Antibiotic stock solution was the same as presented in Materials and Methods from Chapter 2 section 2.1.3 Cell Culture. Dilutions from 10^{-4} to 10^{-1} solutions were prepared in relation to the antibiotic stock solution and tested with the different colonies.

gradient device. The gradient device would help dilute the antibiotic solutions and it was necessary to establish a negative control of antibiotic resistance towards the bacteria.

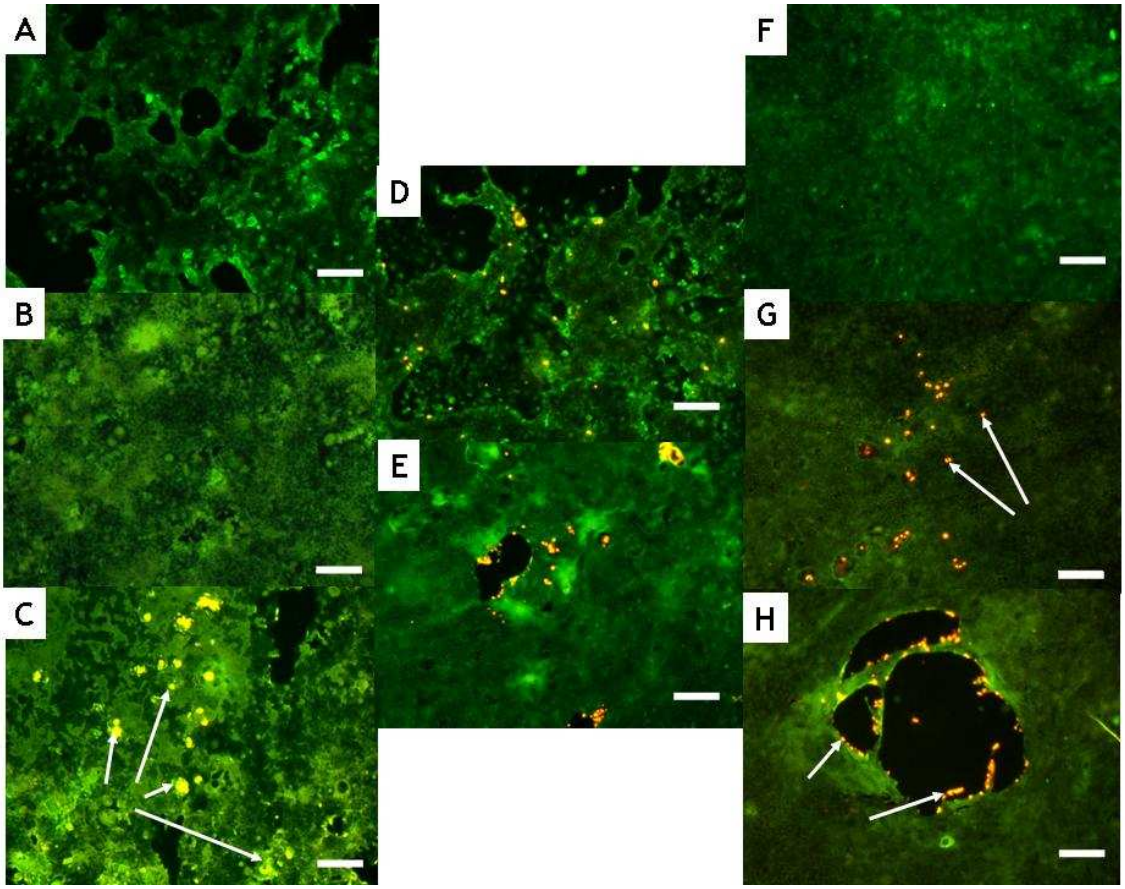

Figure 71: Live-Dead staining of Calu-3 cells to test antibiotic resistance.
The live dead stains used were the SYTO 10 green fluorescent nucleic acid stain for the live cells and the DEAD Red (ethidium homodimer-2) nucleic acid stain from the kit (LIVE/DEAD Reduced biohazard viability/cytotoxicity Kit). A) Calu-3 cells cultured in the absence of the bacteria. B) Calu-3 cells were observed after infecting them with the bacterial species and were put under a dosage of 10^{-1} concentration of antibiotic (2% antibiotic mixture – see 2.1.5 Chapter 2). The green cells were the live stained cells and there was no presence of any dead cells. C) Calu-3 cells infected with bacteria and in 10^{-4} concentration of antibiotic solution. D) The Calu-3 cells were cultured in the presence of bacteria and in the absence of antibiotics. The green cells are alive and the orange yellow cells are the dead cells. E) MDCK cells were observed after infection with the bacterial species was put under a dosage 10^{-1} concentration of the antibiotic. Cells coloured red were the dead cells. F) MDCK cells were cultured in the absence of bacteria G) MDCK cells cultured in the presence of bacteria but in the absence of antibiotics. H) MDCK cells were observed after infection with the bacterial species was put under a dosage 10^{-4} concentration of the antibiotic. Scale = 0.1mm. (white arrows mark the dead cells)

4.3.2.2 Cell interactions with *P. aeruginosa* inside the top/gradient microfluidic device

MDCK cells were maintained within the culture wells, as seen in Figure 72: MDCK being observed after introduction of *P.aeruginosa*, and were allowed to remain in culture for 7

days. These cells were infected with *P. aeruginosa* and they responded to the introduction of the bacteria by initially shrinking in size. At the same time the MDCK cells were found to shrivel and move towards each other.

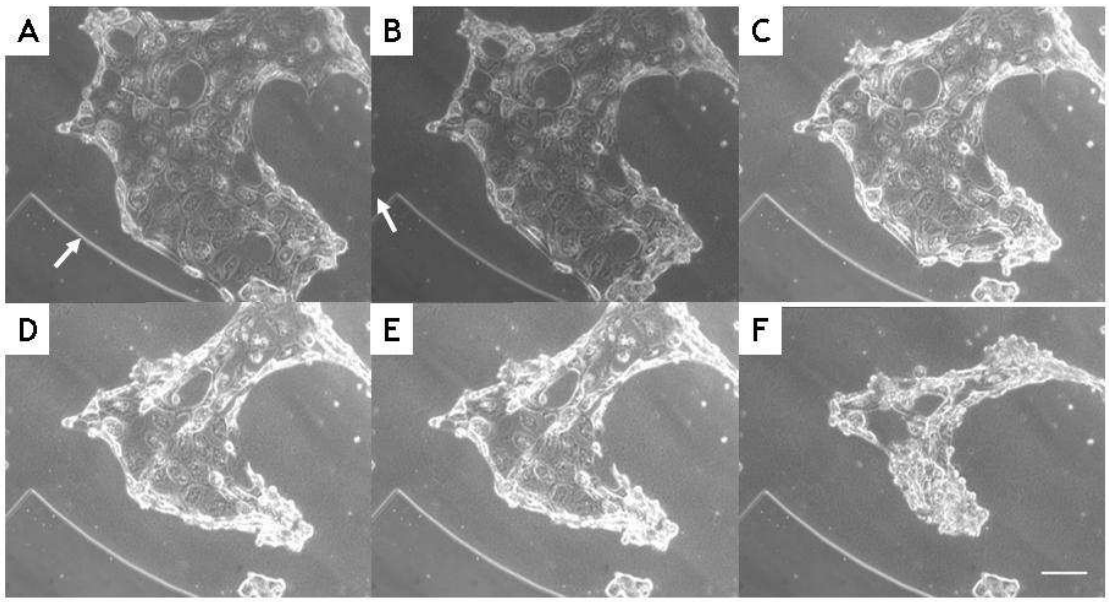

Figure 72: MDCK being observed after introduction of *P.aeruginosa*
The images are a time lapse set showing the reaction of MDCK cells to bacterial infection. The cells were allowed to proliferate within the culture wells for 2-3 days and then infected with a solution of *P.aeruginosa*. From image A) to F) it is evident that the MDCK cell monolayer starts to shrink and cells seem to move closer towards each other, cells were seeded until day 2 and then this happened over 6-7 hrs. Frames A-F were taken 60 minutes/hours apart. Scale bar - 400µm in F. The white arrow in A and B show the cell chamber boundary and the inlet channel respectively.

4.3.3 Discussion and conclusion

The aim here was to observe the effects of the *P. aeruginosa* on epithelial tissue within a contained microenvironment. Microfluidics in this context was an enabling technology where the experiments with the pathogenic bacteria were performed in a safe, enclosed environment. This also helped to reduce both the number of bacteria and the amount of antibiotic solutions used. The P.aeruginosa has been used through literature on epithelial monolayers is commonly judged indirectly using their effect on tight junction-proteins (Jacob 2002, Saavedra 2002, Kazmierczak 2001, Nicolis 2009, Vikströma 2009). The experiments shown in Figure 71 and Figure 72 show the effects of *P. aeroguinosa* on the MDCK monolayers under normal conditions in culture. The different antibiotic solutions were used to observe whether the cell monolayers that were put under the influence of the bacteria would yet survive and also to test which would antibiotics concentration would be the optimal to lead to a resolution of the bacterial infection, and at which the MDCK would still be alive. This meant that we would set a control experiment under static conditions to

test cell responses in presence of antibiotics. Figure 69, where epithelial cell cultures of MDCK cells were maintained inside the multiple cell culture well device. These cells were put under the influence of *P. aeruginosa,* resulting in the rapid shrinking of the monolayer of MDCK cells. These initial results show the short term effects and reactions that were presented here when cells exposed to the bacterial species. However, there were certain microfluidic devices that studied the effects of certain bacterial species and worked on manipulating their behaviour according to chemical stimuli by using a gradient of concentrations. (Larry 2008, Mao 2003, Balasubramanian 2007, Inatomi 2006). Also these most bacterial species like *P. aeruginosa* are motile and possess micro pili, and in constant motion through liquid. However, these motile functions can be controlled to some extent within micro channels (Purcell 1977, Brody 1996). Such examples have shown that high throughput systems could be useful for the study of some micro-organisms.

4.4 Multilayered SU-8 device

The microfluidic devices until this point in the thesis, were being fabricated using PDMS against an SU-8 master substrate. The idea behind this part of the thesis was to develop a device entirely in SU-8 in order to avoid the sealing and bonding processes required for PDMS. Also previously shown silicon nitride membranes have several fabrication steps (see Section 3.1.1, Chapter 3). By using SU-8, the number of fabrication steps as compared to the silicon nitride membrane fabrication, could be reduced and several devices can be prepared in parallel within one day. However, the primary focus of this project was to first assess the fabrication of the middle porous membrane (using SU-8 3005) and then move on to the fabrication process for an entirely encapsulated device. In the first instance the device design was simple which has a single fluidic microchannel at the top and the bottom separated by a microporous membrane. The single channel design is shown in the Figure 73, pointing out the different layers of the device; the bottom channel (layer 1), the middle membrane (layer 2) and the top channel (layer 3).

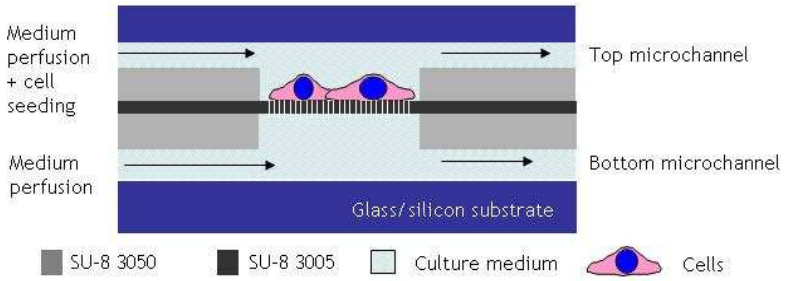

Figure 73: Multilayered device fabricated in SU-8
This is a schematic representation of the working of the multilayered microfluidic device. The SU-8 channels would be sealed on either side with glass or PDMS. The bottom layer, middle porous membrane layer and the top microchannels were to be fabricated in SU-8 the inside the clean room and developed together. Cells would be maintained on the middle porous membrane surface. The entire system would be a sealed device which would reduce leakages.

The SU-8 series is a commonly used negative resist for micro-electro-mechanical systems (MEMS) technologies (Hill 2007, López-Romero 2010, Voskerician 2003). They allow for the fabrication of high aspect ratio structures having stable adhesion with the substrates, with vertical side walls and excellent reactive ion etching resistance. SU-8 fabrication involved the process of exposing the resist to light and in doing so the resist polymerises and hardens (explained in Chapter 2 – Introduction). Once it has polymerised, the SU-8 is non reactive and is resistant to most solvent types. This property made it an extremely useful resist in terms of applications in various fields (del Campo 2007, Keller 2008, Mata 2006). The success of this project largely depended on the properties and characteristic of the SU-8 used. From SU-8 3000 series of photoresist, the SU-8 3050 and the SU-8 3005 were used to create the different layers for this particular device (3050 for the top and bottom layers and 3005 for the middle membrane layer). The viscosity range of SU-8 3000 allowed for film thicknesses of 4 to 120µm in a single coat and also the adhesion to substrates was improved (MicroChem data sheet). SU-8 3000 is also quite transparent, which makes it ideally suited for imaging and handy for cell imaging too. This also made it easy when trying to align the multiple layers during exposure under the mask aligner.

4.4.1 Materials and Methods

4.4.1.1 Multilayered SU-8 device fabrication steps

The designs for the microfluidic device are shown in Figure 74, where the three different layers A) bottom layer, B) the middle membrane layer and C) the top channel designs are seen in a 2D top view. The bottom channel design consists of pillars within the cell culture

well. These pillars were included to support the porous membrane layer. The middle membrane consists of a porous membranes of 3.5 mm diameter with pores of 3 µm diameter spaced 10 µm on a square lattice. The top layer was designed to contain the main cell culture well in which the cells would be maintained and could proliferate over the membrane surface. The images in a), b) and c) give a better understanding of different processing stages for the multilayered SU-8 device when seen in 3D.

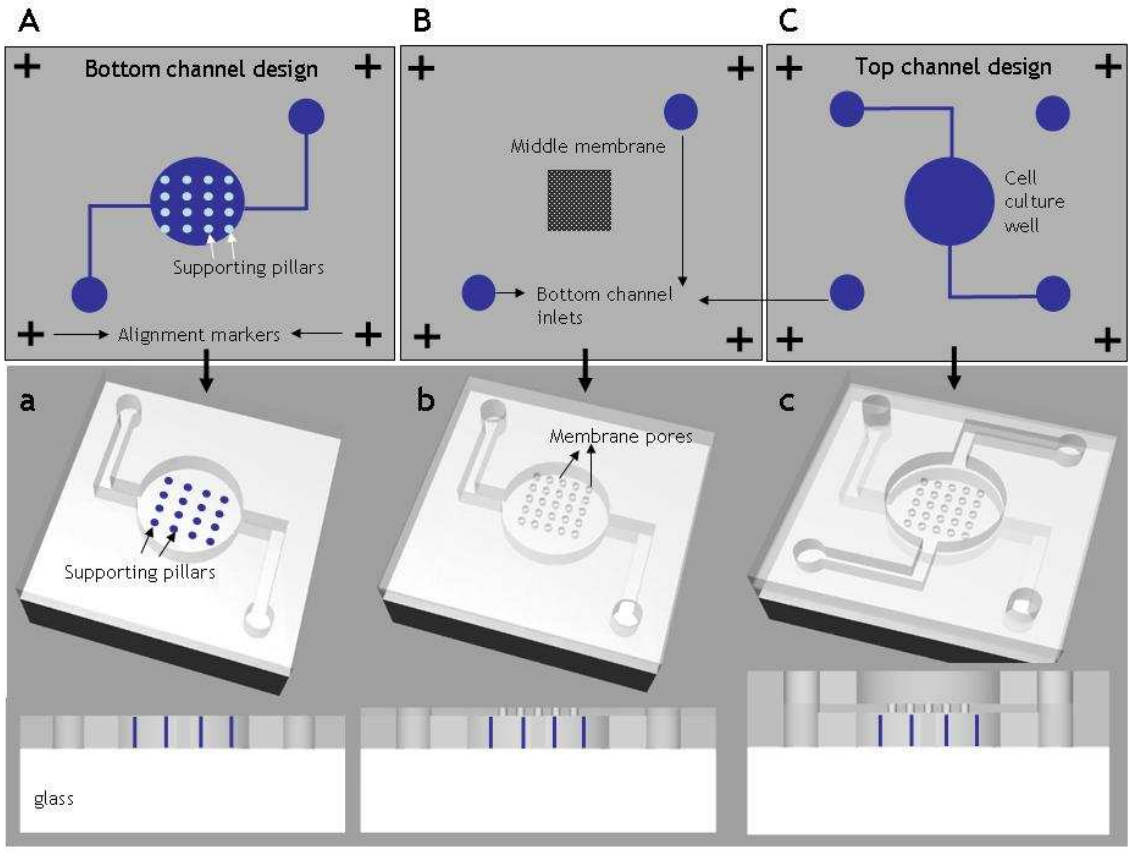

Figure 74: Multilayered SU-8 device design
The device consisted of three parts A) the bottom microfluidic channel which also had the supporting pillars for the membrane layer, B) the middle porous membrane and C) the top microfluidic channel consisting of the main cell culture well. These designs have been represented in 3D images a), b) and c) to give a better understanding of the fluidic device design.

4.4.1.2 Fabrication of the different SU-8 layers

The fabrication procedure consisted of 5 stages presented in Figure 75. Stage 1: SU-8 3050 photoresist was spin coated onto a clean glass slide/coverslip (using a spin speed of 2000 rpm) and then a pre baking step of 95° C for 30 min to achieve a height of ~75 µm (Table 5: SU-8 fabrication scheme showing the nominal and measured resist heights. and the used for this project as given in Table 10). Stage 2: dealt with the exposure of the bottom layer

and exposure details were listed in Table 2. On exposure, the resist was not developed. The development of this layer was continued in Stage 5 of this protocol. Stage 3: SU-8 3005 photoresist was spin coated at 3000 rpm to form a layer with a thickness of 5 µm. The pre bake step for this stage was altered to work as the post exposure bake step for bottom layer. Stage 4: This resist was exposed with a different mask plate designed to fabricate the porous membranes. Exposure times for this stage were different for each of the layers. Therefore it was important to get an optimum exposure setting in order to prevent overexposure of the membrane and the bottom layer. After the exposure step the third layer of SU-8 3050 was spin coated on and then the pre-exposure bake step followed. Stage 5: Using a third mask design, the third layer was exposed and caution was taken while exposing this layer to prevent over exposure of he membrane layer. The entire device would then be baked for 12 min and developed until the microchannels also cleared out from any unexposed photoresist.

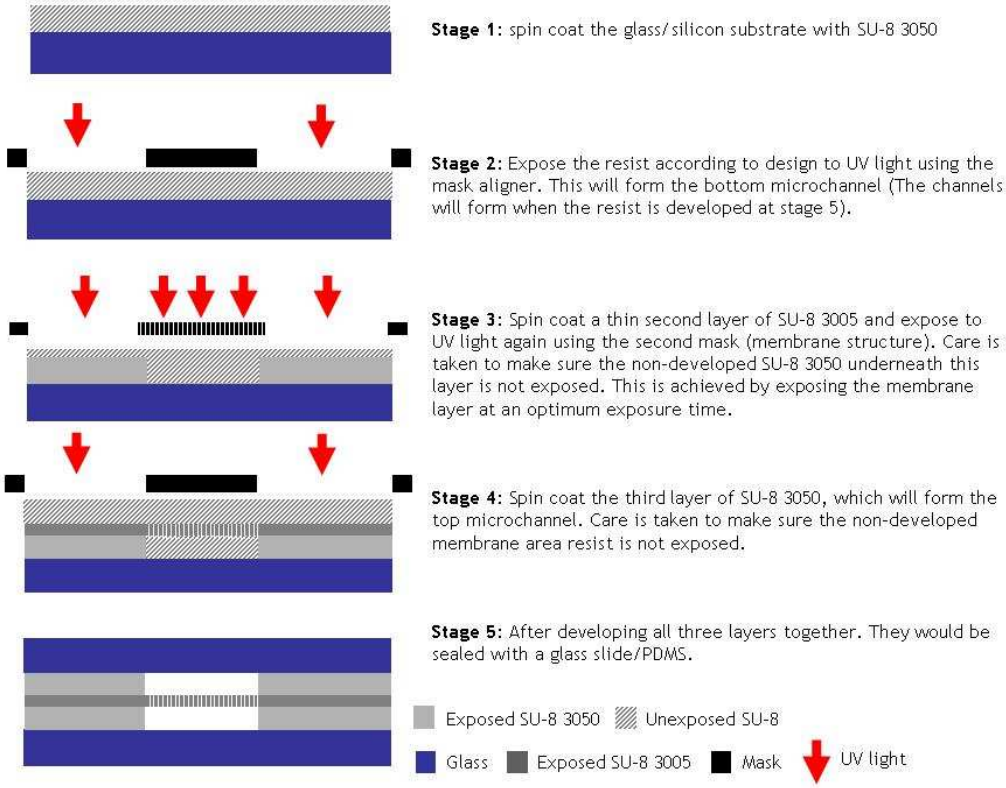

Figure 75; Fabrication steps for the multilayered devices
Stage 1: The SU-8 photoresist 3050 was spin coated on a glass coverslip. This forms the base/bottom microchannels of the device. Stage 2: The mask specifically prepared for this bottom channel design was used to expose the resist. Stage 3: A thinner second layer, in SU-8 3005, was spin coated and exposed using a mask plate specifically designed for the porous membrane. Stage 4: The third/top layer, in SU-8 3050, spin coated and exposed using a mask designed for this layer. Stage 5: The device was finally developed and sealed using a glass coverslip/PDMS. (light grey square – SU-8 3050, blue – Glass, dark grey – SU-8 3005, black – Mask plate, red arrow – UV light)

Step	SU-8 Resist	Process					
		Spin speed		Pre-exp bake	Exposure time	Post-exp bake	Development
		Rpm	Time (s)				
1	3050	500 2000	10 30	95˚C for 30min	35sec	65˚C- 1min 95˚C- 12min Only of you do not wish to proceed to step 2	Develop at the end if you proceed to step 2
2	3005	500 3000	10 30	65˚C- 1min 95˚C- 12min	5, 7.5, 10, 12.5 and 15sec	95˚C- 5-10min Only of you do not wish to proceed to step 3	Develop at the end if you proceed to step 3
3	3050	500 2000	10 30	65˚C- 1min 95˚C-	20, 25, 30, 35 and 40sec	95˚C 12min	Develop until excess resist is removed from microchannels.

Table 10: Steps involved in fabricating the device
The fabrication protocol was used depended on the SU-8 data sheet. {MicroChem. #1899}. The varied times of exposure for layer 2 and 3 were in order to get optimum exposure times for that particular layer.

4.4.2 Results

4.4.2.1 Multilayered SU-8 device

The images in Figure 76 included experiments performed using the fabrication protocol listed in Table 10. In order to optimize the exposure conditions such that the membrane would be formed and the layer below would not be exposed different exposure rates for this layer were used. For the samples shown in Figure 76 A) B) C) and D) the first layer was exposed for 35s, the second membrane layer was exposed for 5s and the third/top layer was exposed for 35s. For the samples shown in E) and F) the difference was in the exposure time of the membrane layer. The middle layer E) which was exposed for 10s seemed to make a difference in results observed. Both sets showed the membrane support pillars, however the porous membrane itself had more visible pores in the 5s exposure images. The membrane area however, in both cases, had collapsed and had an irregular wavy surface structure. This irregularity could be due to the improper development of the respective baking steps leading to stretching and collapsing of the membrane.

The dektak images in Figure 77 show the depth profiles after processing all three layers of the device. The devices with 5s exposures for the membrane layers had a depth of 75±5 µm (n=4) (measured from the top layer to the middle layer). Whereas the devices with a 10s exposure time for the membrane layers had a depth of 68±3 µm (n=4) (measured from the top layer to the middle layer). This variation in depth could be due to either different exposure times and the presence of non-developed resist or even over exposed resist. It was tricky, to ensure proper development of the entire device once fabricated, the development times would vary anywhere from 15 min to 24 hrs depending on the exposure. The development times were so varied, since the developer had to move through the microchannels filled with non-developed SU-8 was obstructing the normal flow and its removal from these channels was very slow. The access points for the developer to enter device parts were from the inlet and outlet connectors on the device (Figure 71 B). The main difficulty was to ensure that all the non-crosslinked resist was removed from the microchannels.

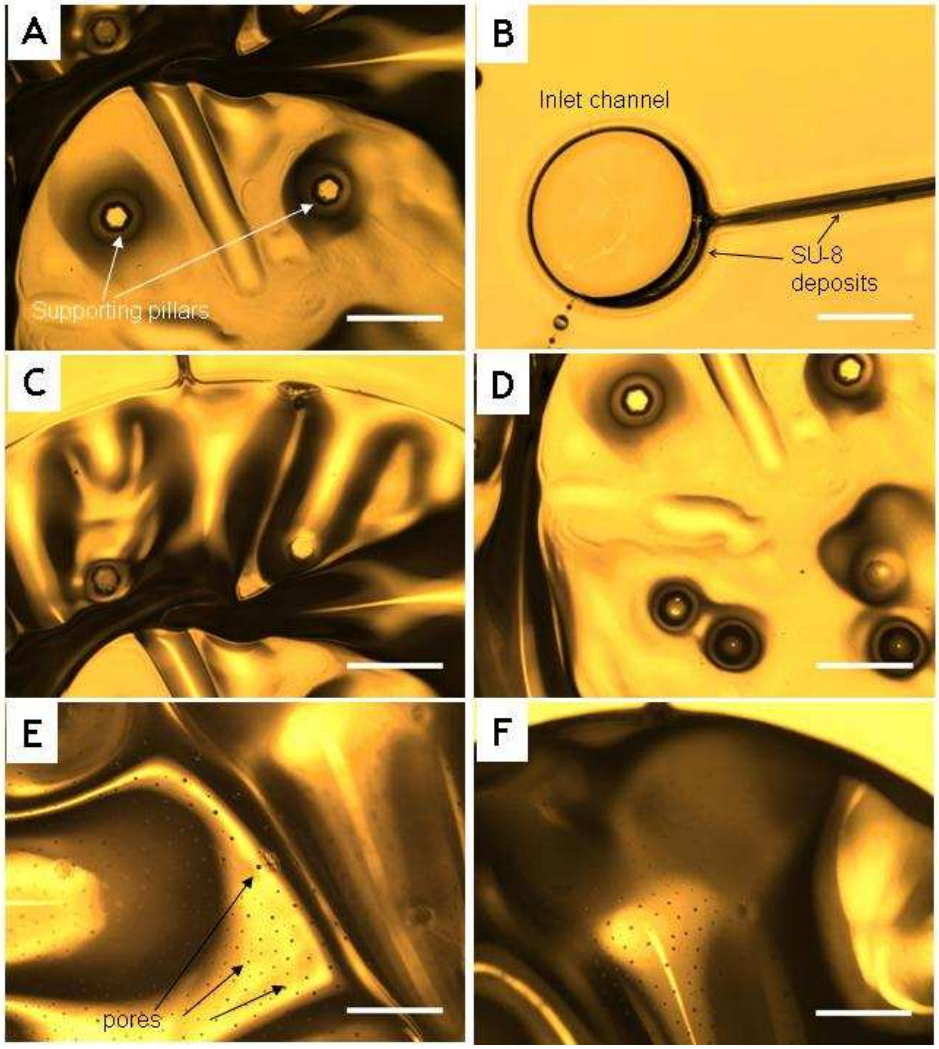

Figure 76: Initial experiments with SU-8 device.
A) The device was developed after processing steps for layer 1: exposure of 35 sec, layer 2: exposure of 5s and layer 3: exposure 35 sec. The image shows the membrane supporting pillars to be intact and the porous membrane area is clear. However the membrane area appears to be extremely wavy and slightly collapsed. B) this is the inlet channel which shows SU-8 on-crosslinked resist residue on the edges of the inlet well and inside the microchannel. C) and D) The device was developed after processing steps for layer 1: exposure of 35 sec, layer 2: exposure of 5s and layer 3: exposure 35 sec. however compared to A), this is much wavier. E) and F) The device was developed after processing steps for layer 1: exposure of 35 sec, layer 2: exposure of 10s and layer 3: exposure 35 sec. The air bubbles seen in these images show the presence of pores within the membrane area. However images of the samples could not properly be captured due to excessive irregularities on the surface. (the scale bars on all samples is 0.5 mm)

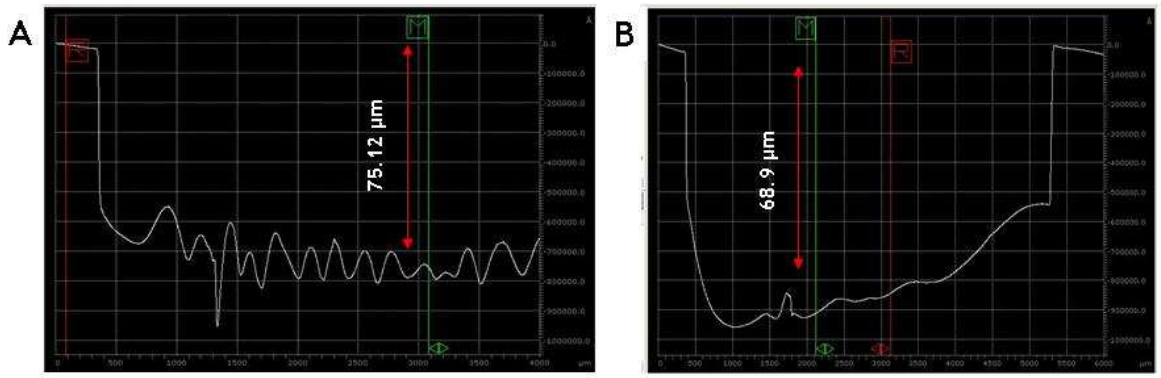

Figure 77: Dektak images for SU-8 devices
A) The device developed after processing steps for layer 1: exposure of 35 sec, layer 2: exposure of 5s and layer 3: exposure 35 sec. The dektak reading for the samples was taken after all three layers were processed. The dektak reading showed a depth of approximately 75.12 µm for this sample. These types of samples ranged from about 75 ± 5 µm (where around 10 samples were measured). B) The device developed after processing steps for layer 1: exposure of 35 sec, layer 2: exposure of 10s and layer 3: exposure 35 sec. The dektak reading for the samples was taken after all three layers were processed. The dektak reading showed a depth of approximately 69 µm for this sample at the deepest end. These depth of the wells was in the range of 68 ± 7 µm (n=4).

In order to address the membrane irregularity in surface structure, each of the layers was spun, pre-baked, exposed, post baked and developed and then observed separately. The first/bottom layer was straight-forward, a one step fabrication (same method as used to fabricate the silicon masters for devices discussed in section 2.1.1). The second, membrane layer was more difficult to make. This layer required the exposure time to be optimised (5, 7.5, 10 and 12.5s) to allow for accurate pore definition (depth and diameter, also that the exposure of this layer should not influence the layer below). In Figure 78 the images showed evidence of experiments performed with two layers and development results. A), B) and C) were three different exposure times of 5, 7.5 and 10s for their respective membrane layers. The image in A) showed evidence of the membrane and it is clearly visible in the D) which was a close up of the membrane. The membrane structure seen in B) was slightly faint however it was marked using a black dotted line in the image. The exposure time being different has had an effect on the membrane and it was also evident in the image C) where the membrane was faintly visible. From these experiments, it was evident that a certain exposure time for the proper development of the membrane was vital. The membrane device for second layer 5s exposure showed the best results of the lot. However, in all these samples there were cracks within the membrane areas. This could be due to long development times, since SU-8 can often begin to contract, therefore making it necessary to use precise development times. Images E) and F) showed evidence of a layer

of overexposed parts of SU-8 layer when using a 15s exposure step for the second layer. These results help identify the problems faced when attempting to fabricate such a device.

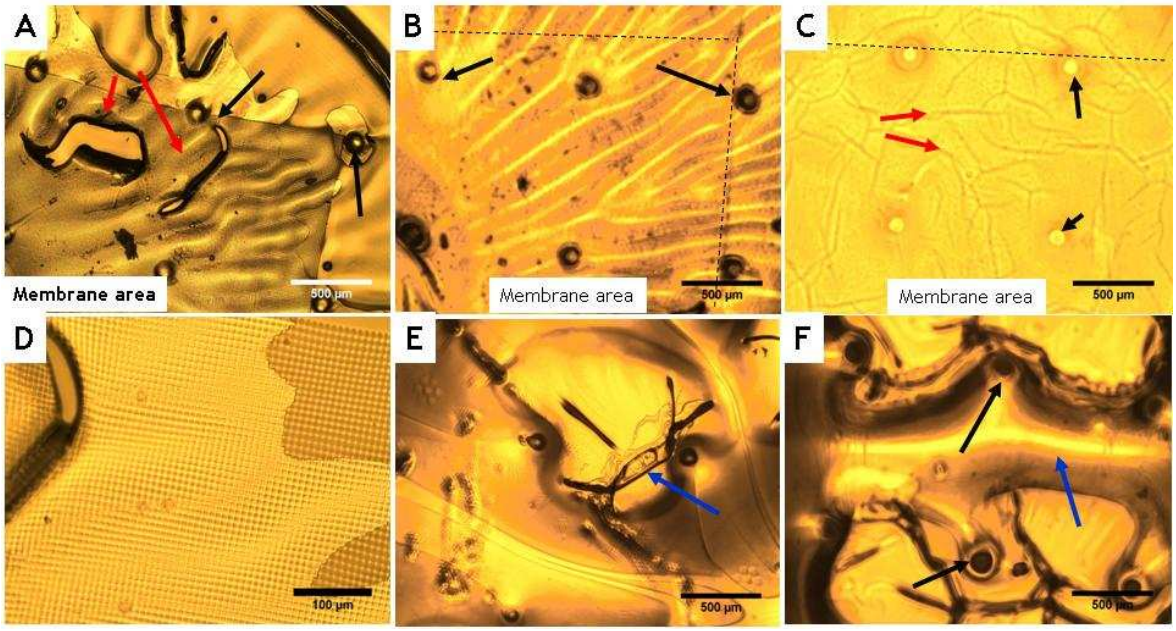

Figure 78: SU-8 device images
A) The exposure time for the membrane layer was 5secs. The membrane area is very clear, however it also shows the presence of cracks. These cracks could be the result of over-development (long development times). The surface is much smoother as compared to previously seen images (less wavy structures).B) Exposure time for the membrane layer was 7.5 sec. The membrane area is slightly visible and in this image it is marked using a black dotted line. The supporting pillars are seen very clearly. C) Exposure time for the membrane layer was 10 sec. The membrane area is slightly visible and in this image it is marked using a black dotted line. The supporting pillars are seen very clearly, however this image shows the presence of cracks again stressing on long development times to be the cause. D) This is a magnified image of the membrane in image A). E) and F) Exposure time for the membrane layers was 12.5 sec. The membrane area is slightly visible but there is presence of overexposed SU-8 visible on the surface. [A,B,C,E and F scale bar is 500 µm and scale bar for D is 100 µm]

4.4.2.2 Multilayered SU-8 cell culture device with integrated gradient generation (Joint project with Kazeem Olayiwola)

This section discusses the possible development of a microfluidic device entirely made in SU-8 which includes a concentration gradient design channels on the top layer and a set of five membranes in parallel (similar to the new multilayered toxicity device explained in Section 4.1.1). This device would allow for five different experiments to be performed in parallel on the same chip. The designs for this multilayered SU-8 gradient device were a slight modification to the multilayered gradient channel device discussed in previous sections of this chapter. The fabrication techniques developed in the previous single membrane SU-8 multilayered device (explained from the above section) were adopted for

this device. Also, the idea of incorporating the gradient device system (like the device design from Figure 52) was thought to add to the value of the device. Each layer had a set of alignment markers to assist during exposure of the remaining layers. The layer 2 (porous membrane layer) and layer 3 (concentration gradient layer) shown in Figure 79 B) and C) respectively, would be ones needing the optimisation methods for the exposure times and development times. In image B) there are five porous membranes each with either the same pore size and the layer had outlet and inlet access points to allow fluid communication between the top and bottom layers. The final top/gradient layer, C), was complex in its design. The concentration gradient would help separate a solution in five different concentrations on one device. [Device dimensions – serpentine channel width = 50µm, cell culture well diameter = 1mm, porous membrane area = 1 mm^2, pore diameter = 1µm, inlet/outlet connector diameter = 1mm, total device area = 20 x 20 mm].

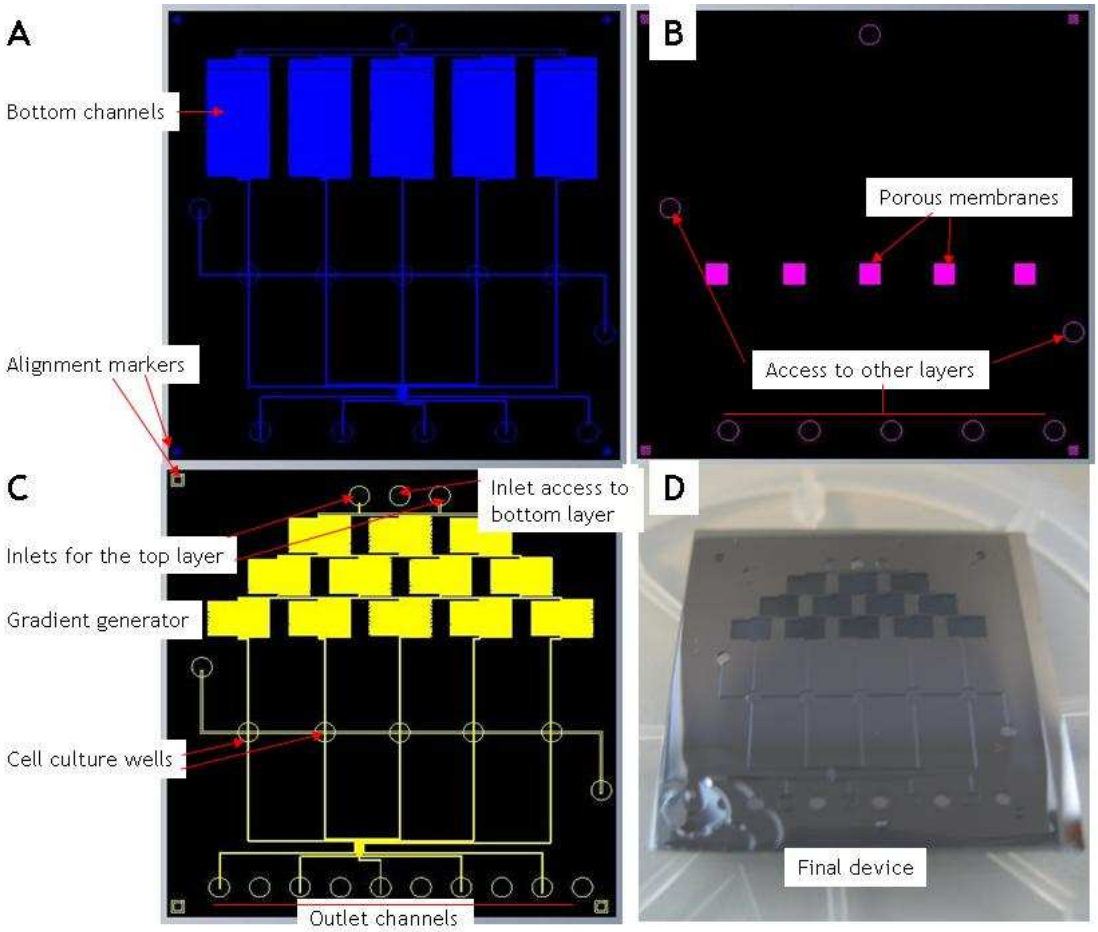

Figure 79: Device design for the multilayered, mutli-cell culture well gradient system.
A) The bottom channels showing the serpentine channels bottom microchannels and the alignment markers. This will form the first layer of the device B) The middle porous membrane showing the five membranes in the centre. This will form the second/middle layer of the device. C) This is the top most layer of the device which consists of the microfluidic concentration gradient system. The Gradient generator feeds the separated solutions into their respective cell culture wells. D) This image is a top view of the final device after being fabricated with all the three layers.

4.4.3 Discussion and conclusion

There are multiple challenges in photolithography, especially with thick SU-8 photoresists (del Campo, 2007). Problems like under-exposure are common and can be difficult and time consuming to work with. If there is not enough U.V exposure over time to drive the cross-linking reaction through the photoresist (all the way to the base), then it could remain unexposed and subsequent development would remove the entire structure off the substrate. The MA-6 (SUSS MicroTec) mask aligner in the JWNC has a lamp and imaging system that transmits 7.1 mW/cm^2 to the resist/substrate. In order to expose the resist an optimum time for exposure is important. Therefore, as the 1^{st} and 3^{rd} layer of the device had a different thickness from the 2^{nd} layer these would need different exposure times that needed to be optimised individually. Another challenge encountered was the aligning of the 2^{nd}, 3^{rd} layer mask to the underlying features this was at all possible SU-8 was transparent over high aspect ration structure (Sato 2006, Mata 2006, López-Romero 2010). If the photoresist is thick, it may not be possible to achieve conformity between the mask and substrate due to edge beading; this could also result in the resist to stick to the mask after exposure. An additional concern when working with SU-8 was its propensity to form an uneven surface if it failed to wet the substrate surface properly. As mentioned above due to the need for alignment the substrates needed to be extremely even which was not always possible as the non homogenous resists surfaces resulted in uneven surfaces which made alignment and conformity to masks difficult leading to uneven exposure patterns. Homogeneous and stable coatings were determined by the substrate surface energy. Being an organic material, SU-8 is rather hydrophobic (contact angle of cured resin 73°), and therefore has difficulties in wetting hydrophilic inorganic substrates, like oxidized silicon wafers, or oxidized glass slides. However, the wetting can be improved by applying commercial primers to the substrate before spin coating SU-8. Primers, like HMDS (hexamethyldisilazane), (OmniCoat from Microchem Inc.), are low molecular weight organic substances which either strongly adsorb or react with the wafer surface forming a thin layer with lower surface energy which can then be wetted by SU-8 (del Campo 2007, Sato 2006, Mata 2006, Keller 2008, MicroChem. Data sheet). Soft baking is again another vital step since it helps to remove the solvent and promotes good adhesion between the substrate and resist. It is typically performed by progressive heating the SU-8 film up to 95°C on a leveled hotplate. Higher soft-bake temperatures (T > 130 °C) may initiate thermal cross-linking even if photoactivation had not taken place. Lower temperatures or short times leave resist films with a high solvent content which will evaporate and therefore generate high film stress during post-exposure baking. Therefore, it was

necessary to optimise the soft/pre-exposure bake times for each device layer (MicroChem. Data sheet, del Campo 2007, Mata 2006).

4.5 Conclusion

In this chapter the focus was mainly on the integration of the different parts of the multilayered microfluidic toxicity testing device. The various parts of this device were developed through the course of this thesis, which were A) the silicon nitride membranes chips (from Chapter 3) designed to bear five adjacent nitride membranes and the TEER analysing electrodes. B) The microfluidic devices that were of two kind, the top gradient device and the bottom microchannels with no gradient. Where the top gradient device was fabricated from a design adopted from the gradient model mixer from Chapter 2. C) The cell culture conditions within the 'static condition' silicon nitride membranes and 'flow conditions' single multilayered devices, revealed that these cells could be used with the integrated system (Chapter 3). When the multilayered testing device was put together, it showed some considerable problems, however there were some relative results with the effective monolayer measurements with TEER that could correlate to the static conditions from Chapter 2. Not all the wells showed TEER measurements, but the ones that did show values were found to be in the range measured under static conditions of 20 $k\Omega cm^2$. The wells that mainly could not be read normally had gas bubbles that restricted the measurement of TEER. This integrated device has the potential to work, however, without a solution for bubble elimination it becomes a difficult task to measure all five channels

On the other application parts discussed in this Chapter, the use of the top gradient channel developed for the integrated device was also used as a standalone device. This standalone device gave an idea of gradient development within the device. With the help of FITC-dextrans the gradient profile could be generated to better understand the working and significance of the mixer. This presented the opportunity to develop parallel projects. One such project mentioned here was with using bacterial species of *P. aeruginosa*. This would help analyse cell monolayer responses to an induced gradient of bacterial infections. Once this was achieved, the bacterial species could be used in conjunction with the multilayered TEER measuring device to test its influence on tight junctions of Calu-3 cells. The other project discussed here was the SU-8 device developed in the attempt to develop functional multilayered devices to study toxicity. The SU-8 membrane devices gave an insight towards a completely sealed disposable device and due to the unique properties of SU-8 having chemically stable structure provide a possibility into a wide range of applications.

5 Final discussion

In order to develop the multilayered microfluidic device the different device parts were tested as ‘stand alone’ projects. The single cell culture microfluidic device, discussed in Chapter 2, was designed to form the top and bottom part of the multilayered membrane device and was tested as a standalone device in order to optimise cell culture conditions and flow regimes within these devices. The microfluidic channels were fabricated in PDMS, this material was commonly used for fabricating microfluidic channels (McDonald 2000). PDMS gained importance in microfluidics due to its long-term stability with several solutions used for cell culture (Klammer 2006, Kallio 2006). It was also compatible to a certain extent to some commonly used solvents, for example 70% ethanol etc (Lee 2003), commonly used for substrate sterilisation before cell culture. One of the properties of PDMS that made it attractive for use with cell culture systems was its gas permeability (Mark 2005, Kallio 2006, Pinnau 2004). The transfer of gases through the system was good for long-term cultures inside the devices. Two different cell lines (Calu-3 and hTert cells) were successfully cultured within these devices over prolonged periods of time (6-8 days, depending on the cell type.) The hTert fibroblast cells reach confluence much earlier than the Calu-3 cells. However, the culture time for the Calu-3 cells was much longer and these cells needed frequent replenishment of culture medium. Many studies have demonstrated microfluidic devices for the use as long term cell culture devices where the authors developed valuable insights on culturing different cell types, also suggesting that the fluid flow inside microchannels applies shear stress to the cells (Yeon 2007, Li N 2003, Leclerc 2004, Lee PJ 2009, Park 2003). When dealing with long-term cultures several parameters had to be considered in order to improve cell survival and proliferation within the microchannels. For example, sterile working conditions inside microchannels, the sufficient supply of nutrients and gases to cells and most of all favourable conditions of flow, such that cells are exposed to a minimum amount of shear stress. This fluid motion was however necessary for replenishment of nutrients and waste removal. Shear stress is experienced by cells when a tangential force such as fluid shear was applied across their surface; optimum- or limiting shear stress values are different for different cell types (Lu 2004, White 2007, Korin 2007, 2009, Frangos 1988). In Chapter 2, the single cell culture device used for maintaining hTert fibroblast and Calu-3 cells, had a calculated shear stress value of 1.2 mPa inside the cell culture well region. The shear stress calculated for the inlet and outlet channels however, was about 30mPa. These devices had favourable conditions for cell culture over long periods of time, in the literature a shear stress within microfluidic channels of 5-20 mPa is deemed suitable for cell survival and proliferation (Korin 2007).

In a first investigation Calu-3 cells were tested for survival under a shear stress of 0.6 - 1.2 mPa (0.5 – 1 µl/min flow rate) within the single cell culture well devices. Calu-3 cells were chosen as a model for the lung epithelium, because of their barrier forming properties, and their prominent use as such a model (Matilainen 2007, Geys 2006, Florea 2003, Foster 2000, Grainger 2006, Fiegel 2003, Mathia 2002).

Impedance measurements on living tissues and cells have seen vast advancements in recent years where miniaturised systems have gained importance. Miniaturised systems decrease the amount of test solutions used, reduce reaction times, allow for batch fabrication processes, and it is also possibile to integrate electrical and optical measurement systems, allowing to perform several experiments in parallel (Auroux 2002, Dittrich 2006, Puleo 2007). In an attempt to miniaturise an impedance measurement system, where the aurhtors studied the increase in resistance signal due to cell coverage over time, Wegener et al (1996) developed a system to measure the resistance of epithelial cell monolayers that were cultured on glass slides with gold electrodes (cells were allowed to grow on these electrode surfaces). Some other devices, where the resistance of cell coverage over time was measured over porous membrane surfaces, developed to study the barrier properties of epithelial and endothelial tissue were also interesting in their approach where they used Transwell polymer membranes (Huh 2007, Kimura 2008, Genes 2007). Huh et al. (2007) presented a device that studied an injury induced on lung epithelial cells by using fluid mechanical stresses. Their device showed the apical and basal microfluidic channels (fabricated in PDMS) that were separated by a porous polyester membrane and lung epithelial cell monolayers (SAECs – primary human small airway epithelial cells), shown in Figure 80, A. They induced a mechanical stress on these cell monolayers using an air plug to exert the force. This device discussed the airway crackling effects and reopening on chip that closely mimicked true physiological stresses in respiratory crackling created due to airway barrier damage (due to mechanical injuries or lung disorders). The paper by Kimura et al. (2008) used transportation assays to test the difference in distribution of the fluorescent dye between the apical and basal fluidic sides of the device and analysing these using optical sensors. (Figure 80 B) shows the cross sectional view and a real size image of the device). The device was fabricated using PDMS chambers and a semipermeable polyester membrane sandwiched between these two chambers. They used human intestine derived Caco-2 cells for their experiments and analysed the transportation of fluorescent dye (rhodamine 123) through these cells. (Wegener, 1996).

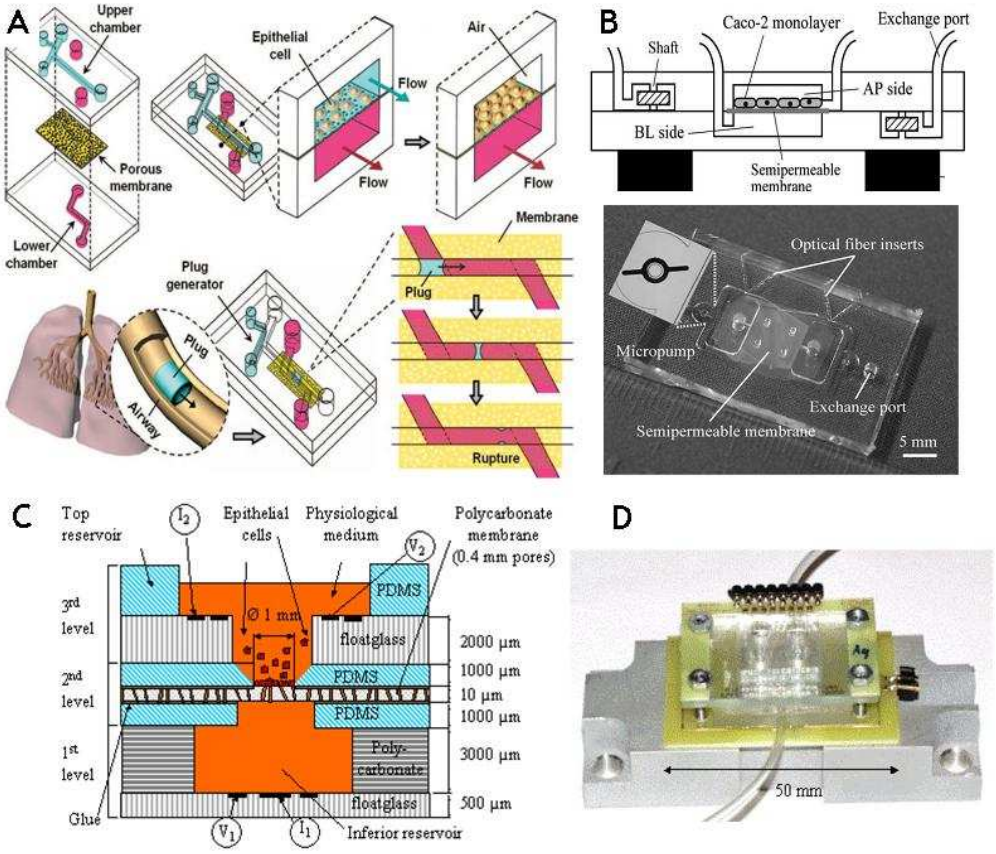

Figure 80: Examples of devices for epithelial studies
A) This device developed by Huh et al (2007) to study the mechanical force effects of air plugs inside a microfluidic device. B) This device was developed by Kimura et al (2008) which show a very unique micro pump system to drive the perfusion channels within a microfluidic device. It mainly discusses transportation assays across epithelial barriers. C) Schematic cross-section showing the three levels of the basic modular tissue measurement structure developed by Hediger et al. D) This is a photograph of the microsystem developed by Herdiger et al. [Pictures C) and D) were obtained from PhD thesis of Serge Herdiger (2000)

Hediger et al. developed a bio-microsystem to test the characteristics of TEER measurements for epithelial cell monolyers. Figure 80 C) Their device consisted of an assembly of three different layers; 1) The first level (starting from the bottom) was an assembly of a float glass wafer on top and a machined 2 mm thick polycarbonate plate, that formed the bottom channel of the device. Silver (Ag) micro-patterned electrodes that were previously deposited on a float glass wafer formed the current electrode - I1 and the concentric voltage electrode - V1. 2) The second level (middle section) of the device was composed of two moulded PDMS layers on either sides of a nano-porous polycarbonate membrane glued in between them. The diameter of the culture sites was 1 mm. 3) The third level (the top, cell seeding section) was similar to the first one with two concentric electrodes I2 and V2. The picture of this device in Figure 80 D) shows that it had four identical cell culture wells on one modular measurement device. This allowed a maximum of four experiments to be run in parallel. Similar to the device presented by Hediger et al.

(2002), the device explained in Chapter 4 used silicon nitride porous membranes (instead of the polycarbonate membranes used by Hediger) inside the cell culture device system and the modular measurement device had the capability to perform five experiments in parallel. Silicon nitride membranes used for cell biology and DNA technology have shown to have certain promise through literature (Harris 2003, Ma 2005, Zhang 2008, Fissell 2006). The main plus point of silicon nitride membranes was that their thickness and pore sizes could be altered according to the required application (Ekkels 2003, Popa 2009, Bal 2009, Yemini 2009, Leen 2008). Silicon nitride membranes used in Chapter 3 and 4, were only 500 nm thick and the pore diameters ranged from 1 µm. Their thickness was most important since the study of cell monolayer involved transport mechanisms and tight junctions using lung epithelial cells. The primary function of lungs involves gas exchange but at the same time it has to function as a protective layer that has as an objective not to allow any harmful environmental agents to enter the body. The barrier function usually is monitored by a thin epithelial cell lining of alveolar cells (Gardner 1993, Cohen 1975, Hermans 1999). These barrier epithelial thicknesses vary from animal to animal, where in most mammals it is in the range of 0.62 µm up to about 1.2 µm (Meban 1980, Weible 1964). Therefore when attempting to model the use of thin membranes (500nm) like silicon nitride membranes, had proven to be a useful tool. These membranes would allow good cell conformation to substrates and provided precise solute transport studies and epithelial resistance measurements. Also the thinness of the membranes meant that there would be less hinderance of the translocating particles between thetop and bottom compartments separated by the membranes. Meaning that the measured translocated material can afford to neglect the presence of the thin membranes and hence resultant translocation of test particles would be mainly dependant on the monolayer of cells and diffusion or active transport through the cell membranes.

Silicon nitride membranes, used as base substrate for cellular membrane studies, are often compared to the conventional polymer Transwell membranes used to test cell layer TEER values and transport of FITC-dextran molecules through cell monolayers. Zhang et al. (2008) for example presented work using rat derived hepatocyte (harvested from Wistar rat liver) cells on top of silicon nitride membranes. These membranes (pore diameter 20 µm, thickness of membranes 1.5 µm) were compared to collagen coated polycarbonate (PC) membranes bearing the same porosity. They used a silicon nitride sandwich culture method, the cells were initially maintained for 24 hrs on a galactose/collagen coated silicon nitride membrane and then a second substrate membrane (silicon nitride) was placed on top of the first substrate. FITC-labelled dextran particles were then used to test for

leakiness and mass transport through the cell monolayers, showing that smaller sized particles translocated easily through the membranes. In another study presented by Ma et al (2005), which involved a co-culture of endothelial cells and astrocytes utilised the silicon nitride membrane substrates as a means to model the blood-brain barrier (this work involved smaller dimensions of pores ranging from approximately 270 to 700 nm and a thickness of 1µm). These silicon nitride membranes were coated with collagen to promote cell adhesion and compared in working with polyethylene teraphthalate (PET). The unique part about their system was that they had used thin (1µm) silicon nitride membranes for the co-culture, they also incorporated a TEER measurement system on their device holder to analyse the integrity of their endothelial and astrocyte co-cultures. They reported TEER values for endothelial cells and astrocytes were quite low compared to co-culture TEER values of 200-800 Ωcm^2. In contrast to some of the work reported here their experiments were performed under static conditions. Similar to these examples stated here, experiments carried out under static conditions were reported in Chapter 3. The silicon nitride membranes used here were also coated in collagen which did produce the best results in terms of the calculated percentage confluency and the TEER measurement systems also tested under static conditions, revealed a very high TEER. However, due to differences in cell types between the experiments reported by Ma et al (2005), their results cannot be directly compared. Therefore, a comparison was derived from the TEER experiments for the polymer membranes showing results with Calu-3 cells from papers by Geys et al (2006, 2007), Foster et al (2000), Rotoli et al (2008), Fiegel et al (2003) and Mathia et al (2002). The afore mentioned authors have shown that Calu-3 cultured on transwell polymer supports reached different TEER values in response to changes in various parameters such as: culture medium, percent of FBS (10% and 2%) and intrusion of nanoparticles on monolayers.

Geys et al (2007) compared certain culture conditions using different FBS concentrations in the culture medium (DMEM) with Calu-3 cells. They showed that the TEER decreased with decreasing concentrations of FBS, so when using 10% FBS the TEER values were 949±182 Ωcm^2 (on 0.4 µm diameter membrane pores) and 500±95 Ωcm^2 (on 3.0 µm diameter membrane pores). In her earlier paper Geys et al. (2006) paper also showed that the TEER values for Calu-3 cells on 3.0 µm pores measured to be 404±83 Ωcm^2 for 10% FBS. Compared to their results the TEER values obtained here on similar Transwell membranes (see Chapter 3) were lower on the smaller 586±12 Ωcm^2 (on 0.4 µm pores) and higher on the larger pores 606±9 Ωcm^2 (on 3.0 µm pores). These differences could be due to the culture conditions: cells were seed at a much lower density of 0.1×10^6 cells/cm^2 and

because a higher concentration of FBS (15 %) was used in the culture medium. An additional difference was that the cell culture medium used was here was EMEM medium instead of DMEM (EMEM was the recommended medium for these cells bought from ATCC-LGC, Promochem). Also the TEER reported here (on Transwell 0.4 and 3μm diameter) was slightly higher compared with this and other papers, Florea et al (2003) and Foster et al (2000) used the same seeding densities but 10% FBS in DMEM got about 400 – 600 Ωcm^2). This suggested that an increase in the percentage of FBS to 15% and use of the preferred EMEM medium had an effect on the TEER values.

On silicon nitride membranes (Chapter 3), Calu-3 cells were maintained under the same culture conditions as mentioned above for the Transwell membrane supports (using EMEM medium and 15% FBS). The results for these experiments showed a good deal of proliferation and growth. These culture conditions for Calu-3 cells along with collagen coated silicon nitride membranes gave values, which were about 20 $k\Omega cm^2$. For these experiments the use of EDTA/versine buffer was implemented as an easy and quick way to disrupt the tight junctions formed between adjacecnt cells. This versine buffer worked well as a positive control solution and the high TEER acquired during the experiments fell rapidly (within minutes of adding the solution to the cell cultures). This showed that the specially designed TEER setup for the silicon nitride membrane devices was in fact measuring the TEER of the cell monolayers. The formation of tight monolayers were also confirmed when using translocation experiments, with silicon nitride membrane and polymer Transwell membranes, the FITC- dextran particles (mol.wt of 4, 70, 500, and 2000 kDa) showed a much higher percentage of diffused dextran molecules on the polymer membranes than that compared to silicon nitride membranes. These comparative results helped to identify the potential for silicon nitride membranes with Calu-3 cells as tool for studying translocation and TEER. However, all these experiments were performed under static (no continuous fluid flow) conditions and the next step was to integrate the different components of the final multilayered device (five cell culture multilayered device). Most of the devices described throughout the literature e.g. Kimura et al (2004), Herdiger et al (2002) and Huh et al (2007), had concentrated on the possibility of performing single experiments using their devices. Hung et al (2005) presented their work where they used an array of cell culture wells allowing drug screening at different dilutions one device.

Chapter 4 presented the possibility of performing five different experiments in parallel along with a gradient generator to develop different dilutions of the test materials. The application of the top fluidic gradient layer was demonstrated using coloured dyes and

FITC-dextran molecules. The aim of using such a gradient device was to automatically generate a series of dilute concentrations of an analyte or solute, creating four concentrations and a control. These would then be automatically introduced into to the five cell culture wells in the device. This device was designed using information from literature on microfluidic gradient models (Dertinger 2001, Jeon 2000). Starting off with the devices described in the papers by Dertinger et al. (2001) and Jeon et al (2000), a 7 row concentration gradient generator was designed, implemented and used to understand the workings of such devices. In collaboration with Ms Kristin Kirchoff, this gradient design was used to create pH gradients across the wide channel. The main purpose for this device was twofold: firstly, it was intended that serial dilutions of test solutes in a defined, reliable, and predictable way would be developed using such a serpentine device. At the same time, this device was used to generate gradients of pH for layer-by-layer (LbL) deposition of molecules to study cell haptotaxis. Similar microfluidic devices were used in the study of cell chemotaxis. The large gradient generator was the appropriate tool to apply pH sensitive LbL layers onto poly-ethylene-imide modified glass following the general techniques laid out by (Kirchhof 2008, Kirchhof 2009). The principle followed here was to first adopt a design from a successful publication and then modify it in order to apply it to other areas of research. (Agrawal 2008, Lin 2005, Jeon 2002, Gunawan 2006). The design was such that the gradient channel was 900µm wide and several millimeters long such that cells migrating on such a substrate could be observed within the broad channels. Following these structures, the top gradient device in Chapter 4 was structured in a way that the gradient profile could be viewed under one field of view upto 20 x magnification.

The successful working of the top gradient generator showed that the dilutions could be achieved within the top/gradient device. The dilutions developed using flow rates between 0.5 and 1 µl/min on the devices with the 2000kDa FITC-dextran molecule solutions. The percentage of dye intensities calculated in each channel was quite close to the expected values of dilution. However, in many of the channels the intensity profiles were not flat, which meant that the mixing was incomplete. This could be due to secondary mixing that resulted from lateral leakage through the channel that interconnected the cell culture wells and had been intended for cell seeding. When two liquids are to be mixed or diluted using microfluidic devices, the length of the mixing channels needs to be of a certain minimum length which is dependant on the diffusion coefficient of the test material, the flow rate and the lateral dimensions of the channel. In a ‘T’ shaped channel the diffusion profile starts at the point at which the two channels meet, if this was compared to the profile that had formed by diffusion at the end of the channel, the time for diffusion was given by the

distance along the channel, if the velocity of fluid was known (Kamholz 1999). Through this relation the diffusion coefficient of the test material dissolved in the buffer could be calculated (buffer was cell culture medium). When the diffusion coefficient in some cases was known then the relation between the diffusion coefficients and time was used, through this the required length for mixing was also calculated. In the case of serpentine channels the diffusion profile was more complex since there were points at which the channels 'met-then split-then met' with other parallel channels (Dertinger 2001, Jeon 2000). The top/gradient device described in detail in Chapter 4 consisted serpentine channels and serpentine connector channels. It was important to check whether each of these channels allowed for the respective concentrations, formed for FITC-dextran, to get mixed before reaching the end of each serpentine. Each serpentine channel was 6 cm in length and the distance required for mixing when calculated for mixing the FITC-dextran 2000kDa (54 nm diameter) was approximately 0.2 mm (at a flow rate of 1 µl/min) (see Appendices). Therefore, the length of each channel should have been more than sufficient for the 2000kDa FITC-dextran molecule to be mixed evenly across the channel crossection at the end of the channel. However, the intentions of the project were to be able to use the mixer device with a wide range of nanoparticles and fluorescent molecules. Because nanoparticles have in general a larger hydrodynamic diameter the top/gradient device was "overdesigned" with channels that were long enough to allow for diffusive mixing of a large range of solutes and even particles.

On forming the different concentrations using the serpentine channels within the top/gradient device, the concentrations were to then flow into five cell culture wells. The cell culture wells allowed five cell experiments to be performed in parallel and under different induced by the previously established concentrations of the test solutes. The cell culture wells were connected to each other via a cell seeding channel that ran perpendicular to these. During cell seeding, the fluid flow through the gradient generating serpentine channels was stopped and thus blocked preventing any cells from entering the serpentine channels. This reduced the clogging of channels by cells and gradient disruption within these. Cells were maintained using the serpentine channels as the medium perfusion channels. Comparing this model to the one developed by Hung et al. (2005), their device was unique in terms of its fabrication and also number of experiments that could be done in parallel. Their device was equipped to perform 10 sets of experiments within one device. They had an integrated gradient system, but most interestingly, their device had a chain of cell culture wells parallel to the gradient and a perpendicular perfusion system that was at a different height in the chamber. This meant that the perfusion channels would not interfere

with the cell seeding or the gradient generation. However, these perfusion channels were connected between all the cell culture wells, which meant that there was some cross talk expected between the adjacent cell culture wells. Similarly, in the top/gradient device, mentioned before, had seeding channels that were perpendicular to the gradient and passed through all the cell culture channels. This meant that there was cross talk between the adjacent cell culture channels. However, in the top/gradient device from Chapter 4, the gradient was disrupted in the top/gradient device when observed. The observation channels showed that the mixing was incomplete in some channels. It was thought that there was either cross talk between the different cell culture wells or that the outlet channels lengths had different flow resistance due to varied lengths. However, when observing the entire device the fluid tended to flow towards the channels with least resistance (when the seeding inlet and outlet connectors were plugged). Even after the outlet channel lengths were adjusted to be of the same length, there was still some incomplete mixing observed within some of the channels at flow rates between 0.6 and 1 µl/min. However, at slightly lower flow rates of 0.025 – 0.25 µl/min the mixing was complete and the peaks of the graphs were homogeneous, but the relative concentrations observed were slightly off compared to the calculated dilution ratios. This observation illustrated that the seeding channels were the root cause for mixing disruption as this allowed the fluid from adjacent cell culture wells to towards adjacent outlet channels. This would mean that future device required different design for the seeding channels. These seeding channels could either be removed completely and cells seeded through the outlet channels (trying to avoid any clogging of the serpentine channels) or by incorporating another layer that had the seeding channel, but this would include an extra fabrication step.

The integration of the multilayered device included; A) the working of the integrated multilayered device was the single well cell culture system. These devices had a success rate (initial fabrication, assembly, fluidic connection, cell seeding and growth), of about 60%.when used with the new device holder design. The results in Chapter 2 showed the percentage of confluence to be almost 80% after day 3 and meaning that most of these devices reached a 100% confluence at day 5/6, when used with Calu-3 cells. The only element missing in this device was the ability to measure the TEER across the membrane and cell monolayers inside the device. The TEER using the single cell culture system was setup only for static conditions. However, the TEER measurement electrodes were incorporated into the multilayered multiple cell culture well device (the top/gradient microfluidic device, silicon nitride membranes, Calu-3 cells and electrodes for TEER). The results with the multilayered multiple channel well device revealed a slightly low

success rate when using Calu-3 cells. However, there were a few measurements of TEER that were available, showing either 1 or 2 wells out of five having a high measurement of TEER. The main reasons this, being that the fluid flow inside this device was often disrupted with the formation of gas bubbles and it was extremely challenging to remove them from the cell culture wells. There were many factors that could have affected the TEER within the device explained in literature for example with changes in temperature, cell- substrate interactions, air bubbles, etc (Forbes 2002, Eley 2002, Lo 1999). The intention was to use the multilayered 5 well device for the continuous analysis of epithelial cell health under the influence of toxins such as nanoparticles, heavy metals, etc. Due to gas bubbles, the device was used to analyse the TEER but the next step was to be the introduction of toxic and non-toxic nanoparticles for analysis.

There are several toxicity testing devices seen through the literature (Bang 2004, Viravaidya 2004, Sin 2004, McAuliffe 2008, Frampton 2008, Diao 2008, Ahn 1998). These devices were however quite different from the final multilayered multiple cell culture well device discussed here. Most of them used different principles and had varied mechanisms to evaluate the toxicity of test materials. Some of these devices used hydrogel matrices (using ECM protein based gels) inside which cells were maintained for long culture periods and are often used for cell patterning and chemotactic cell experiments (Cushing 2007, Meuwly 2007, Prestwich 2008). The other difference with these devices was that they did not require TEER as a measurement system. These devices were used in conjunction with cytotoxicity assays, LIVE/DEAD staining assays, etc, to test for cell responses. These are cell toxicity assays that could be used to test the toxic effects on cells and required another kind of assay to asses the health of these cells prior to inclusion of the toxins (for example a Glucose or lactic acid assay. An inclusion of such a system had been presented by Sin et al (2004), where they incorporated an oxygen detector to monitor the health of cells inside the microchannels. A TEER based systems had been included in the multiple cell culture well device discussed in Chapter 4, which allowed to test the integrity of the cellular monolayers. This meant that cells could be monitored over time when inside the device and when put under an induced toxic effect they would reveal changes in the measurements. Therefore, the TEER based device could act as a method of evaluating the effects on epithelial cell barriers when induced by toxic materials, solutions, etc within separate cell culture wells of the device in a parallel study.

Future Work

The intentions for the final multilayered device were to detect several different types of engineered nanoparticles of known toxic effect and to evaluate their toxicity using the TEER measurements. Since this PhD was a part of the NanoSafe2 project, which was a European funded project and it was structured to provide innovative ideas for better and safer methods handling nanoparticles and nanomaterials (NanoSafe2 2005-2009). The field of nanotechnology has been rapidly developing and the production of new engineered nanoparticles have found benefits in several avenues such as medicine, energy supply, environment, etc (Sperling 2008, Silva 2005, Silva 2004, Sharma 2006, Salata 2007, Salata 2004, Paull 2003, Hoet 2004, Heath 2008, Freitas 2005). Worldwide estimates for the growth of nanoparticles suggest that there would be a probable market of 700- 1000 billion Euro by the end of 2011 (NanoSafe2, 2005-2009). However, the potential side effects of the particles produced and released by this industry are yet poorly understood (Hoet 2004, Stone 2007, Oberdorster 2007, Stone 2006).

Another attractive area would be to develop an ‘air to liquid’ (ATL) interface rather than the current ‘liquid to liquid’ (LTL) interface. The lung epithelia under physiological conditions are in an ATL interface at the alveolar regions, at the air blood barrier. Therefore this sort of system could be interesting when attempting to mimic the physiological conditions of the lung cells (Grainger 2006) and a membrane system such as this would be handy for toxicity testing.

Other future plans for this project were in fact being worked on and were also explained in Chapter 4. The idea of using a bacterial species (*P. aeruginosa*) with the Calu-3 cells and incorporated with the multilayered device for testing was one such avenue for the . Due to the presence of the CFTR receptor in Calu-3 cells, they were often used in conjunction with these bacteria. In CF patients are vulnerable to such bacterial species since these patients show a loss of mucocilliary activity. In which case the mucus dries up on the epithelium and forms plaque like structures. These plaque help bacterial species to colonise and rapidly proliferate, forming a protective biofilm, which is resistant to several antibiotics, hence resulting in chronic lung infections (eg pneumonia). These bacterial species could be used in conjunction with out device and Calu-3 cells, in order to test effects on the tight junction protein disruption (to evade macrophage involvement in physiological conditions) and disrupt cellular tight junctions (de Kerchove 2008, Jacob 2002, Vikströma 2009, Saavedra 2002). It was thought that using this kind of multilayered

device and TEER system could also give a relation between Calu-3 cells and *P. aeruginosa* under the influence of antibiotic solutions and drugs. Hence be used as a drug implementation and testing device for patients with cyctic fibrosis (B. Goldberg 2000, Moreau-Marquis 2008, Gómez 2007).

6 Appendices

Device holder designs diagrams

In some cases the bonding strength was not sufficient, therefore external pressure was applied to press the device and substrate together, to assist this process device holders were designed. The device holders were machined in the mechanical workshop according to specifications. The designs were prepared using CAD software, and each designed for a specific application. Glass slides (which are normally used for cell stainig and imaging) were used to evenly apply pressure had holes drilled in order to allow access for the fluidic connectors. The burs needed to drill the holes were purchased from Diama Int. (500 series diamond burs; 545, 544, 525 and 522). Figure 81, the device clamp shown here could be used with a number of different device types, however it was not ideal when using the multilayered single cell culture devices (with or without silicon nitride membrane. For that reason a different clamp shown in Figure 82, was used exclusively for the single multilayered silicon nitride membrane device. The single device clamps were also quite bulky and often posed problems with rusty screw parts, improper sealing to the outer parts of the PDMS devices and hence resulting in the cracks near the inlet outlet connections causing leakages. Therefore, new plastic device clamps were prepared from plexi-glass slabs shown in Figure 83. These were designed such that the PDMS multilayered devices would fit perfectly well inside the clamp. Also, the entire device was clamped down using bulldog clamps. This proved to be a much better setup compared to the older aluminium device clamps. Finally, Figure 84 shows the device clamp used for the final multilayered multiple channel silicon nitride membrane device used to test the TEER. The device clamp wasdesigned such that each of the electrodes connectors could perfectly screw onto the clamp such that they would be aligned with the electrodes on the chip. The device clamp had glass slides (Figure 84, C) to provide support and sturdiness to the PDMS microchannels when clamped together.

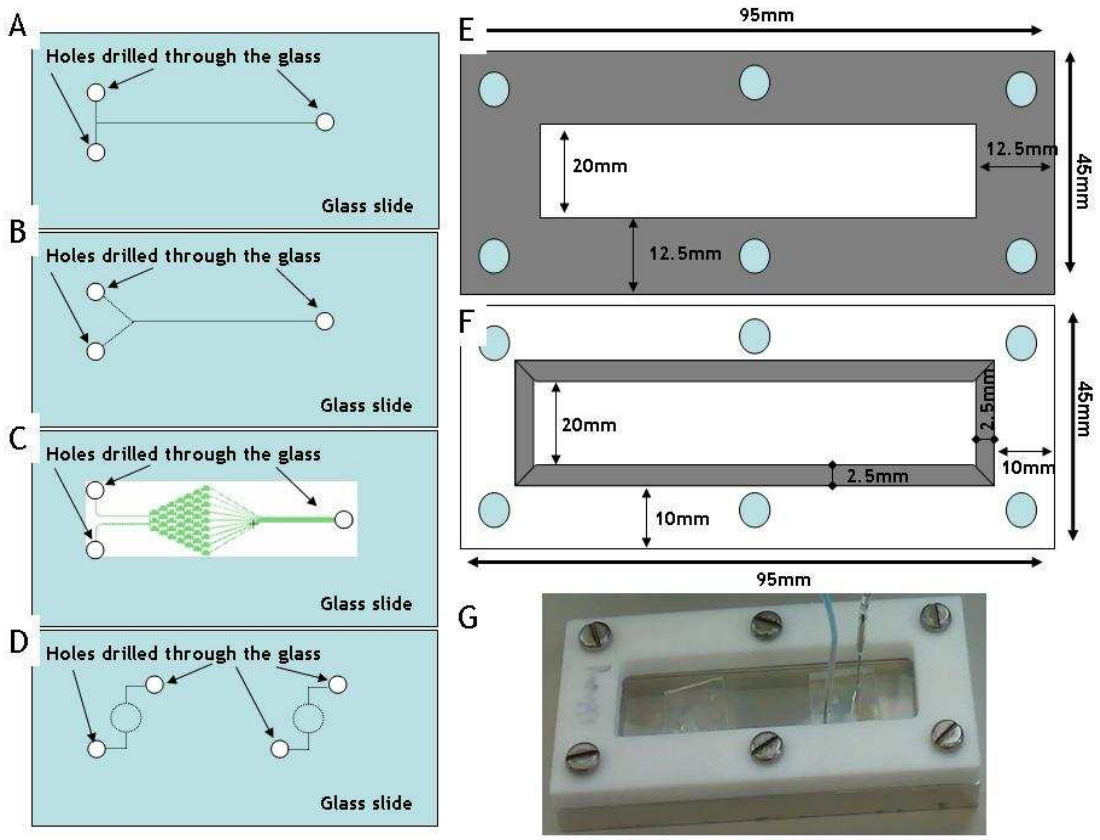

Figure 81: First clamp design: Aluminium and PTFE.
Holes drilled through glass slides using Diama dental burs. Holes were drilled into the glass slides to correctly fit above the A) T-junction microfluidic device, B) Y-shaped layout, C) concentration gradient generator and D) single cell culture well system. For the single culture well system the device holder was useful since it was possible to fit a maximum of 3 devices together. The device holder was designed at the C.C.E and machined in the mechanical workshop, University of Glasgow, James Watt bld. E) this shows the top view of the upper piece of the holder . F) this shows the top view of the bottom piece of the holder. G) This is an image of the holder being used with the devices inside it. The device holder could hold different types of devices.

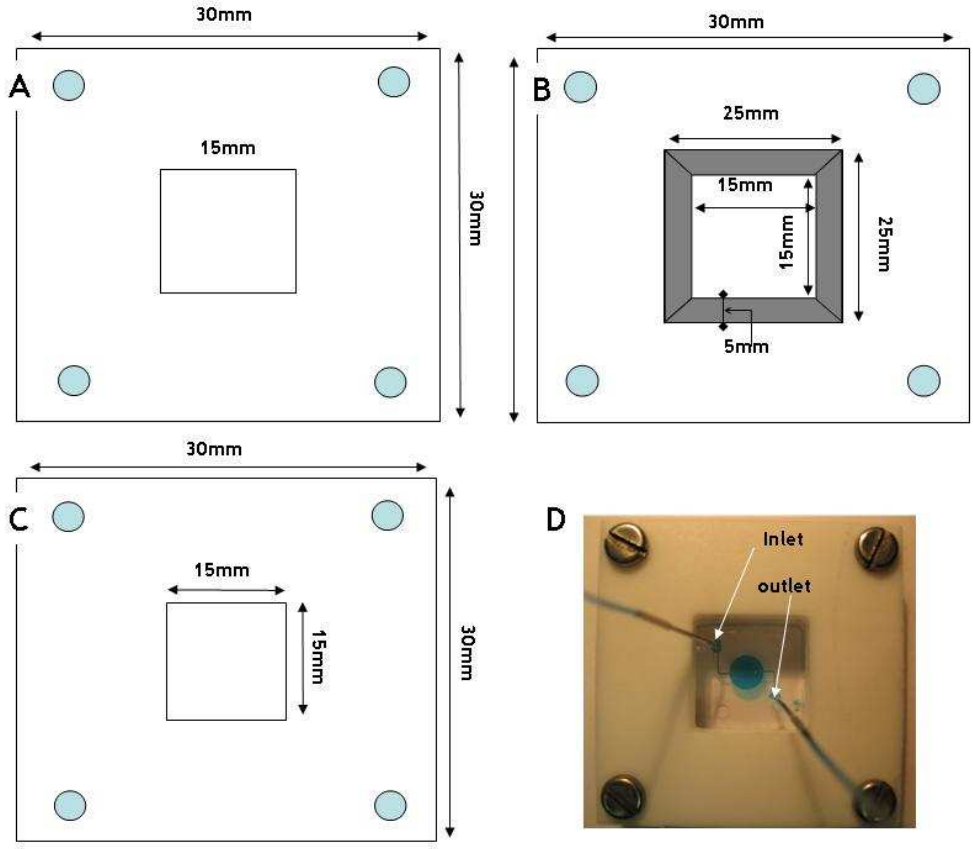

Figure 82: device clamp: Aluminium and PTFE.
(Designed at the C.C.E and machined in the mechanical workshop, University of Glasgow, James Watt Bldg.) A) This is the top PTFE part of the holder. B) this is the bottom part of the holder device which shows the recess area (grey) where the device would fit. C) this shows the bottom view of the holder. D) This is the device Holder shown with the device showing the inlet and outlet channels.

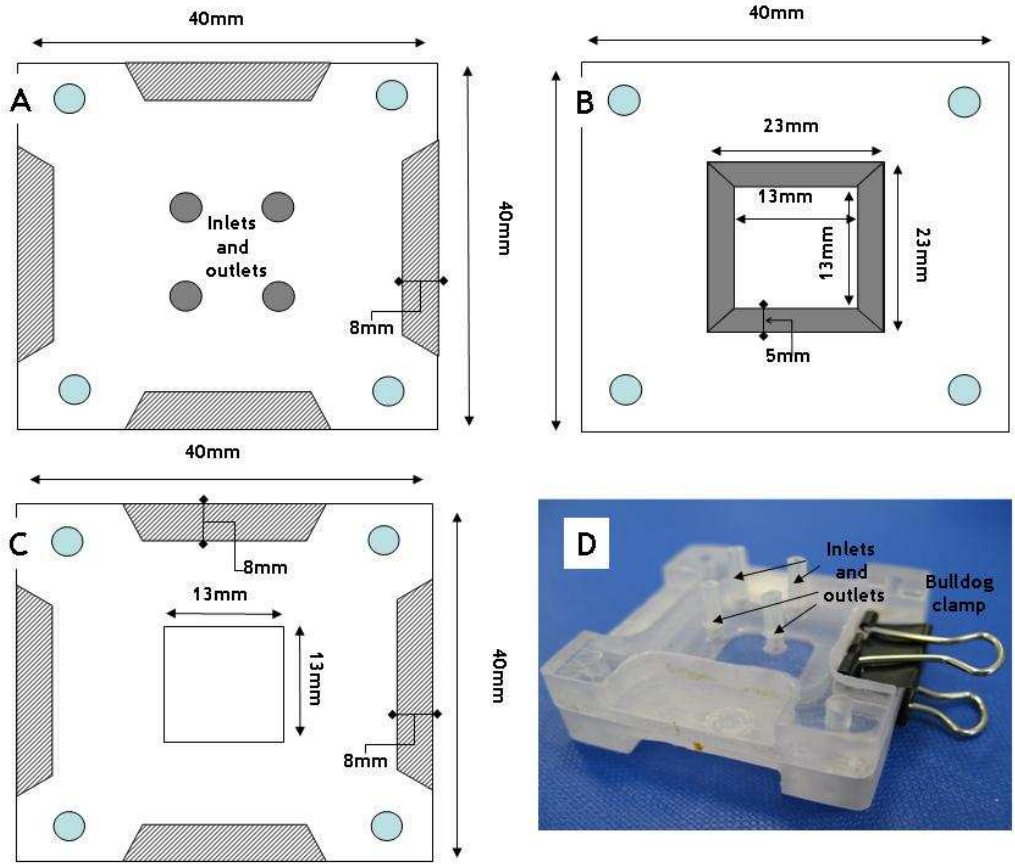

Figure 83: The new device holder prepared to hold the single cell culture device
A) Shows the top view of the top part of the device holder, B) Shows the bottom part of the holder and the recess for the device to fit into. C) This shows the bottom view of the device holder. D) this device clamp can be used with the bulldog clamps and the inlet outlet silicone tubing connectors (meant to give the inlet/outlet connector tubing some rigidity).

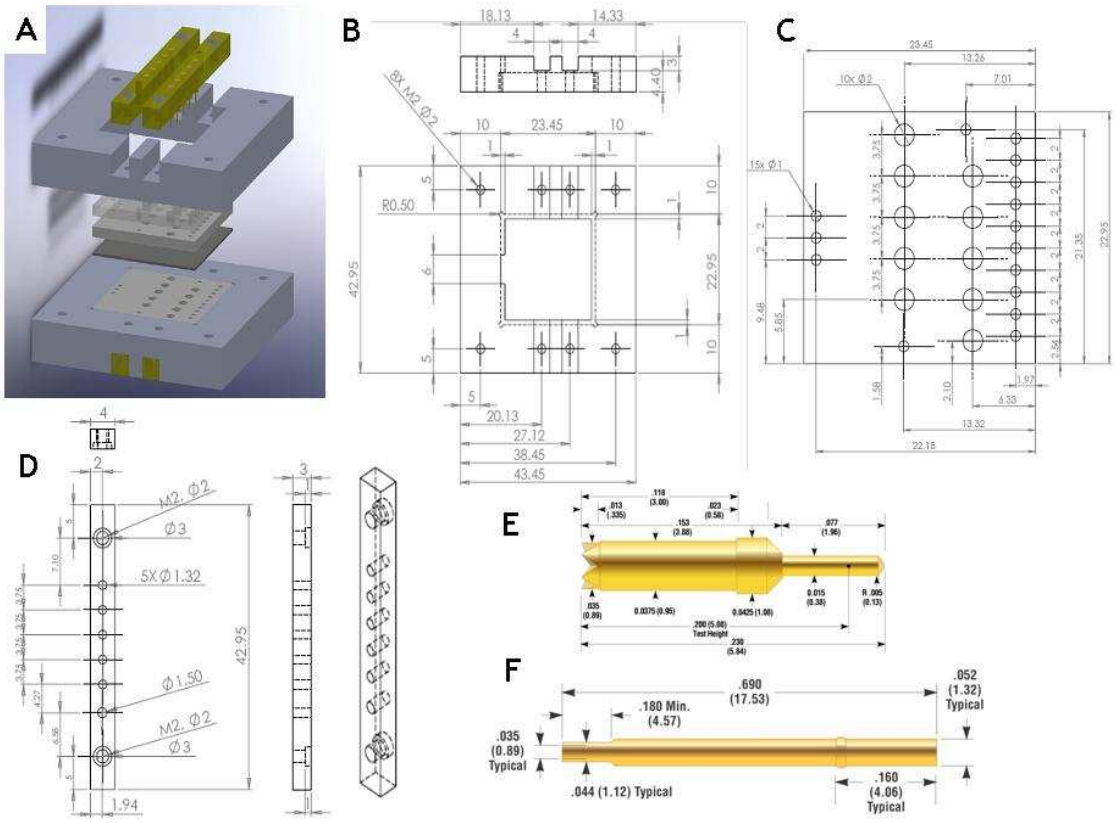

Figure 84: Final device holders for the toxicity device setup.
A) Design in represented in 3D B) Device holder scheme and all measurements are in mm C) Dimensions of the glass slides that support the device inside the holder. D) Dimensions of the electrode holders. E) and F) are the electrical contacts used to measure TEER inside the device.

Calculation Tables

Flow rate (pump) Q_p µl/min	Velocities mm/sec		Shear stress (mPa)	
	Inlet/outlet channels	Cell culture chamber	Inlet/outlet channels	Cell culture chamber
0.5	0.048	0.2×10^{-3}	15	0.6
1	0.096	0.4×10^{-3}	30	1.2
2	0.19	0.8×10^{-3}	59	2.3
5	0.48	2×10^{-3}	147	5.8
10	0.96	4×10^{-3}	295	11.8

Table 11: Shear stress calculations for the single cell culture device
µ = viscosity = 0.0074 g/cm, 5ml syringe diameter (BD scientific) = 12.06 mm, length of inlet/outlet channels ($l_{i/o}$) = 4 mm; height of channels = 0.112 mm; width of channels ($w_{i/o}$) = 0.2 mm; Cell chamber radius (r) = 2.5 mm; height of channel (h) = 0.112 mm; volume of chamber. These calculations were done using equation – 3 and 4.

Flow rate (pump) Q_p µl/min	Velocities mm/sec		Shear stress (mPa)	
	Cell culture chamber	Each serpentine channel	Cell culture chamber	Each serpentine channel
0.5	1.1×10^{-3}	3.2×10^{-3}	7	125
1	2.2×10^{-3}	6.5×10^{-3}	14	251
2	4.4×10^{-3}	13×10^{-3}	28	502
5	11×10^{-3}	32×10^{-3}	71	1255
10	22×10^{-3}	65×10^{-3}	143	2511

Table 12: Shear stress calculations for the multiwell channel device
µ = viscosity = 0.0074 g/cm, 5ml syringe diameter (BD scientific) = 12.06 mm, length of serpentine channel lenght ($l_{i/o}$) = 6 cm; width of serpentine channels ($w_{i/o}$) = 0.050 mm; Cell chamber radius (r) = 1.75 mm; height of channel (h) = 0.058 mm; These calculations were done using equation – 3 and 4.

FITC-dextran MW (kDa)	Stokes radius (nm)	Diffusion coefficients (D_{coeff}) at 37°C ($cm^2\ s^{-1} \times 10^{-7}$)		
		37°C (Xu, 2001)	(using equation 3 from Chapter 1)	
			37°C	**22°C**
4	1.4	6.9	7.1	4.2
70	6	1.9	1.91	1.13
500	14.5	0.6	0.78	0.46
2000	27	0.4	0.42	0.25

Table 13: Diffusion coefficients of the dextran particles
The values given by Xu et al, (2001) were used to compare the calculated values from the diffusion eqution in Chapter 1 and compared at different temperatures. Calculation were done using the Diffusion equations (equation – 6)

7 Bibliography

Abasolo, I., Z. Wang, et al. (2004). "Adrenomedullin inhibits prostate cancer cell proliferation through a cAMP-independent autocrine mechanism." Biochemical and Biophysical Research Communications **322**(3): 878-886.

Absood, A., B. Hu, et al. (2008). "VIP inhibits human HepG2 cell proliferation in vitro." Regulatory Peptides **146**(1-3): 285-292.

Agrawal, N., M. Toner, et al. (2008). "Neutrophil migration assay from a drop of blood." Lab on a Chip **8**(12): 2054-2061.

Agu, R. U., M. Jorissen, et al. (2001). "In vitro nasal drug delivery studies: comparison of derivatised, fibrillar and polymerised collagen matrix-based human nasal primary culture systems for nasal drug delivery studies." J. Pharm. Pharmacol. **53**: 1447 - 1456.

Ahn, I. S., W. C. Ghiorse, et al. (1998). "Growth kinetics of Pseudomonas putida G7 on naphthalene and occurrence of naphthalene toxicity during nutrient deprivation." Biotechnol Bioeng **59**(5): 587-94.

Aijaz, S., M. S. Balda, et al. (2006). "Tight junctions: molecular architecture and function." Int Rev Cytol **248**: 261-98.

Aijaz, S., F. D'Atri, et al. (2005). "Binding of GEF-H1 to the tight junction-associated adaptor cingulin results in inhibition of Rho signaling and G1/S phase transition." Dev Cell **8**(5): 777-86.

Alivisatos, A. P., K. P. Johnsson, et al. (1996). "Organization of 'nanocrystal molecules' using DNA." Nature **382**(6592): 609-11.

Arafat, A., M. Giesbers, et al. (2007). "Covalent biofunctionalization of silicon nitride surfaces." Langmuir **23**(11): 6233-44.

Arafat, A., K. Schroen, et al. (2004). "Tailor-made functionalization of silicon nitride surfaces." J Am Chem Soc **126**(28): 8600-1.

Asgharian, B., W. Hofmann, et al. (2001). "Mucociliary clearance of insoluble particles from the tracheobronchial airways of the human lung." Journal of Aerosol Science **32**(6): 817-832.

Auroux, P. A., D. Iossifidis, et al. (2002). "Micro total analysis systems. 2. Analytical standard operations and applications." Analytical Chemistry **74**(12): 2637-2652.

Babu, J. P., G. D. Jindal, et al. (1990). "Impedance plethysmography: basic principles." J Postgrad Med **36**(2): 57-63.

Bal, B. S., A. Khandkar, et al. (2009). "Fabrication and testing of silicon nitride bearings in total hip arthroplasty: winner of the 2007 "HAP" PAUL Award." J Arthroplasty **24**(1): 110-6.

Balasubramanian, A. K., A. Beskok, et al. (2007). "In situ analysis of bacterial capture in a microfluidic channel." J. Micromech. Microeng. **17**: 1467-1478.

Balda, M. S. and K. Matter (2000). "Transmembrane proteins of tight junctions." Semin Cell Dev Biol **11**(4): 281-9.

Balda, M. S. and K. Matter (2008). "Tight junctions at a glance." J Cell Sci **121**(Pt 22): 3677-82.

Bang, H., S. H. Lim, et al. (2004). "Serial dilution microchip for cytotoxicity test." Journal of Micromechanics and Microengineering **14**(8): 1165-1170.

Barrientos, A. G., J. M. de la Fuente, et al. (2003). "Gold glyconanoparticles: synthetic polyvalent ligands mimicking glycocalyx-like surfaces as tools for glycobiological studies." Chemistry **9**(9): 1909-21.

Barrow, C. S. and W. H. Steinhagen (1982). "Design, construction and operation of a simple inhalation exposure system." Fundam Appl Toxicol **2**(1): 33-7.

Beck, R. E. and J. S. Schultz (1970). "Hindered Diffusion in Microporous Membranes with Known Pore Geometry." Science **170**(3964): 1302-1305.

Becker, H. and C. Gartner (2008). "Polymer microfabrication technologies for microfluidic systems." Anal Bioanal Chem **390**(1): 89-111.

Becker, H. and L. E. Locascio (2002). "Polymer microfluidic devices." Talanta **56**(2): 267-87.

Beebe, D. J., G. A. Mensing, et al. (2002). "Physics and applications of microfluidics in biology." Annual Review of Biomedical Engineering **4**: 261-286.

Beer, N. R., E. K. Wheeler, et al. (2008). "On-Chip Single-Copy Real-Time Reverse-Transcription PCR in Isolated Picoliter Droplets." Analytical Chemistry **80**(6): 1854-1858.

Benson, H.A.E., Sraveiya, V., Risk, S., and Roberts, M. S., (2005) “Influence of anatomical site and topical formulation on skin penetration of sunscreens.” Therapeutics and Clinical Risk Management **1** (3): 209-218.

Bernardin, M. P. and B. E. Lehnert (1995). "Model of particle-alveolar macrophage relationships during the alveolar clearance of a low lung burden of instilled particles." Journal of Aerosol Science **26**(2): 319-333.

Bhattacharya, S. Arindom Datta, Jordan M. Berg, and Shubhra Gangopadhyay (2005). “Studies on Surface Wettability of Poly(Dimethyl) Siloxane (PDMS) and

Glass Under Oxygen-Plasma Treatment and Correlation With Bond Strength.” Journal of Microelectromechanical systems ,**14**(3): 590-597

Black, A. M. S. (1989). "Applied Aspects of Pulmonary Gas Exchange." Current anesthesia and critical care **1**: 19 - 25

Boucher, R. C. (2002). "An overview of the pathogenesis of cystic fibrosis lung disease." Advanced Drug Delivery Reviews **54**(11): 1359-1371.

Brandner, J. M. (2009). "Tight junctions and tight junction proteins in mammalian epidermis." Eur J Pharm Biopharm **72**(2): 289-94.

Breslauer, D. N., P. J. Lee, et al. (2006). "Microfluidics-based systems biology." Molecular Biosystems **2**(2): 97-112.

Brody, J. P. and P. Yager (1997). "Diffusion-based extraction in a microfabricated device." Sensors Actuators A **58**: 13-18.

Brody, J. P., P. Yager, et al. (1996). "Biotechnology at low Reynolds numbers." Biophys. J. **71**: 3430-3441.

Broeckaert, F., A. Clippe, et al. (2000). "Clara cell secretory protein (CC16): features as a peripheral lung biomarker." Ann N Y Acad Sci **923**: 68-77.

Bruchez, M., Jr., M. Moronne, et al. (1998). "Semiconductor nanocrystals as fluorescent biological labels." Science **281**(5385): 2013-6.

Bryce, S. M., J. C. Bemis, et al. (2008). "In vivo mutation assay based on the endogenous Pig-a locus." Environ Mol Mutagen **49**(4): 256-64.

Campodónico, V. L., M. Gadjeva, et al. (2008). "Airway epithelial control of Pseudomonas aeruginosa infection in cystic fibrosis." Trends in Molecular Medicine **14**(3): 120-133.

Cannon, W. C., E. F. Blanton, et al. (1983). "The flow-past chamber: an improved nose-only exposure system for rodents." Am Ind Hyg Assoc J **44**(12): 923-8.

Cassie, A. B. D and Baxter, S (1944). “Wettability of porous surfaces” Trans. Faraday Soc. , **40**, 546.

Cheng, Y.-S. and O. R. Moss (1995). "Inhalation exposure systems." Toxicology Methods **5**(3): 161 - 197.

Chiba, H., M. Osanai, et al. (2007). "Transmembrane proteins of tight junctions." Biochimica et Biophysica Acta (BBA) - Biomembranes **In Press, Corrected Proof**.

Chien LJ, W. J., Hsieh TM, Chen PH, Chen PJ, Lee DS, Luo CH, Lee GB (2009). "A micro circulating PCR chip using a suction-type membrane for fluidic transport." Biomed Microdevices. **11**(2): 359 -67.

Clausen, C., S. A. Lewis, et al. (1979). "Impedance analysis of a tight epithelium using a distributed resistance model." Biophys J **26**(2): 291-317.

Clausen, C. and N. K. Wills (1981). "Impedance analysis in epithelia." Soc Gen Physiol Ser **36**: 79-92.

Cohen, A. B. and W. M. Gold (1975). "Defense mechanisms of the lungs." Annu Rev Physiol **37**: 325-50.

Collard, D., S. Takeuchi, et al. (2008). "MEMS technology for nanobio research." Drug Discovery Today **13**(21-22): 989-996.

Cushing, M. C. and K. S. Anseth (2007). "Materials science. Hydrogel cell cultures." Science **316**(5828): 1133-4.

Darling, R. B. "Lecture presentation EE-527: Microfabrication" Accessed on 21st August 2009 from the following website http://www.ee.washington.edu/research/microtech/cam/PROCESSES/PDF%20FILES/Photolithography.pdf."

de Belder, A. N. "Amersham Bioscience handbook - Dexran particles " (18-1166-12).

De Boeck, M., P. Hoet, et al. (2003). "In vivo genotoxicity of hard metal dust: induction of micronuclei in rat type II epithelial lung cells." Carcinogenesis **24**(11): 1793-800.

de Kerchove, A. J. and M. Elimelech (2008). "Calcium and Magnesium Cations Enhance the Adhesion of Motile and Nonmotile Pseudomonas aeruginosa on Alginate Films." Langmuir **24**(7): 3392-3399.

de la Fuente, J. M. and C. C. Berry (2005). "Tat peptide as an efficient molecule to translocate gold nanoparticles into the cell nucleus." Bioconjug Chem **16**(5): 1176-80.

de la Fuente, J. M., C. C. Berry, et al. (2006). "Nanoparticle targeting at cells." Langmuir **22**(7): 3286-93.

de la Fuente, J. M., M. Fandel, et al. (2005). "Quantum dots protected with tiopronin: a new fluorescence system for cell-biology studies." Chembiochem **6**(6): 989-91.

de la Fuente, J. M. and S. Penades (2004). "Understanding carbohydrate-carbohydrate interactions by means of glyconanotechnology." Glycoconj J **21**(3-4): 149-63.

del Campo, A. and C. Greiner (2007). "SU-8: a photoresist for high-aspect-ratio and 3D submicron lithography." J. Micromech. Microeng. **17**: R81 - R95.

DeMello, A. J. (2003). "Microfluidics - DNA amplification moves on." Nature **422**(6927): 28-29.

Dertinger, S. K. W., D. T. Chiu, et al. (2001). "Generation of gradients having complex shapes using microfluidic networks." Anal. Chem. **73**: 1240-1246.

Devlin, R. B., M. L. Frampton, et al. (2005). "In vitro studies: What is their role in toxicology?" Experimental and Toxicologic Pathology **57**(Supplement 1): 183-188.

Diao, J., L. Young, et al. (2008). "An actively mixed mini-bioreactor for protein production from suspended animal cells." Biotechnol Bioeng **100**(1): 72-81.

Dittrich, P. S., K. Tachikawa, et al. (2006). "Micro total analysis systems. Latest advancements and trends." Analytical Chemistry **78**(12): 3887-3907.

Donaldson, K., D. Brown, et al. (2002). "The pulmonary toxicology of ultrafine particles." Journal of Aerosol Medicine-Deposition Clearance and Effects in the Lung **15**(2): 213-220.

Duhayon, S., P. Hoet, et al. (2008). "Carcinogenic potential of formaldehyde in occupational settings: a critical assessment and possible impact on occupational exposure levels." Int Arch Occup Environ Health **81**(6): 695-710.

Ekkels, P., R. W. Tjerkstraa, et al. (2003). "Fabrication of functional structures on thin silicon nitride membranes." Microelectronic Engineering **67-68** 422 – 429.

Eley, J. G. (2002). "In vitro external factors influencing tight junctions and the accuracy of transepithelial electrical resistance measurement." Journal of the Alabama Academy of Science.

Elghanian, R., J. J. Storhoff, et al. (1997). "Selective colorimetric detection of polynucleotides based on the distance-dependent optical properties of gold nanoparticles." Science **277**(5329): 1078-81.

Ferin, J. (1994). "Pulmonary retention and clearance of particles." Toxicology Letters **72**(1-3): 121-125.

Ferin, J., G. Oberdörster, et al. (1990). "Increased pulmonary toxicity of ultrafine particles? I. Particle clearance, translocation, morphology." Journal of Aerosol Science **21**(3): 381-384.

Fiegel, J., C. Ehrhardt, et al. (2003). "Large porous particle impingement on lung epithelial cell monolayers--toward improved particle characterization in the lung." Pharm Res **20**(5): 788-96.

Fissell, W. H., S. Manley, et al. (2006). "Differentiated growth of human renal tubule cells on thin-film and nanostructured materials." Asaio J **52**(3): 221-7.

Florea, B. I., M. L. Cassara, et al. (2003). "Drug transport and metabolism characteristics of the human airway epithelial cell line Calu-3." Journal of Controlled Release **87**(1-3): 131-138.

Fogh, J., J. M. Fogh, et al. (1977). "One hundred and twenty-seven cultured human tumor cell lines producing tumors in nude

mice." J. Natl. Cancer Inst. **59** 221–225.

Forbes, B. (2000). "Human airway epithelial cell lines for in vitro drug transport and metabolism studies." Pharmaceutical Science & Technology Today **3**(1): 18-27.

Forbes, B. (2002). "Pulmonary epithelial cell culture." Methods Mol Biol **188**: 65-75.

Forbes, B. and C. Ehrhardt (2005). "Human respiratory epithelial cell culture for drug delivery applications." European Journal of Pharmaceutics and Biopharmaceutics **60**(2): 193-205.

Forbes, B., A. Shah, et al. (2003). "The human bronchial epithelial cell line 16HBE14o- as a model system of the airways for studying drug transport." International Journal of Pharmaceutics **257**(1-2): 161-167.

Foster, K. A., M. L. Avery, et al. (2000). "Characterization of the Calu-3 cell line as a tool to screen pulmonary drug delivery." International Journal of Pharmaceutics **208**(1-2): 1-11.

Frampton, J. P., M. L. Shuler, et al. (2008). "Biomedical Technologies for in vitro Screening and Controlled Delivery of Neuroactive Compounds." Cent Nerv Syst Agents Med Chem **8**(3): 203-219.

Frangos, J. A., L. V. McIntyre, et al. (1988). "Shear stress induced stimulation of mammalian cell metabolism " Biotechnology and Bioengineering **32**: 1053 - 1060.

Freitas, R. A., Jr. (2005). "Nanotechnology, nanomedicine and nanosurgery." Int J Surg **3**(4): 243-6.

Gardner, D. E. (1993). "Toxicology of the lungs." Methodologies and technnologies for animal inhalation toxicology studies **Second eddition**: 1.

Geys, J., L. Coenegrachts, et al. (2006). "In vitro study of the pulmonary translocation of nanoparticles: A preliminary study." Toxicology Letters **160**(3): 218-226.

Geys, J., B. Nemery, et al. (2007). "Optimisation of culture conditions to develop an in vitro pulmonary permeability model." Toxicology in Vitro **21**(7): 1215-1219.

Geys, J., B. Nemery, et al. (2007). "Cytotoxicity of SiO2 in A549 cells." Toxicol Appl Pharmacol **220**(2): 225; author reply 226.

Geys, J., A. Nemmar, et al. (2008). "Acute toxicity and prothrombotic effects of quantum dots: impact of surface charge." Environ Health Perspect **116**(12): 1607-13.

Goldberg, B. J. and Pier G. B. (2000). "The role of the CFTR in susceptibility to Pseudomonas aeruginosa infections in cystic fibrosis." Trends in Microbiology **8**(11): 514-520.

Gomez, M. I. and A. Prince (2007). "Opportunistic infections in lung disease: Pseudomonas infections in cystic fibrosis." Current Opinion in Pharmacology **7**: 244–251.

Gómez, M. I. and A. Prince (2007). "Opportunistic infections in lung disease: Pseudomonas infections in cystic fibrosis." Current Opinion in Pharmacology **7**(3): 244-251.

Gonzalez-Mariscal, L., A. Betanzos, et al. (2003). "Tight junction proteins." Progress in Biophysics and Molecular Biology **81**(1): 1-44.

Gonzalez-Mariscal, L., A. Betanzos, et al. (2003). "Tight junction proteins." Prog Biophys Mol Biol **81**(1): 1-44.

Grainger, C. I., L. L. Greenwell, et al. (2006). "Culture of Calu-3 cells at the air interface provides a representative model of the airway epithelial barrier." Pharm Res **23**(7): 1482-90.

Grenha, A., C. I. Grainger, et al. (2007). "Chitosan nanoparticles are compatible with respiratory epithelial cells in vitro." Eur J Pharm Sci **31**(2): 73-84.

Gunawan, R. C., J. Silvestre, et al. (2006). "Cell migration and polarity on microfabricated gradients of extracellular matrix proteins." Langmuir **22**(9): 4250-8.

Haeberle S, Z. R. (2007). "Microfluidic platforms for lab-on-a-chip applications." Lab Chip **7**(9): 1094 - 1110.

Harris, S. G. and M. L. Shuler (2003). "Growth of endothelial cells on microfabricated silicon nitride membranes for an in vitro model of the blood-brain barrier." Biotechnology and Bioprocess Engineering **8**(4): 246-251.

Haswell, S. J. (2006). "Chemical technology: All together now." Nature **441**(7094): 705-705.

Heath, J. R. and M. E. Davis (2008). "Nanotechnology and cancer." Annual Review of Medicine **59**: 251-265.

Hediger, S. (2002). "Biosystems for the culture and electrical characterisation of epithelial cell tissue." PhD Thesis.

Hediger, S., J. Fontannaz, et al. (2000). "Biosystem for the culture and characterisation of epithelial cell tissues." Sensors and Actuators B: Chemical **63**(1-2): 63-73.

Hermans, C. and A. Bernard (1999). "Lung epithelium-specific proteins: characteristics and potential applications as markers." Am J Respir Crit Care Med **159**(2): 646-78.

Hermans, C., B. Knoops, et al. (1999). "Clara cell protein as a marker of Clara cell damage and bronchoalveolar blood barrier permeability." Eur Respir J **13**(5): 1014-21.

Hermans, C., O. Lesur, et al. (1998). "Clara cell protein (CC16) in pleural fluids: a marker of leakage through the visceral pleura." Am J Respir Crit Care Med **157**(3 Pt 1): 962-9.

Hermans, C., M. Petrek, et al. (2001). "Serum Clara cell protein (CC16), a marker of the integrity of the air-blood barrier in sarcoidosis." Eur Respir J **18**(3): 507-14.

Hill, G. C., R. Melamud, et al. (2007). "SU-8 MEMS Fabry-Perot pressure sensor." Sensors and Actuators A: Physical **138**(1): 52-62.

Hoet, P. H., I. Bruske-Hohlfeld, et al. (2004). "Nanoparticles - known and unknown health risks." J Nanobiotechnology **2**(1): 12.

Hull, J. (2003). "Basic science of cystic fibrosis." Current Paediatrics **13**(4): 253-258.

Hung P, J. P., J. Lee; Poorya, Sabounchi; Robert, Lin; Luke, P. Lee (2005). "Continuous perfusion microfluidic cell culture array for high-throughput cell-based assays." Biotechnology and Bioengineering **89**(1): 1-8.

Inatomi, K. I., S. I. Izuo, et al. (2006). "Application of a microfluidic device for counting of bacteria." Letters in Applied Microbiology **43**: 296-300.

Isawa T, T. T., Anazawa Y, Miki M, Motomiya M. (1991). "Technegas for inhalation lung imaging." Nuclear Medical Communication **12**(1): 47-55.

Ismagilov, R. F., A. D. Stroock, et al. (2000). "Experimental and theoretical scaling laws for transverse diffusive broadening in two-phase laminar flows in microchannels." Appl. Phys. Lett. **76**: 2376-2378.

Jacob, T., R. J. Lee, et al. (2002). "Modulation of Cytosolic Ca2+ Concentration in Airway Epithelial Cells by Pseudomonas aeruginosa." Infect. Immun. **70**(11): 6399-6408.

Jain, K. K. (2005). "Nanotechnology in clinical laboratory diagnostics." Clinica Chimica Acta **358**: 37 - 54.

James JM, T. H. (1995). "The use of 99Tcm-Technegas in the investigation of patients with pulmonary

thromboembolism." Nuclear Medical Communication **16**(10): 802-810.

Jeon, N. L. (2000). "Generation of solution and surface gradients using microfluidic systems." Langmuir **16**: 8311-8316.

Jeon, N. L., H. Baskaran, et al. (2002). "Neutrophil chemotaxis in linear and complex gradients of interleukin-8 formed in a microfabricated device." Nature Biotechnology **20**(8): 826-830.

Jeon, N. L., S. K. W. Dertinger, et al. (2000). "Generation of solution and surface gradients using microfluidic systems." Langmuir **16**(22): 8311-8316.

Jiang, X., J. M. Ng, et al. (2003). "A miniaturized, parallel, serially diluted immunoassay for analyzing multiple antigens." J Am Chem Soc **125**(18): 5294-5.

Kallio, J. K.-K. a. P. J. (2006). "PDMS and its suitability for analytical microfluidic devices." Proceedings of the 28th IEEE EMBS Annual Internatioal Conference: 2486 - 89.

Kamholz, A. E. (2004). "Proliferation of microfluidics in literature and intellectual property." Lab on a Chip **4**(2): 16N-20N.

Kamholz, A. E., B. H. Weigl, et al. (1999). "Quantitative analysis of molecular interaction in a microfluidic channel: the T-sensor." Anal. Chem. **71**: 5340-5347.

Kamholz, A. E. and P. Yager (2001). "Theoretical analysis of molecular diffusion in pressure-driven laminar flow in microfluidic channels." Biophys J **80**(1): 155-60.

Kane, R. S. and A. D. Stroock (2007). "Nanobiotechnology: protein-nanomaterial interactions." Biotechnol Prog **23**(2): 316-9.

Kashima, R., Y. Oyake, et al. (1996). "Improved ex vivo/in vitro lymph node cell proliferation assay in guinea pigs for a screening test of contact hypersensitivity of chemical compounds." Toxicology **114**(1): 47-55.

Kato, K. and T. Takayama (2002). "Pseudomonas aeruginosa infection and cystic fibrosis." The Lancet **359**(9302): 262-262.

Kazmierczak, B. I., T. S. Jou, et al. (2001). "Rho GTPase activity modulates Pseudomonas aeruginosa internalization by epithelial cells." Cell Microbiol **3**(2): 85-98.

Keller, S., G. Blagoi, et al. (2008). "Processing of thin SU-8 films." J. Micromech. Microeng. **18**: 125020 (10pp).

Kim, K. Y. (2007). "Nanotechnology platforms and physiological challenges for cancer therapeutics." Nanomedicine-Nanotechnology Biology and Medicine **3**(2): 103-110.

Kirchhof, K. and T. Groth (2008). "Surface modification of biomaterials to control adhesion of cells." Clin Hemorheol Microcirc **39**(1-4): 247-51.

Kirchhof, K., K. Hristova, et al. (2009). "Multilayer coatings on biomaterials for control of MG-63 osteoblast adhesion and growth." J Mater Sci Mater Med **20**(4): 897-907.

Klammer, I., M. C. Hoffman, et al. (2006). "Long-term stability of PDMS-based microfluidic systems used for biocatalytic reactions." J. Micromech. Microeng. **16**: 2425 - 2428.

Knight, J. (2002). "Microfluidics: Honey, I shrunk the lab." Nature **418**(6897): 474-475.

Korin, N., A. Bransky, et al. (2007). "A parametric study of human fibroblasts culture in a microchannel bioreactor." Lab Chip **7**(5): 611-7.

Korin, N., A. Bransky, et al. (2009). "Design of well and groove microchannel bioreactors for cell culture." Biotechnol Bioeng **102**(4): 1222-30.

Lapierre, L. A. (2000). "The molecular structure of the tight junction." Adv Drug Deliv Rev **41**(3): 255-64.

Larry, M. L., M. F. Roseanne, et al. (2008). "Bacterial chemotaxis transverse to axial flow in a microfluidic channel." Biotechnology and Bioengineering **100**(4): 653-663.

Leclerc, E., B. David, et al. (2006). "Study of osteoblastic cells in a microfluidic environment." Biomaterials **27**(4): 586-95.

Leclerc, E., Y. Sakai, et al. (2004). "Microfluidic PDMS (polydimethylsiloxane) bioreactor for large-scale culture of hepatocytes." Biotechnol Prog **20**(3): 750-5.

Leclerc, E., Yasuyuki, Sakai, Teruo, Fujii (2004). "Microfluidic PDMS (Polydimethylsiloxane) Bioreactor for Large-Scale Culture of Hepatocytes." Biotechnology Progress **20**(3): 750-755.

Lee, J. N., C. Park, et al. (2003). "Solvent compatibility of poly(dimethylsiloxane)-based microfluidic devices." Anal Chem **75**(23): 6544-54.

Lee PJ, G. T., Hung PJ (2009). "Dynamic cell culture: a microfluidic function generator for live cell microscopy." Lab Chip **9**(1): 164 -166.

Leen, J. B., P. Hansen, et al. (2008). "Improved focused ion beam fabrication of near-field apertures using a silicon nitride membrane." Opt Lett **33**(23): 2827-9.

Li N, T. A., Folch A (2003). "Biology on a chip: microfabrication for studying the behavior of cultured cells." Crit Rev Biomed Eng **31** (5-6): 423 - 88.

Lin, F., C. M. C. Nguyen, et al. (2005). "Neutrophil migration in opposing chemoattractant gradients using microfluidic chemotaxis devices." Annals of Biomedical Engineering **33**(4): 475-482.

Lin, Y. C., C. H. Ho, et al. (1997). "Fibroblasts Contracting Collagen Matrices Form Transient Plasma Membrane Passages through which the Cells Take Up Fluorescein Isothiocyanate-Dextran and Ca2'

" Mol Biol Cell **8**: 59 - 71.

Lo, C. M., C. R. Keese, et al. (1995). "Impedance analysis of MDCK cells measured by electric cell-substrate impedance sensing." Biophys J **69**(6): 2800-7.

Lo, C. M., C. R. Keese, et al. (1999). "Cell-substrate contact: another factor may influence transepithelial electrical resistance of cell layers cultured on permeable filters." Exp Cell Res **250**(2): 576-80.

López-Romero, D., C. A. Barrios, et al. "High aspect-ratio SU-8 resist nano-pillar lattice by e-beam direct writing and its application for liquid trapping." Microelectronic Engineering **87**(4): 663-667.

Lu, H. K., L. Y., Wang, W. M. Lauffenburger, D. A. Griffith, L. G, Jensen, K. F. (2004). "Microfluidic Shear Devices for Quantitative Analysis of Cell Adhesion." Anal. Chem. **76**(18): 5257-5264.

Lu, S. L., R. Duffin, et al. (2009). "Efficacy of Simple Short-Term in Vitro Assays for Predicting the Potential of Metal Oxide Nanoparticles to Cause Pulmonary Inflammation." Environmental Health Perspectives **117**(2): 241-247.

Lundqvist, M., J. Stigler, et al. (2008). "Nanoparticle size and surface properties determine the protein corona with possible implications for biological impacts." Proc Natl Acad Sci U S A **105**(38): 14265-70.

Lynch, I., T. Cedervall, et al. (2007). "The nanoparticle-protein complex as a biological entity; a complex fluids and surface science challenge for the 21st century." Adv Colloid Interface Sci **134-135**: 167-74.

Ma, S. H., L. A. Lepak, et al. (2005). "An endothelial and astrocyte co-culture model of the blood-brain barrier utilizing an ultra-thin, nanofabricated silicon nitride membrane." Lab on a Chip **5**(1): 74-85.

Madou, M. J. (2002). "Fundamentals of Microfabrication - The Science of Miniaturization." **Second edition** 3.

Manford, F., A. Tronde, et al. (2005). "Drug permeability in 16HBE14o- airway cell layers correlates with absorption from the isolated perfused rat lung." European Journal of Pharmaceutical Sciences **26**(5): 414-420.

Mao, H. B., P. S. Cremer, et al. (2003). "A sensitive, versatile microfluidic assay for bacterial chemotaxis." Proc. Natl Acad. Sci. USA **100**: 5449-5454.

Mark, J. M., H. Allcock, et al. (2005). "Inorganic Polymers." Cary, NC, USA **Oxford University Press** chp 4.

Marquis, B. J., S. A. Love, et al. (2009). "Analytical methods to assess nanoparticle toxicity." Analyst **134**(3): 425-39.

Mata, A., A. Fleischman, J., et al. (2006). "Fabrication of multi-layer SU-8 microstructures." J. Micromech. Microeng. **16**: 276–284.

Mathia, N. R., J. Timoszyk, et al. (2002). "Permeability characteristics of calu-3 human bronchial epithelial cells: in vitro-in vivo correlation to predict lung absorption in rats." J Drug Target **10**(1): 31-40.

Matilainen, L., T. Toropainen, et al. (2007). "In vitro toxicity and permeation of cyclodextrins in Calu-3 cells." Journal of Controlled Release **In Press, Corrected Proof**.

Matter, K. and M. S. Balda (1999). "Occludin and the functions of tight junctions." Int Rev Cytol **186**: 117-46.

Matter, K. and M. S. Balda (2003). "Signalling to and from tight junctions." Nat Rev Mol Cell Biol **4**(3): 225-36.

Mazzola, L. (2003). "Commercializing nanotechnology." Nat Biotechnol **21**(10): 1137-43.

McAuliffe, G. J., J. Y. Chang, et al. (2008). "Development of a gastrointestinal tract microscale cell culture analog to predict drug transport." Mol Cell Biomech **5**(2): 119-32.

McDonald, J. C., D. C. Duffy, et al. (2000). "Fabrication of microfluidic systems in poly(dimethylsiloxane)." Electrophoresis **21**(1): 27-40.

McDonald, J. C. and G. M. Whitesides (2002). "Poly(dimethylsiloxane) as a material for fabricating microfluidic devices." Accounts of Chemical Research **35**(7): 491-499.

Meban, C. (1980). "Thickness of the air-blood barriers in vertebrate lungs." J Anat **131**(Pt 2): 299-307.

Mendes, F., L. Doucet, et al. (2004). "Immunohistochemistry of CFTR in native tissues and primary epithelial cell cultures." Journal of Cystic Fibrosis **3**(Supplement 2): 37-41.

Meuwly, F., P. A. Ruffieux, et al. (2007). "Packed-bed bioreactors for mammalian cell culture: bioprocess and biomedical applications." Biotechnol Adv **25**(1): 45-56.

MicroChem. and www.microchem.com "SU-8 3000 series data sheet."

Miner, M. E. and N. C. Gonzalez (1975). "Variations in pulmonary gas exchange due to changes in pulmonary artery pressure and flow." J Surg Res **18**(4): 431-5.

Mirkin, C. A., R. L. Letsinger, et al. (1996). "A DNA-based method for rationally assembling nanoparticles into macroscopic materials." Nature **382**(6592): 607-9.

Moreau-Marquis, S., B. A. Stanton, et al. (2008). "Pseudomonas aeruginosa biofilm formation in the cystic fibrosis airway." Pulmonary Pharmacology & Therapeutics **21**(4): 595-599.

Muhlfeld, C., B. Rothen-Rutishauser, et al. (2008). "Interactions of nanoparticles with pulmonary structures and cellular responses." Am J Physiol Lung Cell Mol Physiol **294**(5): L817-29.

Mukhopadhyay, R. (2007). "When PDMS isn't the best. What are its weaknesses, and which other polymers can researchers add to their toolboxes?" Anal Chem **79**(9): 3248-53.

NanoSafe2 (2005-2009). "Project Report." http://www.nanosafe.org/scripts/home/publigen/content/templates/show.asp?P=66&L=EN.

Nawrot, T. S., K. Nackaerts, et al. (2007). "Lung cancer mortality and fine particulate air pollution in Europe." Int J Cancer **120**(8): 1825-6; author reply 1827.

Nemmar, A., P. H. Hoet, et al. (2003). "Diesel exhaust particles in lung acutely enhance experimental peripheral thrombosis." Circulation **107**(8): 1202-8.

Nemmar, A., P. H. Hoet, et al. (2006). "Translocation of ultrafine particles." Environ Health Perspect **114**(4): A211-2; author reply A212-3.

Nemmar, A., P. H. Hoet, et al. (2002). "Passage of inhaled particles into the blood circulation in humans." Circulation **105**(4): 411-4.

Nemmar, A., B. Nemery, et al. (2003). "Pulmonary inflammation and thrombogenicity caused by diesel particles in hamsters: role of histamine." Am J Respir Crit Care Med **168**(11): 1366-72.

Nguyen, N. T. and S. T. Wereley (2006). "Fabrication techniques for microfluidics " Fundamentals and applications of microfluidics

(Second edition): 55 - 110.

Nguyen, N. T. and Z. G. Wu (2005). "Micromixers - a review." Journal of Micromechanics and Microengineering **15**(2): R1-R16.

Nicolis, E., I. Lampronti, et al. (2009). "Modulation of expression of IL-8 gene in bronchial epithelial cells by 5-methoxypsoralen." International Immunopharmacology **9**(12): 1411-1422.

Oberdorster, G. (1995). "Lung particle overload: implications for occupational exposures to particles." Regul Toxicol Pharmacol **21**(1): 123-35.

Oberdorster, G. (2001). "Pulmonary effects of inhaled ultrafine particles." Int Arch Occup Environ Health **74**(1): 1-8.

Oberdorster, G. (2002). "Toxicokinetics and effects of fibrous and nonfibrous particles." Inhal Toxicol **14**(1): 29-56.

Oberdörster, G., J. Ferin, et al. (1997). "Alveolar macrophage cluster formation: A clearance mechanism for large particles in mouse lungs?" The Annals of Occupational Hygiene **41**(Supplement 1): 554-560.

Oberdorster, G., A. Maynard, et al. (2005). "Principles for characterizing the potential human health effects from exposure to nanomaterials: elements of a screening strategy." Part Fibre Toxicol **2**: 8.

Oberdorster, G., V. Stone, et al. (2007). "Toxicology of nanoparticles: A historical perspective." Nanotoxicology **1**(1): 2-25.

Oberdorster, G., M. J. Utell, et al. (1986). "Bronchial and alveolar absorption of inhaled 99mTc-DTPA." Am Rev Respir Dis **134**(5): 944-50.

Paris, L., L. Tonutti, et al. "Structural organization of the tight junctions." Biochimica et Biophysica Acta (BBA) - Biomembranes **In Press, Corrected Proof**.

Park, T. H. and M. L. Shuler (2003). "Integration of cell culture and microfabrication technology." Biotechnol Prog **19**(2): 243-53.

Paull, R., J. Wolfe, et al. (2003). "Investing in nanotechnology." Nat Biotechnol **21**(10): 1144-7.

Petty, R. T., H. W. Li, et al. (2007). "Attachment of cells to islands presenting gradients of adhesion ligands." Journal of the American Chemical Society **129**(29): 8966-+.

Phalen, R. F. (1976). "Inhalation exposure of animals." Environ Health Perspect **16**: 17-24.

Phalen, R. F., R. C. Mannix, et al. (1984). "Inhalation exposure methodology." Environ Health Perspect **56**: 23-34.

Pier, G. B. (2002). "CFTR mutations and host susceptibility to Pseudomonas aeruginosa lung infection." Current Opinion in Microbiology **5**(1): 81-86.

Piiper, J. (1994). "Alveolar-capillary gas transfer in lungs: development of concepts and current state." Adv Exp Med Biol **345**: 7-14.

Piiper, J. and P. Scheid (1971). "Respiration: alveolar gas exchange." Annu Rev Physiol **33**: 131-54.

Pinnau, I. and Z. He (2004). "Pure- and mixed-gas permeation properties of polydimethylsiloxane for hydrocarbon/methane and hydrocarbon/hydrogen separation." Journal of Membrane Science **244**: 227-233.

Pollard, T. D. and W. C. Earnshaw (2002). "Cell Biology ".

Popa, A. M., P. Niedermann, et al. (2009). "Fabrication of nanopore arrays and ultrathin silicon nitride membranes by block-copolymer-assisted lithography." Nanotechnology **20**(48): 485303.

Prestwich, G. D. (2008). "Engineering a clinically-useful matrix for cell therapy." Organogenesis **4**(1): 42-7.

Puleo, C. M., H. C. Yeh, et al. (2007). "Applications of MEMS technologies in tissue engineering." Tissue Engineering **13**(12): 2839-2854.

Purcell, E. M. (1977). "Life at low Reynolds number." Am. J. Phys. **45**: 3-11.

Reyes, D. R., D. Iossifidis, et al. (2002). "Micro total analysis systems. 1. Introduction, theory, and technology." Analytical Chemistry **74**(12): 2623-2636.

Rhee, M. and M. A. Burns (2008). "Microfluidic assembly blocks." Lab Chip **8**(8): 1365-73.

Robin, M., P. Dong, et al. (2002). "Serum levels of CC16, SP-A and SP-B reflect tobacco-smoke exposure in asymptomatic subjects." Eur Respir J **20**(5): 1152-61.

Rotoli, B. M., O. Bussolati, et al. (2008). "Non-functionalized multi-walled carbon nanotubes alter the paracellular permeability of human airway epithelial cells." Toxicology Letters **178**(2): 95-102.

Saavedra, M., M. Vasil, et al. (2002). "Pseudomonas aeruginosa-Human Airway Epithelial Cell Interaction." Chest **121**: 40S–41S.

Saavedra, M., M. Vasil, et al. (2002). "Pseudomonas aeruginosa-human airway epithelial cell interaction: effects of iron on inflammation and apoptosis." Chest **121**(3 Suppl): 40S-41S.

Sakagami, M. (2006). "In vivo, in vitro and ex vivo models to assess pulmonary absorption and disposition of inhaled therapeutics for systemic delivery." Advanced Drug Delivery Reviews **58**(9-10): 1030-1060.

Salata, O. (2004). "Applications of nanoparticles in biology and medicine." J Nanobiotechnology **2**(1): 3.

Salata, O. (2007). "Nanotechnology in therapeutics: hydrogels and beyond." J Nanobiotechnology **5**: 5.

Sato, H., H. Matsumura, et al. (2006). "An all SU-8 microfuidic chip with built-in 3D fine structures." J. Micromech. Microeng. **16**: 2318 - 2322.

Sayes, C. M., K. L. Reed, et al. (2009). "Can in vitro assays substitute for in vivo studies in assessing the pulmonary hazards of fine and nanoscale materials? ." J Nanopart Res **11**: 421 - 431.

Schneeberger, E. E. and R. D. Lynch (1992). "Structure, function, and regulation of cellular tight junctions." Am J Physiol **262**(6 Pt 1): L647-61.

Schneeberger, E. E. and R. D. Lynch (2004). "The tight junction: a multifunctional complex." Am J Physiol Cell Physiol **286**(6): C1213-28.

Seagrave, J., J. D. McDonald, et al. (2005). "In vitro versus in vivo exposure to combustion emissions." Experimental and Toxicologic Pathology **57**(Supplement 1): 233-238.

Service, R. F. (2004). "Nanotoxicology. nanotechnology grows up " Science **304**: 1732–1734,.

Sharma, P., S. Brown, et al. (2006). "Nanoparticles for bioimaging

" Adv. Colloid Interface Sci. **.** pp. 123, 471-null.

Shim, J., T. F. Bersano-Begey, et al. (2003). "Micro- and nanotechnologies for studying cellular function." Current Topics in Medicinal Chemistry **3**(6): 687-703.

Sia, S. K. and G. M. Whitesides (2003). "Microfluidic devices fabricated in poly(dimethylsiloxane) for biological studies." Electrophoresis **24**(21): 3563-3576.

Sieben, V. J., C. S. D. Marun, et al. (2007). "FISH and chips: chromosomal analysis on microfluidic platforms." Iet Nanobiotechnology **1**(3): 27-35.

Silva, G. A. (2004). "Introduction to nanotechnology and its applications to medicine." Surg Neurol **61**(3): 216-20.

Silva, G. A. (2005). "Nanotechnology approaches for the regeneration and neuroprotection of the central nervous system." Surg Neurol **63**(4): 301-6.

Silva, G. A. (2006). "Neuroscience nanotechnology: progress, opportunities and challenges." Nat Rev Neurosci **7**(1): 65-74.

Silva, G. A. (2007). "Nanotechnology approaches for drug and small molecule delivery across the blood brain barrier." Surgical Neurology **67**(2): 113-116.

Sin, A., K. C. Chin, et al. (2004). "The design and fabrication of three-chamber microscale cell culture analog devices with integrated dissolved oxygen sensors." Biotechnol Prog **20**(1): 338-45.

Sin, A., K. C. Chin, et al. (2004). "The Design and Fabrication of Three-Chamber Microscale Cell Culture Analog Devices with Integrated Dissolved Oxygen Sensors." Biotechnol. Prog **20**: 338 - 345.

Soloviev, M. (2007). "Nanobiotechnology today: focus on nanoparticles." J Nanobiotechnology **5**: 11.

Song, L., S. Nadkarni, et al. (2004). "Microfluidic channels with well-defined spatial and temporal chemical gradients to study chemotaxis in dictyostelium discoideum." Biophysical Journal **86**(1): 482A-483A.

Sperling, R. A., P. Rivera Gil, et al. (2008). "Biological applications of gold nanoparticles." Chem Soc Rev **37**(9): 1896-908.

Stiles, D. K. and B. A. Oakley (2005). "Four-point electrode measurement of impedance in the vicinity of bovine aorta for quasi-static frequencies." Bioelectromagnetics **26**(1): 54-8.

Stone, V. (2000). "Environmental air pollution." American Journal of Respiratory and Critical Care Medicine **162**(2): S44-S47.

Stone, V. (2006). "Nanoparticle toxicity." Comparative Biochemistry and Physiology a-Molecular & Integrative Physiology **143**(4): S123-S123.

Stone, V., H. Johnston, et al. (2007). "Air pollution, ultrafine and nanoparticle toxicology: Cellular and molecular interactions." Ieee Transactions on Nanobioscience **6**(4): 331-340.

Sturm, R. and W. Hofmann (2009). "A theoretical approach to the deposition and clearance of fibers with variable size in the human respiratory tract." Journal of Hazardous Materials **In Press, Accepted Manuscript**.

Sukhorukov, G. B., A. L. Rogach, et al. (2005). "Nanoengineered polymer capsules: tools for detection, controlled delivery, and site-specific manipulation." Small **1**(2): 194-200.

Sun Y, K. Y. (2006). "Polymeric microfluidic system for DNA analysis." Anal Chim Acta **556**(1): 80 - 96

Tabling, P. (2005). "Diffusion, mixing and separation in microsystems." Introduction to Microfluidics 130 - 187.

Taccetti, G., S. Campana, et al. (1996). "Pseudomonas aeruginosa infection in patients with cystic fibrosis." The Journal of Pediatrics **129**(4): 619-620.

Taylor, A. E. and K. A. Gaar, Jr. (1970). "Estimation of equivalent pore radii of pulmonary capillary and alveolar membranes." Am J Physiol **218**(4): 1133-40.

Taylor, A. E., A. C. Guyton, et al. (1965). "Permeability of the Alveolar Membrane to Solutes." Circ Res **16**: 353-62.

Terheggen-Lagro, S. W. J., G. T. Rijkers, et al. (2005). "The role of airway epithelium and blood neutrophils in the inflammatory response in cystic fibrosis." Journal of Cystic Fibrosis **4**(Supplement 2): 15-23.

Theodore, J., E. D. Robin, et al. (1975). "Transalveolar transport of large polar solutes (sucrose, inulin, and dextran)." Am J Physiol **229**(4): 989-96.

Tirella, A., M. Marano, et al. (2008). "A microfluidic gradient maker for toxicity testing of bupivacaine and lidocaine." Toxicol In Vitro **22**(8): 1957-64.

Torous, D., N. Asano, et al. (2006). "Performance of flow cytometric analysis for the micronucleus assay--a reconstruction model using serial dilutions of malaria-infected cells with normal mouse peripheral blood." Mutagenesis **21**(1): 11-3.

Urban, J. J., D. V. Talapin, et al. (2006). "Self-assembly of PbTe quantum dots into nanocrystal superlattices and glassy films." J Am Chem Soc **128**(10): 3248-55.

Vanoirbeek, J. A., M. Tarkowski, et al. (2004). "Respiratory response to toluene diisocyanate depends on prior frequency and concentration of dermal sensitization in mice." Toxicol Sci **80**(2): 310-21.

Vanoirbeek, J. A., M. Tarkowski, et al. (2006). "Validation of a mouse model of chemical-induced asthma using trimellitic anhydride, a respiratory sensitizer, and dinitrochlorobenzene, a dermal sensitizer." J Allergy Clin Immunol **117**(5): 1090-7.

Vikströma, E., L. Buib, et al. (2009). "The junctional integrity of epithelial cells is modulated by Pseudomonas aeruginosa quorum sensing molecule through phosphorylation-dependent mechanisms." Experimental Cell Research (315): 313 – 326.

Villa-Vega, K. R., Takemoto, J. K., Yanez, J, A., Remsberg, C. M., Forrest, M. L., Davies, N. M., (2008). "Clinical toxicities of nanocarrier systems." Advanced Drug Delivery Reviews. 60: 929-938.

Viravaidya, K., A. Sin, et al. (2004). "Development of a microscale cell culture analog to probe naphthalene toxicity." Biotechnol Prog **20**(1): 316-23.

Voskerician, G., M. S. Shive, et al. (2003). "Biocompatibility and biofouling of MEMS drug delivery devices." Biomaterials **24**(11): 1959-67.

Walker, G. M., J. Q. Sai, et al. (2005). "Effects of flow and diffusion on chemotaxis studies in a microfabricated gradient generator." Lab on a Chip **5**(6): 611-618.

Walker, G. M., H. C. Zeringue, et al. (2004). "Microenvironment design considerations for cellular studies." Lab Chip **4**: 91 - 97.

Warheit, D. B. (2004). "Nanoparticles: Health impacts?" Materials Today **7**(2): 32-35.

Warheit, D. B., W. J. Brock, et al. (2005). "Comparative pulmonary toxicity inhalation and instillation studies with different TiO2 particle formulations: Impact of surface treatments on particle toxicity." Toxicological Sciences **88**(2): 514-524.

Warheit, D. B., J. F. Hansen, et al. (1997). "Inhalation of high concentrations of low toxicity dusts in rats results in impaired pulmonary clearance mechanisms and persistent inflammation." Toxicology and Applied Pharmacology **145**(1): 10-22.

Warheit, D. B. and M. A. Hartsky (1988). "Assessments of Pulmonary Macrophage Clearance Responses to Inhaled Particulates." Scanning Microscopy **2**(2): 1069-1078.

Warheit, D. B., B. R. Laurence, et al. (2004). "Comparative pulmonary toxicity assessment of single-wall carbon nanotubes in rats." Toxicological Sciences **77**(1): 117-125.

Wegener, J., M. Sieber, et al. (1996). "Impedance analysis of epithelial and endothelial cell monolayers cultured on gold surfaces." J Biochem Biophys Methods **32**(3): 151-70.

Weibel, D. B. and G. M. Whitesides (2006). "Applications of microfluidics in chemical biology." Current Opinion in Chemical Biology **10**(6): 584-591.

Weible, E. R. and B. Knight (1964). "A morphometric study on the thickness of the pulmonary air-blood barrier." The Journal of Cell biology **1**: 367 - 384.

Weigl, B. H., R. L. Bardell, et al. (2003). "Lab-on-a-chip for drug development." Advanced Drug Delivery Reviews **55**(3): 349-377.

Weiss, L. (1983). "Cell and tissue biology " Textbook of Histology **Sixth Edition**: 113-150; 753-813.

White, C. R. and J. A. Frangos (2007). "The shear stress of it all: the cell membrane and mechanochemical transduction." Philosophical Transactions of the Royal Society B: Biological Sciences **362**(1484): 1459-1467.

Whitesides, G. M. (2005). "Nanoscience, nanotechnology, and chemistry." Small **1**(2): 172-9.

Whitesides, G. M. (2006). "The origins and the future of microfluidics." Nature **442**(7101): 368-73.

Wong, B. A. (2007). "Inhalation exposure systems: design, methods and operation." Toxicol Pathol **35**(1): 3-14.

WPI, W. P. I. I. "http://www.wpiinc.com." WPI Inc.

Wu, M. H., J. P. Urban, et al. (2006). "Development of PDMS microbioreactor with well-defined and homogenous culture environment for chondrocyte 3-D culture." Biomed Microdevices **8**(4): 331-40.

Xu, G. and M. J. Groves (2001). "Effect of FITC-dextran molecular weight on its release from floating cetyl alcohol and HPMC tablets." Journal of Pharmacy and Pharmacology **53**: 49-56.

Xu, H., H. M. Vanhooren, et al. (2004). "Pulmonary toxicity of polyvinyl chloride particles after repeated intratracheal instillations in rats. Elevated CD4/CD8 lymphocyte ratio in bronchoalveolar lavage." Toxicol Appl Pharmacol **194**(2): 122-31.

Yamamoto, Y., T. Yamamoto, et al. (1991). "Impedance plethysmography in human limbs. Part 1. On electrodes and electrode geometry." Med Biol Eng Comput **29**(4): 419-24.

Yamamoto, Y., T. Yamamoto, et al. (1992). "Impedance plethysmography for blood flow measurements in human limbs. Part 2. Influence of limb cross-sectional area." Med Biol Eng Comput **30**(5): 518-24.

Ye, H., Z. Gu, et al. (2006). "Kinetics of ultraviolet and plasma surface modification of poly(dimethylsiloxane) probed by sum frequency vibrational spectroscopy." Langmuir **22**(4): 1863-8.

Yemini, M., B. Hadad, et al. (2009). "The controlled fabrication of nanopores by focused electron-beam-induced etching." Nanotechnology **20**(24): 245302.

Yeon, J. H. and J. K. Park (2007). "Microfluidic cell culture systems for cellular analysis." Biochip Journal **1**(1): 17-27.

Young, E. W. and D. J. Beebe (2010). "Fundamentals of microfluidic cell culture in controlled microenvironments." Chem Soc Rev **39**(3): 1036-48.

Zaouk, R., B. Y. Park, et al. (2006). "Fabrication of polydimethylsiloxane microfluidics using SU-8 molds." Methods Mol Biol **321**: 17-21.

Zhang, S., L. Xia, et al. (2008). "Microfabricated silicon nitride membranes for hepatocyte sandwich culture." Biomaterials **29**(29): 3993-4002.

Zhang, Z. X., Z. Shen, et al. (2005). "Microarrays of DNA and protein integrated on microfluidic chip." Acta Chimica Sinica **63**(18): 1743-1746.